METAMORPHIC AND STRUCTURAL EVOLUTION OF
ARCHEAN ROCKS IN THE KESKARRAH BAY AREA,
POINT LAKE, DISTRICT OF MACKENZIE, N.W.T.

VALERIE A. JACKSON, B.Sc.

NOTICE

AVIS

Canada

Permission has been granted to the National Library of Canada to microfilm this thesis and to lend or sell copies of the film.

The author (copyright owner) has reserved other publication rights, and neither the thesis nor extensive extracts from it may be printed or otherwise reproduced without his/her written permission.

L'autorisation a été accordée à la Bibliothèque nationale du Canada de microfilmer cette thèse et de prêter ou de vendre des exemplaires du film.

L'auteur (titulaire du droit d'auteur) se réserve les autres droits de publication; ni la thèse ni de longs extraits de celle-ci ne doivent être imprimés ou autrement reproduits sans son autorisation écrite.

METAMORPHIC and STRUCTURAL EVOLUTION

of ARCHEAN ROCKS

in the KESKARRAH BAY AREA, POINT LAKE,

DISTRICT OF MACKENZIE, N.W.T.

submitted by
Valerie A. Jackson B.Sc.

in partial fulfillment of the M.Sc. degree

May 1989

National Library
of Canada

Bibliothèque nationale
du Canada

Canadian Theses Service

Service des thèses canadiennes

NOTICE

AVIS

THE QUALITY OF THIS MICROFICHE
IS HEAVILY DEPENDENT UPON THE
QUALITY OF THE THESIS SUBMITTED
FOR MICROFILMING.

LA QUALITE DE CETTE MICROFICHE
DEPEND GRANDEMENT DE LA QUALITE DE LA
THESE SOUMISE AU MICROFILMAGE.

UNFORTUNATELY THE COLOURED
ILLUSTRATIONS OF THIS THESIS
CAN ONLY YIELD DIFFERENT TONES
OF GREY.

MALHEUREUSEMENT, LES DIFFERENTES
ILLUSTRATIONS EN COULEURS DE CETTE
THESE NE PEUVENT DONNER QUE DES
TEINTES DE GRIS.

View northeast from Point Lake (foreground) showing
terrane underlain by the sillimanite-bearing schists
of the Itchen Formation, which are intruded by
small, leucocratic pegmatite bodies.

ABSTRACT

The Keskarrah Bay area, Point Lake, N.W.T. is underlain by Archean rocks of the Slave Province that form two distinct lithotectonic elements: a sialic basement terrane, consisting of high-grade gneisses and granodiorite, and a supracrustal terrane, known as the Itchen Lake region supracrustal belt, comprising metavolcanic and metasedimentary rocks of the Yellowknife Supergroup.

Conditions of regional metamorphism are documented mainly from metamorphic mineral assemblages in turbidites, which comprise greywacke-mudstone and subordinate iron formation and Fe-rich sediments. The sequential development of the key metamorphic index minerals chlorite, biotite, cordierite, andalusite and sillimanite in pelitic lithologies and garnet, staurolite or Ca and Fe-rich clino-amphibole in Fe-rich sediments occurred dominantly through continuous rather than discontinuous metamorphic reactions. The measured trends of increasing $Mg:Fe$ ratios of the index minerals (cordierite > muscovite > chlorite > biotite > amphibole > staurolite > garnet) are used to demonstrate changes in AFM topology, from which the continuous reactions are interpreted.

The pattern of metamorphic isograds is attributed to a single, progressive low pressure regional metamorphic event. Metamorphic grade increases both eastwards towards the Tarta batholith, and westwards towards the basement gneisses and

the Pointless batholith. Prograde metamorphism in the supracrustal rocks was synchronous with retrograde metamorphism in the basement terrane. Peak metamorphic conditions, which reached a maximum of about 600°C +/- 50°C and 4.0 +/- 1.6 kbar, were attained toward the end of deformation. The P-T distribution throughout the area is consistent with the presence of a distant thermal dome that formed in the area of eventual batholith emplacement.

Three or possibly four phases of deformation have been recognized in the supracrustal terrane. Proximity to basement is considered to have had an influence on the orientation and intensity of structures developed during the first two phases of deformation. East-west trending isoclinal folds (F_1) and a penetrative S_1 fabric produced during D_1 are recognized mainly along the western edge of the supracrustal belt. D_2 resulted in the formation of north-south trending main phase F_2 folds that refold F_1 and are overturned to the west, and an S_2 foliation, both of which predominate throughout much of the map area. Post-D_2 deformations produced crenulations of the S_2 foliation, an L-S fabric defined by elongate biotite porphyroblasts and southeast- and northeast-trending biotite schistosities (tentatively designated S_3 and S_4). These fabrics, which are well developed in central and eastern exposures of the metaturbidites, are unrelated to large scale folding.

The polyphase deformation (D_x) in the basement terrane that led to the formation of the basement gneisses predated

deposition of the Yellowknife Supergroup. After deposition
of the Yellowknife Supergroup, the basement gneisses
adjacent to the supracrustal rocks were deformed by
north-trending mylonitic foliations and large scale folds,
which are correlated with S_2 and F_2 respectively in the
supracrustals. West-verging recumbent folds (pre-D_2?) in the
gneisses may indicate the formation of nappes, which m y
have also affected the supracrustal rocks.

The westward overturning of main phase F_2 folds in the
supracrustal terrane is towards basement. A similar
relationship is observed in parts of the southern Slave
Province, thus the formation of these folds represents a
major tectonic event in the Slave Province. The suggested
deformational history of the Itchen Lake region supracrustal
rocks is that of a west-verging fold-and-thrust belt.

ACKNOWLEDGEMENTS

DEDICATION

This thesis is dedicated to my mother and father.

TABLE OF CONTENTS

LIST OF FIGURES

LIST OF TABLES

LIST OF ABBREVIATIONS

Musc	Muscovite
Chl	Chlorite
Bio	Biotite
Cord	Cordierite
And	Andalusite
Alsil	Aluminosilicates
Sill	Sillimanite
Plag	Plagioclase
Garn	Garnet
Alman	Almandine
Gross	Grossular
Spess	Spessartine
Staur	Staurolite
Amph	Amphibole
Op	Opaque
Cc	Calcite
Ilm	Ilmenite
To	Tourmaline
Sp	Sphene
Ap	Apatite
Zi	Zircon
Rf	Rock fragment
CHZ	Chlorite Zone
ECHZ	Eastern Chlorite Zone
WCHZ	Western Chlorite Zone
BZ	Biotite Zone
EBZ	Eastern Biotite Zone
WBZ	Western Biotite Zone
CZ	Cordierite Zone
AZ	Andalusite Zone
SZ	Sillimanite Zone
A*Z	Muscovite-free Andalusite Zone
S*Z	Muscovite-free Sillimanite Zone
SCB	Sillimanite-Cordierite-Biotite Assemblage
SAB	Sillimanite-Andalusite-Biotite Assemblage
SCAB	Sillimanite-Cordierite-Andalusite-Biotite Assemblage
SABM	Sillimanite-Andalusite-Biotite-Muscovite Assemblage
$X_A B$	Molecular proportion of Component A in Mineral B
Kd	Distribution coefficient
O.R	Outer rim of garnet porphyroblast
I.R	Inner rim of garnet porphyroblast
M/FM	Mg/Mg+Fe from atomic proportions in mineral analyses
FeO, Fe^{2+}	= total Fe in analyses carried out by electron microprobe

1.0 INTRODUCTION

This thesis is primarily a metamorphic and structural study of some Archean rocks in the Slave Province of northern Canada. In this first section some of the general characteristics of the Slave Province will be reviewed before the new data and interpretations of the tectonometamorphic history of a small part of the Itchen Lake greenstone belt, Keskarrah Bay area are presented.

1.1 Slave Structural Province

1.1.1 General Statement

The Slave Province of the northwestern Canadian Shield is an Archean crustal remnant consisting of both low- to medium-grade granite-greenstone terranes and medium- to high-grade gneiss terranes (Figure 1; Stockwell, 1961; McGlynn and Henderson, 1970, 1972). The supracrustal rocks in the greenstone belts are interconnected over large areas, but locally isolated by the intervening granitic and gneissic regions. In many respects the greenstone belts are similar to those found in the Superior Province of southern Canada, and in the Archean blocks of Australia and southern Africa (Goodwin, 1981). The most abundant lithologies, ie. mafic and felsic volcanic rocks and greywacke-mudstones of turbiditic origin, are similar to those recorded elsewhere in young Archean cratons. However, two points of distinction

Figure 1: Generalized geologic map of the Slave Province of the northwestern Canadian Shield (inset diagram) modified after McGlynn (1977) and Padgham (1981) showing: known locations of basement to the Yellowknife Supergroup (BL - Benjamin Lake area, CR - Cameron River area, HR - Hackett River area, IL - Indin Lake area, PL - Point Lake area, RL - Ross Lake area, YK - Yellowknife area) and the Thelon Front (TF). Outlined area represents the Itchen Lake region (Bostock, 1980) which is enlarged in Figure 3 and includes the area of this study.

1 Aphebian cover rocks (includes Bear and Churchill Provinces and platformal Goulburn and Epworth Groups).

2 Granitoids.

3 Gneissic equivalents of the Yellowknife Supergroup (may include some older rocks).

4 Mainly greywacke - mudstone turbidites of the Yellowknife Supergroup.

5 Mainly felsic - intermediate volcanics of the Yellowknife Supergroup with probable calc-alkaline affinities ('Hackett River' type).

6 Mainly mafic volcanics of the Yellowknife Supergroup with tholeiitic affinities ('Yellowknife type').

7 Gneissic granitoids (probable basement to the Yellowknife Supergroup).

8 Boundary of the Slave Province.

9 Fault.
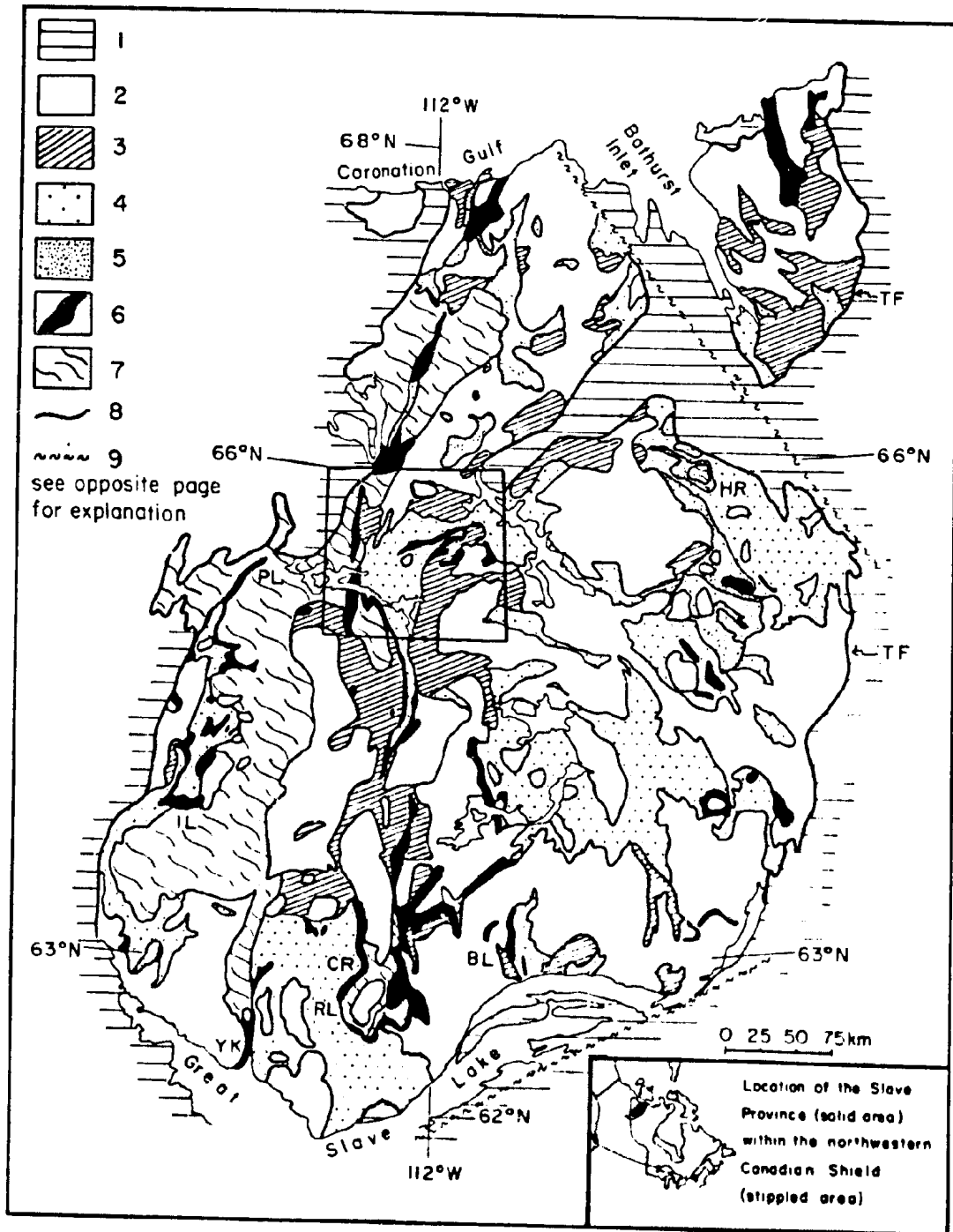
are that in the Slave Province sediments are much more abundant than volcanic rocks, and that ultramafic lavas are rare.

The relationship between the high-grade gneiss terranes and the supracrustal belts is not everywhere certain (Thompson, 1978; Easton, 1985). The gneissic regions may be highly metamorphosed and deformed equivalents of the supracrustals or remnants of an older basement upon which the supracrustals were deposited. Basement-cover relations are well preserved in some localities (Figure 1; Baragar and McGlynn, 1976).

Radiometric ages support the existence of a circa 2.8 to 3.0 Ga basement terrane of granitic to tonalitic composition (Nikic et al., 1975; Frith et al., 1977; Krogh and Gibbins, 1978; Scharer and Allègre, 1982; van Breemen et al., 1987). Deposition of the supracrustal rocks, known as the Yellowknife Supergroup (Henderson, 1970), occurred about 2670 Ma ago (Green and Baadsgaard, 1971: Lambert and Henderson, 1980; Frith and Loveridge, 1982; Henderson et al., 1987; van Breemen et al., 1987), and may have been completed within a 10 to 15 Ma time span (Henderson, 1981). Granitoid rocks were emplaced into the supracrustals between 2500 to 2600 Ma ago (Green and Baadsgaard, 1971; Frith and Loveridge, 1982; Henderson et al., 1987; van Breemen et al., 1987) and local migmatization and remobilization of older sialic terranes may also have occurred at this time (Padgham, 1981). The pan-Slave low pressure-type metamorphic

event occurred about 2600 Ma ago, with the metamorphic culmination either coinciding with or pre-dating the last stages of deformation (Thompson, 1978).

1.1.2 Yellowknife Supergroup

Basalt-andesites with tholeiitic differentiation trends, abundant in the southern and western parts of the Slave Province, comprise the 'Yellowknife' type volcanic rocks (Figure 1; Padgham, 1981; Frith, 1982). Many of these linear volcanic belts are thought to approximate the original margins of the supracrustal basins (Henderson, 1981) as they commonly form the base of the supracrustal sequence and occur along the contact with gneissic or granitic rocks that are suspected or proven to be basement. Calc-alkaline ardesite-rhyodacite volcanic rocks of the 'Hackett River' type (Padgham, 1981; Frith, 1982), which are abundant in the northeastern part of the Slave Province, may form both at the base of the cover sequence and as centers within the sedimentary succession. Lambert (1976, 1978, 1982a) has documented caldera complexes in these calc-alkaline rocks.

Generally overlying the volcanic rocks is a sedimentary sequence dominated by immature greywacke-mudstones of turbiditic affinity (Henderson, 1975, 1981). Tuffaceous layers found within the turbidites locally attest to continued volcanism during sedimentation (Padgham, 1985). Henderson (1975) and Jenner et al. (1981) suggested that in the Yellowknife area turbidites were derived from a mixed

felsic volcanic and granitic and/or gneissic source terrane. Recently Easton (1985) has determined that mafic volcanic rocks contributed significant amounts of detritus to the turbidites of the Point Lake area.

Conglomerate, with or without associated fluvial sandstone, is found at several localities within the Slave Province and typically shows a spatial relationship to volcanic or basement rocks (McGlynn and Henderson, 1970, 1972; Henderson, 1975; Henderson and Easton, 1977a; Henderson, 1981). Henderson (1981) suggested that the depositional environment for these rocks may have been that of a rising fault scarp.

Chemical sediments, such as limestone and iron formation comprise a very small part of the sedimentary succession and are found at the interface between felsic volcanics and turbidites. Iron formation, which is locally auriferous, also occurs widely as discontinuous beds within the turbidites (Padgham, 1981).

1.1.3 Pre-Yellowknife Supergroup Rocks

The best documentation of the sialic basement to the Yellowknife Supergroup is found at Point Lake where two different lithologies have been identified as part of a basement terrane: 1) a 3155 Ma old granitic body (Krogh and Gibbins, 1978) is unconformably overlain by conglomerate of the Yellowknife Supergroup that contains boulders of the granite (Stockwell, 1933; Henderson and Easton, 1977a, b);

and 2) tonalitic to granitic gneiss is unconformably overlain by mafic volcanic rocks (Easton et al., 1981). However, basement-cover relations at Point Lake are controversial. The conglomerate was interpreted as a rift sediment by Henderson and Easton (1977a), Henderson (1981) and Easton (1985), but as a syn-thrusting molasse by Kusky (1987). The high strain zone that locally marks the gneiss-supracrustal boundary was suggested to be a reverse or reactivated normal fault by Henderson (1981), Easton (1985) and Fyson (1987), but was interpreted as a deep level thrust by Kusky (1987).

Elsewhere in the Slave Province the existence of basement has been inferred from: 1) the lack of intrusive relationships between granitoids and the surrounding Yellowknife Supergroup (Heywood and Davidson, 1969); 2) the presence of mafic dikes that cross-cut the granitoids, metamorphic complexes and overlying volcanic rocks, but not the younger turbidites (Davidson, 1972; Baragar and McGlynn, 1976; Lambert, 1982b); and 3) the presence of clasts in metasediments that are similar to the underlying gneissic rocks (Frith and Hill, 1975). A relatively large part of the western Slave Province is characterized by mixed gneissic rocks (Figure 1), some of which may prove to be part of an older basement terrane rather than deeply uplifted keels of the Yellowknife Supergroup.

1.1.4 Intrusive Rocks

Detailed studies have documented the diversity of intrusive complexes in the Slave Province (Atkinson, 1987; King et al., 1988). Batholiths and plutons range from granite to diorite, with most being granite-granodiorite, however in some areas tonalite, quartz diorite and diorite predominate (Henderson and Thompson, 1980, 1981). The latter may be spatially and genetically linked to mafic and intermediate volcanic rocks (Frith and Roscoe, 1980; ; Frith et al., 1977; Jackson et al., 1987) and may pre-date intrusion of granite-granodiorite (Henderson and Thompson, 1980, 1981; Frith and Loveridge, 1982). Small bodies of metagabbro are related to mafic volcanism in some areas (Henderson and Easton, 1977a, b; Bostock, 1980; Helmstaedt, 1985), but ultrabasic rocks are rare (Baragar and McGlynn, 1976; Henderson and Thompson, 1981; Gibbins, 1986). Pegmatites are locally abundant (Kretz, 1969; Bostock, 1980; McKinnon, 1982; Meintzer and Cerney, 1983).

Granitoid intrusions in the Yellowknife Supergroup are generally syn- to postkinematic but it is not unusual to find that in any one area there is a range in the age of pluton emplacement relative to deformation (eg. Fyson and Frith, 1979; King et al., 1988). Subordinate intrusions of dioritic to gabbroic compositions are generally pre- to synkinematic.

1.1.5 Regional Metamorphism

Documentation of metamorphic conditions in the
Yellowknife Supergroup of the Slave Province is aided by the
abundance of turbidites, which are sufficiently aluminous to
have developed some of the key metamorphic mineral
assemblages typical of pelitic rocks. The predominance of
andalusite-sillimanite assemblages indicates that low
pressure, bathozone 2 (Carmichael, 1978) type regional
metamorphism prevailed throughout the Slave Province. The
distribution of the regional metamorphic zones, after
Thompson (1978), is shown in Figure 2.

In general low-grade metasediments are characterized by
the presence of chlorite, muscovite and biotite (Thompson,
1978). The onset of medium-grade metamorphism is widely
indicated by the first appearance of knotted schists
(Thompson, 1978). The knots commonly consist of cordierite,
but andalusite may be present as well as, or occur instead
of cordierite. Sillimanite first appears in rocks of
medium-grade.

High-grade metamorphism may be characterized by the
breakdown of muscovite in the presence of quartz to form
K-feldspar and sillimanite (Winkler, 1976), delineating a
K-feldspar + sillimanite isograd (second sillimanite
isograd), as in the eastern Point Lake area (King, 1981). In
general the zones of high-grade rocks are characterized by
gneisses and/or migmatites (first appearance of granitic
pods) derived from medium-grade metasediments. Kyanite

Figure 2: Regional metamorphic zones in the Slave Province
(from Thompson, 1978). Letter symbols as for
Figure 1, with G = granulite facies, KY = kyanite
localities.

dotted pattern   = low grade

vertical rule   = medium grade

horizontal rule   = high grade

dot - dash line   = boundary of Slave Province

solid heavy line = trend of volcanic belts

unpatterned portion within Slave Province =

granitoids
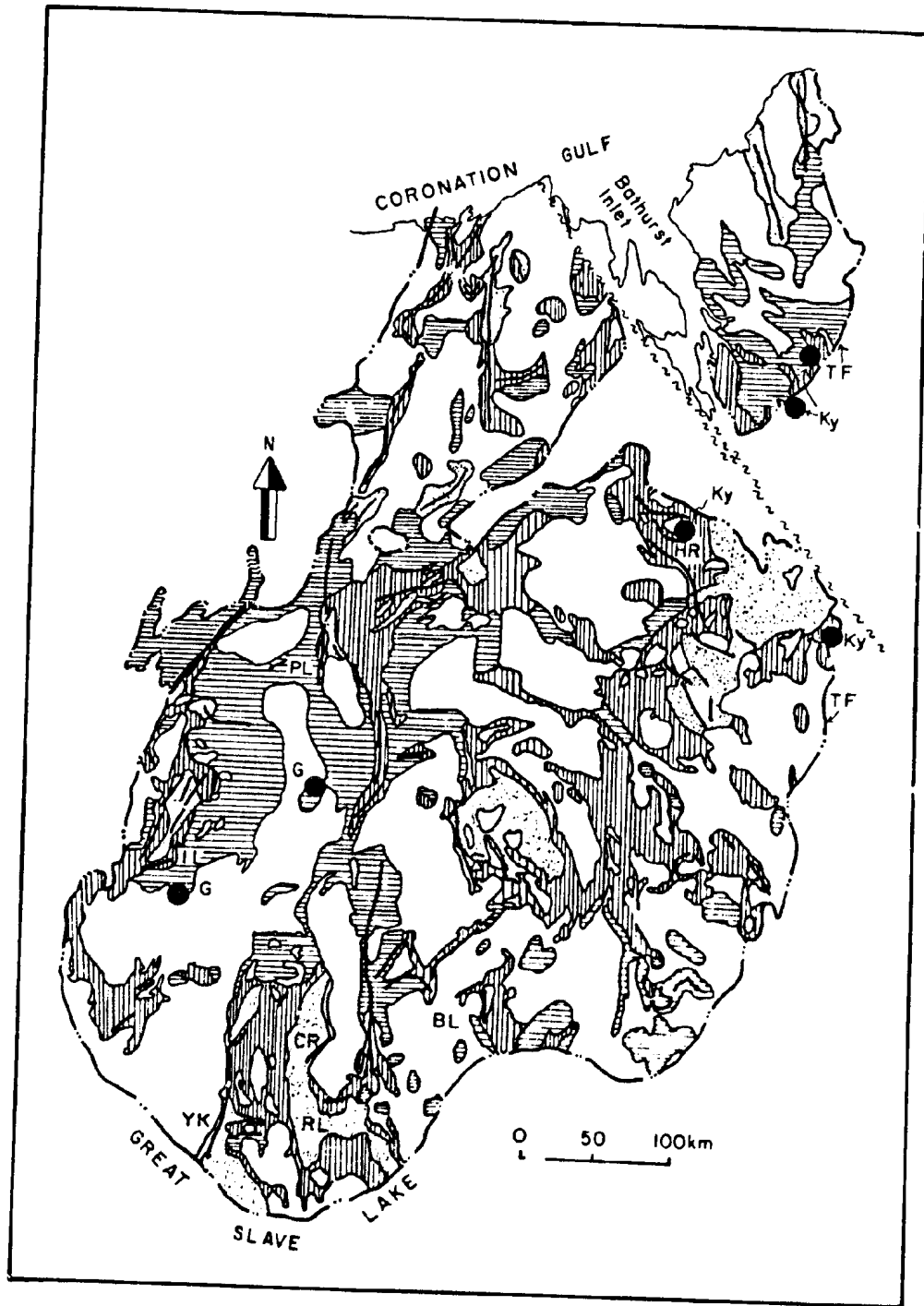
occurrences (Figure 2) document local variations to intermediate-pressure metamorphism within medium to high grade rocks (Percival, 1979). Granulite facies mineral assemblages are recognized only locally within the Slave Province (Figure 2). Many but not all of the high-grade metamorphic zones are adjacent to granitoid rocks (Figure 2).

1.1.6 Structural Synthesis

Throughout the Slave Province, patterns of deformation within the supracrustal belts are broadly similar in style (Thompson, 1978; Fyson, 1981; Fyson and Helmstaedt, 1988). Generally, early folds associated with D_1 are recognized by reversals in bedding facing directions; these F_1 folds are isoclinal with steeply dipping axial planes and variably plunging axes; they typically lack an axial plane cleavage. Thompson (1978) noted that the presence of basement blocks may cause the variable orientations of D_1 structures.

During D_2, pre-existing F_1 folds were either tightened or refolded, depending on their initial orientation. The main phase regional F_2 folds are typically north-south trending, have steeply dipping axial traces and variable plunges, and were formed throughout the Slave Province.

Later deformational events produced regional foliations without associated large scale folds and resulted in the reorientation of the axial traces of the main phase F_2 folds into parallelism with the borders of batholiths and larger

plutons. These deformational events may be associated with granite emplacement (Fyson, 1981).

Fyson (1981, 1982, 1984a) and Fyson and Helmstaedt (1988) have synthesized the structural geology of a large part of the southern Slave Province. Fyson (1981) established; 1) the development of the regional F_2 folds prior to granite emplacement; 2) the predominance of westward overturning of F_2 folds and 3) the formation of both F_2 fold fan axes and S_2 cleavage fan axes were related to regional compression during emplacement and uplift of the granitic plutons. Fyson (1982, 1984b) suggested that major refold patterns were developed in response to strike-slip movement of basement blocks along early formed crustal faults.

1.1.7 Basin Development

The origin of greenstone belts in Archean terranes has been vigorously debated for over a decade, with much of the discussion being centered on the nature of the basement to the supracrustal sequences - the Slave Province is no exception (eg. Green and Baadsgaard, 1971; Drury, 1977). More recent models for the Slave Province prefer a dominantly sialic basement, although both the coherency of this crustal block during greenstone formation and the mechanism(s) of basin formation remain disputed.

The accordance observed in the lithology, stratigraphy and orientations and styles of regional folds and foliations

together with the lack of significant accumulations of ultramafic rocks and the widespread development of low-pressure andalusite-sillimanite metamorphic mineral assemblages led to the speculation that the Slave Province behaved as a coherent crustal segment and to the proposal of extensional tectonic models. For instance, the intracontinental rift models of Henderson (1981) and Easton (1985) envisage small ensialic basins created during extensive block faulting of a coherent sialic crust, leading to the formation of graben-like structures. However, re-examination of many of these features has led to the proposal of horizontally directed compressional tectonic models. Hoffman (1986) suggested that the Slave Province originated as a prograding trench-arc system. Helmstaedt and Padgham (1986) considered the Yellowknife Greenstone Belt to have developed in a back-arc basin setting. Fyson and Helmstaedt (1988) inferred that the 'Yellowknife' type belts are remnants of the floor of marginal basins and models for emplacement of these belts are comparable to either allochthonous or autochthonous ophiolites. 'Hackett River' type volcanics may then have been emplaced in an accreted arc terrane, as Hoffman (1986) suggested. Kusky (1986, 1989) proposed that the Slave Province originated through the collision between an Archean microcontinent (represented by the western gneiss terrane) and a paired accretionary prism (central sedimentary terrane) and island-arc system ('Hackett River' type volcanics) that formed over an east-

dipping subduction zone. Kusky (1986) suggested that all 'Yellowknife' type greenstone belts are allochthonous.

1.2 Regional Geologic Setting

The Itchen Lake region, which includes the thesis study area, lies in the west-central Slave Province (Bostock, 1980; Figures 1 and 3). The northern half of this region contains Proterozoic cover rocks of the Goulburr. and Epworth Groups. The Yellowknife Supergroup forms the northern part of a supracrustal belt, which in the Itchen Lake region is pronouncedly arcuate, but to the south forms an elongate north-trending greenstone belt about 80 kilometers long. This predominantly metasedimentary belt contains two main areas of volcanic rocks known as the Central and Western volcanic belts (Figure 3; Bostock, 1980). It is bounded to the west by granitoid rocks and their host basement gneisses (Henderson and Easton, 1977a, b; Bostock, 1980; Easton et al., 1981, 1982; Henderson, 1981) and to the north and east by granitic batholiths and gneissic equivalents of the Yellowknife Supergroup (Bostock, 1980; King, 1981).

1.3 General Geology of the Keskarrah Bay Area

The Keskarrah Bay area lies along the western margin of the supracrustal belt that spans part of the Itchen Lake region (Figure 3). Volcanic rocks in the area comprise the
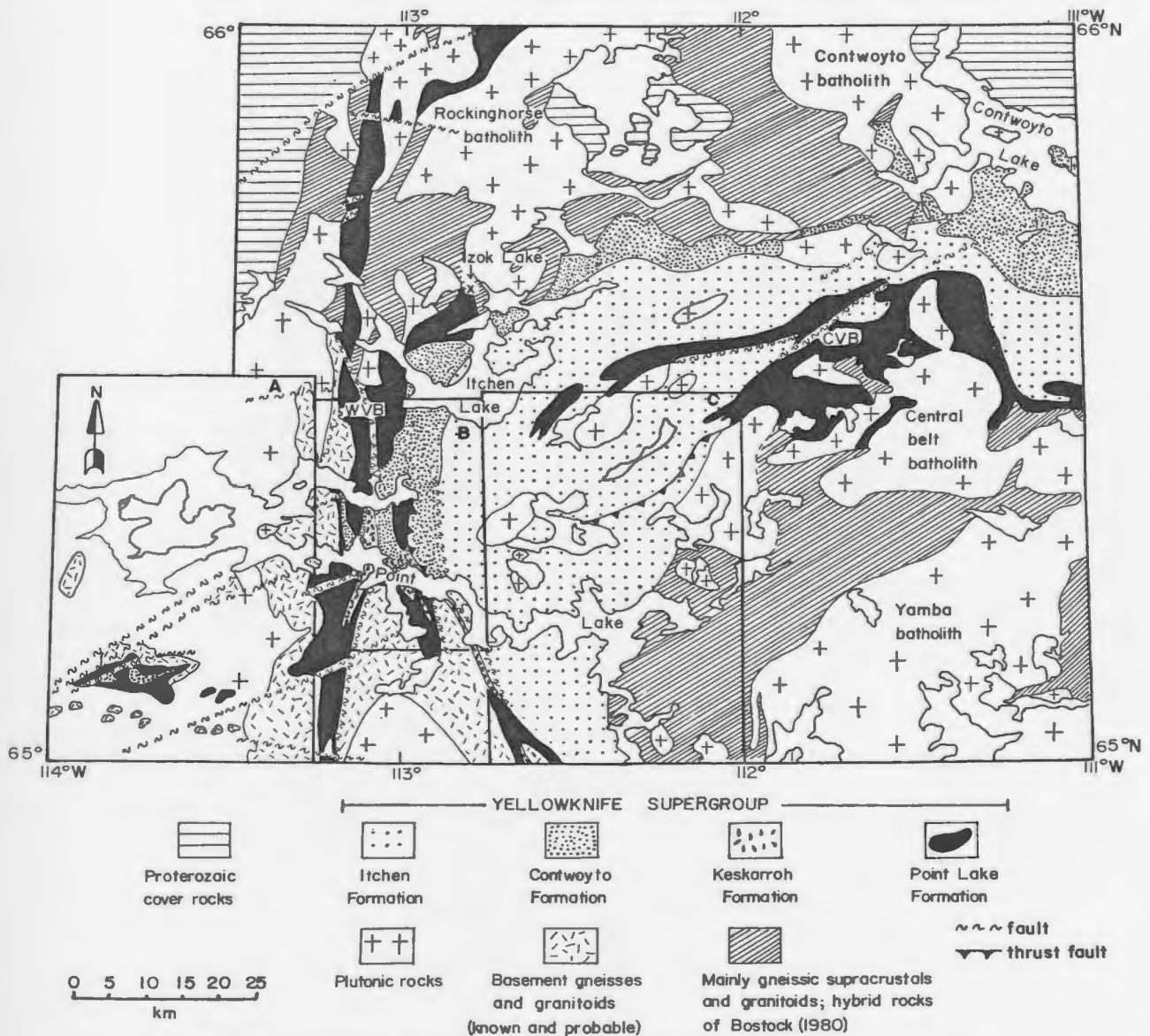
Figure 3: Geology of the Itchen Lake region (modified after Bostock, 1980). Outlined portions represent areas mapped by: Easton et al., 1982 (A), Henderson and Easton, 1977b (B), and King, 1981 (C). This study lies within area B.

WVB Western Volcanic Belt CVB Central Volcanic Belt

Western volcanic belt (Bostock, 1980). The distribution of lithologies is summarized in Figure 4 (the complete geologic map, Figure 5, is included in the pocket). The reader is referred to the previous works of: Bostock (1980), for petrological and lithological descriptions of the supracrustal rocks; Jackson (1983, 1984) for lithologic descriptions; Henderson and Easton (1977a, b) for stratigraphic information; Easton et al. (1981, 1982) for description of the basement gneisses and the 'Pointless' batholith and McKinnon (1982) for detailed petrology and geochemistry of granites and pegmatites. Kusky (1987) examined the basement-cover relationships in the Point Lake area.

Evidence in the study area (Figure 4) suggests that the Yellowknife Supergroup was deposited on a sialic basement terrane consisting of gneiss (unit 1) and granodiorite (unit 2). In different locations within or near the map area, banded mafic volcanic rocks of the Point Lake Formation (unit 3) and mafic flows (unit 4) and Keskarrah Formation conglomerate (unit 8) all interfinger to form the base of the supracrustal sequence (Henderson and Easton, 1977a, b). The unconformity between conglomerate (unit 8) and the 3155 Ma old granodiorite (unit 2; Stockwell, 1933; Henderson and Easton, 1977a, b; Krogh and Gibbins, 1978), is exposed in the study area (Figure 4). Additional evidence for basement-cover relations comes from a paleoweathering zone which is found locally within this granodiorite (Easton, 1985). A

Figure 4

Generalized Geological Map
of the Keskarrah Bay Area

(modified after Henderson
and Easton, 1977a)

```
0          5
  |———————|
     km
```

ITCHEN   LAKE

NORTH
ARM

Tree
Bay

FUBAR
FAULT

POINT

Keskarrah
Bay

LAKE

N

Legend:

| 12 | Adamellite |
| 11 | Granite |

YELLOWKNIFE SUPERGROUP

Itchen Formation (10)
(medium-grade)

Contwoyto Formation: low-grade
(9a), medium-grade (9b)

Keskarrah Formation (8)

Point Lake Formation

Rhyolite (6)

Dacite (5)

Mafic flows (4)

Banded mafic volcanics(3), Gabbro (3a)

BASEMENT

Granodiorite-granite (2)

Gneiss (1)   fault, reverse fault

antiform, overturned antiform

synform, overturned syn'orm   } F$_2$

small stock of granodiorite, southwest of Tree Bay (Figure
4), may also represent a basement block: surrounding mafic
flows face away from the granodiorite (see map of Henderson
and Easton, 1977b) and are not intruded by it. Relationships
between the gneissic basement rocks and the supracrustals
are more obscure. Easton et al. (1981) documented an angular
unconformity between banded mafic volcanic rocks and
gneisses about 5 kilometers west of the southwestern corner
of the map area. Within the map area the volcanics of unit 3
are either in fault contact with the gneisses, or are
penetratively folded and in apparent conformable contact
with them. However, Kusky (1987 and pers. comm.) suggests
that these volcanics are allochthonous and were emplaced
during westward directed thrusting of the supracrustal
terrane.

Turbidites of the Contwoyto and Itchen Formations (units
9 and 10) overlie and interfinger with the volcanic rocks
and conglomerate. Thin, discontinuous, and locally
auriferous, layers of iron formation (unit 9c) are found
within the turbidites of the Contwoyto Formation (Figure 5).
The main accumulation of felsic volcanic rocks (units 5 and
6) is also found within this turbidite sequence. Impure
siliceous carbonate (unit 7) occurs along the eastern
contact of these felsic volcanic units (Figure 5).

Contact relationships within the supracrustal succession
are often obscured by shearing along fault zones (mainly in
the volcanic and conglomerate units) and folding (mainly in

the turbidite units), but lateral interdigitation of all the supracrustal units is suggested (see also Henderson and Easton, 1977a, b).

Granite and pegmatite (units 11 and 12) intrude the supracrustal sequence and the basement gneisses. Small bodies that intrude the sillimanite-bearing metaturbidites of the Itchen Formation (see Frontispiece) were likely derived by partial melting of the sediments at depth (McKinnon, 1982). Diabase dikes of several ages are noted (Henderson and Easton, 1977a, b), the youngest form part of the Mackenzie Dike Swarm and intrude all units in the area.

1.4 History of Geological Exploration

At Keskarrah Bay, Stockwell (1933) recognized volcanics and a spectacular boulder conglomerate overlying what he suspected to be granitic basement. Subsequent reconnaissance surveys were carried out by Fraser (1964). During the summers of 1964 to 1966 Bostock mapped the Itchen Lake region at a scale of 1:250,000 and in a 1980 memoir established the formational nomenclature for the region.

Henderson and Easton (1977b) mapped the Keskarrah Bay area at a scale of 1:50,000, documented the unconformity, suspected by Stockwell, between the conglomerate and the granite body and outlined the main metamorphic and structural trends. In 1979 Indian and Northern Affairs Canada (INAC) initiated a 1:30,000 scale mapping program in

the Itchen Lake region. King (1981) studied the structure and metamorphism of the supracrustals in the eastern Point Lake area, and mapping associated with this study was completed in the western Point Lake area (Jackson, 1983, 1984). Easton et al. (1981) mapped the gneisses and granitoids ('Pointless' batholith) in the western Point Lake area (Figure 3).

Mineral exploration in the Itchen Lake region began in 1957. The Canadian Nickel Company Limited discovered gold in iron formation contained within metasediments at Contwoyto Lake (Figure 3) in 1961. This property now belongs to Echo Bay (the Lupin mine). In 1975 Texasgulf Inc. (now Kidd Creek Mines) discovered a base metal deposit at Izok Lake (Figure 3) in quartzofeldspathic gneisses of probable volcanic origin. Giant Yellowknife Mines has recently explored the gold potential of the metasediments southwest of the north arm of Point Lake ('Tree' claims). Lhotka and Nesbitt (1989) examined the geological setting and petrological characteristics of iron formation in the Contwoyto Lake-Point Lake region.

1.5 Aims of this Study

Much information is available on the stratigraphy and petrology of the lithologic units in the Keskarrah Bay area (section 1.3). In this thesis the metamorphic history and

structural characteristics of the area are documented, with emphasis on the supracrustal rocks.

The extensive metagreywacke-mudstone turbidites of the Yellowknife Supergroup in the Keskarrah Bay area exhibit a variation in metamorphic grade and provide an ideal suite for the investigation of metamorphic reactions and estimation of crustal conditions presented in this study. The presence of iron formation within these turbiditic rocks allows an examination of the influence of bulk composition on the resultant mineral assemblages. The mineral assemblages developed in the metabasites provide additional constraints on the conditions of metamorphism in the Keskarrah Bay area.

The metamorphic gradients previously outlined by Henderson and Easton (1977b) indicate both an eastward and westward increase in grade. The eastward rise in metamorphic grade continues through into the eastern Point Lake area (King, 1981), so investigations in this study permit correlation with the eastern area. The noted westward metamorphic gradient toward the area underlain by the basement gneiss complex poses several questions: 1) is the western gradient temporally related to the eastern regional gradient and if so what is the nature of the intervening metamorphic depression? 2) if the western gradient is unrelated to the eastern one, why does it increase toward a basement terrane? and 3) does the basement terrane contain evidence of this metamorphism?

Furthermore the Keskarrah Bay area provides an opportunity to study the effects of deformation on a basement-cover sequence within the Slave Province. The presence of gneissic basement blocks to the Yellowknife Supergroup allows the following questions to be addressed: 1) did the presence of a basement block exert an influence on the style of deformation or orientation of structural elements within the supracrustals? and 2) did the deformational events that affected the supracrustals leave a structural signature in the basement gneisses?

1.6 Methods of Study and Data Collection

Float equipped aircraft chartered from Yellowknife provide the easiest access to Point Lake, although canoe travel is possible. Ice break-up at Point Lake is usually sufficiently advanced by the first or second week in July to allow access. At Itchen Lake it is slightly later. The field season is limited by deteriorating weather conditions in mid-late August, during which time snow squalls may begin.

Geological mapping was carried-out in the Keskarrah Bay area during the summers of 1981 and 1982, with a total of about 15 weeks spent in the field. Mapping was completed by a two-person traversing team, with the deHavilland Beaver aircraft chartered by INAC providing logistical back-up.

The map of Henderson and Easton (1977b) was used as a basis for the choice of study area and location of traverses. The geological map (Figure 5) incorporates much of their data together with the results of this study. Traversing was planned around four main points of interest: 1) to examine the stratigraphy defined by Henderson and Easton (1977a, b); 2) to document metamorphic conditions and further delineate major isograds; 3) to define the main structural elements; and 4) to explore the possibility of correlating the metamorphic and structural characteristics of the Keskarrah Bay area with those of the surrounding areas in order to suggest a regional tectonic setting.

All major lithologies were sampled and examined in thin section. Sampling of the turbiditic units was undertaken from a metamorphic and structural viewpoint, so the samples contained representative and, if possible, a maximum number of metamorphic mineral phases and displayed the main fabric elements.

2.0 METAMORPHISM

2.1 Introduction

Regional metamorphism of the Yellowknife Supergroup
rocks in the Keskarrah Bay area is documented largely on the
basis of metamorphic mineral assemblages observed within the
metaturbidites of the Contwoyto and Itchen Formations (units
9 and 10). The sequential development of the key metamorphic
index minerals biotite, cordierite, andalusite and
sillimanite defines the four respective isograds which have
been mapped in the field and are shown in Figure 6. The
isograds outline five metamorphic zones, corresponding to
the index minerals previously listed, with the addition of
the chlorite zone at lowest grades. Identification of the
metamorphic reactions leading to the formation of the index
minerals allows redefinition of the isograds into reaction
isograds.

The metamorphic grade in the area thus ranges from
low-grade (greenschist facies) to medium-grade (middle
amphibolite facies), and the observed paragenetic sequence
indicates that low pressure-type metamorphism prevailed, as
documented elsewhere in the Slave Province (Thompson, 1978;
Bostock, 1980; King, 1981). The distribution of metamorphic
isograds (Figure 6) determined for the turbidite units
indicates an increase in grade to both the east and west
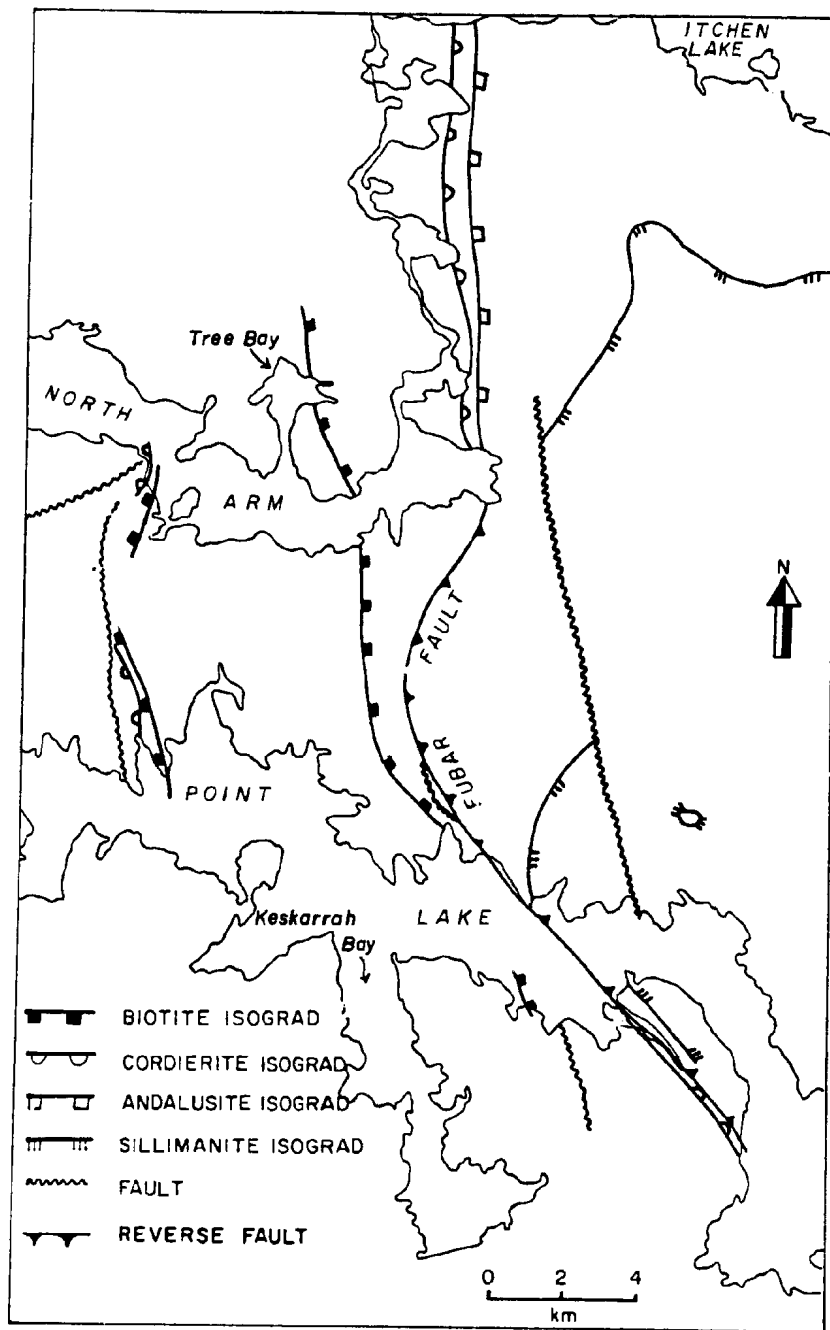
Figure 6: Metamorphic isograds of the Keskarrah Bay area defined for greywacke compositions. Symbols are on the high-T side of isograds.

LEGEND:
- BIOTITE ISOGRAD
- CORDIERITE ISOGRAD
- ANDALUSITE ISOGRAD
- SILLIMANITE ISOGRAD
- FAULT
- REVERSE FAULT

from a low centered about the Keskarrah Formation
conglomerate (unit 8).

The eastern prograde metamorphic sequence consists of
all five metamorphic zones, however it is evident that these
zones have , in part, been telescoped by the Fubar fault
(eg. andalusite zone rocks are displaced against those of
the biotite zone). Only the first three zones are recognized
in the western sequence. The western sequence also shows
evidence of a retrograde event, locally accompanied by
shearing, that resulted in the complete replacement of
cordierite porphyroblasts by sericite and chlorite and the
alteration of biotite to chlorite. Even in the rocks that
show the least evidence of retrogression, it is apparent
that mineral chemistry has been altered and thus the
documentation of prograde regional metamorphism in the
Keskarrah Bay area is necessarily based on data from the
eastern metamorphic sequence. Although data from the western
sequence are presented they cannot be used to depict trends
in mineral chemistry as a result of increasing metamorphic
grade, nor can they provide a basis for the inference of
prograde metamorphic reactions.

2.2 Methods

Locations of the metamorphic isograds were approximated
in the field on the basis of the locations of index
minerals, and reaction isograds were defined through

petrographic study. The nature of the index mineral-forming reactions and changes in mineralogical compositions with metamorphic grade were determined from electron microprobe analyses of participating mineral species. Limited X-ray diffraction analysis of samples from the eastern belt of low-grade Contwoyto Formation established the relative degree of low-grade metamorphism. Thin sections of the turbidite rocks from all metamorphic grades were stained to determine the presence and relative abundance of K-feldspar. Whole rock geochemistry was carried out on several samples of metasediments from both low and medium grades of metamorphism. Laboratory methods involved in most of the analytical techniques are given in the appendices. Microprobe work on such fine grained rocks was difficult, and this is reflected in the quality of some of the analyses. Average mineral compositions for samples analysed from each metamorphic zone are tabulated in Appendix A, which also contains a location map for all samples analysed by the various methods. Additional analyses are given in Appendix B.

Metamorphism of volcanic and associated carbonate rocks of the Point Lake Formation and conglomerate of the Keskarrah Formation is documented mainly through petrographic observations with limited microprobe analyses.

2.3 Bulk Composition of Metaturbiditic Rocks

The formation of a paragenetic sequence developed during progressive regional metamorphism is dependent on the bulk composition of the rocks in question. In particular, variations in bulk composition may play a crucial role in the documentation of continuous reactions.

In the turbidite succession, the subtle compositional differences between greywacke and mudstone in a graded sequence are reflected in contrasting metamorphic mineral assemblage and microstructural development. Variations in the relative abundances of the mineral constituents in the greywackes considered in this study reflect subtle compositional differences. For instance, the lack of muscovite in some of the medium-grade rocks probably reflects less potassic compositions than in the muscovite-bearing equivalents.

A more drastic compositional difference is observed between the greywackes and iron formation (unit 9c). The bulk composition of the iron-rich sediments is reflected in the metamorphic mineral assemblages and mineral compositions, most particularly in the common occurrence of garnet which is conspicuously absent in the greywackes.

Five samples, including different portions of a graded bed, were analysed to determine their whole-rock geochemistry. The sample population should be larger in order to present conclusive results. However, since the bulk

composition can also be determined on the basis of mineral assemblage, these analyses are included for illustrative purposes. The analyses (Table 1) are comparable to others from the Contwoyto and Itchen Formations in the Keskarrah Bay area (Easton, unpublished data; McKinnon, 1982), with the exception that $Na_2O:K_2O$ ratios are anomalously and inexplicably low (elevated K_2O contents). However, when plotted on an AKF diagram (Figure 7) their positions are consistent with respect to the observed mineralogies (i.e. chlorite and muscovite at low grades). The bulk rock analyses have also been plotted on an AFM diagram (Figure 7). However, in this case the compositional range is inconsistent with the observed mineralogies (i.e. biotite-cordierite-bearing samples fall outside the biotite-cordierite field). Phase considerations, particularly that the assemblage chlorite-biotite is superseded by that of cordierite-biotite (see below), suggest that a more Mg-rich Al-poor bulk composition (below the field of chlorite compositions and within the cordierite-biotite field; x on Figure 7) is more likely.

2.4 Metamorphic Zones

2.4.1 Chlorite Zone (CHZ)

Metagreywackes and mudstones of the Contwoyto Formation that outcrop adjacent to the Point Lake Formation mafic flows (unit 4) and Keskarrah Formation conglomerate (unit 8)

TABLE 1: Whole-rock Geochemistry of Metaturbiditic Rocks

	1a	1b	1c	2	3
SiO_2	72.10	62.10	57.80	58.10	59.90
TiO_2	0.44	0.63	0.72	0.62	0.54
Al_2O_3	13.10	17.90	18.90	19.00	17.90
FeO	3.66	5.21	6.40	5.89	6.53
Fe_2O_3	0.95	0.93	1.45	1.56	0.63
MnO	0.06	0.08	0.10	0.09	0.05
MgO	2.10	3.19	3.52	3.72	3.50
CaO	1.35	0.36	0.93	0.48	0.27
Na_2O	2.00	0.49	1.21	1.88	1.24
K_2O	2.54	4.15	4.02	3.53	3.96
P_2O_5	0.06	0.04	0.04	0.13	0.16
LOI	2.17	4.14	4.39	4.57	3.59
TOTAL	100.53	99.22	99.48	99.57	98.27

1a, 1b, 1c: sample 81-V-373 from the western biotite zone of the Contwoyto Formation; coarse, medium and fine-grained fractions of a graded bed.
2: sample 81-V-451a from the eastern chlorite zone of the Contwoyto Formation.
3: sample 81-V-450b from the andalusite zone of the Contwoyto Formation.

Figure 7: AKF plot and AFM projection showing whole-rock compositions of metaturbidites (see Table 1) from the Keskarrah Bay area (solid rectangles). Dotted line outlines compositional field of other Slave Province metagreywackes and metapelites presented in Thompson (1978). Rock composition referred to throughout the text is denoted by (x); this composition is consistent with observed mineral assemblages.

Note: for all AKF plots

$A = (Al_2O_3) - ((Na_2O) + (K_2O) + (CaO))$

$K = (K_2O)$

$F = (FeO) + (MgO) + (MnO)$

for all AFM plots

$A = (Al_2O_3) - 3(K_2O)/(Al_2O_3) - 3(K_2O) + (FeO) + (MgO)$

$F, M = M/FM = MgO/(MgO + FeO)$

$() = $ weight % oxide/molecular weight of oxide

field of
Muscovite
compositions

field of
Chlorite
compositions

field of
Cordierite
compositions

field of
Biotite
compositions

M/FM

+ quartz, muscovite and
plagioclase

M/FM

M/FM
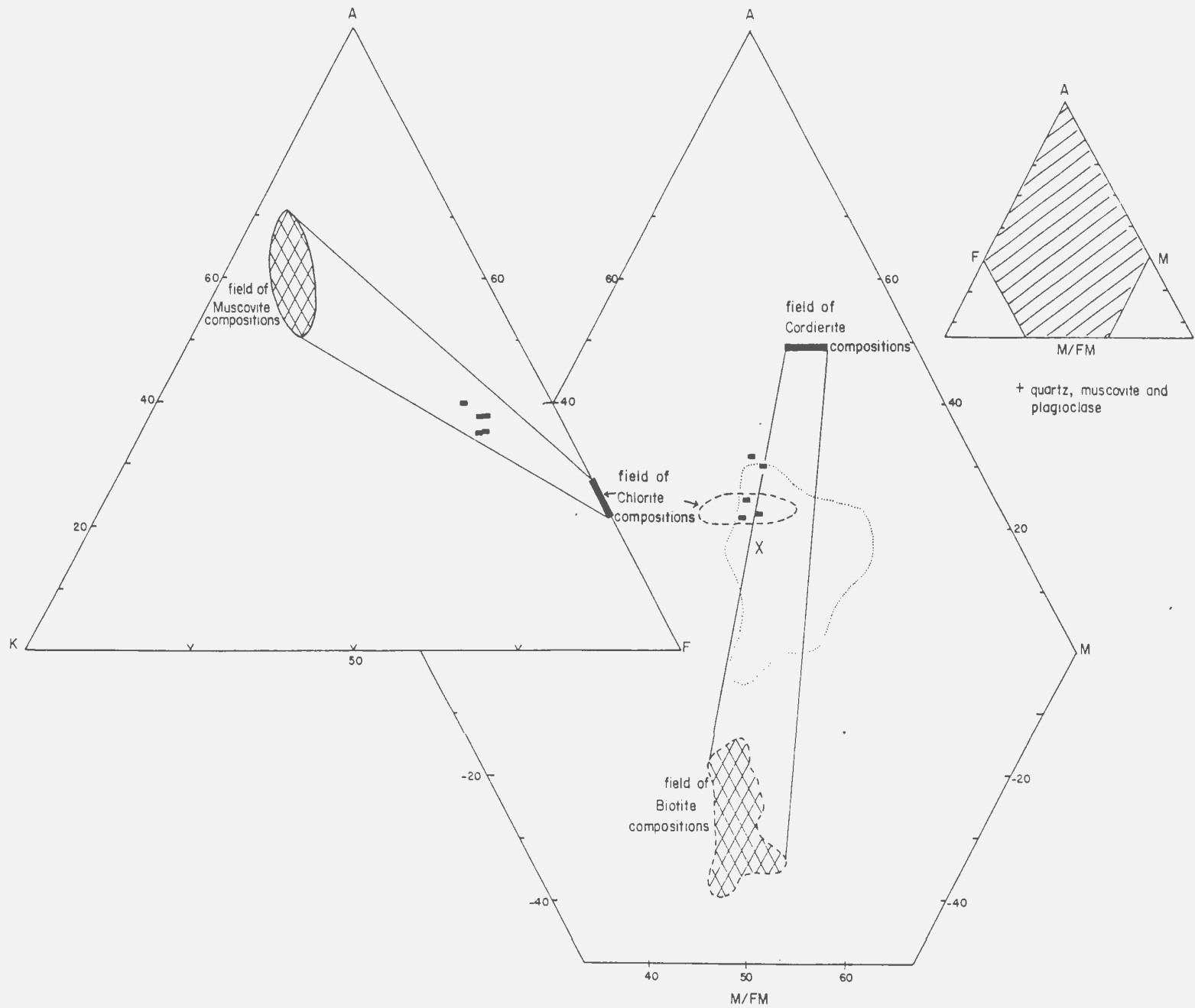
record the lowest metamorphic grades observed in the turbidite units (Figure 6).

Below the biotite isograd greywackes contain abundant relict sedimentary features. Throughout much of the eastern chlorite zone (ECHZ) and parts of the western CHZ (WCHZ) detrital quartz and plagioclase (albite) grains remain unrecrystallized (Figure 8) and the rocks contain a variably developed disjunctive cleavage (Powell, 1979). However WCHZ rocks also contain textures indicative of extensive recrystallization and locally have a schistose microstructure (Figure 9) suggesting that these rocks have been more highly strained than those in ECHZ.

The matrix of the CHZ greywackes is predominantly composed of chlorite, muscovite and recrystallized quartzofeldspathic material. Detrital plagioclase grains are often crowded with sericite flakes, suggesting that some of the micas were in part derived from the breakdown of plagioclase. Muscovite and chlorite tend to be finer grained throughout the ECHZ (in many samples they are < 0.06 mm long) than in the WCHZ (grain lengths of 0.30-0.10 mm are common). However, there is considerable overlap in the grainsize of these minerals. The modal proportions of muscovite and chlorite are variable, although these are fine-grained rocks and abundances are difficult to determine. Opaque phases, present in amounts of up to 5%, typically consist of ilmenite, sulfides (pyrite, pyrrhotite and lesser chalcopyrite) and minor hematite.

Figure 8: Photomicrograph of metagreywacke from the eastern CHZ. Plane light. Detrital quartz and albite retain angular shapes of clastic grains. Weak fabric oriented east – west. Length of section shown approximately 3.4 mm.

Figure 9: Photomicrograph of metagreywacke from western CHZ. Note preferred alignment of quartz clasts, development of quartz-mica beards (indicative of pressure solution processes) and strong schistosity in comparison to greywacke of Figure 8. Plane light. Length of section shown approximately 3.4 mm.
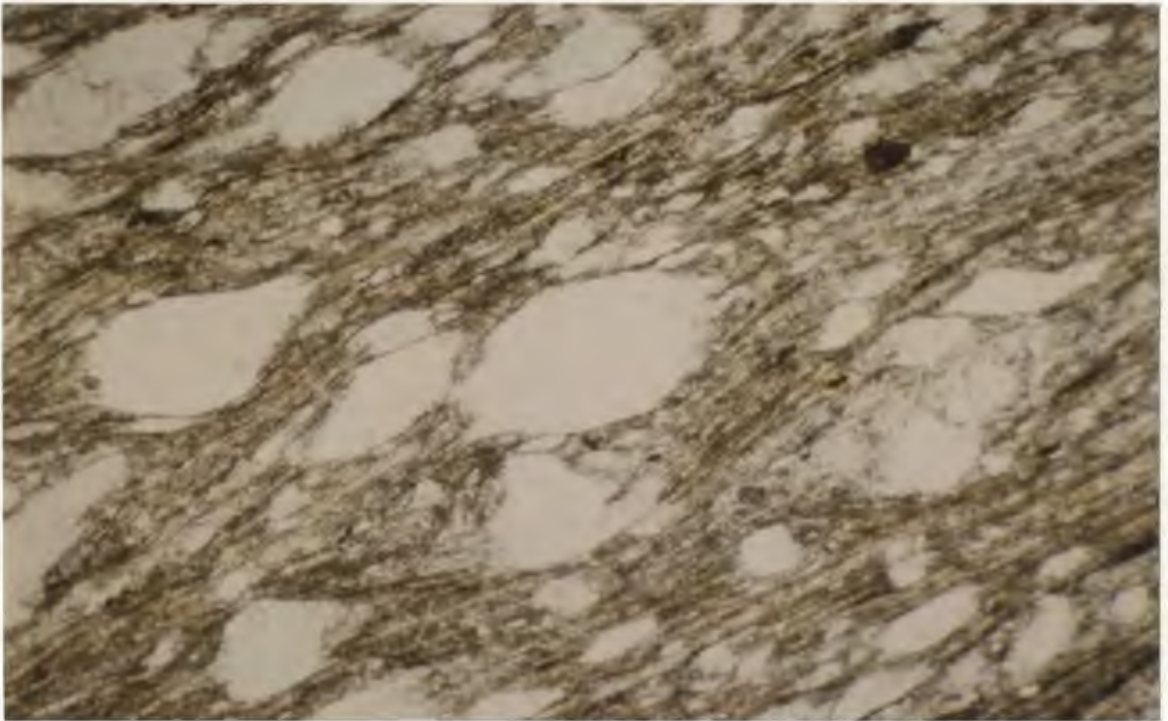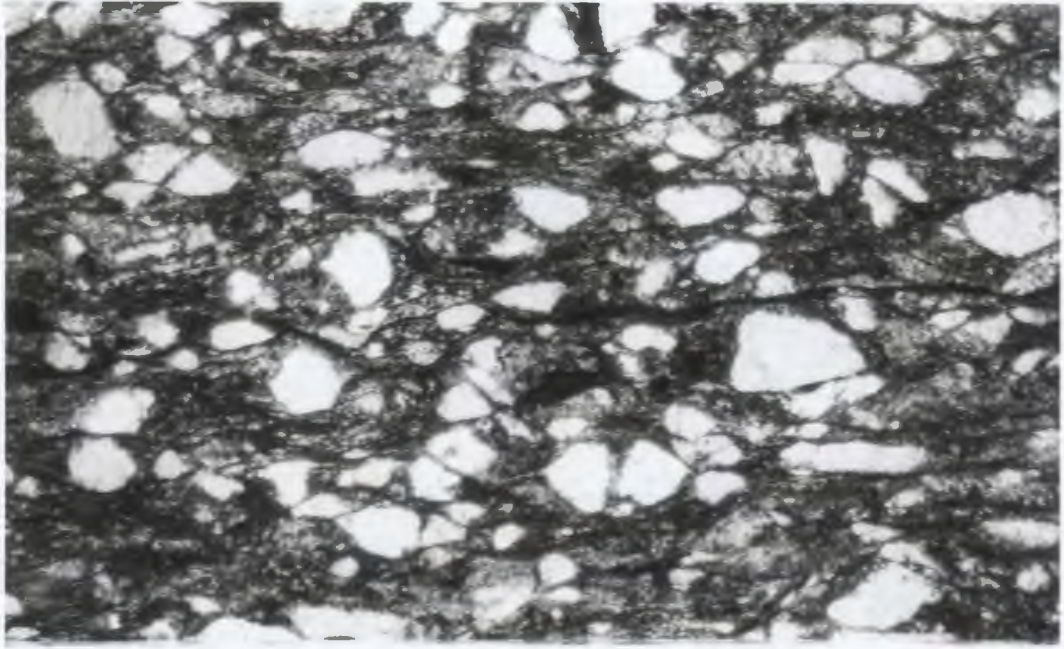
In thin section chlorites exhibit pale green to colorless pleochroism with anomalous birefringent colors ranging from khaki (k-chlorite) to blue or purple (b-chlorite; note that the use of the terms k- and b-chlorite is strictly informal). Differing chlorite compositions are suggested by the range in birefringent colors, however all analysed chlorites fall in the compositional field of ripidolite (Hey, 1954). In many of the samples there is no microtextural distinction between the two chlorites, but in the WCHZ there is some microstructural evidence indicating that the formation of b-chlorite post-dated k-chlorite, and that b-chlorite is retrograde in origin. Muscovites range in texture from fine-grained sericitic aggregates intergrown with chlorite, to distinct crystals and rare porphyroblasts that overgrow the finer grained matrix phyllosilicates.

The characteristic sub-assemblage typical of the CHZ is muscovite-chlorite; observed assemblages are listed in Table 2. In AKF space (Figure 10) the CHZ rocks are represented by the two-phase assemblage chlorite-muscovite. Chlorites have a very limited range of composition in this diagram, whereas coexisting muscovites are more variable, presumably due to variations in celadonite content. Muscovite-chlorite tie lines generally do not cross and the lateral shift in tie lines thus reflects variations in bulk rock compositions. X-ray diffraction analyses of the lowest grade rocks within the ECHZ showed that neither pyrophyllite

TABLE 2: Mineral Assemblages of the Metagreywackes

Metamorphic Zone	Musc	Chl	Bio	Cord	And	Sill	Qtz	Plag	Rf	Op	Cc	Sp	To	Ap	Zir
CHZ	X	Xx	-	-	-	-	Xd	Xd	Xx	xa	xa	ad	ad	a	a
BZ	Xx	Xx	Xx	-	-	-	Xd	Xd	x	xa	xa	ad	ad	a	a
CZ	X	-r	X	X	-	-	X	X	-	xa	-	a	a	a	a
AZ	Xx	-r	X	X-	X	-	X	X	-	xa	-	a	a	a	a
A*Z	pr	-r	X	Xx-	X	-	X	X	-	xa	-	a	a	a	a
SZ	Xx	-r	X	Xx-	Xx-	Xx	X	X	-	xa	-	a	a	a	a
S*Z	pr	-r	X	Xx-	Xx-	Xx	X	X	-	xa	-	a	a	a	a

X = major component
x = minor component
- = mineral not present

a = accessory phase
d = detrital phase
r = retrograde phase

p = post-tectonic phase

This is a summary table compiled from many petrographic observations. Where more than one symbol is present, it refers to different samples.
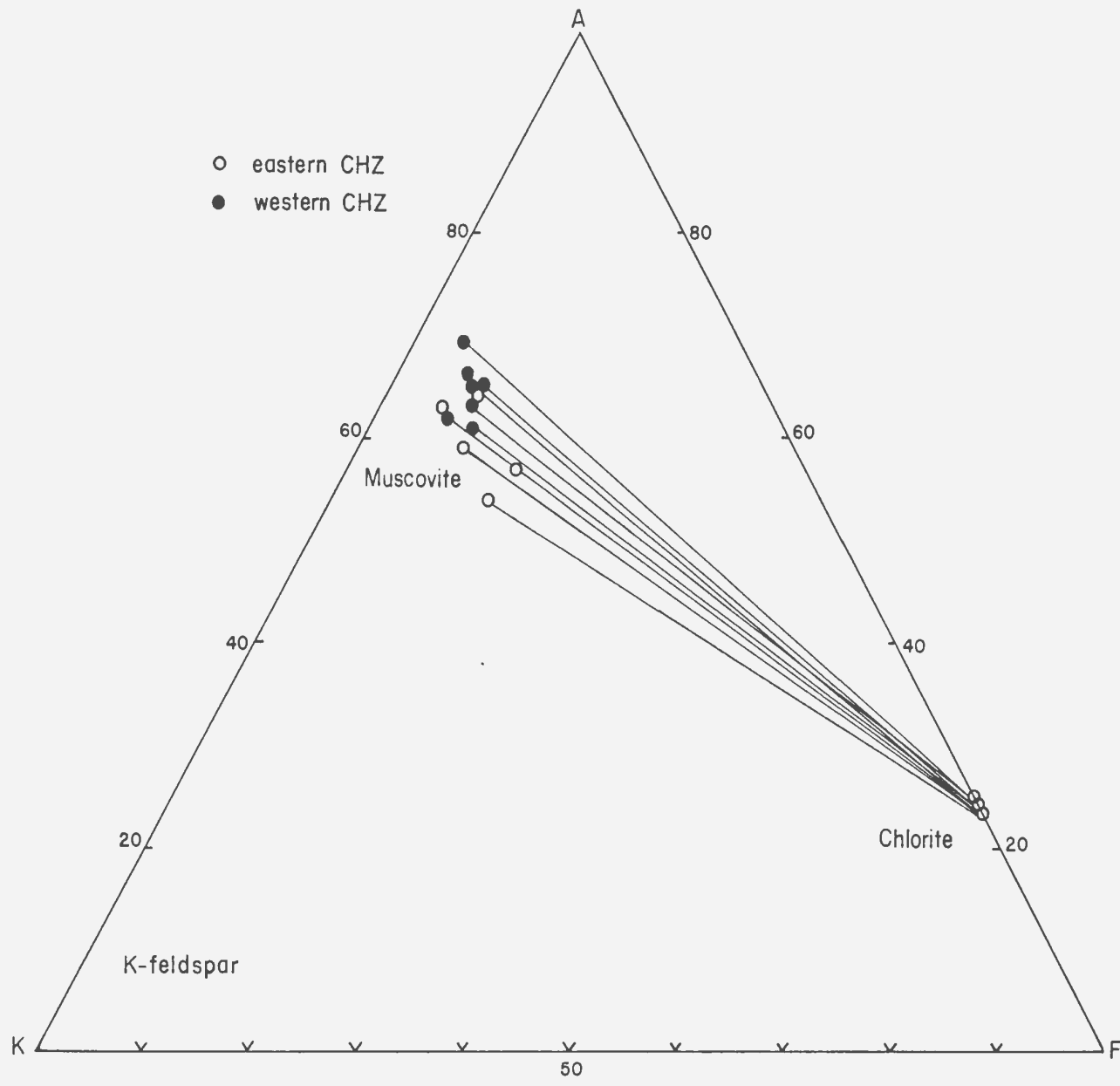
Figure IO : AKF plot of the mineral assemblage   chlorite-muscovite from both eastern and western CHZ's.

nor paragonite are present in sufficient amounts to be determined and that all phyllosilicates are highly crystalline (Appendix C).

Table A.5 lists the average chemical compositions of chlorite, muscovite and plagioclase from both the eastern and western CHZ's. Most plagioclase analyses and optical determinations from both relict and recrystallized grains fall in the albite compositional range (An 0.2- 10), with a single analysis falling in the andesine range. The two sets of chlorite analyses from the eastern zone have similar chemical compositions (M/FM = .46); whereas chlorites from the western zone have variable Fe and Mg contents (.66 > M/FM > .41). In principle this could be due to: a) variations in bulk rock composition; b) variations in metamorphic conditions; or c) alteration of the mineral chemistry due to retrograde metamorphism (see above). To ascertain the influence of point (c) the chlorite analyses have been arranged according to the degree of visible retrograde metamorphism in Table A.5 (samples 105 and 392a being visually fresh, and samples 395 and 223 being the most altered). K-chlorite (see above) is the only chlorite present in the fresh samples, whereas altered samples contain in addition abundant b-chlorite and the remaining samples contain only minor b-chlorite. In comparing the two extreme groups of analyses it can be seen that where k-chlorite is the only chlorite present, the M/FM ratio is higher (.656 to .594) than for those in which b-chlorite is

abundant (.411 to .456). These observations suggest
retrograde metamorphism may be the main factor governing the
M/FM ratios of the WCHZ chlorites, and examination of Table
A.5 shows that the reduction of M/FM ratio is due to both Mg
loss and Fe gain within altered chlorites.

The composition of WCHZ muscovites also shows a
relationship to the extent of visual retrograde
metamorphism; muscovites from samples (105 and 392a) showing
no visible evidence of retrogression have higher M/FM ratios
(.682 and .675) than those from altered samples (395 and
223) which have M/FM muscovite in the range .433 and .502.
In this case the lower M/FM values of the latter are due to
Fe-enrichment rather than Mg-depletion (Table A.5).

Paragonite contents (Na/Na+K) of the muscovites range
from 4 to 11% and celadonite (Tschermak's substitution, see
2.5.5) contents are low. Following the works of Velde (1965)
and Guidotti and Sassi (1976), the higher and more variable
celadonite contents of muscovites from the ECHZ, suggests
that rocks of the ECHZ are of lower grade than those of the
western zone.

2.4.2 Biotite Zone (BZ)

The first appearance of biotite in rocks of greywacke
compositions delineates the biotite isograd and marks the
boundary between the biotite zone (BZ) and lower grade CHZ
(Figure 6). However, biotite is found locally in iron
formation within the CHZ, below the biotite isograd as

defined for greywackes. The formation of biotite during low-grade metamorphism is known to be dependent on the bulk rock composition and has been previously recorded as forming first in Fe-rich compositions, then in greywackes and subsequently in more aluminous pelitic compositions (Mather, 1970).

In AKF space (Figure 11) BZ rocks are represented by the three-phase assemblage chlorite-muscovite-biotite. Crossing tie lines likely reflect variations in the composition of muscovite. The AFM diagram (Figure 12) is projected through muscovite of ideal composition (Thompson, 1957), such that in this topology BZ rocks are represented by the two-phase assemblage chlorite-biotite. From the M/FM ratios of chlorite-biotite pairs, it can be seen that chlorite is as Mg-rich or Mg-richer than coexisting biotite, consistent with the expected element partitioning.

The western biotite isograd is well defined, at least along it's northern boundary. However the extent of retrogression during shearing of these rocks, a factor which is considered to be particularly important for the southern part of the zone, has not been ascertained. Definition of the eastern biotite isograd is hampered by a combination of poor exposure, faulting and associated alteration, and by the presence of units of iron-rich and carbonate-rich compositions. BZ rocks on the peninsula near Tree Bay (Figure 6) may represent slightly more Fe-rich greywacke
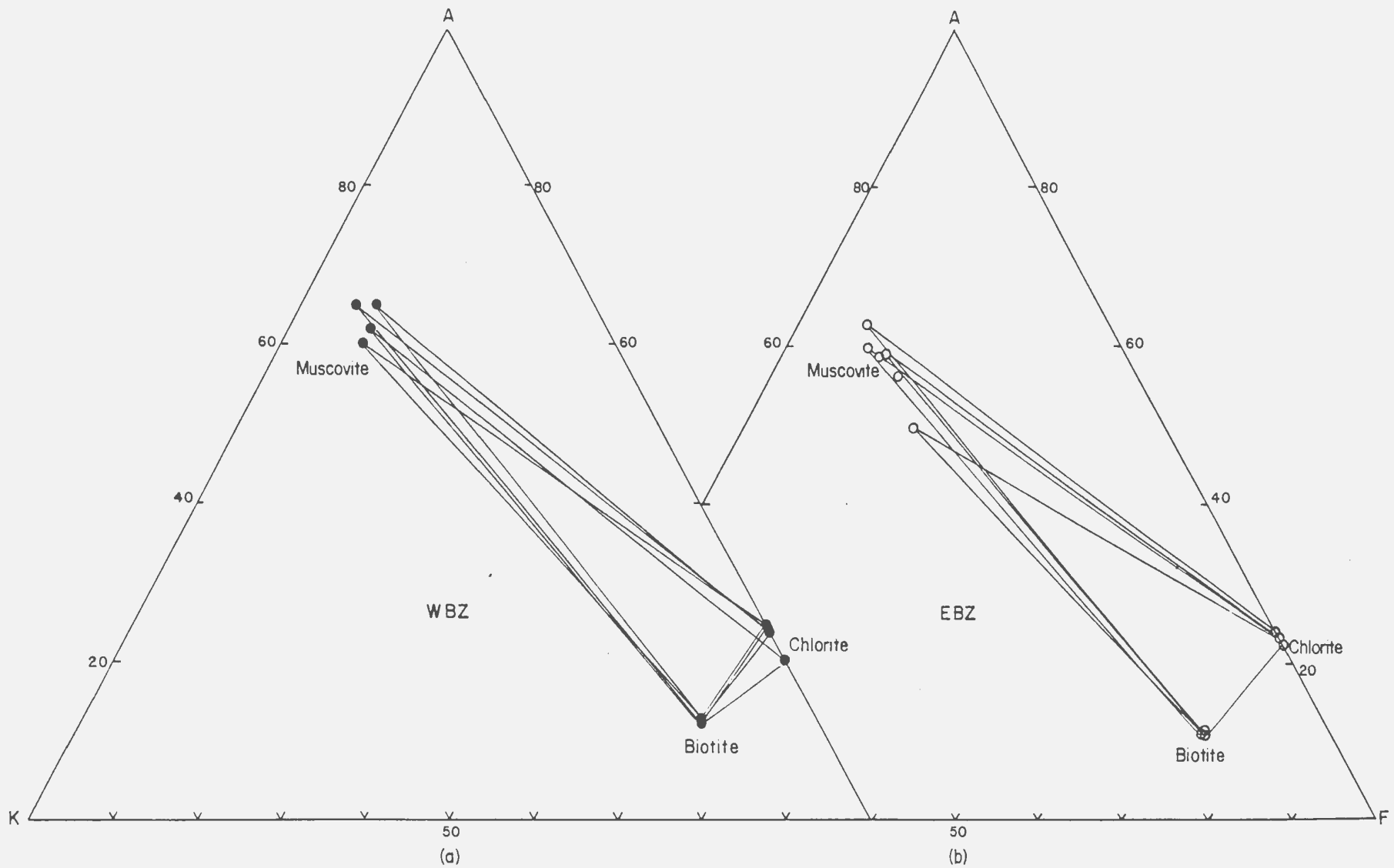
Figure II : AKF plot of the three-phase BZ mineral assemblage chlorite - muscovite - biotite for both the western (a) and eastern (b) zones.
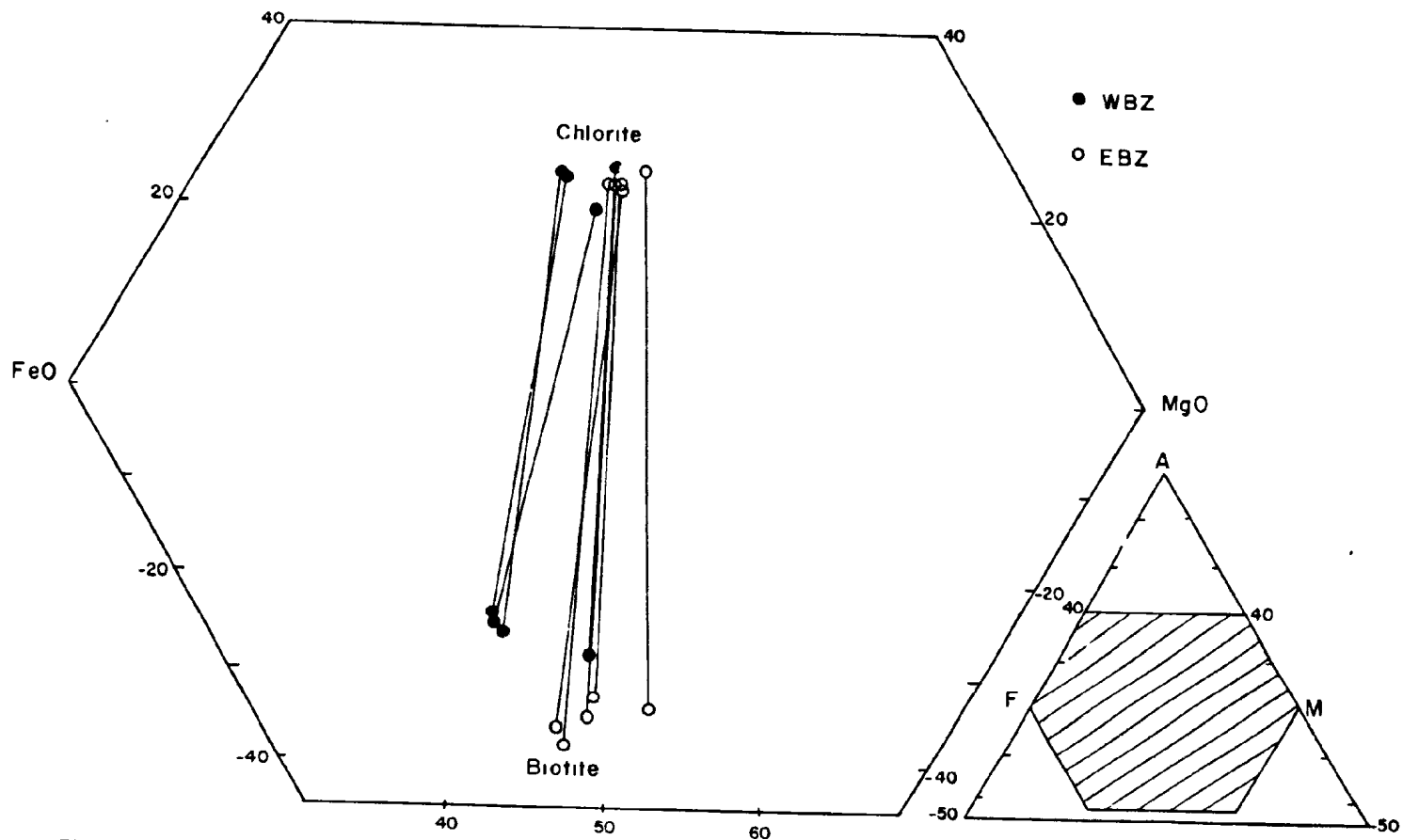
Figure 12 : A portion of the AFM diagram showing the two-phase BZ mineral assemblage biotite - chlorite for both the eastern (open circles) and western (solid circles) zones. Inset diagram shows the portion of the AFM diagram used for plotting.

compositions, as iron formation and disseminated magnetite are abundant in this area.

Throughout the low-grade rocks biotite is first observed microscopically as minute flakes intergrown with aligned muscovite and chlorite. Biotite shows no consistent spatial association with disseminated opaque minerals (ilmenite, sulfides, minor hematite and rutile), but in some samples biotite has formed in areas once occupied by opaque - mica pressure solution seams that form the disjunctive cleavage in CHZ rocks. Biotite may also form aggregates with no apparent preferred alignment. Within the phyllitic to schistose rocks of the WBZ, detrital quartz and plagioclase (oligoclase) grains tend to be more recrystallized (Figure 13) than in the CHZ and EBZ, although apparently unrecrystallized plagioclase (albite) grains can be observed.

In the BZ, as in the CHZ, the modal abundance of phyllosilicates is variable; however there is a lower relative abundance of chlorite (most notable in the WBZ). A lightening in color of the BZ rocks reflects the increase in modal abundance of micas and coincides with a general coarsening of grain size.

Within the EBZ, near the Fubar fault (Figure 6), the metasediments contain biotite poikiloblasts (Figure 14). The poikiloblasts are subidioblastic to xenoblastic and oriented at high angles to the S_2 schistosity (defined by the planar alignment of biotite, muscovite and chlorite).

Figure 13: Photomicrograph of metagreywacke from the western BZ. Note recrystallization of quartz clasts. Top, plane light. Bottom crossed nicols. Length of sections shown approximately 5.0 mm.
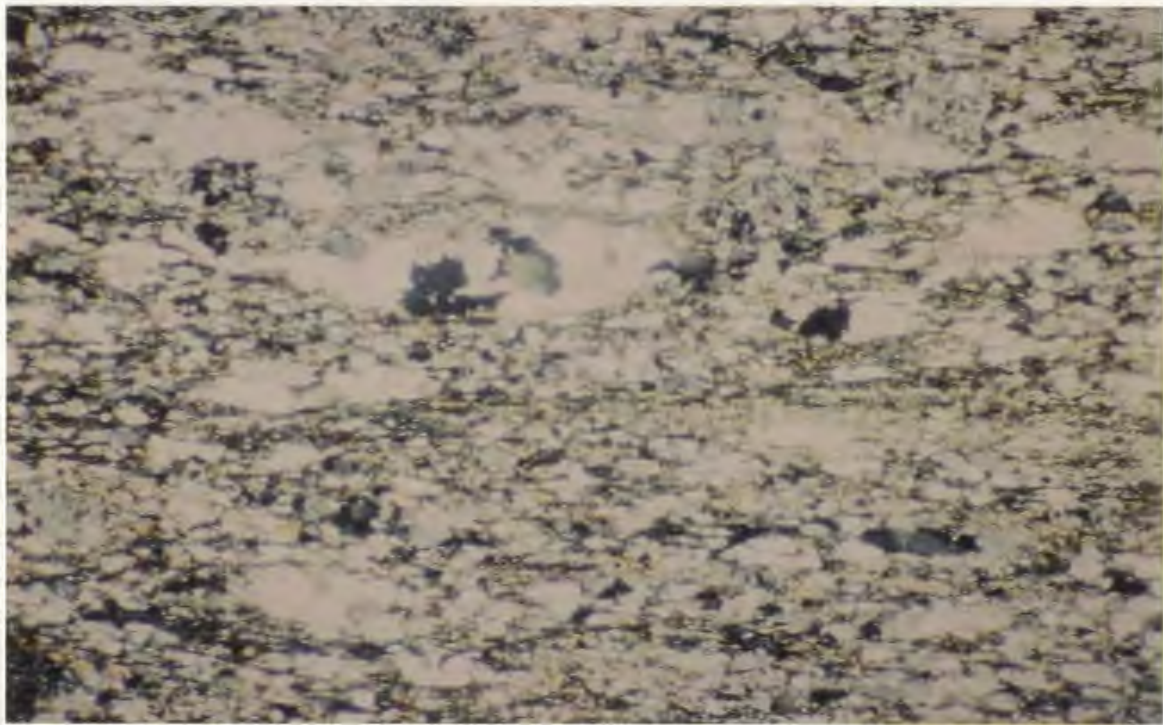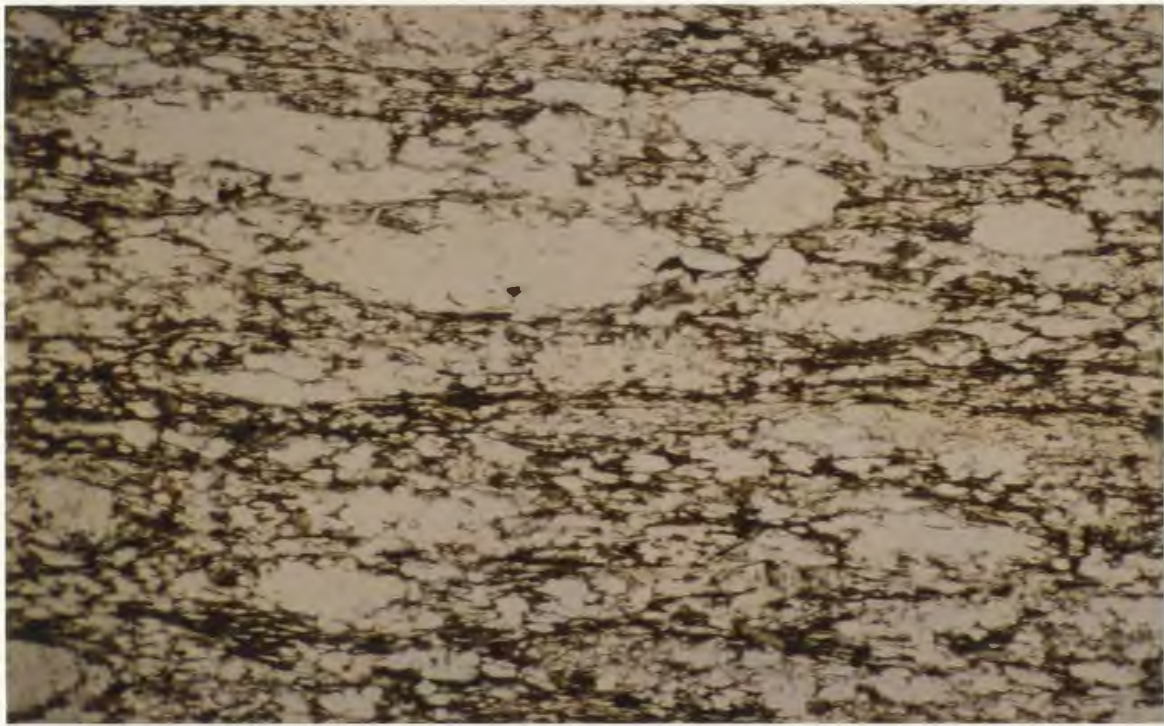
Figure 14: Photomicrograph of biotite porphyroblasts from an
eastern BZ metaturbidite. Note alignment of
porphyroblasts at a high angle to matrix fabric
(S_2). Plane light. Width of section shown
approximately 0.6 mm.

Microstructural relations of biotite porphyroblasts are discussed more fully in section 3.2.3. The BZ phyllites become schistose approximately coincident with the formation of biotite poikiloblasts.

Representative BZ mineral assemblages are listed in Table 2 and average chemical analyses of biotite, muscovite, chlorite and plagioclase in BZ are presented in Table A.6. Plagioclase compositions fall into two groups, An 1-10 and An 20-45, corresponding to albite and oligoclase-andesine, respectively.

WBZ rocks show microscopic evidence of retrograde metamorphism similar to rocks in the WCHZ. However, with an increase in the visual extent of retrograde metamorphism in these BZ rocks, the change in M/FM ratios of muscovite and chlorite is directly opposite to that for CHZ. This may imply that a different exchange reaction took place involving another phase, presumably biotite. Samples which contain no visible evidence of retrograde metamorphism and contain only k-chlorite (eg. sample 398) have the lowest M/FM ratio. In comparison, those which contain mainly retrograde b-chlorite (eg. sample 373) have appreciably higher M/FM ratios (Mg-enriched and Fe-depleted). Biotite compositions do not show this same relationship and appear to be independent of the visually determined extent of retrogression, perhaps because biotite is more abundant than either chlorite or muscovite. Variations in the composition

of muscovite, chlorite and biotite from the EBZ likely
result from differing rock compositions.

Average muscovites from both BZs differ little in
paragonite and celadonite contents from those in CHZ.
However, muscovites from the EBZ have higher and more
variable celadonite contents than WBZ muscovites.

Chlorite and biotite from the WBZ are generally more
Fe-rich (lower M/FM ratios) than those from the east.

2.4.3 Cordierite Zone (CZ)

The first appearance of cordierite, delineated by the
cordierite isograd (Figure 6), marks the onset of medium-
grade metamorphism (Winkler, 1976). Cordierite zone (CZ)
rocks outcrop in both eastern and western belts of the
Contwoyto Formation. However, western CZ rocks are
extensively altered, containing completely sericitized and
pinnitized cordierites. The description of the CZ that
follows is therefore based on observations within the
eastern sequence. Location of the eastern cordierite isograd
is made difficult by the lack of exposure in northern areas
and the presence of a felsic volcanic center through which
the cordierite isograd cannot be defined because of
inappropriate bulk composition. As indicated on Figure 6,
the narrow belt of CZ rocks cannot be traced along its
strike through the central part of the map area, where
post-metamorphic movement along the Fubar fault may have
partly removed the surface expression of the CZ.

The mineral assemblages found within the CZ are listed in Table 2. In AKF space CZ rocks are represented by the three-phase assemblage cordierite-biotite-muscovite (Figure 15) and muscovite compositions are seen to be more restricted in comparison to BZ rocks (Figure 13). The two-phase sub-assemblage cordierite-biotite characterizes the CZ in AFM space (Figure 15).

Distinguishing features of the CZ, apart from the diagnostic presence of cordierite porphyroblasts are: 1) the complete lack of chlorite in the equilibrium assemblage; 2) the overall coarser grain size of the matrix constituents (muscovite, biotite, quartz) with respect to the BZ equivalents; 3) the complete recrystallization of detrital quartz and plagioclase grains; 4) the increased abundance and grain size of accessory tourmaline; and 5) the visual increase in modal abundance of biotite and possibly muscovite.

In thin section cordierite commonly forms irregular poikiloblasts incorporating matrix constituents such as recrystallized quartz grains, muscovite, biotite and ilmenite. However, many cordierite porphyroblasts either lack, or contain appreciably less biotite than the matrix (Figure 16 a,b). Figure 16b shows a cordierite porphyroblast that has overgrown a biotite-rich layer, but only trace amounts of biotite are present within the cordierite. The trace of bedding is faintly visible within the cordierite, marked by a band containing slightly more opaques than the
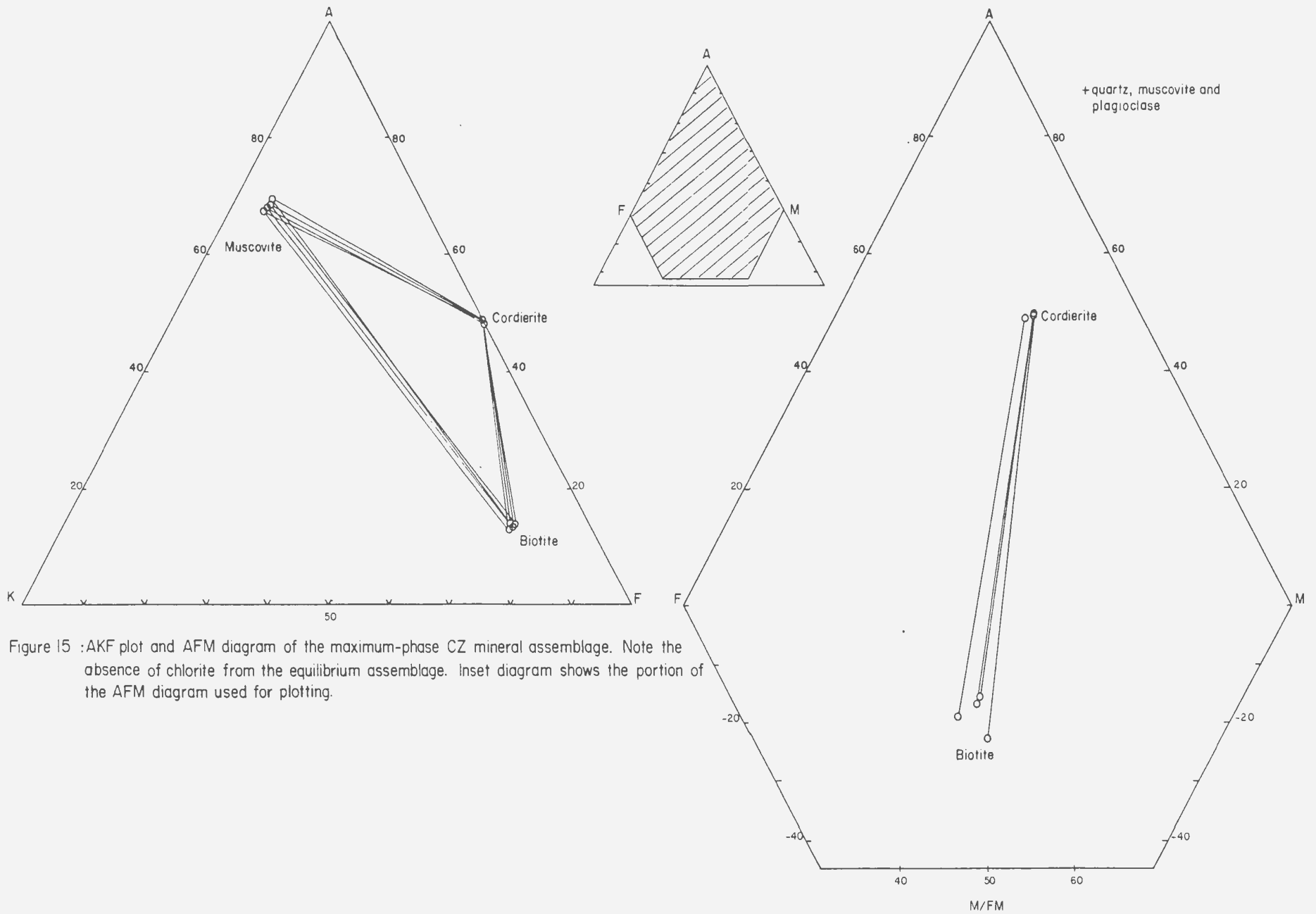
Figure 15 : AKF plot and AFM diagram of the maximum-phase CZ mineral assemblage. Note the absence of chlorite from the equilibrium assemblage. Inset diagram shows the portion of the AFM diagram used for plotting.

Figure 16: A; Photomicrograph of part of a cordierite

porphyroblast and its relationship to the

schistosity. Plane light. Length of section shown

approximately 3.4 mm.

B; Sketch from a thin section showing cordierite

porphyroblasts that have overgrown biotite-rich

layers.

A.

B

Cord

Cord

biotite-rich
layer

Cord

hematite-rich
seams

fracture
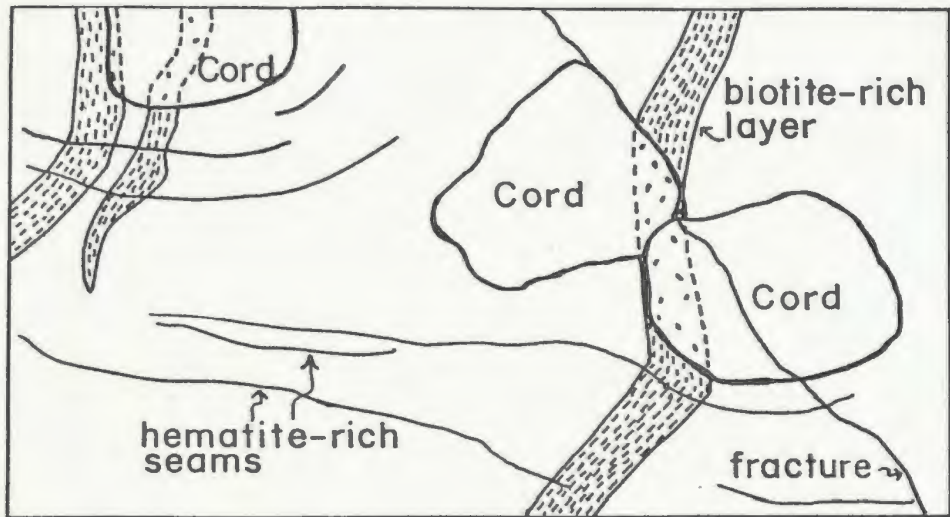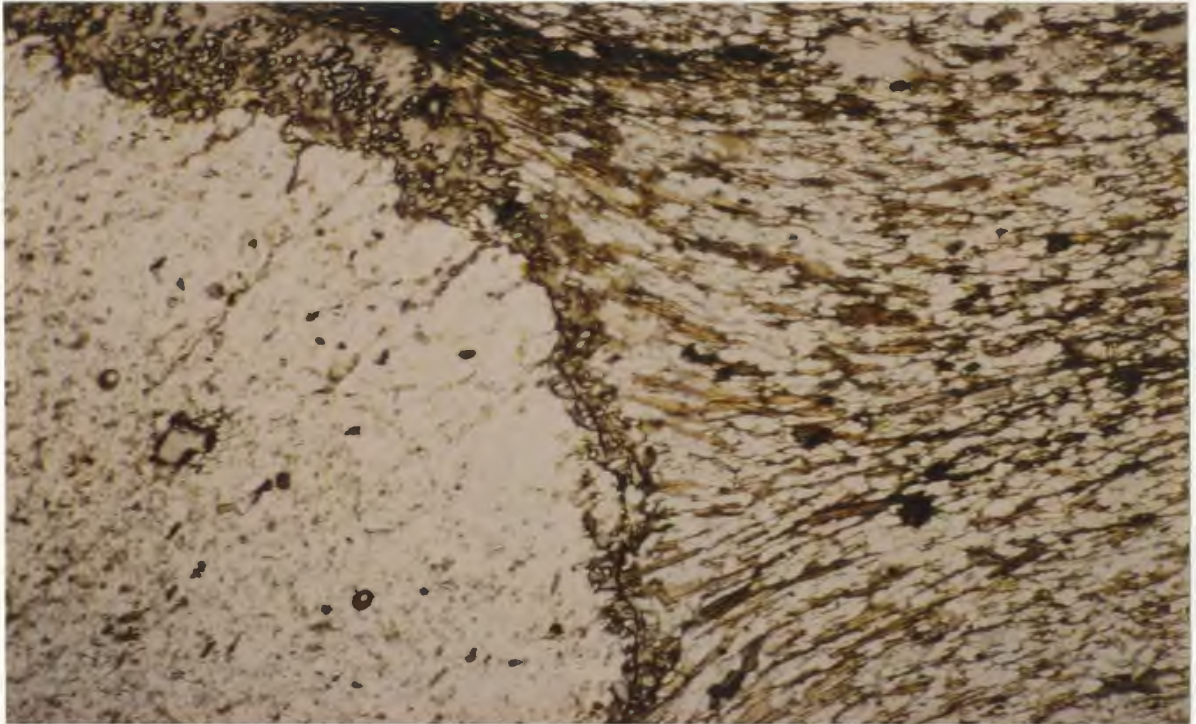
2 x actual size

rest of the cordierite. On the basis of this textural evidence biotite appears to have been involved in cordierite formation.

Quartz inclusions within cordierite porphyroblasts are often finer grained than quartz of the matrix, suggesting that: 1) there was excess quartz in the area of cordierite growth and the included quartz is a product of the cordierite-forming reaction (similar to the ubiquitous quartz 'inclusions' in staurolite described by Carmichael, 1969) and 2) the matrix quartz recrystallized to a coarser grain size while that within the cordierite did not.

Chemical analyses of cordierite, biotite, muscovite and plagioclase (Table A.7) represent two samples from the CZ and two samples from an area within the andalusite zone (Appendix A) that were found to contain cordierite as the only porphyroblastic phase. Average plagioclase compositions fall in the field of oligoclase (Table A.7).

Cordierite, with an average M/FM ratio of 0.64, represents the most Mg-rich mineral phase in the CZ. Small amounts of Na_2O (averaging 0.36 weight percent) and MnO are incorporated into the cordierite structure. Muscovites are noticeably less celadonitic and contain a greater proportion of paragonite (average Na/Na+K = 17.5%) than muscovites from the BZ. Biotite and muscovite included in cordierite porphyroblasts differ somewhat in composition from those in the matrix (Appendix B). Biotites tend to be more potassic and less titaniferous and muscovites more magnesian.

Biotite porphyroblasts tend to have lower M/FM ratios and contain less K_2O than biotite of the matrix (Appendix B). These compositional differences are slight and have been disregarded in calculations of the average biotite compositions.

2.4.4 Andalusite Zone (AZ)

The first appearance of andalusite in greywackes marks the andalusite isograd, with the andalusite zone occurring upgrade from the CZ (Figure 6). In central parts of the map area, adjacent to the Fubar fault, the first medium-grade rocks observed contain both andalusite and cordierite and hence have been assigned to the AZ. However, as mentioned previously, the presence of AZ rocks and absence of CZ rocks adjacent to the lower grade BZ in this area is attributed to displacement on the Fubar fault. Definition of the andalusite isograd is not precise in the northern part of the map area. However it is clear that the area underlain by the AZ is much broader than that of the CZ (Figures 5 and 6). AZ rocks have been mapped in both the Contwoyto and Itchen Formations and thus transecting the lithological boundary between the two formations in the northeastern part of the map area (Figures 5 and 6). AZ rocks have not been identified in the western sequence.

Mineral assemblages observed within the AZ are given in Table 2. The characteristic sub-assemblage is represented by andalusite-cordierite-biotite-muscovite. AZ rocks and

muscovite-free rocks (denoted A*Z) are not illustrated in AKF space in this text. An AKF plot of the AZ maximum-phase assemblage requires that four phases be represented, which would seem to contradict the phase rule. However, Miyashiro (1973, p.129) and Turner (1981, p.186) point out that this number of phases can be depicted because of inherent features of the AKF diagram (i.e. Mg and Fe are grouped together). A*Z rocks can be represented on an AKF plot by the three phase assemblage andalusite-cordierite-biotite.

In the AFM diagram (Figure 17) AZ rocks are represented by the three-phase assemblage cordierite-biotite-andalusite.

In outcrop pale pink poikiloblastic knots of andalusite are often difficult to distinguish from cordierite knots, but andalusite in the form of large euhedral pink chiastolite crystals is readily identifiable. In thin section chiastolite crystals lack inclusions, except for the dusting of opaques and other impurities or narrow zones of poikiloblastic andalusite that form the characteristic cruciform pattern. The terminations of some of the crystal faces are marked by convex outward aggregates of biotite or opaque minerals. This may be indicative of the forceful nature by which the chiastolite grew, with the impurities excluded from the crystal structure during its growth (Ferguson et al., 1980). In some samples chiastolite is surrounded by irregular, spongy poikiloblastic andalusite rims. Andalusite poikiloblasts are commonly seen to rim or form between cordierite porphyroblasts (Figure 18), a

Figure 17 :AFM diagram of the maximum-phase AZ mineral
assemblage andalusite-cordierite-biotite. Inset diagram
shows the portion of the AFM diagram used for
plotting.
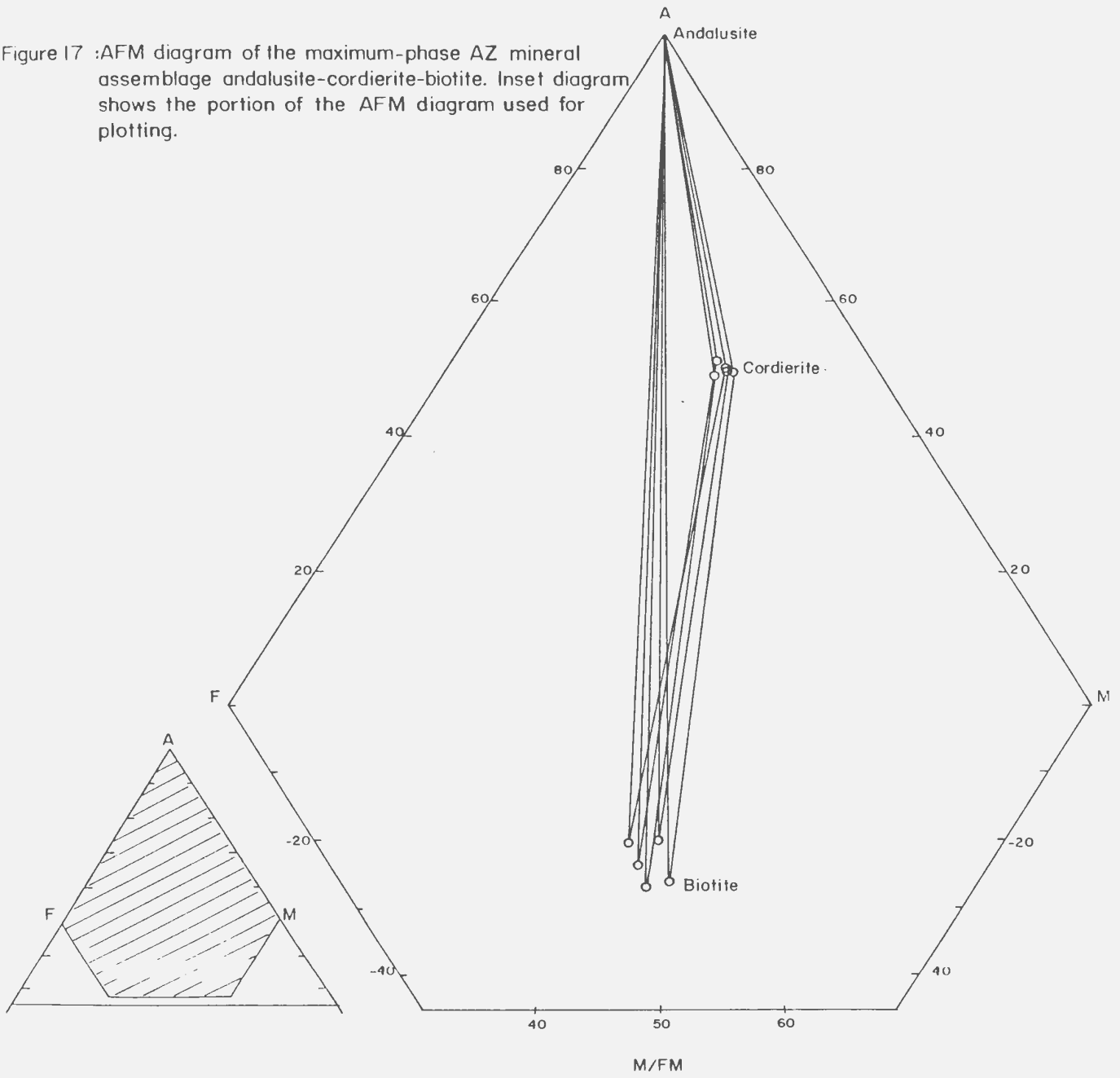
Figure 18: Photomicrograph of a SZ metaturbidite showing poikiloblastic andalusite interstitial to and partly rimming cordierite porphyroblasts, a relationship also observed in the AZ. Sillimanite prisms have grown in andalusite. Top, plane light, bottom, crossed nicols. Length of sections shown approximately 3.4 mm.
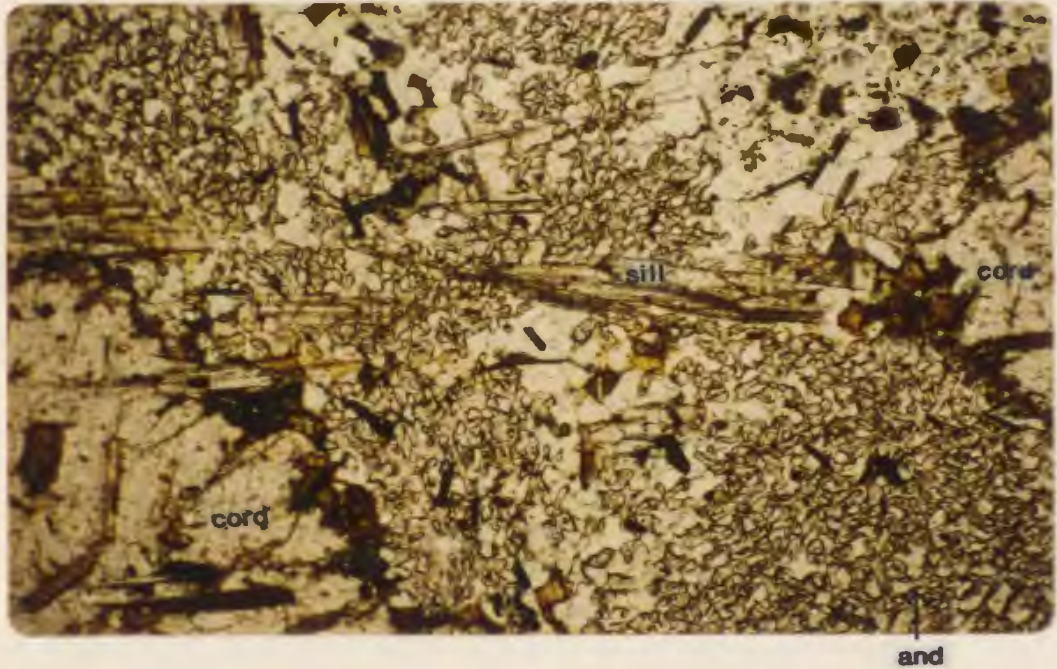
relationship also observed in the eastern Point Lake area by King (1981). The poikiloblasts contain abundant inclusions of quartz, biotite and opaques, but are never seen to include muscovite, even though some have grown within muscovite-rich layers. The exclusion of muscovite from andalusite suggests muscovite is involved in andalusite formation.

The presence of biotite-rich rims around some andalusite crystals may be indicative of the formation of new biotite during the production of andalusite or that biotite was not involved in andalusite formation and was excluded from the growing porphyroblast (see above).

Cordierite does not decrease in modal abundance within the AZ and cordierite porphyroblasts that are rimmed or partly surrounded by andalusite appear to be in textural equilibrium. Locally within the AZ, cordierite porphyroblasts are considerably larger (>4 to 5 cm) than those of the CZ. Additionally, cordierite may form clear xenoblastic rims on andalusite, attesting to continued growth of cordierite in the AZ. Xenoblastic cordierite may also be concentrated in irregular bands within the matrix. In contrast to the CZ, the modal abundance of biotite contained within some cordierite porphyroblasts is often only slightly lower than the biotite content of the matrix.

This may suggest that the formation of some cordierite in the AZ took place by a different reaction than that which initially produced cordierite in the CZ.

Biotite and muscovite throughout much of the AZ differ little in textural relationships from their appearance in the CZ, with the exception of the previously described relationships to andalusite. Slight changes in the modal abundance of muscovite may reflect minor variations in bulk rock composition. However, several samples from the upper portion of the AZ lack matrix muscovite (A*Z) and it is uncertain whether this lack of muscovite reflects a different rock composition, or that muscovite was consumed in the production of andalusite, or a combination of both factors. These samples contain large muscovite crystals, that cross-cut the tectonic fabric(s) defined by biotite, and are not considered to be part of the equilibrium assemblage.

The chemical compositions of cordierite, biotite, muscovite and plagioclase from the assemblage andalusite-cordierite-biotite-muscovite are given in Table A.8, together with the cordierite-free and muscovite-free (A*Z) assemblages. Analyses of andalusite yielded a few tenths of a per cent Fe (probably Fe_2O_3) in the otherwise pure Al_2SiO_5 formula.

Average AZ cordierites are slightly more magnesian than those of the CZ. Biotite, muscovite and plagioclase compositions of the two zones are similar. In those rocks in which muscovite is not part of the equilibrium assemblage (A*Z), biotite is more potassic and titaniferous, whereas cordierite is more Fe-rich (lower M/FM values). It is

presumed that the consumption of muscovite in the A*Z led to these enrichment trends in cordierite and biotite. For example, AZ muscovites contain approximately 0.60 to 0.80 weight percent TiO_2 and A*Z biotites are enriched in TiO_2 by approximately the same amount.

2.4.5 Sillimanite Zone (SZ)

The lower boundary of the sillimanite zone (SZ) is delineated by the sillimanite isograd (Figure 6). In south central and northern exposures the sillimanite isograd transects bedding and structural trends, while in the central part of the map area the SZ is truncated by a major north-trending fault (Figures 4 and 6). Near the lower boundary of the SZ, outcrop-sized pockets of AZ rocks can be found. The SZ occurs only in the eastern metaturbidite sequence and represents the highest metamorphic grade attained within the map area. Within the SZ, numerous adamellite and tourmaline-garnet-bearing pegmatite (McKinnon, 1982) intrusions are found.

Sillimanite first appears as microscopic fibrolite needles in andalusite-muscovite-bearing turbidites. Upgrade within the SZ sillimanite is seen to rim and finally replace both andalusite and cordierite and in far eastern exposures sillimanite forms a porphyroblastic phase.

Microstructural associations of sillimanite with coexisting mineral phases include: a) large needle-like prisms within and projecting from andalusite (Figure 18); b)

fine sprays of sillimanite needles nucleated on biotite (rarely muscovite) in the quartz-rich matrix (Figure 19); c) chaotic mats of fibrolite intergrown with biotite that have overgrown coarse-grained plagioclase and polygonal quartz and may include bleb-like andalusite relics; d) prismatic and/or fibrolitic sillimanite found within or near felsic clots that consist of coarse grained plagioclase and quartz (+/- muscovite) and irregularly shaped relics of andalusite (Figure 20); and e) fibrolite nucleated on embayed and pinnitized cordierite relics. Muscovite as a matrix phase is part of the equilibrium assemblage throughout most of the medium-grade CZ and AZ rocks. However a large portion of the SZ contains rocks in which muscovite is absent from the matrix assemblage (denoted S*Z). Instead, where present, muscovite forms either large, randomly oriented plates cross-cutting the biotite fabric(s) (as in the A*Z), and is considered to be a retrograde phase, or it occurs within the felsic clots (see above) which record the transition from andalusite to sillimanite. In this latter situation muscovite is a part of the equilibrium assemblage.

The following mineralogical change can be interpreted to indicate an increase in metamorphic grade within the SZ, provided that bulk rock composition remains constant: as the abundance of sillimanite increases, the abundances of cordierite, andalusite and muscovite decrease and plagioclase and biotite contents increase. As in the A*Z, the absence of muscovite from the matrix assemblage in the

Figure 19: A; Photomicrograph showing andalusite replaced by

biotite. Fibrolitic sillimanite has nucleated on

biotite. Plane light. Length of section shown

approximately 4.0 mm.

B; photomicrograph of a SZ metaturbidite showing

andalusite (high relief) replaced by biotite

(peripheral to andalusite). Sillimanite is

present elsewhere in the thin section. Plane

light. Length of section shown approximately 4.0

mm.

A.

B
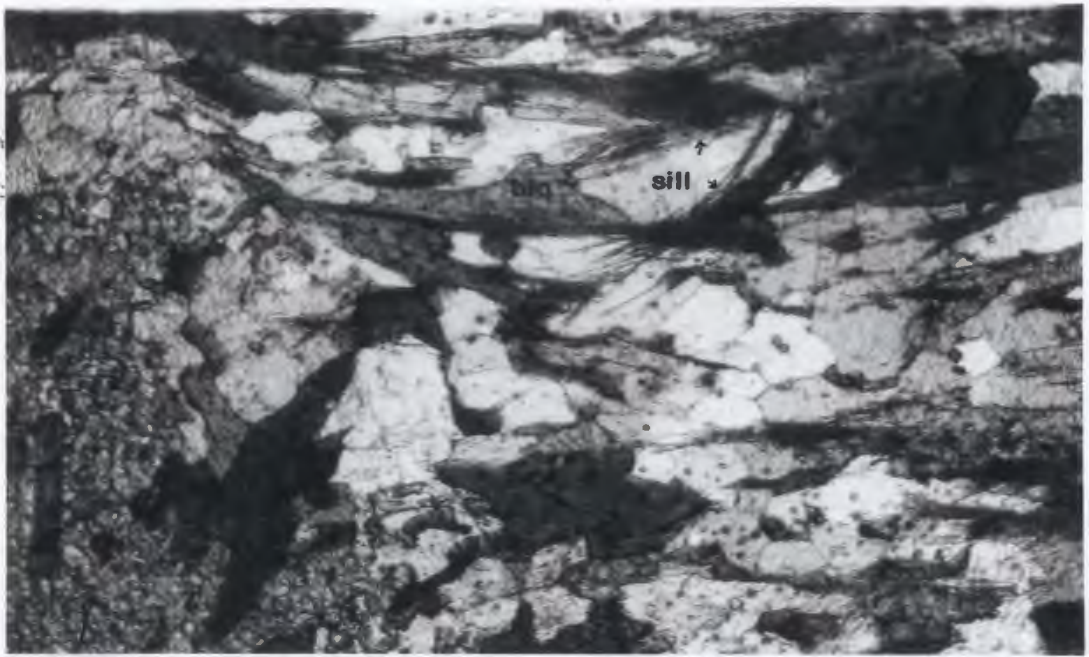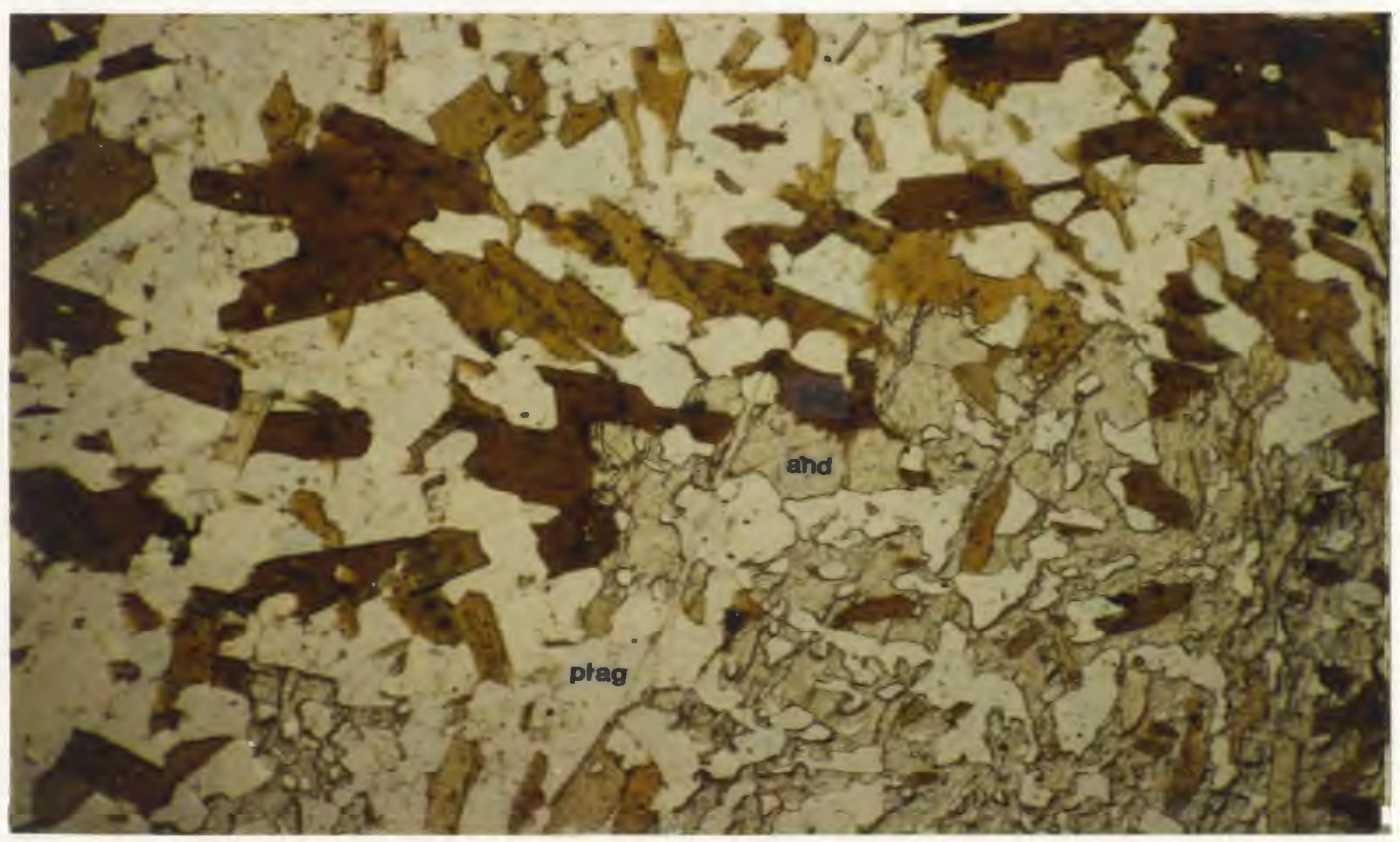
Figure 20: A; Photomicrograph showing andalusite blebs in
felsic clots consisting of coarse grained
plagioclase (clear). Note fine fibrolite sprays
associated with biotite (center top edge of
photograph). Plane light. Length of section shown
approximately 4.0 mm.

B; photomicrograph showing prismatic sillimanite
(lower left) and irregular andalusite relics in
felsic clots consisting of coarse grained
plagioclase and muscovite. Plane light. Length of
section shown approximately 4.0 mm.

A
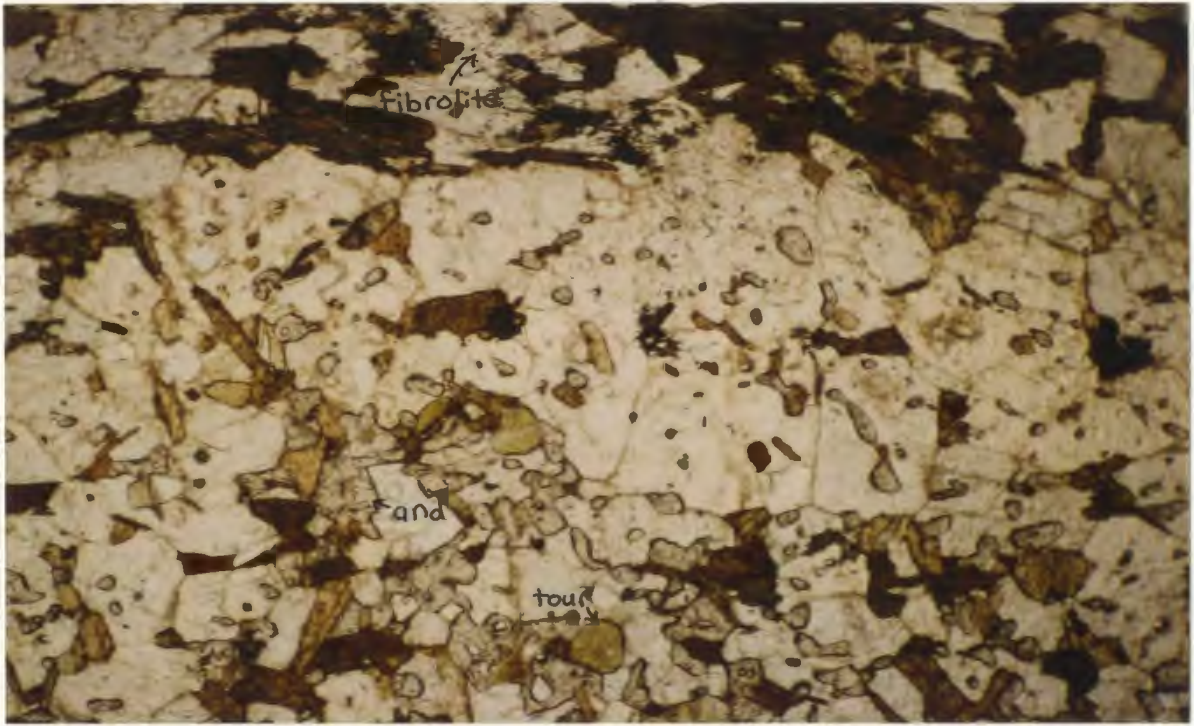
B
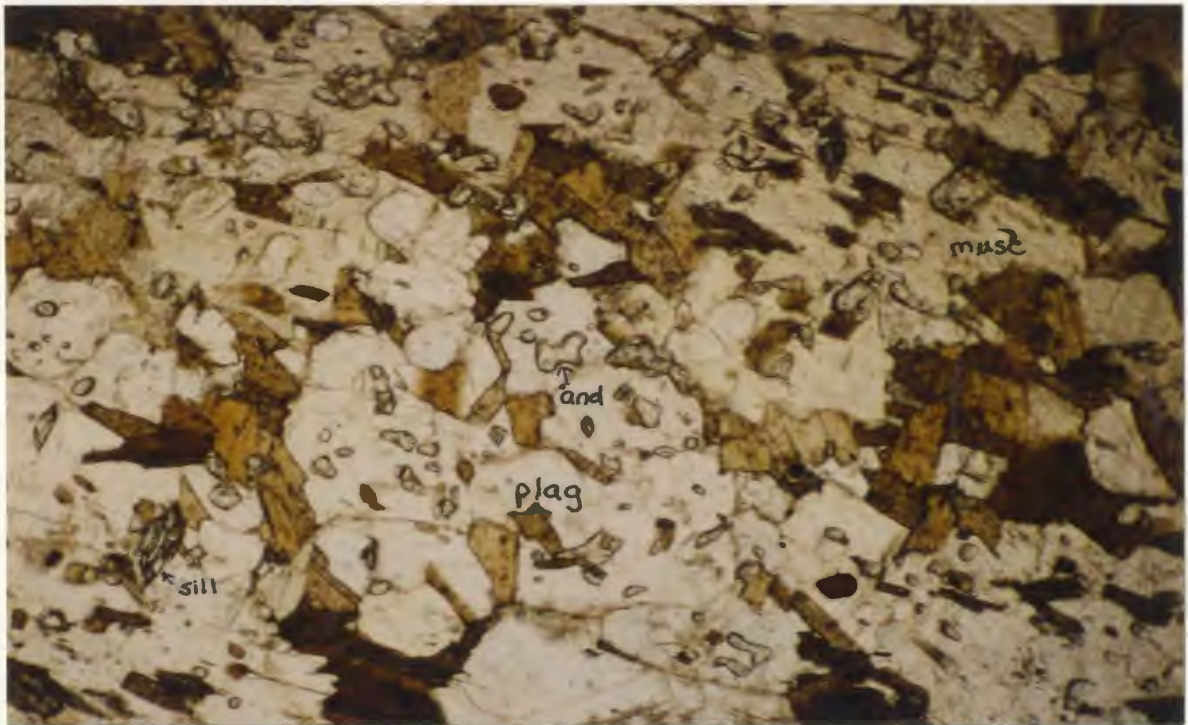
S*Z may indicate either variation in bulk composition or consumption related to the formation of sillimanite, or a combination of both factors.

In Table 2 the SZ maximum-phase assemblage, in which andalusite persists metastably with sillimanite, is listed together with those assemblages that lack one or more of andalusite, cordierite and matrix muscovite (S*Z; SCAB, SCB, SAB; see abbreviations page xv). Mineral compositions of most of these phases are given in Table A.9. Average analyses of cordierite, biotite, muscovite and plagioclase from the SZ differ little from those of the AZ, although SZ micas contain greater amounts of titanium. Individual cordierites in the SZ may be more Mg-rich than those in the AZ but the difference is minimal, so that the position of the SZ assemblage in AFM space changes little from that of the AZ (Figure 21).

In the cordierite-free assemblage sillimanite-andalusite-biotite-muscovite (SABM), muscovite and biotite are more magnesian than in the maximum-phase assemblage. Biotite compositions from the S*Z assemblages differ from those in the muscovite-bearing SZ assemblages in that they contain the highest TiO_2 contents recorded in the turbidites (up to an average of 2.16 average weight percent, with biotite in sample 81-V-264 containing a maximum 2.85 weight percent TiO_2).

In AFM space, the SZ maximum-phase assemblage is represented by the three-phase subtriangle cordierite-

Figure 21: AFM diagram of the maximum-phase SZ mineral assemblage sillimanite-andalusite-cordierite-biotite. Note that andalusite is metastable in the presence of sillimanite and both aluminosilicates are present at the A-apex. Solid circle and heavy tie-line represent the two-phase assemblage sillimanite-biotite. Inset diagram shows the portion of the AFM diagram used for plotting.

A Sillimanite/
   Andalusite

80   80

60   60

Cordierite

40   40

20   20

F   M

20   20

Biotite

40   40

40   50   60

M/FM
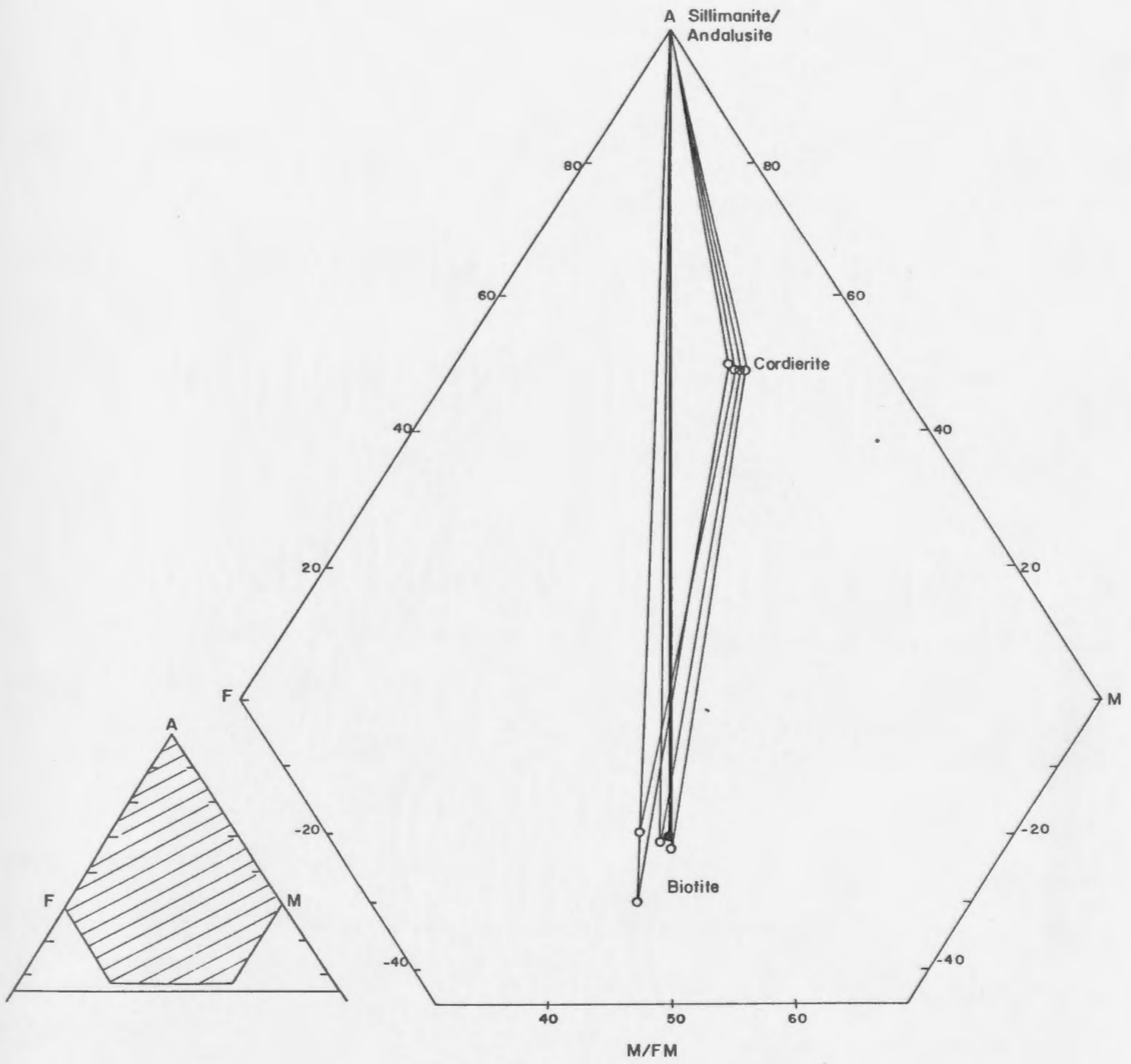
biotite-aluminosilicate, with both andalusite and sillimanite present at the A-apex (Figure 21). The cordierite-free assemblage from the SZ plots as the two-phase assemblage aluminosilicate-biotite (Figure 21). The observation that this tie-line crosses those for assemblages containing cordierite implies that the aluminosilicate-cordierite-biotite subtriangle has migrated to Mg-richer compositions with increasing metamorphic grade, consistent with the consumption of cordierite.

2.5 Variations in Mineral Compositions with Metamorphic Grade

2.5.1 General Statement

The effect of metamorphism on a prograde sequence may be documented not only through the changes in mineral assemblages (discontinuous reactions), but also through the changes in individual mineral compositions across metamorphic zones, due to partitioning of elements between coexisting phases during continuous reactions. Since it is clear from AFM topologies that continuous reactions are dominantly controlled by variations in the M/FM ratios of coexisting phases, a part of the discussion that follows will deal with changes in Mg and Fe contents of the coexisting phases. Other compositional changes in the mineral phases, which may not be apparent in AFM diagrams, are also discussed.

2.5.2 Plagioclase

Plagioclase is present in the low-grade greywackes as detrital grains and as part of the fine-grained quartzofeldspathic matrix. Detrital grains from the low-grade rocks often have ragged grain boundaries and contain abundant sericite and chlorite, indicating lack of equilibrium with the matrix constituents. An-contents of these grains are variable, from albite (An <1) to andesine (An 45). Matrix plagioclases likely recrystallized and attained equilibrium with other matrix components. Most matrix plagioclases analyzed from the CHZ are albite (An 0.2 to 11.6). Albite and oligoclase are found in the BZ, with the latter more common in the WBZ.

In medium-grade rocks the rarely observed detrital plagioclase grains are partly recrystallized and plagioclase is most commonly found in the quartz-rich matrix surrounding the porphyroblastic phases. Plagioclase compositions in the CZ, AZ, A*Z, SZ and S*Z are generally in the oligoclase range (An 11 to An 30), although one analysis of andesine (An 31.8) comes from the AZ, and an albite composition has been determined in the SZ.

The range of plagioclase compositions throughout the study area is shown in Figure 22. With increasing metamorphic grade plagioclase should become progressively more calcic, with the amount of calcium available in the rock system placing an upper limit on this tendency. Figure 22 illustrates that: (1) at low grades plagioclase of albite
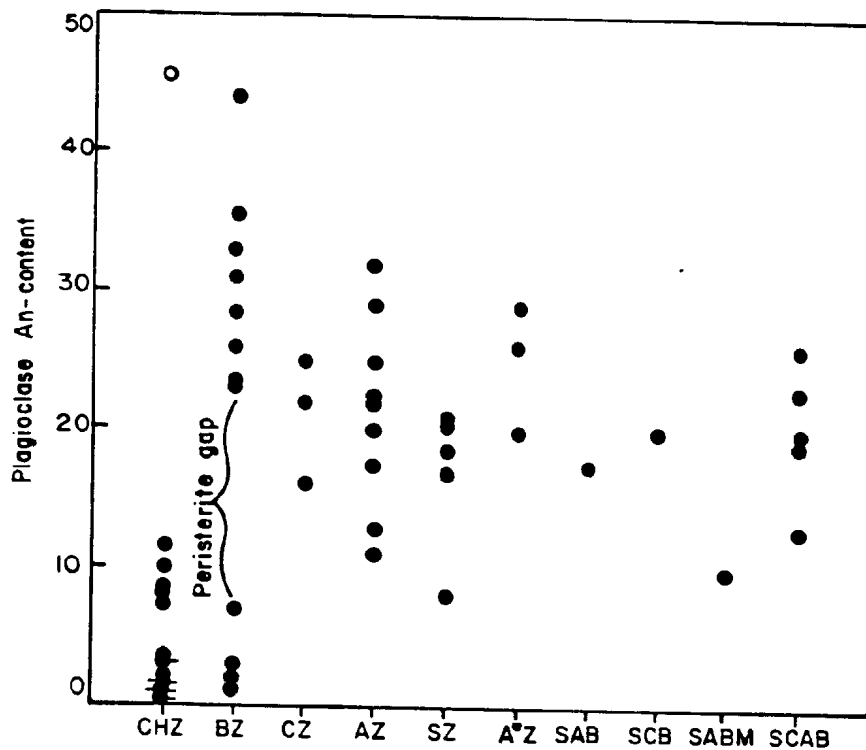
Figure 22: Variation in An-content of plagioclase with metamorphic grade from eastern zone metaturbidites. Abbreviations as listed on page xiv. Ticks on data points indicate number of analyses: O ticks=1 analysis, 1 tick= 2 analyses, 2 ticks= 3 analyses. Open circle represents possible relict grain.

composition is common; (2) BZ plagioclases show evidence of peristerite unmixing (see also Table 4); (3) at medium grades plagioclase is more calcic (oligoclase). Evidence of peristerite unmixing was not found in CHZ rocks and, although exsolution in these plagioclase grains may occur on a sub-microscopic scale, it is likely that insufficient data points were analysed to document this phenomenon. Plagioclase analyses from low-grade rocks that yielded An-contents greater than An 30 are suspected to represent relict grains. However those from the BZ represent relict grains which are recrystallized. These high An values are likely due to the fact that plagioclase is present only in minor amounts in these rocks, so that by medium-grade it may have attained maximum An-contents.

2.5.3 Opaque Phases

No systematic investigation into compositional changes of the opaque phases was made in this study. Visual inspection did not reveal significant changes in the modal amount of opaque minerals related to increasing metamorphic grade. Ilmenite and rutile are found in greywackes of all metamorphic grades. Magnetite, graphite and sulfides (pyrrhotite, pyrite and chalcopyrite) were also noted, but are less abundant than the titaniferous oxides.

2.5.4 Chlorite

Several distinct habits of chlorite can be recognized:
a) chlorite, dominantly with khaki interference colors
(k-chlorite), that forms small platelets aligned with
muscovite and/or biotite in the matrix of the low-grade
rocks; b) chlorite with blue-purple interference colors
(b-chlorite) that forms fine-grained, randomly oriented
platelets or fine-grained aggregates often occurring in
pressure shadows around detrital grains in low-grade rocks
(esp. WCHZ and WBZ); c) large randomly oriented, idioblastic
and often twinned chlorites with anomalous interference
colors, which are quite common in medium-grade rocks and
which post-date tectonic fabrics and appear to form
pseudomorphs of biotite porphyroblasts; and d)
coarse-grained sprays of chlorite within and associated with
cordierite porphyroblasts. Ramsay (1974) considered that
type (d) chlorite was an indirect product of cordierite
formation; however, in this study a consistent association
between type (d) chlorite and cordierite porphyroblasts was
not found. Only type (a) chlorite is considered to be part
of the equilibrium assemblage. Type (b) chlorite is
pertinent to the discussion of the western metamorphic
sequence (see above); types (c) and (d) retrograde chlorites
are not dealt with further here. Ramsay and Kamineni (1977)
described chlorites similar to those listed above from the
Yellowknife area.

The atomic proportions in chlorite analyses presented in the various tables have been calculated on the basis of 18 oxygens. Anhydrous totals approximate 90%, comparable to data presented in Deer et al. (1966). Following the classification of Hey (1954) all analyzed chlorites fall within the compositional field of ripidolite. Note that all chlorite analyses presented throughout the text represent type (a) chlorite, with the single exception of the analysis marked with (**) in Table A.5 and Figure 23, which is type (b) retrograde chlorite.

The main compositional features of the low-grade chlorites are summarized in Figure 23. Al and Si contents of chlorites remain relatively constant throughout both the CHZ and BZ. The variation in Al/Mn+Fe+Mg is rather restricted and unaffected by the more dispersed Mg/Fe+Mn ratios. Fe-rich chlorites have lower Al-contents, indicating the substitution of Fe^{3+} for Al (McNamara, 1965), whereas a sympathetic relationship exists between Al and Mg.

Figures 23a and b show that chlorites from the EBZ are generally more Mg-rich than those from the ECHZ. This implies that the production of biotite, a more Fe-rich mineral than chlorite, led to the consumption of Fe-chlorite, with the average chlorite composition becoming more Mg-rich. These observations are comparable to those of Cooper (1972; see below). Chlorites from the WCHZ and BZ do not show this pattern; in Figure 23b it can be seen that these chlorites show a Mg-depletion trend toward the biotite

Figure 23: Compositional variation of chlorite with

metamorphic grade illustrated by:

(A) The range in M/FM ratios of chlorite from the

CHZ (i) and BZ (ii) for both eastern (open

circles) and western (solid circles) sequences.

Inset diagram shows portion of AFM diagram used

for plotting.

(B) The mineral formula in terms of atomic

proportions from calculated analyses presented in

tables.   Arrows indicate approximate trend toward

higher metamorphic grade: (i) southern part of

western low-grade rocks; (ii) northern part of

western low-grade rocks and; (iii) eastern belt

of low-grade rocks (data points are not connected

because of the irregular distribution of the

samples). Both (i) and (ii) have a retrograde

overprint denoted by (*) (see text). Chlorite

analysis with ** (sample 373) is retrograde in

origin.

A

B
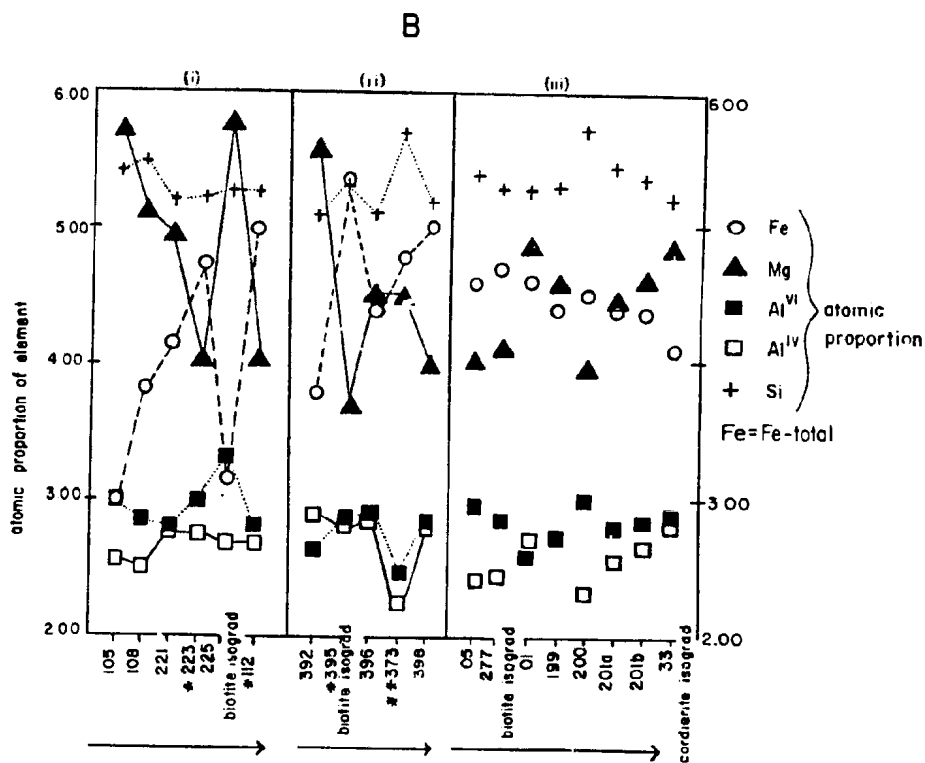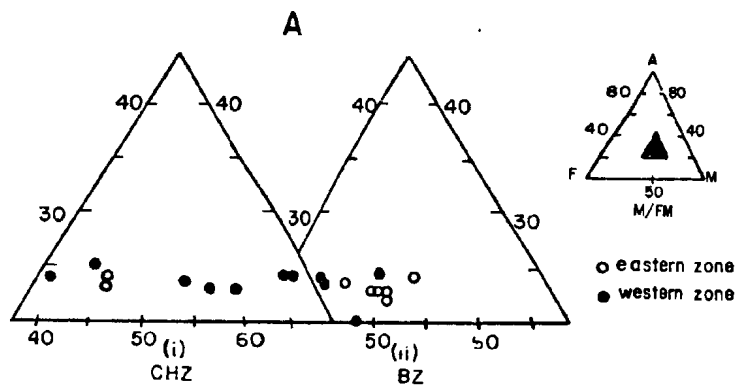
isograd, but Mg-enrichment at or just above the isograd. These effects are interpreted to be due to the widespread retrograde overprinting discussed in 2.4.1 and 2.4.2.

Variations in the chemical composition of chlorite with increasing metamorphic grade are controversial. Cooper (1972) suggested that M/FM ratios of chlorite increased with metamorphic grade; however, A.B. Thompson (1976) pointed out that the change in M/FM ratios of a mineral phase is dependent on continuous reactions taking place in the rock. In rocks of similar composition and metamorphic grade to the low-grade rocks of this study, Brown (1967), Mather (1970) and Ramsay (1973a, b) noted no compositional trends in chlorite related to metamorphic grade. Ramsay (1973b) observed that chlorite is the only mineral prior to the formation of biotite that can accommodate the large quantities of Mg contained within the rock, whereas Fe can be contained in the opaque phases present. He thus argued that the Mg-content of chlorite reaches a maximum at reasonably low grades. However, it is necessary to consider that a large amount of muscovite is usually present in pelites and that muscovites at low grade contain a significant proportion of the celadonite molecule. In these and other studies (Cooper, 1972; Ramamohana Rao, 1977; Carmignani et al., 1982) the bulk composition of the host rock is stressed as being an important influence on the composition of chlorite.

2.5.5 Muscovite

The microstructural habits of muscovite have been previously described and can be summarized into five main types: 1) fine-grained sericitic flakes in the matrix in CHZ and parts of BZ rocks; 2) coarse grained platelets in the BZ through to the SZ that partly define the matrix fabric(s); 3) large plates associated with the felsic clots of the S*Z; 4) coarse-grained plates, cross-cutting the biotite fabric(s) of the matrix; and 5) long, slender laths that may be concentrated within cordierite porphyroblasts. Only the first three types are considered pertinent to this discussion. Types 4 and 5 are retrograde in these rocks, although Ramsay (1974) and Ramsay and Kamenini (1977) suggested that type 5 may be a by-product of the cordierite-forming reaction.

Muscovite compositions have been suggested to vary systematically with increasing metamorphic grade (Guidotti, 1973; Guidotti and Sassi, 1976) and some of the documented trends were suggested as possible petrogenetic indicators (Guidotti and Sassi, 1976), notably: (1) variation in the contents of celadonite (Tschermak's substitution; Mg, Fe, Si $= Al^{vi}, Al^{iv}$); and (2) variation in content of paragonite (substitution of Na for K; the extent of solid solution between the pure end members paragonite and muscovite). In all cases the authors stress the importance of considering bulk composition and/or mineral assemblage (in particular

limiting assemblages) in the application of muscovite as a petrogenetic indicator.

The muscovite formula cation proportions were calculated on the basis of 22 oxygens. It is appropriate to note here that difficulties were encountered during analyses of muscovites by electron microprobe. These difficulties, the most notable of which is the accuracy of K-content, are described in Appendix A. It is suggested in Appendix A that the error in K-values determined by electron microprobe is standard, being consistently low (by about 1%, in comparison to wet chemical analyses). Therefore it is reasoned that the data can be used to document variations in K-content. Weight percent oxide totals obtained by electron microprobe analysis should indicate a water content of about 4% (Deer et al., 1966) and possibly up to 7% (Ramsay, 1973b). Some muscovites analyzed in this study show a deficit in totals of up to 10%. Since all analyzed muscovites are also low in total alkali cations it is uncertain whether this deficiency is related to inaccurate analyses or actual vacancies in cation sites. Visual inspection of the data also shows that some of the lowest weight percent totals are associated with low silica contents, suggesting inaccuracies in silica analysis.

Systematic changes in muscovite composition are evident throughout the paragenetic sequence developed in the Keskarrah Bay area. Variations in oxide proportions in muscovites from the different metamorphic zones are shown

graphically in Figure 24. Total Al-contents increase at the expense of Mg and Fe indicating celadonite substitution. Titanium contents of muscovites increase systematically with metamorphic grade and, with the exception of the slight decrease in the CZ (Figure 24) these trends are consistent with those observed elsewhere (Kwak, 1968; Guidotti, 1970). Y-site total occupancy (Al^{vi}, Fe, Mg, Ti) is in excess of the ideal value (4.00) and although the range of Y-site values is relatively restricted and narrows with increasing grade, no other distinct prograde trend is noted (Figure 25).

Muscovites from all grades are deficient in X-site cations (Na, K), but a prograde filling of this site is noted, except for in the CZ where total X-site cations decrease (Figure 25), but Na is elevated. Butler (1967) suggested that cation deficiency in the X-site may enhance the ability of muscovite to accept Na ions in this site. McNamara (1965) suggested that deficiencies in the alkali sites may be balanced by an excess of octahedral cations (Y-site), as is observed by Evans and Guidotti (1966) and in this study.

The celadonite content of muscovite is low, as indicated on the SAF (Figure 26; see figure caption for diagram explanation) and AKF diagrams (Figure 27). The compositional fields outlined in these diagrams enclose the low-grade rocks (CHZ,BZ) and medium-grade rocks (CZ,AZ,SZ).In both the SAF and AKF diagrams it is apparent that muscovites from
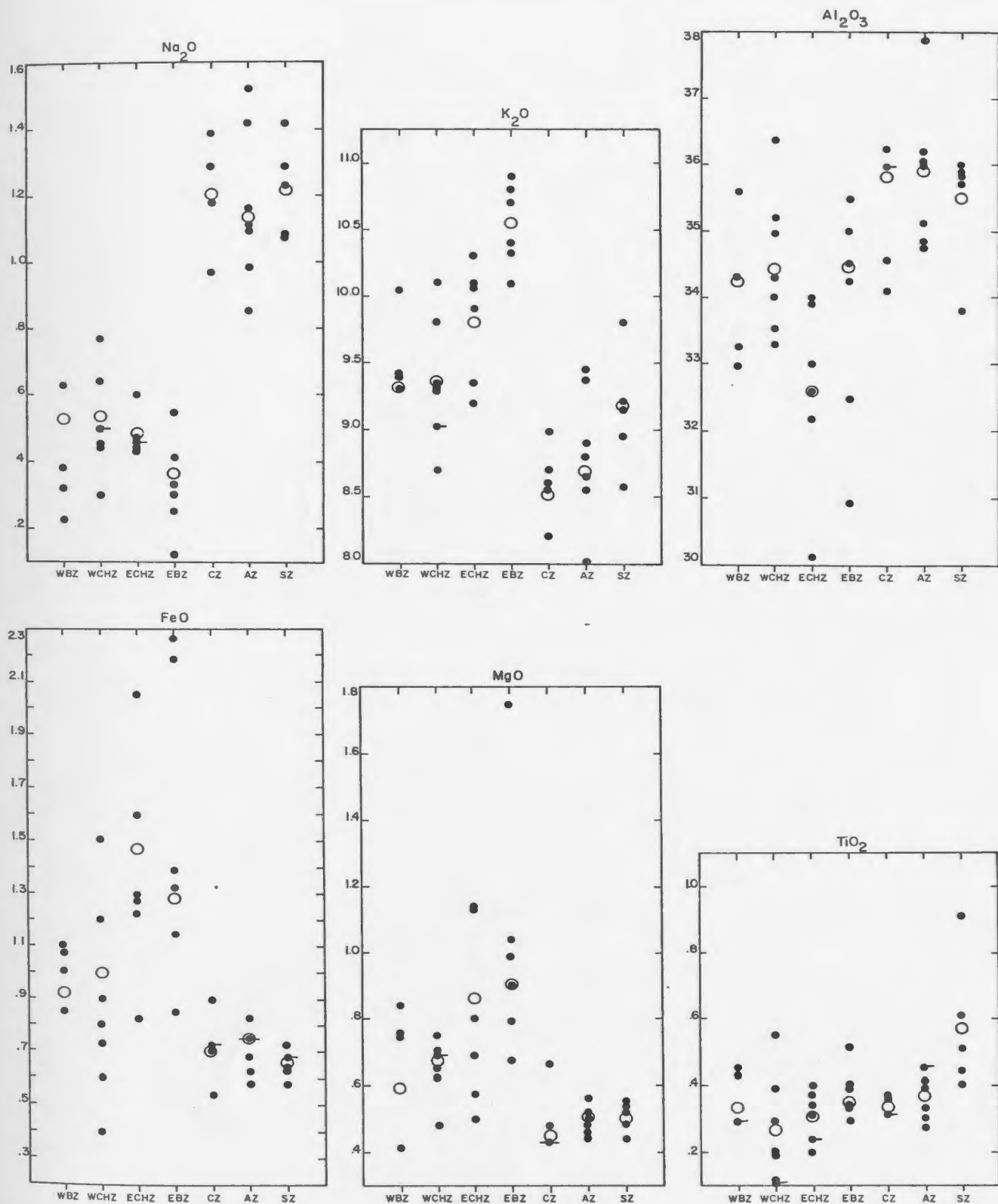
Figure 24: Compositional variations in muscovite with metamorphic grade. Data shown as oxide percent from analyses presented in tables. FeO=Fe-total. Average analyses (open circles). Ticks on data points indicate more than one analysis.
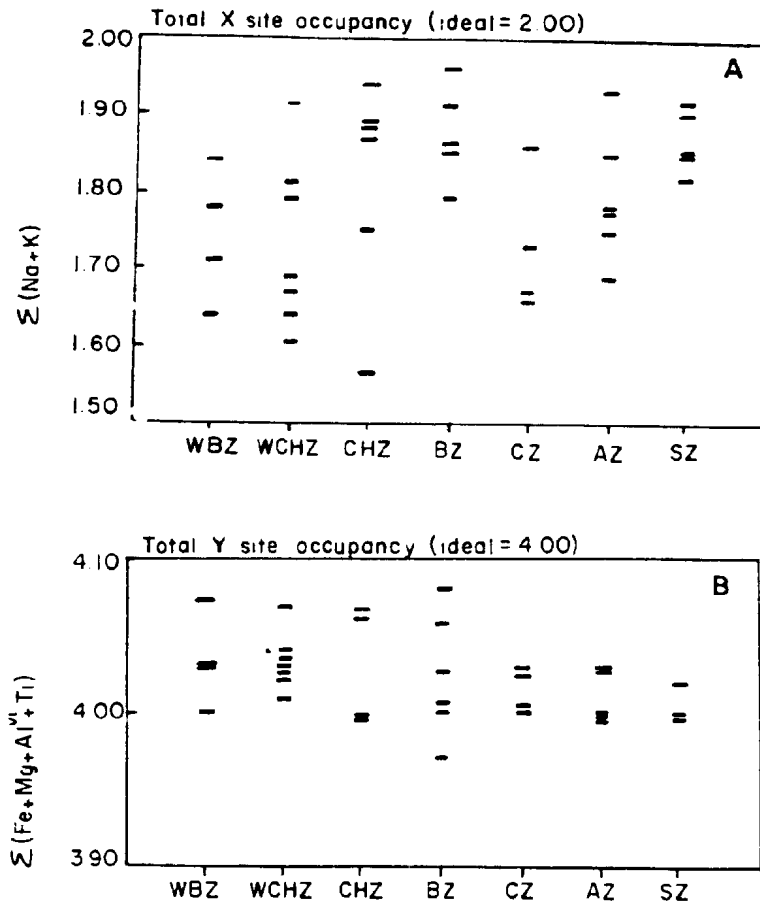
Figure 25 : Variation in total X-site (A) and Y-site (B) occupancy in analysed muscovites related to metamorphic grade. Note X-site occupancy is less than ideal while Y-site occupancy is greater than in ideal muscovite.

Figure 26: Muscovite analyses from all metamorphic zones plotted on a portion of the SAF diagram (see inset diagram for explanation of co-ordinates) to show the change in celadonite content with metamorphic grade. Dotted line outlines the field of low-grade rocks, dashed line outlines the field of medium-grade rocks in this study. Note that there is no distinct change in celadonite content of muscovite between CHZ and BZ.

Figure 27 : Muscovite analyses from all zones plotted on a portion of the AKF diagram (see inset diagram above). Note the distinctive change in muscovite composition at medium grade and no clear distinction between CHZ and BZ.

Legend:
- ● ECHZ
- ◉ WCHZ
- ○ EBZ
- ⊙ WBZ
- □ CZ
- × AZ
- ✳ SZ
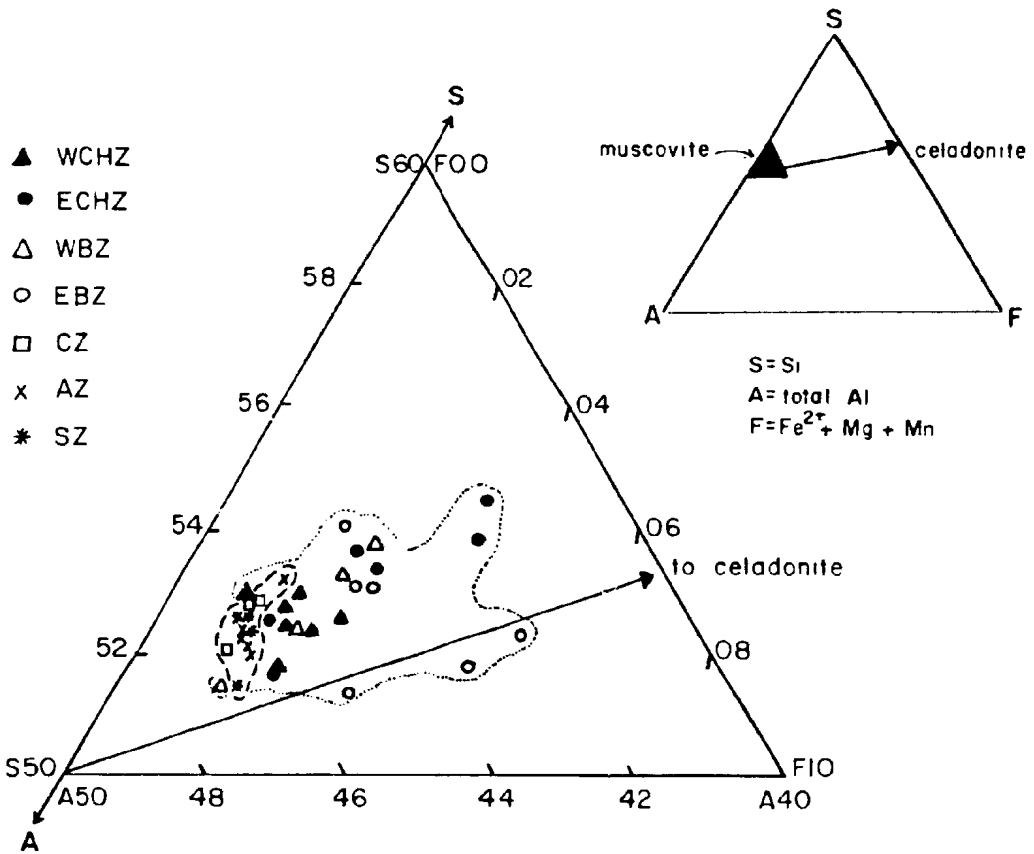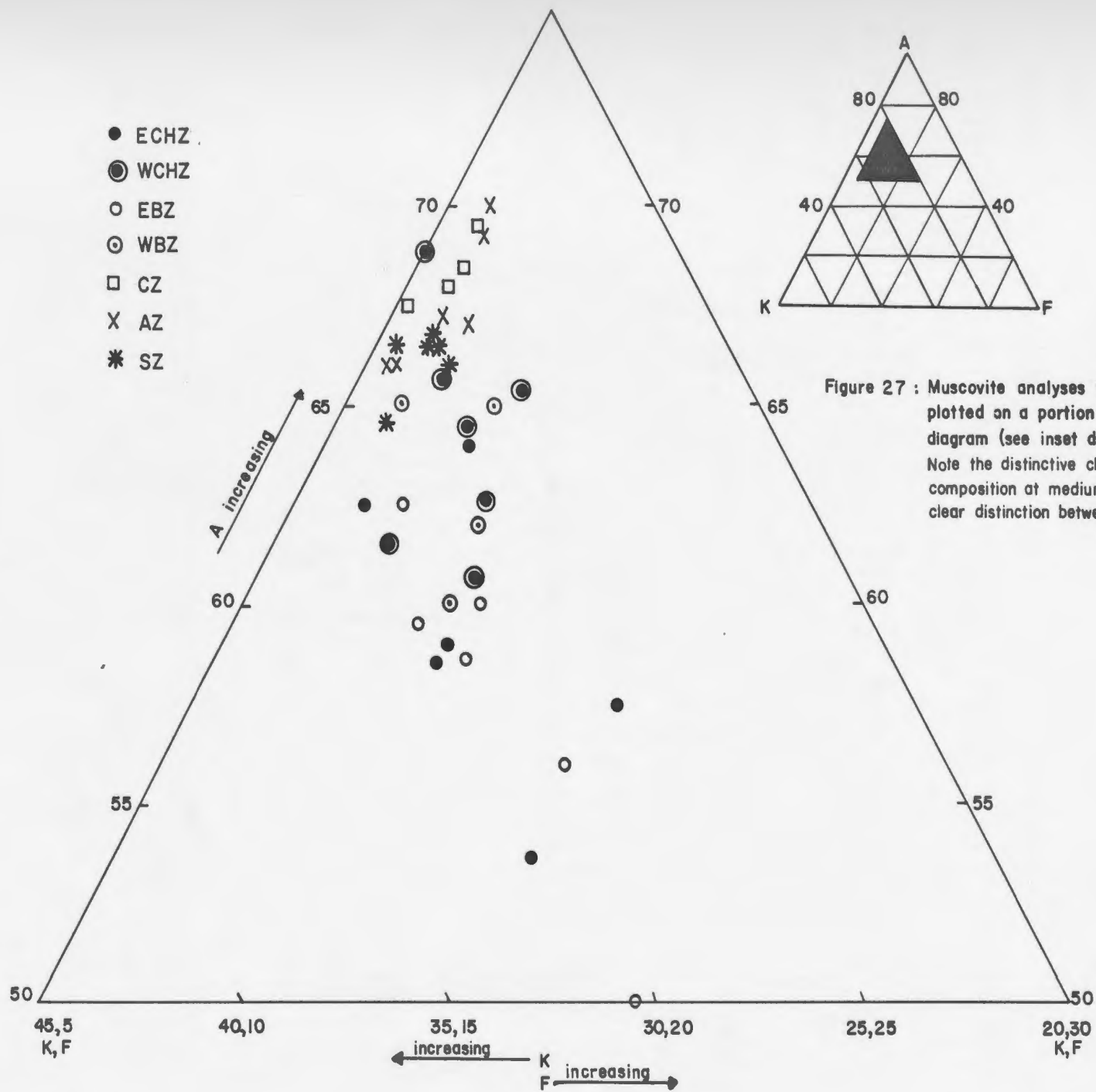
the two eastern low-grade zones show the most variation and
highest celadonite contents, the variation presumably being
a function of variable bulk composition. It is important to
note that in both these diagrams muscovites from the CHZ
overlap with those of the BZ; indeed some BZ muscovites are
more celadonitic than those from CHZ. Celadonite content
declines sharply at the CZ (Figures 24 - 27), with decreases
recorded in both Fe and Mg (Figure 24). At the AZ a slight
increase in Fe and Mg with a concomitant decrease in Al
denotes more celadonitic muscovite. Muscovites from
cordierite-free assemblages of the AZ have a higher
celadonite content than those from cordierite-bearing rocks.
Titanium contents are also elevated. SZ muscovites are lower
in Al and Fe but higher in K. Muscovites from the A*Z and
S*Z assemblages containing cordierite have lower M/FM values
(and lower celadonite contents) than AZ and SZ equivalents
(Figure 29a). Those lacking cordierite have higher M/FM
ratios, reflecting a decrease in Fe-content.

In Figure 28 the X_{Mg} (= Mg/Mg+Fe) values of muscovite
have been plotted against those of chlorite and biotite and
the data indicate that: (1) muscovite is more magnesian than
coexisting biotite and generally more magnesian than
coexisting chlorite; (2) the distribution coefficient (Kd)
approaches unity for the mineral pair muscovite-chlorite
and; (3) Kd for the mineral pair muscovite-biotite does not
appear to be temperature sensitive.
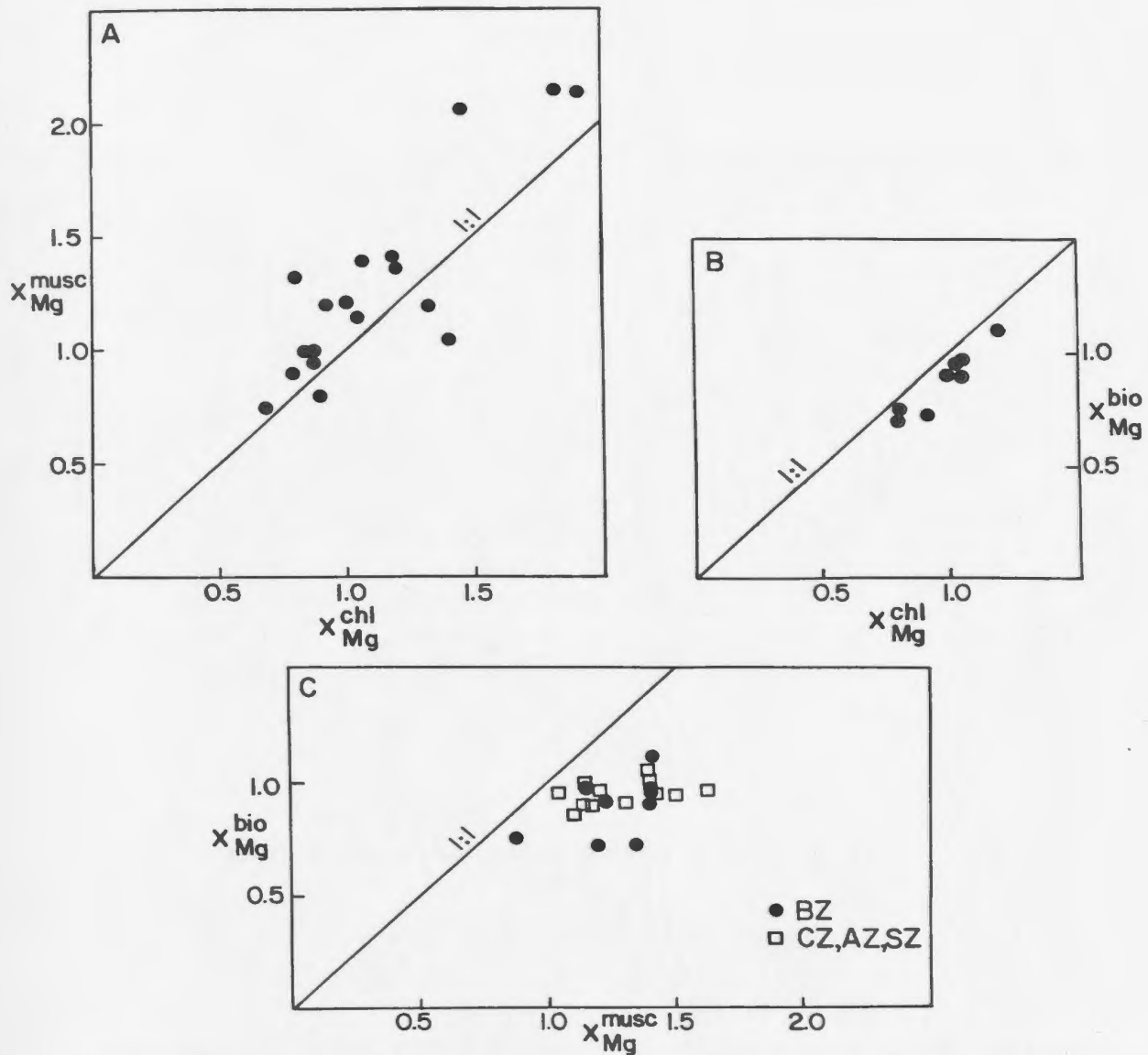
Figure 28 : X_{Mg} (=Mg/Mg+Fe); in muscovite plotted against that in chlorite (A);
in biotite plotted against that in chlorite (B) and muscovite (C).
Fe = total iron.
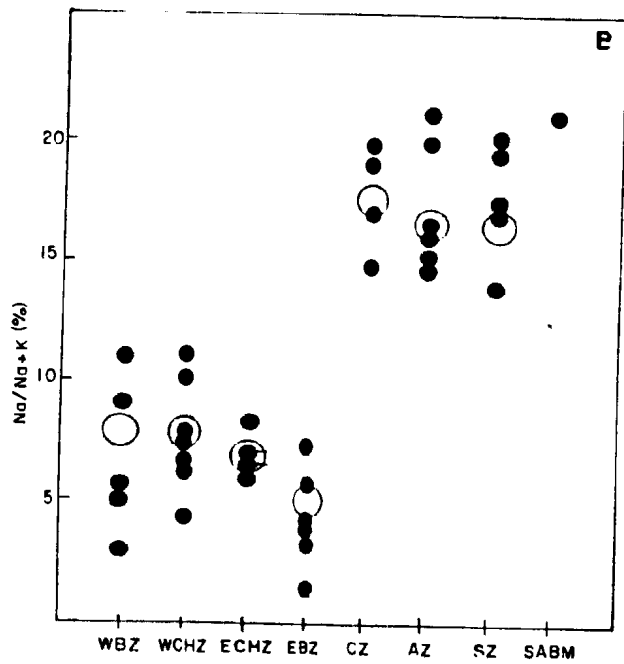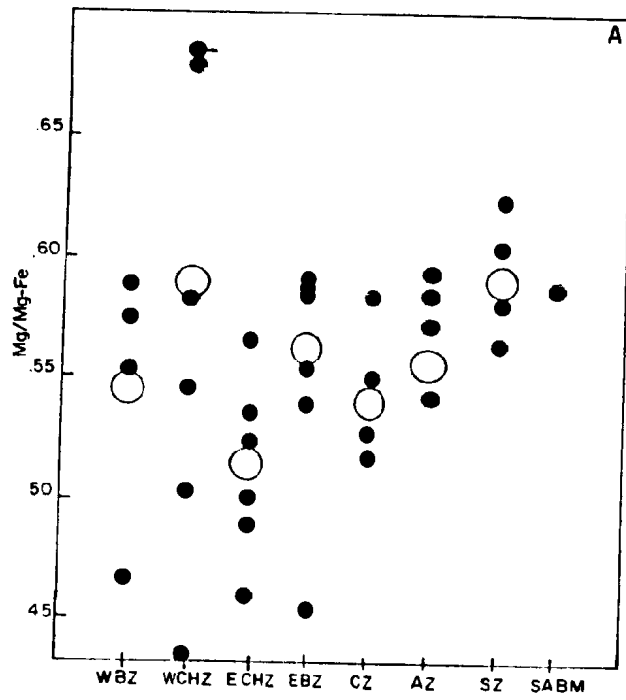
Figure 29:Variation in Mg/Mg+Fe (A) and Na/Na+K (B) ratios of muscovite
with metamorphic grade. For abbreviations see page xiv.
Average analyses (large circles). Fe= total iron.

Numerous studies have documented the decrease in celadonite content of muscovite with increasing metamorphic grade (Velde, 1965; Cipriani et al., 1968; Mather, 1970; Guidotti, 1970; Ramsay, 1973b; Guidotti and Sassi, 1976). For a given pressure the substitution of Fe and Mg into the muscovite crystal structure is less favored at higher temperatures, and muscovite compositions approach ideality (Velde, 1965; Guidotti and Sassi, 1976). The results of this study support this conclusion, with the most abrupt decrease in celadonite content occurring at the onset of medium-grade metamorphism (first appearance of cordierite). Brown (1967) however, noted that the celadonite content of muscovite from the low-grade rocks in his study showed no dependence on metamorphic grade and Carmignani et al. (1982) have documented an increase in celadonite content of muscovite with the incoming of biotite.

Na and K contents of muscovite define distinct and antithetic trends with increasing metamorphic grade (Figure 24). A plot of Na/Na+K (Figure 29b) shows the paragonite content of muscovite from each zone. In the eastern sequence paragonite content decreases from the CHZ to the BZ and from the CZ to the SZ, but the most notable change in muscovite composition occurs at the CZ, where there is a jump of about 10% in the Na/Na+K ratio. Muscovite compositions from the AZ, in those assemblages seen not to contain cordierite, have elevated Na/Na+K ratios (~15 - 20%) in comparison with cordierite-bearing specimens (~2 - 12%). A few of the late

cross-cutting muscovites from the A*Z and S*Z were analyzed (Appendix B). Na/Na+K ratios are in all cases the same or lower than AZ and SZ muscovites of the equilibrium assemblage.

Guidotti (1969, 1973) pointed out that in order to examine the variation in paragonite content of muscovite with metamorphic grade, limiting assemblages must be used. The data shown in Figures 24-29 are restricted to a limiting assemblage only for CZ, AZ and SZ rocks where the assemblage muscovite-plagioclase-biotite exists in high-Al rocks (eg. cordierite and/or aluminosilicate-bearing assemblages; see also Guidotti, 1973). Muscovite is as rich in Na, K and Al as possible for a particular grade in these zones only.

The prograde trend toward increasing paragonite content of muscovite in Al-rich, paragonite-free rocks has been reported to reverse when an aluminosilicate phase is formed, so that a plot of Na/Na+K versus metamorphic grade is described by a bell-shaped curve that mimics relationships in the muscovite-paragonite pseudobinary phase diagram (Guidotti, 1970; Guidotti and Sassi, 1976; Evans and Guidotti, 1966). These authors also noted that Na/Na+K values underwent abrupt changes on crossing a dehydration isograd. The plot of Na/Na+K versus metamorphic grade for the muscovites in this study (Figure 29b) shows a very abrupt change at the boundary between the BZ and the CZ, which is presumably related to the cordierite forming reaction. The decline in Na/Na+K values upon the appearance

of an aluminosilicate phase (AZ) is as predicted, but this is a subordinate effect compared to the increase in values from the BZ to CZ. In comparison, muscovite analyses presented by King (1981) show no significant decrease in paragonite content until the K-feldspar-sillimanite (second sillimanite) zone.

In aluminosilicate-bearing assemblages, the Na-contents of plagioclase and Na/Na+K ratio of coexisting muscovite are theoretically interrelated (Evans and Guidotti, 1966; Guidotti and Sassi, 1976). By projecting the assemblage muscovite-plagioclase-aluminosilicate through Al_2SiO_5 and onto the $CaAlO_2$-$NaAlO_2$-$KAlO_2$ plane it is seen that albite coexists with Na-rich muscovite while Ca-rich plagioclase should coexist with progressively K-richer muscovites (Guidotti and Sassi, 1976). Figure 30 shows the relationship between X_{Na} (= Na/Na+K) muscovite and X_{Na} plagioclase (where X_{Na} = Na/Na+K+Ca) for the metamorphic zones of this study. The low-grade (CHZ and some BZ) and medium-grade (CZ, AZ, SZ) samples form two distinct populations. Muscovites from the low-grade rocks are generally low in paragonite content and coexist with either albite or oligoclase. Medium-grade muscovites have higher paragonite contents and coexist with more Ca-rich plagioclase (oligoclase-andesine). A similar trend in low- to medium-grade rocks is suggested by the data presented by King (1981; indicated on Figure 30), but the trend reverses at high grade (i.e. both plagioclase and muscovite become
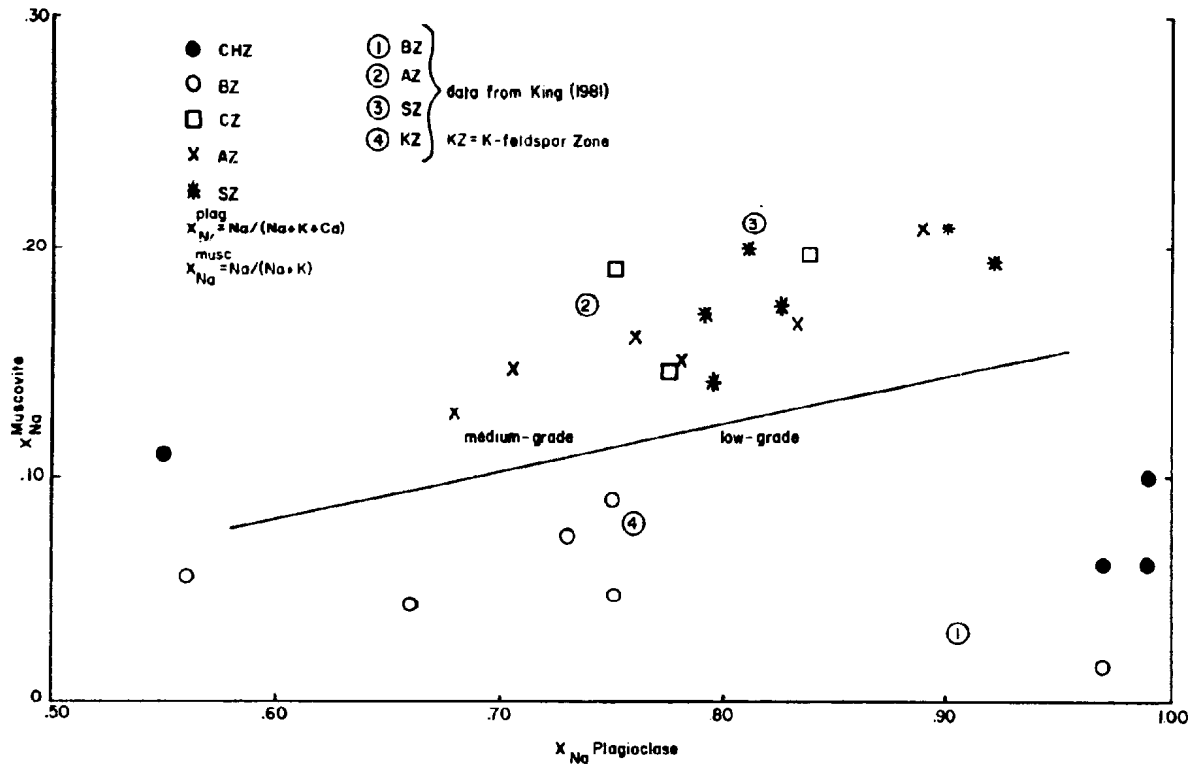
Figure 30: The relationship between X_{Na} Muscovite, X_{Na} Plagioclase and metamorphic grade. Line drawn approximates boundary between low and medium-grade rocks, which form two distinct populations.

less sodic; Figure 30). The results of this study for the high-Al limiting assemblages are comparable with those of Guidotti and Sassi (1976). At the higher grades discussed by Guidotti and Sassi (1976), and as shown by King's data (Figure 30), both muscovite and plagioclase are progressively depleted in Na. Since muscovite apparently exchanges Na for K and plagioclase exchanges Na for Ca, there must be a Na 'sink' in these high-grade rocks. Perhaps Na is taken up in the formation of new plagioclase or in the production of K-feldspar (i.e. upper SZ or K-feldspar zone).

2.5.6 Biotite

Structural formulas of biotite presented in the various tables are calculated on the basis of 22 oxygens. Anhydrous totals indicate (OH,F) contents of 2-6% which are approximately within the range presented in Deer et al. (1966). Inaccuracy in the Si analyses (Appendix A) may account for some of the variations in anhydrous totals.

Commonly observed changes in biotite composition with metamorphic grade include variations in Mg, Fe, Al, Ti and possibly Na and K. Kamineni and Carrara (1973), using a statistical method, discovered significant differences in the Fe, Mg, Al and Ti contents between porphyroblastic and fabric-forming biotites. However, although visual inspection of the biotite analyses from this study indicates small chemical differences between biotites in the two microstructural settings, no consistent trends were

- 96 -

distinguished (Appendix B) and the two types are not
separated in the analysis which follows.

Average biotite analyses for each metamorphic zone are
graphically represented in Figure 31, from which several
important and distinct trends in biotite composition can be
seen. Mg-contents increase slightly (by about 1%) at the CZ.
Above the CZ Mg-content is roughly constant. Fe-content
(Fe-total) declines at the CZ and declines steadily until
the SZ, where it again increases. Fe-contents of biotite
from the S*Z are lower than those of biotites in muscovite
bearing rocks (SZ).

M/FM ratios of biotite are illustrated on an AFM diagram
and plotted versus metamorphic grade in Figure 32. Biotites
from the WBZ have lower M/FM ratios than those from the
eastern zone. Biotite analyses connected by the arrow in
Figure 32 are from the EBZ and CZ, immediately below and
above the cordierite isograd respectively. Biotite is most
Mg-rich adjacent to the CZ, but within the CZ biotite shifts
to more Fe-rich and more aluminous compositions (see below).

In Figure 28 it can be seen that X_{Mg} biotite is less
than X_{Mg} chlorite and muscovite and X_{Mg} ratios of coexisting
chlorite-biotite show an approximately linear distribution
(similar to the results of Cooper, 1972). The lack of a
linear relationship between X_{Mg} muscovite and biotite is
contrary to the results of Evans and Guidotti (1966) and
Butler (1967) and may be due to the presence of an other
element (eg Fe^{3+}) in one or both micas. Both minerals show a

Figure 31: Variation in biotite composition with metamorphic grade. Data shown as oxide percent from analyses presented in tables. FeO = total Fe. Ticks on data points indicate number of analyses: 0 ticks = 1 analysis, 1 tick = 2 analyses, 2 ticks = 3 analyses. Average (large open circle) does not include data points represented by open squares (Mg-rich samples adjacent to the CZ). For abbreviations see page xv.
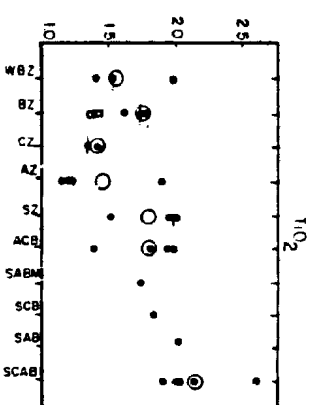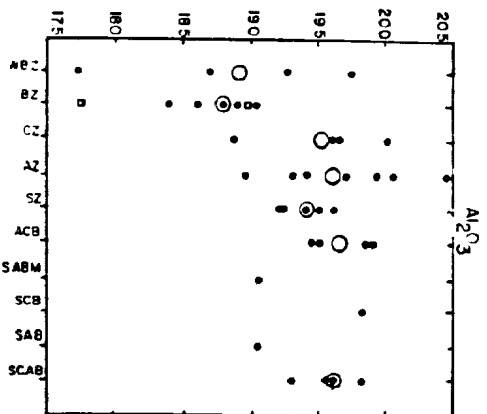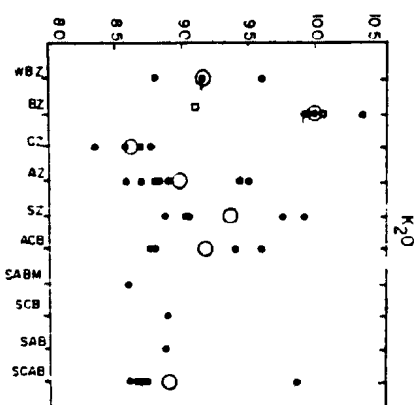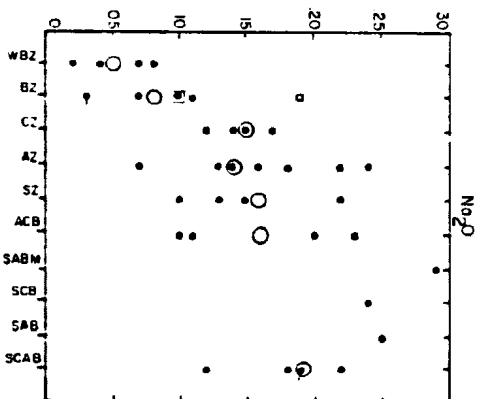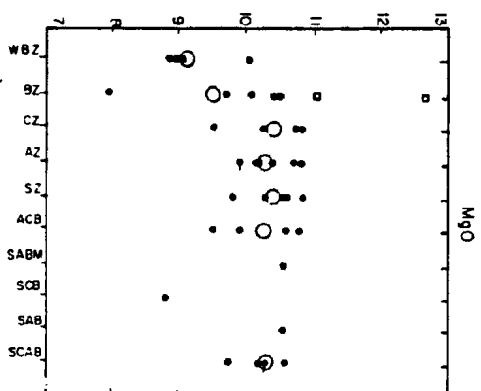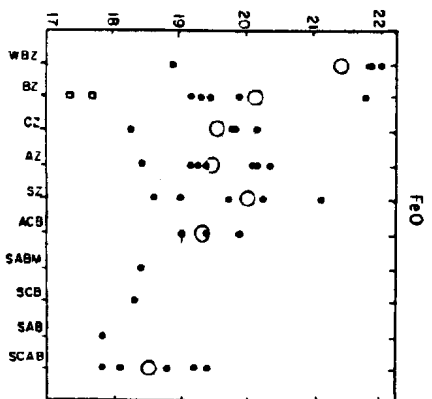
Figure 32: Variation in M/FM ratio of biotite with

metamorphic grade. (A) AFM projection of biotite

compositions from various metamorphic grades.

Arrow in this diagram represents change in

biotite composition with the formation of

cordierite, connecting samples from immediately

below and at the cordierite isograd. Inset

diagram shows the portion of the AFM diagram used

for plotting.

(B) M/FM ratios of biotite plotted against

metamorphic grade. Average (open circle) does

not include data points shown as open squares

(see Figure 31). For abbreviations see page xv.
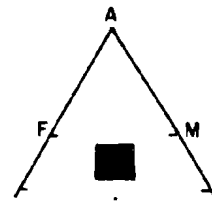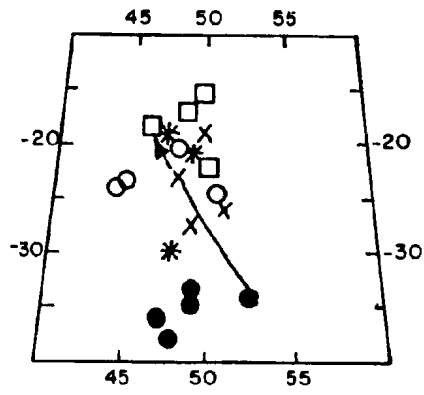
A
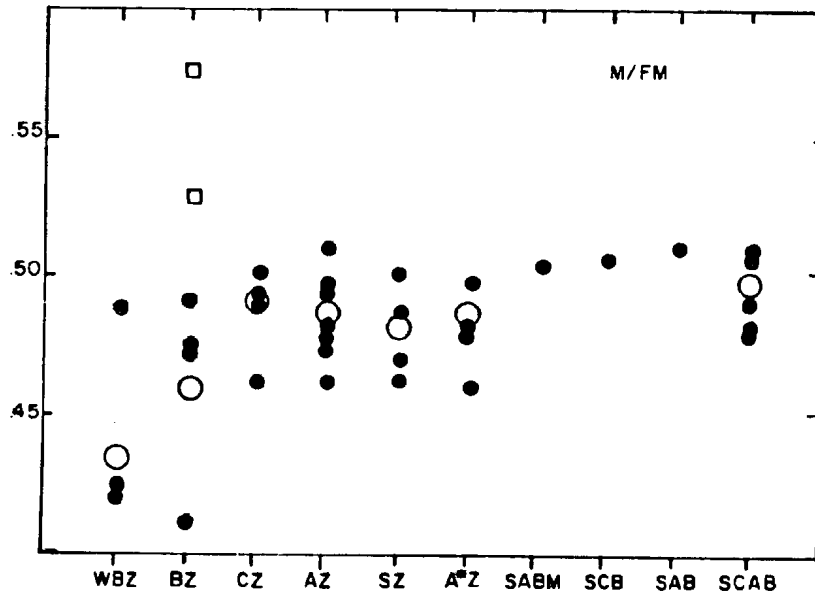
B

general trend toward increasing M/FM values with increasing metamorphic grade.

Total Al contents in biotite generally increase throughout the metamorphic sequence, although a slight decrease is noted in the SZ (lower Al^{vi} content). The AFM diagram (Figure 32a) shows a distinct jump in total Al at the CZ. The introduction of an Al-rich phase (cordierite and/or aluminosilicate) indicates that the rock is Al saturated and biotite is then as Al-rich as possible. Biotites from the assemblages lacking andalusite (i.e. CZ and some of the S*Z) have the highest octahedral Al contents.

Biotite shows a trend toward increasing Ti-content with metamorphic grade (Figure 31), similar to the trend for muscovite. Ti-contents of both micas decrease slightly at CZ. In some S*Z biotites there is an abrupt increase in Ti.

Total Y-site (Fe, Mg, Al^{vi}, Ti, Mn) occupancy is highest for biotites from the CZ and lowest in the BZ and muscovite-free A*Z and S*Z assemblages.

Deficiencies in X-site alkali cations are apparent in all analyzed biotites and appear to vary with metamorphic grade, with biotite from low-grade rocks being nearest to ideal (Figure 31). Total alkali content decreases at the CZ, but subsequent increases in the AZ and SZ are slight and decreases are noted in the S*Z. The small amount of Na present in the biotites shows systematic and continuous increases with metamorphic grade in all the muscovite-

bearing assemblages. Biotites contained within cordierite porphyroblasts are slightly enriched in K relative to biotite in the matrix (Appendix B).

The abrupt decrease in K-content of biotites at the CZ is puzzling, as K in muscovites also decreases. Since the micas are the only abundant and significant K-bearing phases, the coupled decline implies that K may have been removed from the rock system, but another possibility is that there may have been an increase in the total mica content (see 2.4.3).

Other evidence of K-loss comes from some SZ rocks in which biotite has been completely retrogressed to chlorite, except in the immediate vicinity of andalusite relics and sillimanite. These altered rocks define a patchy zone 1-2 km from a major fault. Thus retrogression may be due to the migration of fluids through an extensive microfracture system, suggesting that these rocks may not have behaved as a closed system with respect to K.

2.5.7 Cordierite

The structural formula for cordierite is calculated on the basis of 18 oxygens. Oxide weight percents may be up to approximately 2% less than 100% and, because the cation totals per structural formula are very close to the ideal 11, this deficiency is attributed to the presence of fluids. The analyzed cordierites contain minor quantities of Na (0.04 to 0.07 atoms per formula unit). Cordierite from all

zones is the most Mg-rich phase present, having higher M/FM ratios than coexisting biotite and muscovite (Figure 33). In addition, cordierite is the only ferromagnesian mineral in the analysed assemblages (of greywacke compositions) other than chlorite to contain small but significant amounts of Mn.

The main compositional changes in cordierite examined in this paragenetic sequence are variations in MgO and FeO contents (Figure 34). M/FM ratios (not shown) increase slightly throughout the CZ, AZ and SZ and cordierite in the S*Z has the highest M/FM ratio. A*Z cordierites have higher FeO contents and the lowest average M/FM ratios.

It is of interest to note that in many samples cordierite porphyroblasts show evidence of alteration (pinnitization). In thin section this alteration is generally readily visible and restricted to porphyroblast rims or fractures within the porphyroblast. Microprobe analyses of the altered portions of cordierite yielded variable results which are presented in Appendix B. In addition, several analyses of one visually unaltered cordierite porphyroblast yielded consistently nonstoichiometric results (Appendix B) which appear to be the result of incipient pinnitization.
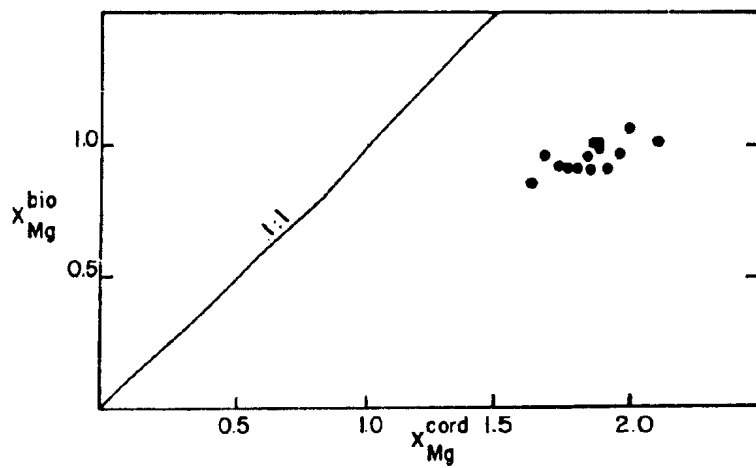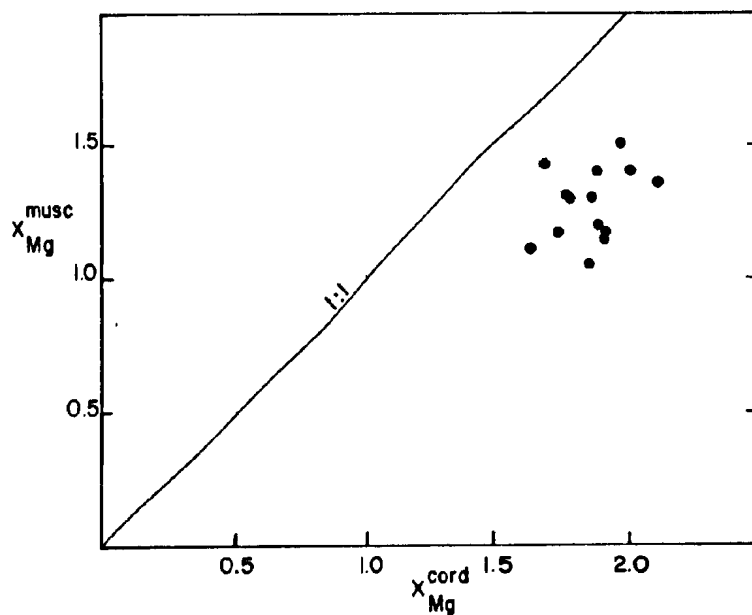
Figure 33: X_{Mg} $(= Mg / Mg + Fe)$ in biotite (A) and muscovite (B) plotted against that in cordierite. Fe = total iron.
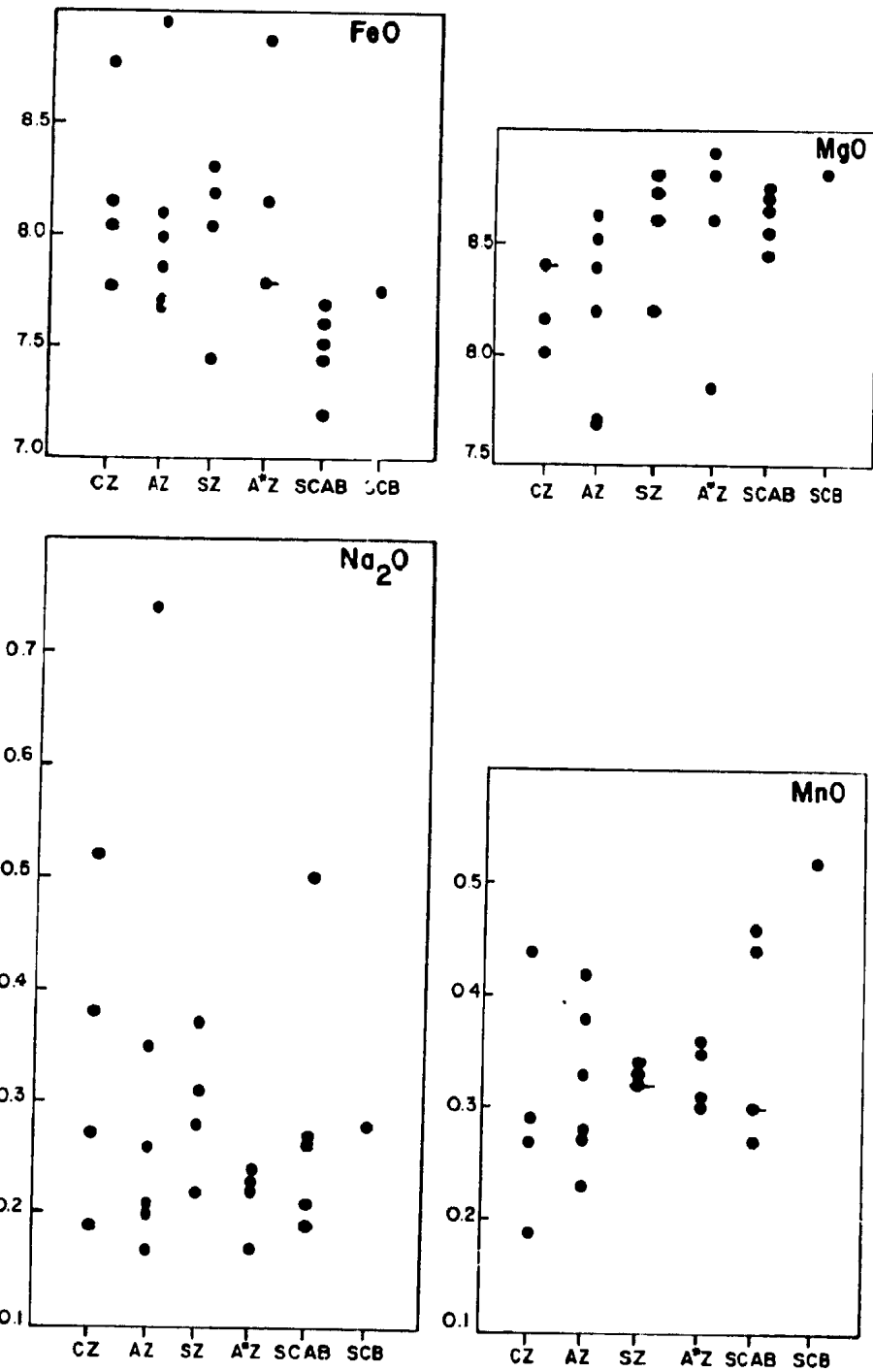
Figure 34: Variation in cordierite composition with metamorphic grade. The main
compositional changes are in FeO and MgO contents. Ticks indicate more
than one data point (see Figure 22). Abbreviations as page x v.

2.6 The Approach to Equilibrium

2.6.1 General Statement

Several factors must be considered in determining whether the rocks attained or approached equilibrium during metamorphism: a) textural evidence; b) the number of phases represented in the mineral assemblages; and c) chemical evidence and element partitioning between coexisting phases. Features suggestive of disequilibrium in the Keskarrah Bay suite include:

1. The presence of two microstructurally distinct chlorites in the WCHZ and WBZ rocks.

2. Retrogression of biotite to chlorite and cordierite and andalusite to chlorite and sericite.

3. Detrital plagioclase grains in some low-grade rocks (particularly the CHZ) have ragged grain boundaries and are partly altered to sericite.

4. Partial conversion of andalusite to muscovite, biotite, plagioclase or sillimanite and cordierite to sillimanite.

5. The ragged appearance of some biotite grains within cordierite porphyroblasts.

6. The metastable persistence of andalusite in the presence of sillimanite, resulting in four phases in AFM space.

7. The lack of systematic and consistent element partitioning (eg. Mg-Fe) between some coexisting phases.

Features suggesting achievement of equilibrium include:

1. Sharp grain contacts are generally observed between the various phases (even in the case of andalusite rims on cordierite) and most of the phases are found in mutual contact.

2. The absence of detrital grains from medium-grade rocks and portions of the BZ.

3. Most assemblages can be reasonably represented on phase diagrams.

4. Compositional zoning of the minerals has not been recorded.

5. Some coexisting phases are shown to have systematic and consistent element partitioning (eg. Mg-Fe; see above).

In the medium-grade rocks much of the evidence for disequilibrium is probably due to retrograde metamorphism. In most cases however, retrograde mineralogies can be distinguished petrographically from the minerals representative of the prograde event, and therefore retrograde effects can be eliminated from the discussion that follows. In the low-grade rocks, particularly tnose of the western sequence, microstructures suggest a retrograde metamorphic event affected the rocks. This is of particular importance in defining the biotite isograd for these rocks, as in some rocks it is difficult to distinguish a CHZ rock that never formed biotite from a retrogressed BZ rock.

Textural evidence in part suggests metastability (points 2-6 above). The sluggish nature of the andalusite-sillimanite transition (Turner, 1981) may be responsible for

the presence of andalusite in the SZ, which is a common occurrence in many areas. The ragged nature of biotite contained within cordierite porphyroblasts may reflect rather rapid increases in metamorphic conditions, during which the minerals were unable to equilibrate, as suggested by Ramsay (1974).

2.6.2 Chemical Equilibrium

Numerous studies have documented that the distribution of elements between coexisting mineral pairs that have attained equilibrium varies in an orderly fashion as a function of P T and fugacity of the volatile constituents. In the pelitic rock system the variation and distribution of Mg and Fe between coexisting minerals is frequently a useful indicator of the attainment of chemical equilibrium.

The X_{Mg} values for the mineral pairs muscovite-chlorite, chlorite-biotite, muscovite-biotite, muscovite-cordierite and biotite-cordierite have been compared (Figures 28, 33). Table 3 contains X_{Mg} ratios for chlorite, muscovite, biotite and cordierite and Kd values for the mineral pairs of each metamorphic zone. These data establish the sequence of Mg:Fe as cordierite > muscovite >chlorite > biotite, which has been used to predict phase relations during progressive metamorphism (A.B. Thompson, 1976).

At constant P, T and fH_2O, the points on a Kd diagram should be distributed in a cluster (at constant rock composition) or show an approximately linear relationship

TABLE 3: X_{Mg} Ratios and Kd Values for Coexisting Mineral Pairs for All Metamorphic Zones

ZONE	Sample no.	XMg/Chl	XMg/Musc	XMg/Bio	XMg/Cord	KdMusc/Chl	KdChl/Bio	KdMusc/Bio	KdCord/Musc	KdCord/Bio
ECHZ	05a	.87	.99			1.14				
	277a	.87	.94			1.08				
WCHZ	105	1.91	2.14			1.12				
	392	1.46	2.07			1.42				
	108	1.33	1.19			.90				
	221	1 20	1.37			1.14				
	223	.84	1.01			1.20				
	225	1.82	2.15			1.18				
	395	.70	.77			1.10				
EBZ	01a	1.06	1.39	.89		1.31	1.19	1.56		
	199a	1.05	1.41	.97		1.34	1.08	1.45		
	200	.88	.81			1.22				
	201a	1.01	1.23	.91		1.10	1.11	1.35		
	201b	1.05	1.15	.97		1.01	1.08	1.19		
	2-33	1.18	1.42	1.11		1.20	1.06	1.28		
WBZ	112	.80	1.34	.72		1.68	1.11	1.86		
	396	1.03	1.42	.95		1.40	1.08	1.50		
	398	.79	.87	.74		1.10	1.07	1.18		
	373	.93	1.21	.72		1.30	1.29	1.68		
CZ	2-54b		1.20	.97	1.87			1.24	1.56	1.93
	2-3		1.10	.86	1.63			1.28	1.48	1.90
	132		1.05	.95	1.84			1.11	1.75	1.94
	2-163		1.39	1.00	1.87			1.39	1.35	1.87
AZ	439		1.43	.96	1.67			1.49	1.17	1.74
	2-176		1.39	1.05	1.98			1.32	1.42	1.89
	427		1.17	.90	1.91	1.30	1.63	2.12		
	2-173		1.16	.98	1.90			1.18	1.64	1.94
	39		1.16	.92	1.73			1.26	1.49	1.88
	2-22b		1.31	.89	1.75			1.47	1.34	1.97
SZ	2-21		1.51	.95	1.95			1.59	1.29	2.05
	342		1.63	.97			1.68			
	346		1.36	1.01	2.09			1.35	1.54	2.07
	340		1.28	.89	1.84	1.44	1.44	2.07		
	307		1.28	.88	1.78	1.46	1.39	2.02		

Average Kd Values:	WCHZ	ECHZ	WBZ	EBZ	CZ	AZ	SZ
KdMusc/Chl	1.22	1.11	1.36	1.18			
KdChl/Bio			1.14	1.10			
KdMusc/Bio			1.55	1.36	1.26	1.34	1.50
KdCord/Musc					1.52	1.43	1.41
KdCord/Bio					1.91	1.92	2.06

XMg mineral = (Mg/Mg+Fe+Mn) (Fe/Mg+Fe+Mn). Kd(Mg) = XMg(mineral A)/XMg(mineral B)

(rock composition varied) if equilibrium was attained or approached (Kretz, 1961; Bartholomé, 1962). Kd values for chlorite-biotite and cordierite-biotite pairs shown in Table 3 are comparable to those presented in Osberg (1971).

In contrast, Kd values for coexisting muscovite-biotite and cordierite-muscovite (Table 3; Figures 28, 33) are variable, suggesting chemical equilibrium was not attained. However, other indices that suggest an approach to equilibrium between these two mineral pairs are: 1) textural evidence, with muscovite being in contact with both biotite and cordierite; 2) average Kd values show systematic prograde changes (Table 3); and 3) the diffuse systematic variation seen in a plot of X_{Na} muscovite versus X_{Na} biotite (Figure 35; because of the jump in muscovite paragonite content at the CZ, the points in this plot tend to form two clusters). Thus there is a considerable body of evidence pointing to the fact that muscovite reached equilibrium with coexisting cordierite and biotite, and the irregularities observed in muscovite X_{Mg}, which influences the Kd values, may be related to other elements substituting for Fe and Mg in the muscovite crystal structure (McNamara, 1965).

Although the evidence is conflicting, it appears reasonable to assume that for the most part the rocks in the Keskarrah Bay area approached equilibrium. The observed equilibrium textures provide a basis for the proposed mineral - forming reactions and reaction mechanisms that follow.
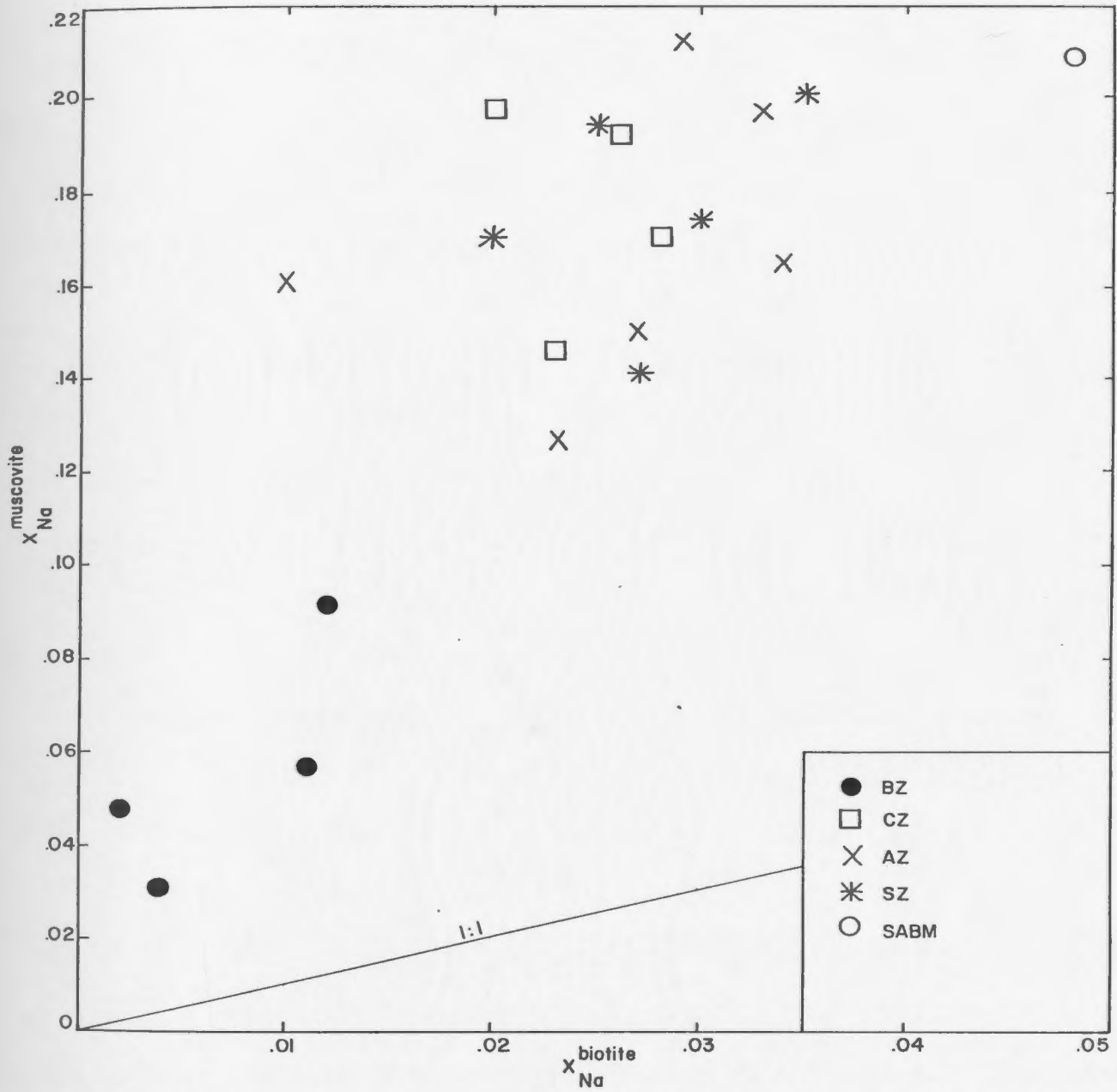
Figure 35 : X_{Na} (= Na / Na + K)   in muscovite plotted against that in biotite. Low-grade and medium-grade rocks form two distinct populations reflecting the increase in paragonite molecule in muscovites at medium grades.

2.7 Index Mineral-forming Reactions

2.7.1 General Statement

On the basis of textural and compositional evidence presented in the previous sections, the reactions leading to the formation of the index minerals are discussed below. In addition the metamorphic zones, which were previously identified according to the first appearance an index mineral, are renamed in full to correspond with the proposed metamorphic reaction. Because of the effects of retrograde metamorphism on the rocks from the western sequence, the reactions proposed in this section are based on data from the eastern prograde sequence.

As noted previously, the lowest grade rocks are characterized by the assemblage chlorite-muscovite-quartz-plagioclase; the CHZ is referred to in full as the muscovite-chlorite zone.

2.7.2 Biotite-forming Reactions

Above the biotite isograd the stable mineral assemblage is muscovite-chlorite-biotite-quartz-plagioclase, with the diagnostic sub-assemblage of the BZ being muscovite-chlorite-biotite.

Numerous reactions have been proposed in the literature to account for the formation of biotite in low-grade metapelites and metagreywackes. In the study area, in rocks

of both the CHZ and BZ, K-feldspar is either absent or present only in trace amounts, so the reaction proposed by Mather (1970), which involves K-feldspar could not have been significant. Thus some or all of the remaining minerals, chlorite, muscovite, plagioclase, quartz and the opaque phases (ilmenite and rutile) must have reacted to form biotite. A decrease in modal abundance of chlorite with the formation of biotite indicates that chlorite is consumed during this reaction. The data also indicate that chlorite became Mg-richer as a result of the reaction.

Since muscovite is the only K-rich phase present in CHZ rocks, it must have either been consumed to produce biotite or, as Tilley (1926) suggested, it may have contributed K for the production of biotite, leaving a K-poorer muscovite in the BZ. The data are inconclusive with respect to changes in celadonite content of muscovite with the appearance of biotite: some BZ muscovites are less celadonitic than CHZ muscovites, as would be expected if (Mg+Fe+Mn) was depleted and contributed to the production of biotite (Ernst, 1963; Ramsay, 1973a,b; Guidotti and Sassi, 1976), but others are more celadonitic. Therefore it seems unlikely that muscovite (celadonite) contributed significant Mg or Fe for the production of biotite. However, ilmenite is ubiquitous to both the CHZ and BZ and may have been consumed in small amounts to contribute Ti and Fe to the production of biotite.

An-contents of plagioclase change in the BZ, with albite compositions being subordinate to oligoclase. However, it has not been ascertained whether plagioclase plays a role in biotite formation.

Considering the evidence presented above a generalized biotite-forming reaction for these rocks could have had the form:

Fe-chlorite + muscovite +/- ilmenite = biotite + quartz +/- magnetite + H_2O (R.1)
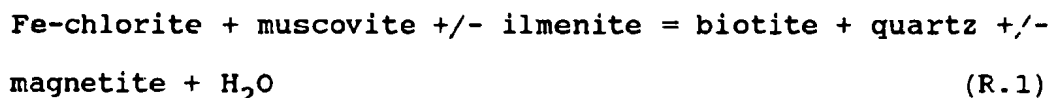
where the involvement of ilmenite as a reactant requires that some magnetite be produced or that oxygen is a product (i.e. bulk reduction of the rock). Reaction R.1 is similar to that proposed by Ramsay (1973a), with the exception that K-feldspar is not a by-product.

2.7.3 Cordierite-forming Reactions

CZ rocks are characterized by the assemblage cordierite-biotite-muscovite-quartz-plagioclase and thus are referred to in full as the cordierite-biotite-muscovite zone.

The formation of cordierite through the frequently proposed reaction involving chlorite + muscovite + aluminosilicate as reactants (Hess, 1969) is not tenable in the study area since low-grade rocks are not seen to contain an aluminosilicate phase. The bulk composition of the rocks plots below the muscovite-chlorite tie line in AKF diagrams

and within the chlorite-biotite two-phase field in AFM
diagrams (Figure 7). Thus it is possible that the formation
of cordierite took place by a continuous reaction of the
type:

muscovite + chlorite + quartz = cordierite + biotite + H_2O

(R.2)
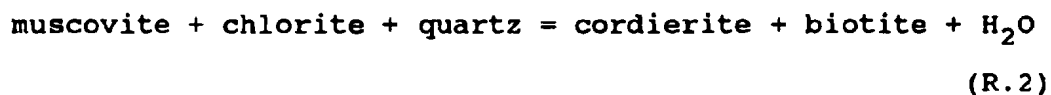
which is consistent with the measured intermediate X_{Mg} of
chlorite compared to those of the products biotite and
cordierite. This is a crossing tie line reaction in AKF
space (Figure 36). According to Schreyer and Yoder (1961),
Hess (1969) and Seifert (1970) the cordierite-biotite two-
phase field progressively moves to more Fe-rich compositions
with increasing T, sweeping across the cordierite-biotite-
chlorite three-phase subtriangle (Figure 37a). However, in
the present case Fe-chlorite was already consumed by
reaction R.1, leaving only relatively Mg-rich chlorite
remaining for reaction R.2. The absence of chlorite in CZ
rocks is interpreted to indicate that reaction R.2 took
place during the initial stages of cordierite formation,
while Mg chlorite was still available. However, it is likely
that a significant proportion of cordierite was produced by
a reaction involving biotite and muscovite, which are both
present below the cordierite isograd. It has already been
noted that biotite is commonly depleted within cordierite
porphyroblasts relative to the matrix and that biotite
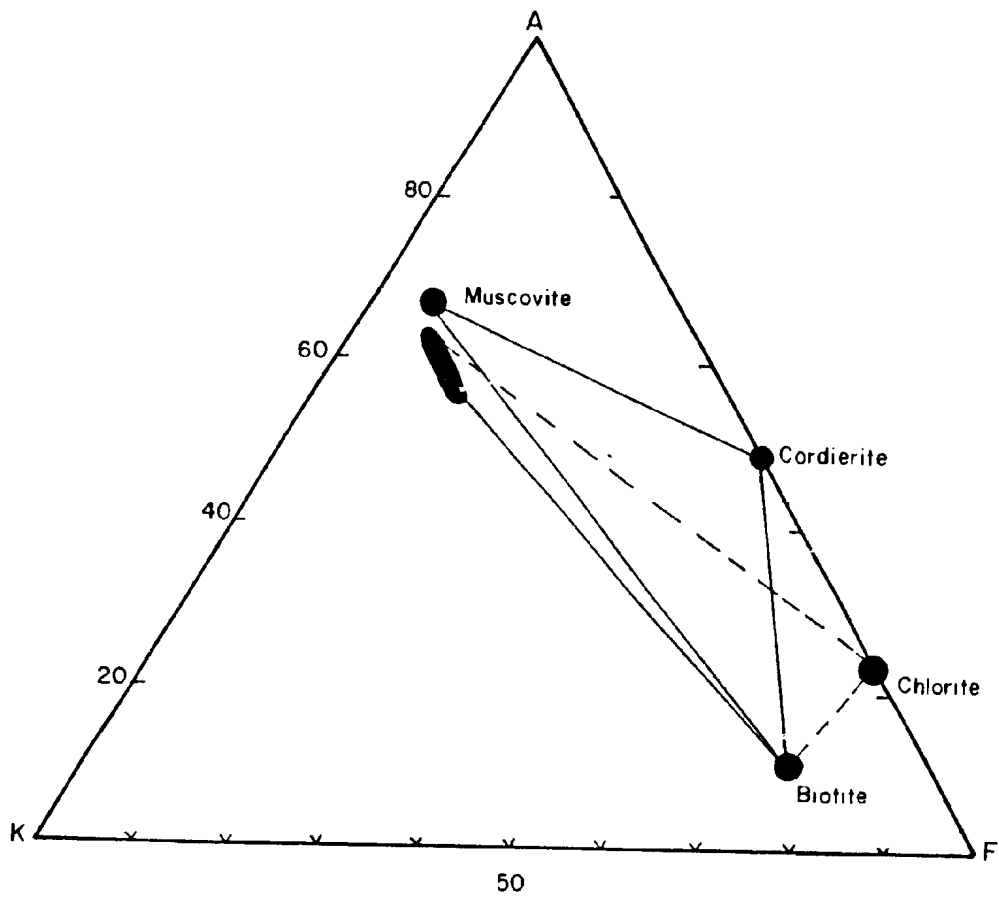
Figure 36: AKF diagram illustrating the changes in tie line topology with the formation of cordierite by reaction R.2.

Figure 37: AFM projections of continuous and discontinuous
reactions leading to the formation of cordierite
(reaction R.3, a-b), andalusite (reactions R.4
and R.5, b-c) and sillimanite (reactions R.6 and
R.7, d). Arrows indicate the direction of
subtriangle migration across AFM face during
continuous reactions. X is the inferred bulk
composition of average metagreywackes in the
Keskarrah Bay area (as explained in section 2.3).

(a)

(b)

(c)

(d)
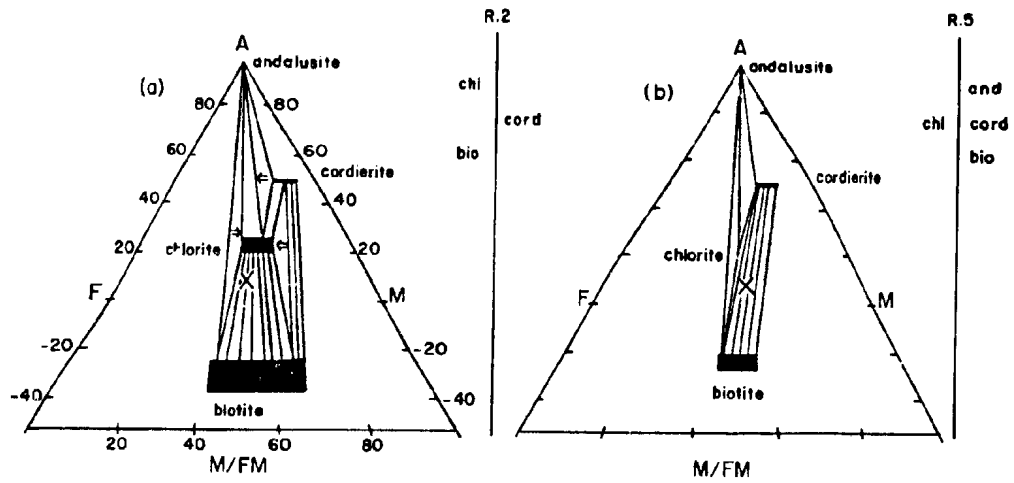
All assemblages include quartz, muscovite, plagioclase and ilmenite. Bulk composition of the rocks (x).

with sillimanite, andalusite is metastable

- 119 -
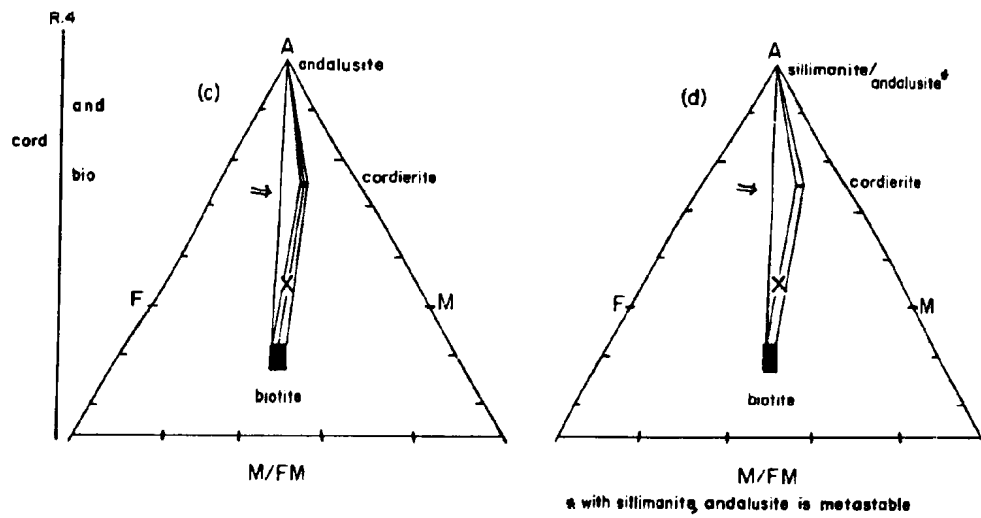
compositions change (becoming richer in Fe, Al and Na) across the cordierite isograd. Although muscovite displays little textural evidence of involvement in the cordierite-forming reaction, it decreases in modal abundance and also undergoes major compositional changes at the cordierite isograd (Figures 24 - 30, 35), becoming less celadonitic and containing a greater percent of the paragonite molecule. Thus reaction R.3 may describe the formation of some of the cordierite:

$$\text{Mg-biotite} + \text{muscovite}_1 = \text{cordierite} + \text{muscovite}_2 \qquad (R.3)$$
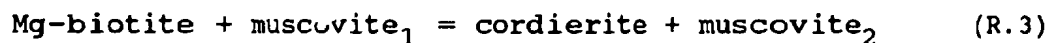
in which musc_1 is K-richer and more celadonitic than musc_2. However, although biotite involvement is implied by the textures, there is no significant change in M/FM biotite at the CZ (Figure 32b), which may imply that a significant proportion of Mg and Fe for cordierite came from celadonitic muscovite, as indicated by the analyses (Figures 24, 29a). Seifert (1970) suggested that phengite-poor muscovite will coexist with cordierite and phlogopite (biotite in this case), which is supported by the data in this study.

Plagioclase does not appear to be involved in cordierite formation, but it may have contributed Na to muscovite and biotite (see sections 2.5.4 and 2.5.5).

Ilmenite forms abundant inclusions within cordierite and therefore does not appear to be a necessary phase in cordierite formation.

Reaction (R.2) is a continuous reaction (Thompson, 1978), the nature of which in AFM space is illustrated in Figure 37. Although chlorite is no longer present in the cordierite-bearing rocks of this study, it theoretically does not disappear from all bulk compositions in the AFM topology at this stage. As reaction R.2 continues, the cordierite-biotite-chlorite subtriangle migrates across the AFM face toward the F apex, resulting in the formation of cordierite first in more Mg-rich bulk compositions and later in more Fe-rich compositions. This movement of the subtriangle results in a shrinkage of the chlorite-biotite two-phase field at the expense of the cordierite-biotite two-phase field. In the study area the compositions of chlorite and biotite below the cordierite isograd and cordierite and biotite above the isograd indicate that the subtriangle encompasses a small area in AFM space (Figure 37). Thus only a slight shift of the tie lines toward the F apex is required to cross the bulk composition of the rocks, leaving only the assemblage cordierite-biotite. Reaction R.3, involving predominantly a change in the composition of muscovite, cannot be depicted in AFM space.

2.7.4 Andalusite-forming Reactions

The assemblage andalusite-cordierite-biotite-muscovite-quartz-plagioclase characterizes rocks of the AZ and these rocks are referred to in full as the andalusite-cordierite-biotite zone.

Since andalusite forms at higher grade than cordierite
and the concomitant disappearance of chlorite in the
paragenetic sequence, it is possible that it forms via a
reaction involving cordierite and/or muscovite as reactants.
This type of reaction was proposed for other areas of the
Slave Province (Heywood and Davidson, 1969; Thompson, 1978).
Heywood and Davidson noted that in such a reaction both
cordierite and muscovite would decrease in abundance while
biotite would increase.

In the rocks of this study, although partial rims of
andalusite on cordierite suggests that cordierite was in
some way involved in andalusite production, no change in the
modal abundance of cordierite has been recorded. Indeed it
appears that cordierite growth continued in the AZ
(cordierite rims on andalusite). Marginally increased M/FM
ratios of cordierite are the only noted compositional
changes in this mineral.

Textural evidence points to the fact that muscovite was
consumed during the formation of andalusite, but for the
most part this occurred only locally, i.e. in the precise
area that andalusite nucleated. Compositionally muscovite
records slight decreases in paragonite content and minor
increases in Fe and Mg. Presumably the consumption of some
muscovite to form andalusite left residual Fe and Mg (in
small amounts as the muscovites are not highly celadonitic)
that was taken up by the remaining muscovites.

Matrix muscovite was completely consumed in some rocks within the AZ (denoted A*Z). The disappearance of muscovite in these rocks is presumably related to the formation of andalusite, but possibly also cordierite, and suggests A*Z rocks are slightly less potassic than AZ equivalents.

Textural evidence also indicates that biotite was not a reactant in the andalusite-forming reaction and that possibly some new biotite was produced (biotite enriched zones around andalusite). Changes in biotite composition in the AZ include minor increases in Al, K and Ti contents (Figure 31) which may indicate that biotite accommodated some of the residual elements during the partial consumption of muscovite. Both Ti and K contents are higher in biotite from the A*Z than in the AZ equivalents, consistent with a decrease in the modal abundance of muscovite.

The proposed andalusite-forming reaction, which is compatible with textural and chemical evidence is:

cordierite + muscovite +/- ilmenite = andalusite + biotite + quartz +/- albite +/- rutile,   (R.4)
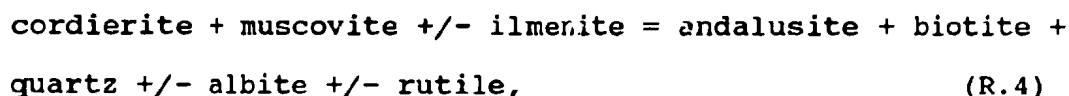
which is a modified version of that proposed by Heywood and Davidson (1969) and Thompson (1978).

The continuous nature of reaction R.4 in AFM space is illustrated in Figure 37. Andalusite is formed together with cordierite in more Fe-rich compositions once the stability field of chlorite is exceeded by the discontinuous reaction

chlorite + muscovite + quartz = cordierite + andalusite +

biotite + H_2O (R.5)
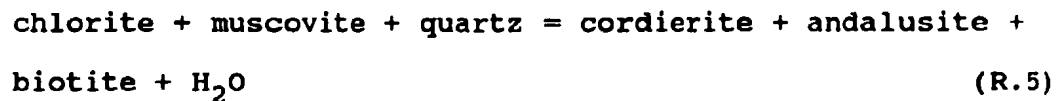
(Winkler, 1976; Thompson, 1978), allowing the coexistence of andalusite, cordierite and biotite. Reaction R.5 is a terminal reaction for chlorite in muscovite-bearing rocks (Hess, 1969) in that chlorite compositions are reduced to a single point in the diagram and subsequently chlorite is reacted out of the system. Although chlorite is not observed to be part of the equilibrium assemblage of either the CZ or AZ rocks in this study, Reaction R.5 may be responsible for the continued growth of cordierite within parts of the AZ. Once the three-phase subtriangle andalusite-cordierite-biotite is formed, it migrates toward Mg-richer compositions via progressive Mg-enrichment of coexisting cordierite and biotite (Figures 31 and 34).

The cordierite isograd is located down-grade of the andalusite isograd because the bulk composition of the rocks is sufficiently Mg-rich in this area that it is intersected by the cordierite-chlorite-biotite subtriangle rather than the andalusite-chlorite-biotite subtriangle (Figure 37).

2.7.5 Sillimanite-forming Reactions

The SZ, the highest grade zone in the study area, is characterized by the assemblage sillimanite+/-andalusite-cordierite-biotite-muscovite-quartz-plagioclase and is

referred to in full as the sillimanite-cordierite-biotite-muscovite zone.

Three reactions can be related to the formation of sillimanite. The direct polymorphic transition of andalusite to sillimanite, represented by sillimanite needles or prisms that have grown within andalusite porphyroblasts, is indicative of the reaction

andalusite = sillimanite   (R.6).

However this direct transition appears to have been rather rare.   Within the SZ the depletion of cordierite and muscovite and increase in relative abundance of biotite is consistent with the continuous reaction

cordierite + muscovite = sillimanite + biotite + quartz + H_2O (R.7)
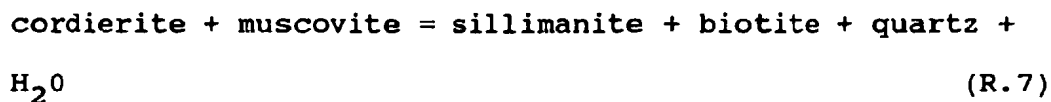
which is the sillimanite analogue of reaction R.4, and in which Fe-cordierite is progressively replaced by the product assemblage (see Tables A.8 and A.9; Figures 31 and 34). As a result of this reaction, many of the SZ rocks were found to lack muscovite in the equilibrium assemblage (S*Z), although some contain minor amounts of late muscovite. The consumption of muscovite in the S*Z led to the formation of more biotite and changes in biotite composition, most notably an increase in Ti-contents. Reaction R.7 has been

experimentally investigated by Seifert (1970) in the pure system KMASH. In the system KFMASH the reaction is continuous and results in the sillimanite-cordierite-biotite subtriangle shifting to more Mg-rich compositions (Figure 37), as indicated by increasing M/FM ratios of cordierite. Eventually the subtriangle breaches the bulk composition of the rocks leaving the two-phase assemblage sillimanite (+/-andalusite) - biotite.

In muscovite-free S*Z assemblages, sillimanite growth appears to have occurred by an indirect process involving plagioclase, biotite, quartz and relict muscovite as intermediary phases in a set of complex cation exchange reactions of the type first described by Carmichael (1969). The textural features within the felsic clots (see 2.4.5), which provide microstructural evidence of these exchange reactions are summarized as follows:

1. Andalusite is replaced by biotite and is partly surrounded by coarse-grained quartz. Sillimanite nucleates on biotite at some distance from andalusite (Figure 19).

2. Andalusite is embayed by biotite and coarse-grained plagioclase (Figures 19,20) and in some instances biotite in turn is embayed by plagioclase. Plagioclase and quartz may form a conspicuous rim around andalusite. Sillimanite needles or prisms nucleate on biotite and within plagioclase and quartz (Figure 19). A residual opaque phase can be seen within sillimanite-biotite aggregates. Eventually the site once occupied by andalusite is marked by a coarse-grained

aggregate of plagioclase and quartz, that contains
sillimanite prisms and locally minute andalusite relics
(Figure 20) and may have a biotite-fibrolite rim.

3. Andalusite is replaced by biotite. Large muscovite
plates and peripheral coarse-grained plagioclase engulf
andalusite and partly digested biotite (Figure 20).
Sillimanite prisms have grown in both muscovite and
plagioclase and nucleated on biotite.

4. In one sample coarse-grained tourmaline is associated
with 2 and 3; tourmaline is replaced by biot:.te and
fibrolite has nucleated on both biotite and tourmaline.

2.8 Iron Formation and Iron-rich Metasediments

2.8.1 Introduction

Discontinuous layers of iron formation and iron-rich
sediments (unit 9c), generally less than 1-2 meters thick,
are interlayered with turbidites of the Contwoyto Formation
(Figure 5). Henderson and Easton (1977a) and Bostock (1980)
described the facies variation and distribution of iron
formation in the Keskarrah Bay area.

Minerals developed during metamorphism of iron-rich
metasediments (unit 9c) include garnet, staurolite, biotite,
chlorite and Ca and Fe-Mg-Mn amphibole. The presence of
amphibole in iron formation rather than garnet or staurolite
is a result of less aluminous bulk rock composition. In
general there is a gradation between turbiditic sediment and

sulfide-bearing amphibolitic iron formation, which may
include intermediary compositions such as iron-rich
turbidites and sulfide-bearing pelitic iron formation (see
section 2.8.5 and Ford, 1988). In this study the effects of
metamorphism on iron formation are focused mainly on data
obtained from the more aluminous, pelitic compositions,
although several amphibole-bearing iron formations are
described. Bostock (1977) investigated low-alumina,
amphibole-bearing iron formation from the Itchen Lake
region.

2.8.2 Amphibole-bearing Iron Formation

Three samples of amphibole-bearing iron formation were
examined: two samples (82-V-58a, 76a) are from the BZ and
one (81-V-36b) is from the AZ (see Appendix A for sample
locations). The amphiboles of both BZ samples are blue-green
and form coarse-grained radiating porphyroblasts. In sample
82-V-58a, these porphyroblasts are partly rimmed by
colorless amphibole and are set in a fine-grained matrix of
biotite, chlorite, quartz and feldspar. Epidote also occurs
within a calcite-rich layer. In sample 82-V-76a,
Ca-amphibole porphyroblasts are concentrated in layers,
where they are set in a matrix of felt-like mats or
aggregates of biotite which enclose recrystallized detrital
grains of quartz and feldspar. The amphibole-rich layers are
interbanded with fine scale quartz-magnetite layers, in

which there is only minor amphibole. Magnetite is the only opaque phase identified in both samples.

Analyses of amphibole-biotite pairs are given in Table A.10. In 82-V-76a the Ca-amphibole is ferro paryasitic hornblende (Leake, 1978), whilst in 82-V-58a cummingtonite-grunerite (63% grunerite end member) occurs. Coexisting biotite from both samples is Fe-rich; M/FM values are 0.30 and 0.34. Plagioclase in 82-V-58a is oligoclase (An 20).

At medium grades garnet is commonly associated with amphibole-bearing iron formation, an association that was also noted by Bostock (1977) in the Itchen Lake region. One sample (81-V-36b) examined from the AZ contains garnet and brown amphibole (probably gedrite). The amphibole is altered to an Fe-rich brown-orange chlorite and garnet and biotite are also chloritized. Analyses of garnet, biotite and the altered amphibole are given in Table A.10. Both ilmenite and pyrrhotite are also present.

Both amphibole analyses presented above are from the BZ, hence the data does not allow an examination of either the variation in amphibole composition or mineral assemblage with metamorphic grade. For this reason some of Bostock's (1977) results are included here. Bostock (1977) analysed the compositions of coexisting hornblende-grunerite, hornblende-grunerite-garnet and hornblende-cummingtonite from silicate iron formation in the Itchen Lake region, in an attempt to determine any variation in Mg-Fe partitioning

between amphiboles that might reflect changes in metamorphic grade. He found that "the degree of alumina contamination of the iron formation beds is probably the predominant factor affecting the Fe-Mg distribution in amphiboles..." and listed the important factors governing the composition of the amphiboles as: 1) the Mg/Fe ratio of the iron formation layer; 2) the alumina content of the layer, which affects the distribution of Fe-Mg in coexisting amphiboles through the degree of alumina substitution in Ca-amphibole; 3) the occurrence of Fe-rich garnet, which produces higher Mg/Fe ratios in coexisting amphiboles and; 4) oxygen fugacity (the influence of this significant factor was not examined by Bostock because Fe^{3+} determinations were not of high enough accuracy).

2.8.3 Chlorite - Biotite Zone

The low-grade iron-rich samples examined are fine-grained shales or mudstones consisting predominantly of chlorite with lesser biotite, quartz and plagioclase. Some samples contain trace amounts of K-feldspar. Muscovite is either present in small quantities or absent from these assemblages. Two of the samples (81-V-122, 137) contain abundant hematite and carbonate.

Analysed chlorites and biotites are enriched in Fe relative to those from metagreywackes (Table A.11, Figure 38). Where muscovite is present it is celadonitic and Fe-rich, containing 3-4% FeO (total Fe as FeO). In Fe-rich
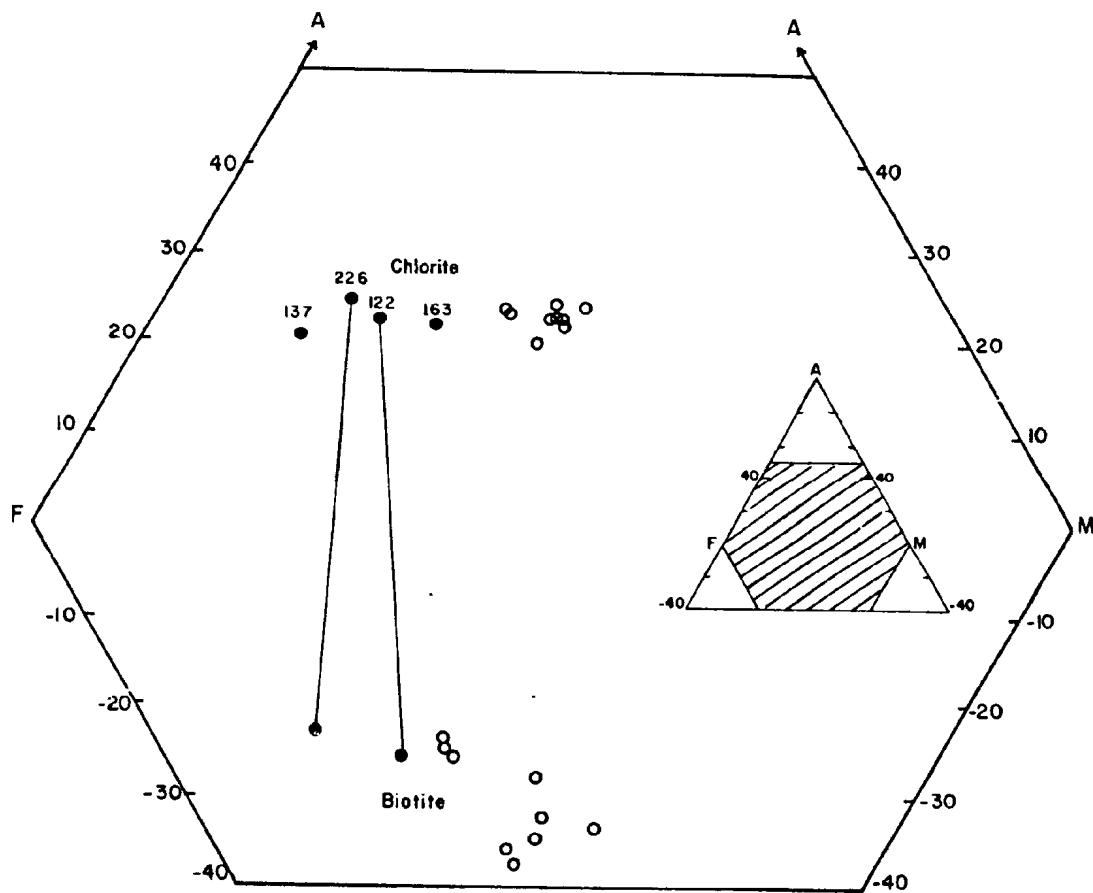
Figure 38: AFM projection showing M/FM ratios of chlorite and biotite from low-grade iron-rich metasediments (solid circles) compared with those from metagreywacke compositions (open circles). Inset diagram shows the portion of the AFM diagram used for plotting.

bulk compositions, such as iron formation, biotite forms at lower grades than in greywackes. In AKF space (Figure 39) the muscovite-chlorite-biotite subtriangle is displaced toward the KF face in comparison with that for greywackes.

2.8.4 Garnet +/- Staurolite-bearing Assemblages

At medium-grades of metamorphism the iron formation and associated Fe-rich turbidites may contain garnet, staurolite, biotite, quartz, plagioclase, magnetite, ilmenite, pyrrhotite and rare K-feldspar. In addition cordierite, andalusite and sillimanite are also found in some of the Fe-rich metasediments, and in many of these cases garnet and staurolite are metastable relics. Garnet and/or staurolite-bearing assemblages are not observed prior to medium-grades (also noted by Bostock, 1977). The mineral assemblages observed in the medium-grade Fe-rich compositions are listed in Table 4 and mineral compositions for most of these assemblages are given in Table A.12. Coexisting minerals are depicted in AFM topology in Figure 40. Iron enrichment of the Contwoyto Formation turbidites adjacent to iron formation demonstrates that a range of bulk compositions exists. The degree of iron enrichment can be gauged both by the mineral phases present and by the Fe-Mg contents of these phases (see 2.8.5).

Figure 39: AKF diagram illustrating the modelled
relationship between the first appearance of
biotite, celadonite content of muscovite and rock
composition (adapted from Mather, 1970). In
iron-rich, low-alumina rocks (rock 1) biotite
coexists with celadonite-rich muscovite (M1). As
temperature increases the amount of celadonite
substitution in muscovite decreases, muscovite
compositions migrate toward the A - apex (M2 then
M3) and the muscovite-chlorite-biotite stability
field shifts so that progressively more aluminous
rock compositions become biotite bearing (rock 2
then rock 3).
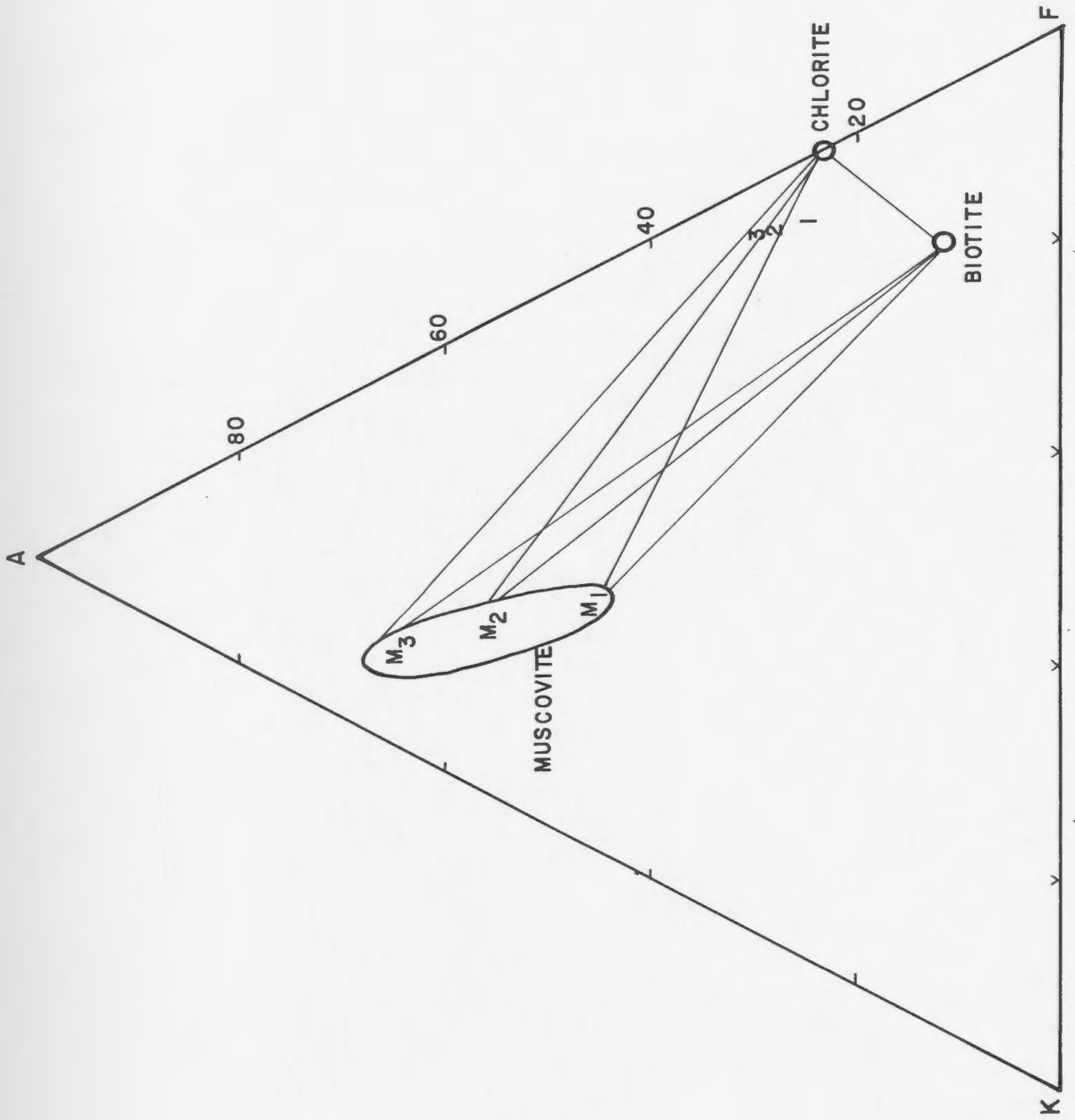
TABLE 4 : Observed Garnet +/- Staurolite-bearing Assemblages

```
Garnet   - biotite
Garnet   - biotite -      (staurolite)
Garnet   - biotite -      cordierite -  (staurolite)
Garnet   - biotite -      andalusite -  sillimanite - (staurolite)
Garnet   - biotite -      cordierite -  andalusite - sillimanite -
(staurolite)
Biotite - cordierite -(garnet)
Biotite - cordierite - sillimanite - (garnet)
Biotite - cordierite - sillimanite - (staurolite)
Biotite - cordierite - andalusite  - muscovite - (staurolite)
Biotite - cordierite - (staurolite) - muscovite*
Biotite - andalusite - sillimanite  - (staurolite) - (cordierite)
- muscovite*
Biotite - cordierite - andalusite -  muscovite
```

Minerals in brackets may represent metastable relics.
Asterisk (*) denotes post-tectonic muscovite

Figure 40: AFM projection of mineral assemblages in iron

formation and iron-rich metasediments. Method of

projecting through plagioclase for muscovite-free

assemblages is after Thompson and Bard (1982).

Assemblages have been plotted on several diagrams

to lessen tie-line overlap.

```
(A)  4 - sample 214b - staur- garn-bio
     5 - sample 23    - garn-bio
     6 - sample 383d - garn-bio
     7 - sample 38    - garn-bio
    10 - sample 39    - cord-bio-staur*
(B)  3 - sample 252  - cord-bio-garn*-sill**
     9 - sample 347a - and/sill-cord-bio-staur*
(C)  2 - sample 143  - garn-and-bio-staur*
         cord-and-bio-staur*
(D)  1 - sample 15a  - garn-and/sill-bio-staur*
     8 - sample 55h  - cord-and-bio-musc
    11 - sample 153  - cord-and/sill-bio-staur*
```

* relict phase
** sillimanite observed in outcrop and sample but
not in thin section.
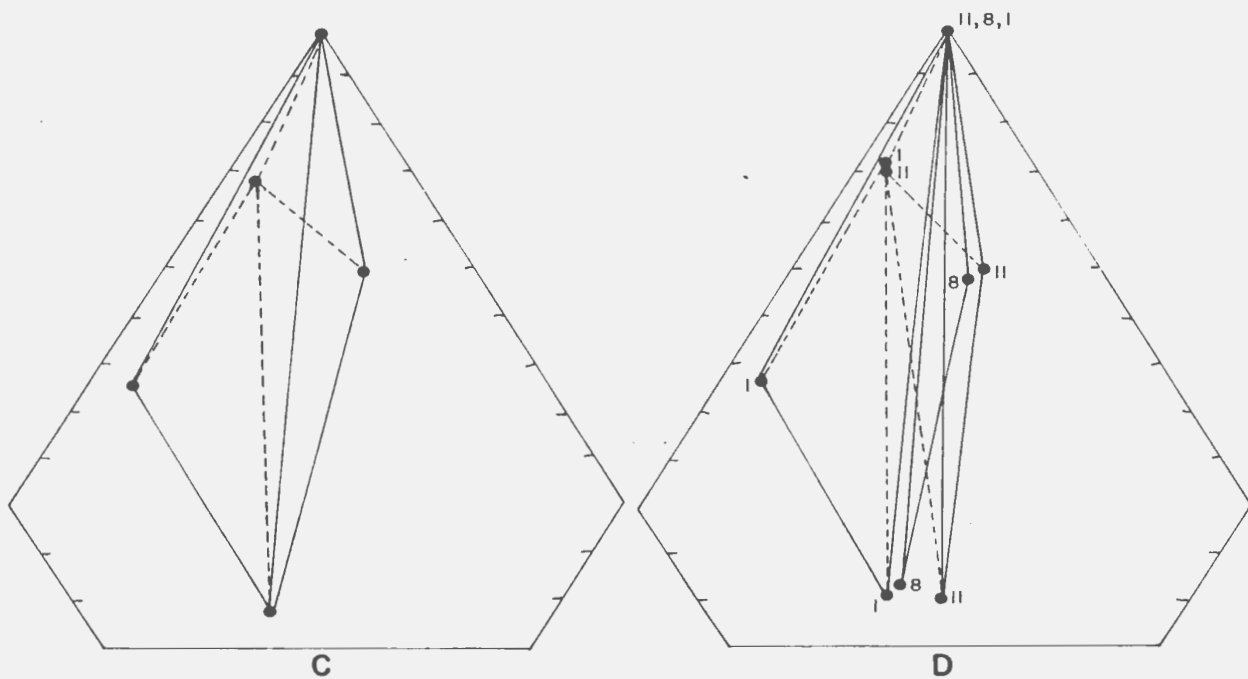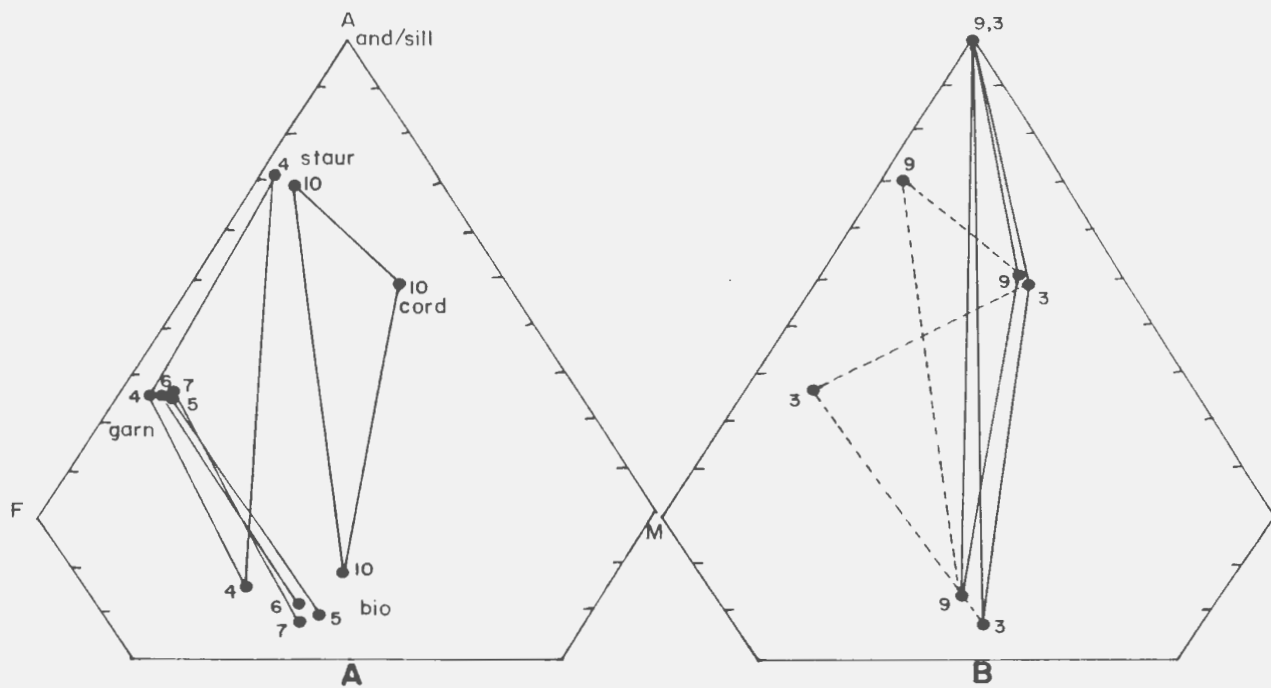
i) Garnet

Garnets vary from idiomorphic porphyroblasts contained within the quartzofeldspathic biotite-rich matrix or within andalusite porphyroblasts, to embayed relics surrounded by coarse-grained quartz and plagioclase in the matrix or in cordierite porphyroblasts. In one sample of the garnet-cordierite-biotite assemblage garnet is present as embayed relics in the matrix but as idioblastic porphyroblasts in a plagioclase-rich layer isolated from cordierite. Rotation of some garnets with respect to the external matrix foliation is apparent, although other garnets completely overgrow the matrix fabrics.

Garnet is the most Fe-rich phase present in these rocks, consisting of 75-87% almandine molecule (Table A.12). Garnets from the assemblages garnet-biotite and garnet-staurolite-biotite tend to be the most almandine-rich, while those found in cordierite-bearing assemblages have higher pyrope contents (Table A.12). The garnets are commonly zoned; inclusion-rich cores are surrounded by inclusion-free rims with locally a dusting of opaques (rutile/ilmenite?) delineating cores from rims. Compositionally the cores usually contain more Ca and Mn and less Fe and Mg than the rims (Table A.12), exhibiting normal zoning (Hollister, 1966). One garnet (81-V-383d) was found to be compositionally homogeneous, containing no discernible or consistent chemical trend from core to rim. Garnet from

sample 81-V-38 shows a trend toward more Fe and Ca and less Mn and Mg in the core than in the rim.

ii) Staurolite

Staurolites range in size from 5 mm poikiloblasts to much less than 0.1 mm relics, and are rarely idioblastic in outline. Small embayed or subidioblastic twinned crystals of staurolite are found within xenoblastic cordierite, where they form armored relics (Figure 41). Staurolite relics within the matrix and less commonly within cordierite, are often embayed by coarse-grained quartz, plagioclase and biotite and in some samples are associated with randomly oriented chlorite laths.

In a sillimanite-bearing sample (81-V-15a), staurolite is embayed by and included within andalusite porphyrcblasts (Figure 42). In the matrix of this sample staurolite is surrounded by coarse-grained plagioclase crystals. Garnet from this sample is idioblastic.

Staurolite is partly replaced by garnet in sample 81-V-214b. Here, staurolite is pre/syn-biotite schistosity; garnet on the other hand post-dates the biotite schistosity. The foregoing relationships suggest that staurolite formed prior to garnet in this rock.

Variations in staurolite composition are dependent on the associated mineral assemblage (Table A.12, Figure 40); staurolite coexisting with garnet-biotite has the lowest

Figure 41: Photomicrograph of staurolite relics in
          cordierite. Plane light. Length of section shown
          approximately 2.9 mm.

Figure 42: Photomicrograph showing staurolite embayed by
          andalusite and subidioblastic garnet
          porphyroblasts in andalusite. Crossed nicols.
          Length of section shown approximately 3.0 mm.
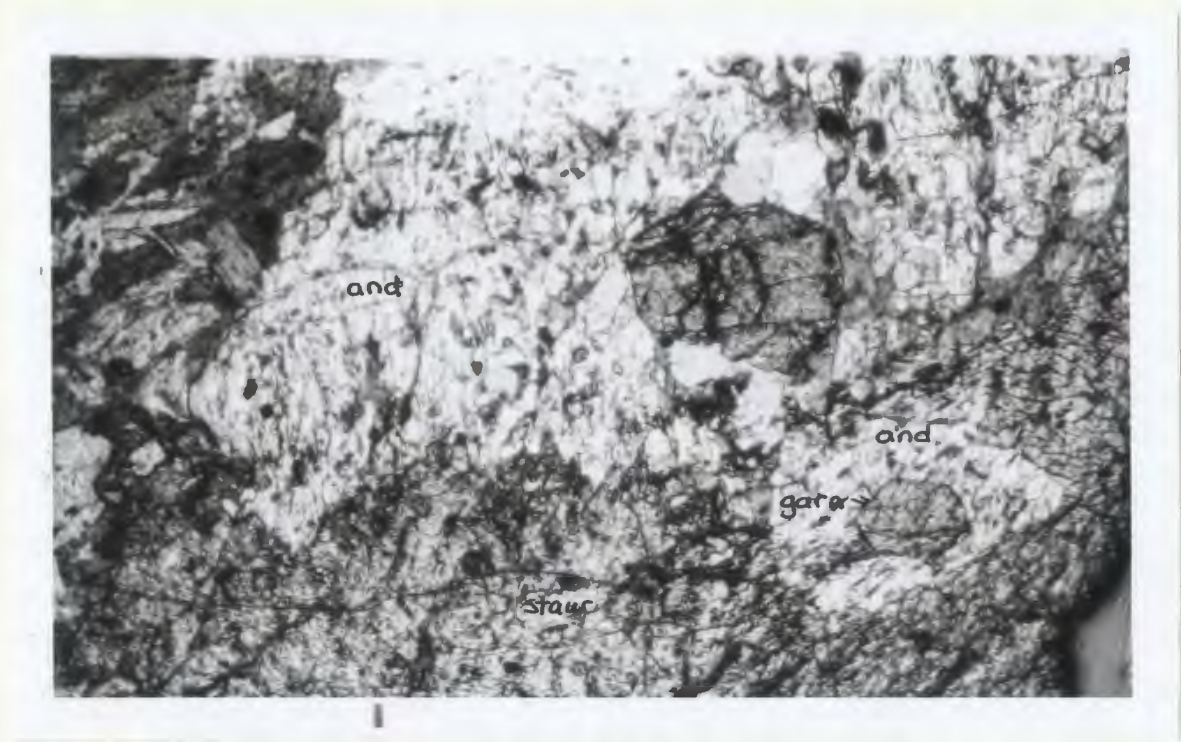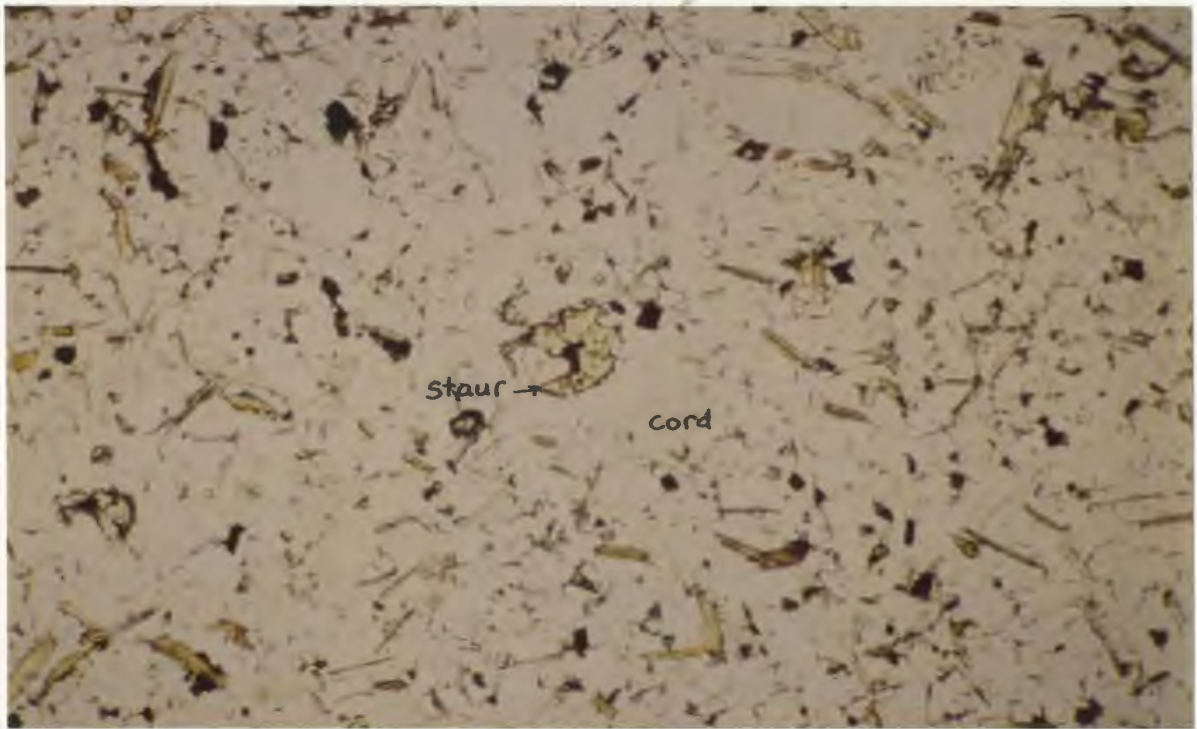
M/FM ratio, while that from cordierite and/or aluminosilicate-bearing assemblages is more Mg-rich.

iii) Biotite

In many instances biotites from the Fe-rich rocks have lower M/FM ratios than those in the muscovite-bearing greywackes (Figure 43). The most Fe-rich biotites are found in the assemblage garnet-staurolite-biotite, while the most Mg-rich occurs with garnet and cordierite (Table A.12, Figure 40, 43). In the remaining assemblages M/FM ratios of biotite in iron formation and greywacke may differ only slightly.

2.8.5 Compositional Considerations

The mineral assemblages that have been described do not represent a single, uniformly Fe-rich composition: they are representative of a range of compositions. This is because of the variable degree of iron enrichment of the interlayered greywacke rocks. The mineralogical effect of this progressive enrichment is illustrated below.

Whether or not the iron enrichment of the greywackes is primary or metamorphic cannot be determined from the data presented in this study. However, Ford (1988) carried out a thorough geochemical investigation of iron formation in the Slave Province (including the Tree claims found in this study area). He concluded that the progression from bordering metasediments to pelitic iron formation to
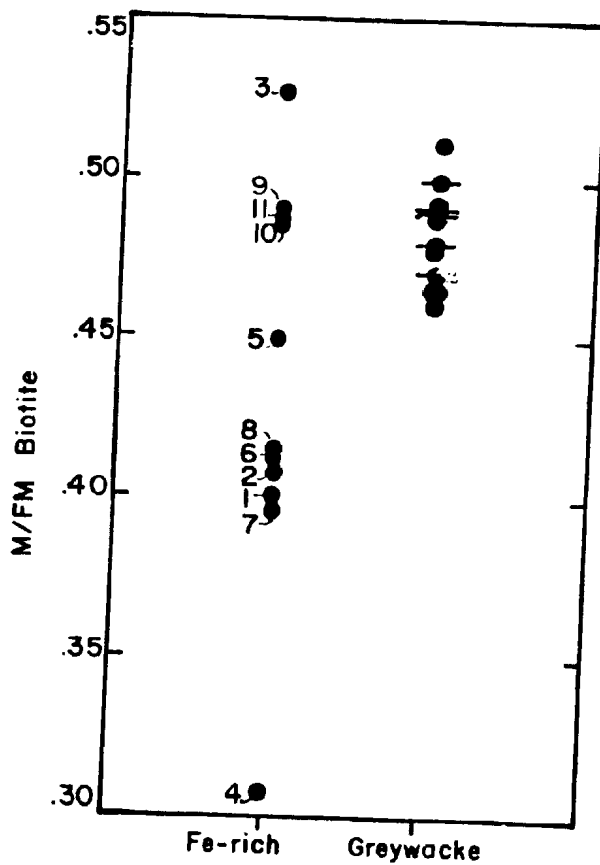
Figure 43: Comparison of M/FM ratios of biotite
from iron formation and iron-rich meta-
sediments with those occurring in greywacke
compositions. Sample numbers as in
Figure 40. Ticks on data points indicate
number of analyses greater than one.

amphibolitic iron formation represents an original continuous spectrum of decreasing clastic sediment and increasing chemical sediment.

A sequence of three samples from the AZ was collected from within a garnet-bearing iron formation layer and up to two meters from the layer (Figure 44). It was found that the abundance of garnet decreased from greater than 50% (sample a; Figure 44) to less than 2-3% (sample b) over a distance of about one meter. All the rocks within this interval contain the assemblage garnet-biotite, but two meters away garnet no longer occurs. The most distant sample (d) contains staurolite, cordierite, andalusite, biotite and muscovite, with staurolite present as inclusions in cordierite. The mineral assemblages and bulk rock compositions are depicted in AFM topology (Figure 44), along with an intermediate assemblage of garnet-biotite-staurolite (sample c) which was not observed but has been recorded elsewhere in the area. Possible rock compositions to account for the range of assemblages are also shown.

In another location, a sample (81-V-55h) collected adjacent to garnetiferous iron formation was found to contain the maximum-phase AZ mineral assemblage (i.e andalusite-cordierite-biotite). However, the analysed ferromagnesian minerals are Fe-richer than greywacke equivalents (Table A.12, Figure 40).

The variation in Fe-content of aluminous metasediments adjacent to an iron formation layer is thus reflected in: 1)

Figure 44: The influence of bulk rock composition on type and abundance of ferromagnesian minerals. (A); AFM projection of a sequence of samples collected from the AZ within and adjacent to a layer of iron formation showing the variation in mineralogy. Projection uses method of Thompson and Bard (1982). (B); abundances of ferromagnesian minerals as a function of bulk rock composition. See text for explanation.

alsil
A

staurolite

cordierite

garnet

● Fe-rich metasediment

○ Metaturbidite

A

F

M

a ● ● b ●(c) ● d ○

biotite

gt-bio   gt-bio-st   (st)-cd-and-bio-ms

>50%gt   2-3%gt

a   b   c   d

iron formation   <1m   >1m   2m's

B
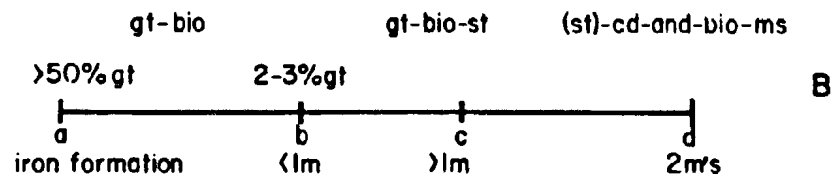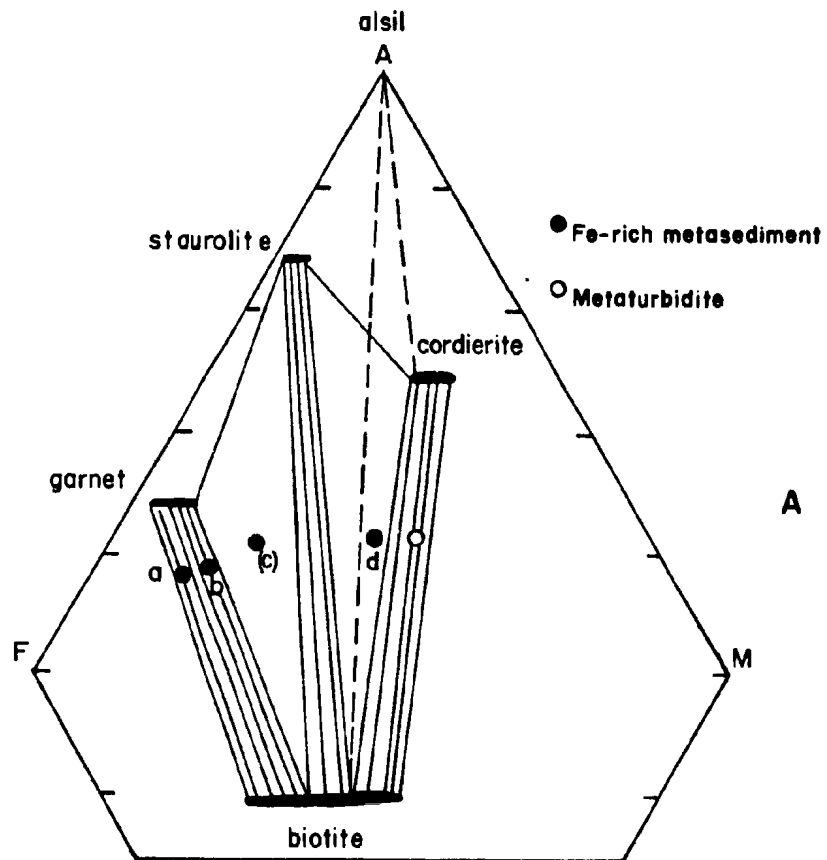
the modal abundance of garnet; 2) the presence of staurolite and 3) the Fe-content of cordierite, biotite and muscovite.

2.8.6 Reactions in Garnet +/- Staurolite Assemblages

All assemblages containing garnet and/or staurolite (Table 4) coexist with plagioclase, quartz and ilmenite. Muscovite is absent from most of these assemblages and as such is not considered as a participant in the majority of the reactions to be proposed. The available Al and K in these rocks may have been used to form biotite rather than muscovite. However, it is also possible that the rocks were muscovite-bearing originally but that muscovite was reacted out of the system.

Chlorite is part of the equilibrium assemblage of the low-grade rocks, but in many of the medium-grade rocks it appears retrograde in origin as a result of the alteration of garnet and biotite. Whether chlorite coexisted with staurolite when cordierite and andalusite formed is not clear from the microstructures (see also Thompson, 1978).

The reactions to be proposed for the garnet +/- staurolite assemblages are represented on a sequence of AFM diagrams (projected through plagioclase), following the principles of Thompson and Bard (1982; Figure 45). X1 through X4 are inferred bulk compositions and their progress is followed through reactions inferred from the observed mineral assemblages.

Figure 45: Depiction of reactions occurring in iron-rich garnet/staurolite assemblages as a function of bulk composition and increasing metamorphic grade. See text for explanation. Method of plotting after Thompson and Bard (1982).

A

staurolite

60 60

40 40

garnet chlorite

20 x_1 x_4 0 20

x_1

x_2

-20 -20

F M

biotite

(a)

R9 R11

chl staur garn staur

bio musc bio

musc chl H2O

qtz

H2O

A

cordierite

x_3

x_1 x_4 0

x_2

F M

(b)

R12

chl cord

musc staur

qtz bio

H2O

A

x_3

x_1 x_4 0

x_2

F M

(c)

R13

aluminosilicate

staur cord

bio musc

qtz H2O

x_3

x_4 0

x_1

x_2

F M

(d)

R14 A

staur and

musc bio

qtz H2O

cord

x_3

x_1 x_4 0

x_2

F M

(e)

R15 R16 A

staur and garn

and staur

musc bio musc

qtz bio

qtz H2O

H2O

x_3 x_4 0

x_1

x_2

F M

(f)

Garnet is considered to have formed at or near the onset of medium-grade metamorphism. The continuous reaction

$$Fe\text{-chlorite} + quartz = garnet + H_2O \qquad\qquad (R.8)$$
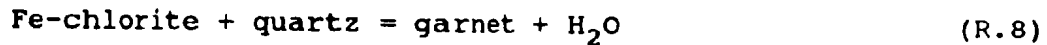
(modified from Chakraborty and Sen, 1967) leads to the association garnet-chlorite-biotite in rock x1 (Figure 45a). Biotite and remaining chlorite become more Mg-rich as a result of this reaction. The most Fe-rich assemblage observed occurs in the two-phase region garnet-biotite (rock x2), which remains stable throughout all the topological changes in the sequence.

The presence of staurolite in chlorite-bearing rocks has not been established as neither chlorite nor muscovite is found in the staurolite-garnet-biotite assemblages. However, their previous existence is assumed (see above and Figure 45a), so that formation of the staurolite-biotite-garnet assemblage may have occurred by the continuous reaction

$$chlorite + muscovite = staurolite + biotite + quartz + H_2O$$
$$(R.9)$$
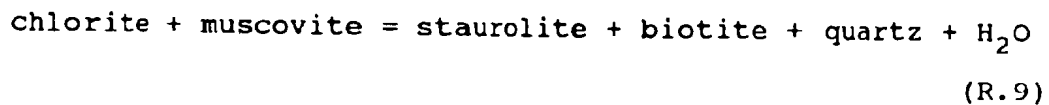
(Figure 45b; Hosheck, 1969).

In rocks that contain both staurolite and garnet, microstructural evidence indicates that staurolite was the earlier formed of the two minerals. The formation of garnet

from staurolite may thus have proceeded via a continuous reaction of the type

staurolite + chlorite + quartz = garnet + H_2O (R.10).
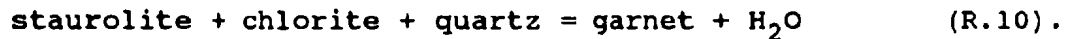
It is possible to balance such a reaction without the presence of an aluminosilicate to compensate for excess Al in the products, if approximately 12 times the amount of garnet is formed as staurolite is destroyed.

The formation of staurolite prior to garnet is possible only in rocks that were initially in the staurolite-chlorite two-phase region (x3 in Figure 45). Subsequently rock x3 is overridden by the staurolite-garnet-chlorite subtriangle and the abundance of garnet increases at the expense of chlorite and staurolite. The discontinuous reaction

garnet + chlorite + muscovite = staurolite + biotite + H_2O

(R.11)
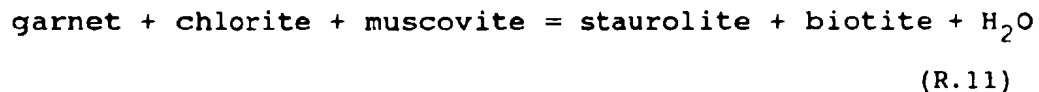
simultaneously accounts for the coexistence of staurolite and biotite in rock x3 and the disappearance of chlorite from rock x1, leaving the assemblage garnet-staurolite-biotite in this more Fe-rich bulk composition (Figure 45b).

The continuous reaction R.9 results in an increase in the proportions of staurolite and biotite and a decrease in chlorite content, leaving rock x3 in the staurolite-biotite field (Figure 45b-c). The staurolite-biotite-chlorite

- 151 -

subtriangle eventually encompasses rock x4 (originally
containing chlorite-biotite) as it shifts to Mg-richer
compositions (Figure 45c).

The stable coexistence of cordierite and staurolite
(which is implied but not observed) may be related to the
discontinuous reaction

chlorite + muscovite + quartz = staurolite + cordierite +
biotite+ H_2O (R.12).
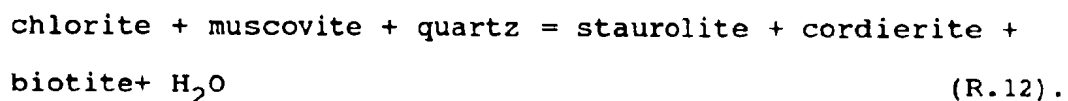
Note that rock o subsequently lies in the cordierite-biotite
two-phase region of medium-grade metamorphism (Figure 45d,
e) and that rock compositions x1, 2 and 3 are unaffected by
this reaction.

The presence of minute staurolite relics within
cordierite porphyroblasts suggests that the breakdown of
staurolite led to the formation of cordierite which may be
explained by the continuous reaction

staurolite + biotite + quartz = cordierite + muscovite + H_2O

                           (R.13).
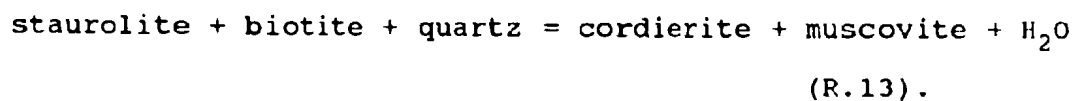
This reaction results in the depletion of staurolite and an
increase in the proportion of cordierite in rock x4.

In theory the coexistence of staurolite and cordierite
should be terminated by the discontinuous reaction

staurolite + cordierite + muscovite + quartz = andalusite + biotite + H_2O (R.14)
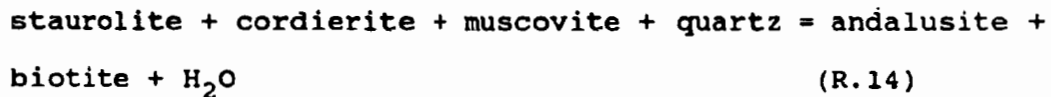
so that rocks x4 and o enter the three-phase region cordierite-biotite-aluminosilicate (Figure 45 e-f).

Reactions R.13 and R.14 could account for the observed staurolite relics within cordierite which itself rims or is partly surrounded by andalusite, if the growth of cordierite isolated staurolite from other reacting phases, or if muscovite was totally consumed so the reaction R.14 ceased before all staurolite was consumed.

Rock x3 enters the three-phase staurolite-andalusite-biotite region (Figure 45f) through the continuous reaction

staurolite + muscovite + quartz = aluminosilicate + biotite + H_2O (R.15).
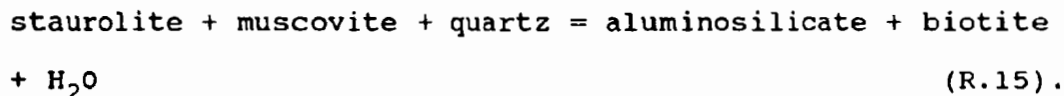
The final breakdown of staurolite in the presence of muscovite occurs by the discontinuous terminal reaction

staurolite + muscovite + quartz = garnet + andalusite + biotite +H_2O (R.16)
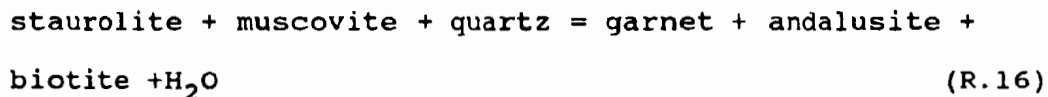
(Figure 45f; Hollister, 1966; Richardson, 1970). In the absence of muscovite, staurolite breakdown would occur at slightly higher temperatures by the reaction

staurolite + quartz = garnet + andalusite + H_2O (R.17).

Reactions R.16 and R.17 account for the unstable appearance of staurolite (as relict inclusions in other phases) in the assemblages staurolite-garnet-biotite-aluminosilicate (rock x3), and imply that staurolite stability was been exceeded in both muscovite-bearing and muscovite-free rocks.

Relatively unambiguous mineral parageneses in Fe-rich aluminous rocks such as these make the interpretation of reactions much easier than for greywackes. In addition many of the reactions have been experimentally calibrated and can be reasonably located on a petrogenetic grid, in comparison to some of the reactions determined for greywacke compositions.

Iron formation typically occurs within turbidites of the Contwoyto Formation; only rarely are the Itchen Formation turbidites rich enough in iron to have formed garnet (or other Fe-rich ferromagnesian minerals). Since Itchen Formation metasediments occur continuously eastward from within the Keskarrah Bay area to east of the eastern Point Lake area and adjacent to the Yamba batholith (Bostock, 1980; King, 1981), there is a lack of information on the metamorphic mineralogies formed in Fe-rich rocks at higher grades than those described herein.

2.9 Point Lake and Keskarrah Formations

2.9.1 Metabasites, Point Lake Formation

Mafic metavolcanics (unit 4) in the central part of the map area were examined in order to compare their metamorphic signature with that of the turbidites of the Contwoyto Formation (unit 9a), which record low grade (CHZ) metamorphism. In Figure 46 the distribution of the mineral assemblages observed in these metabasites is illustrated, as well as the approximate locations of the boundaries between the chlorite, chlorite-actinolite and chlorite-actinolitic hornblende zones. The trends of the isograds separating these zones (Figure 46) together with the isograd distribution shown for greywackes suggest that the metamorphic grade increases from a low in exposures east of unit 2 (Figure 46) outwards towards both the northwest and southwest (Figure 6). However, as will be shown below, a discrepancy may exist between the metamorphic grade recorded by the metabasites and that recorded by the adjacent metasediments.

Results of the limited microprobe analyses of amphibole-bearing metabasites are listed in Table A.13 and are plotted on an ACF diagram in Figure 47. Amphibole compositions range from actinolite to ferro-tschermakitic hornblende (Leake, 1978) with increasing grade. Chlorites display a prograde trend toward more magnesian compositions and decrease in modal abundance. Epidotes contain about
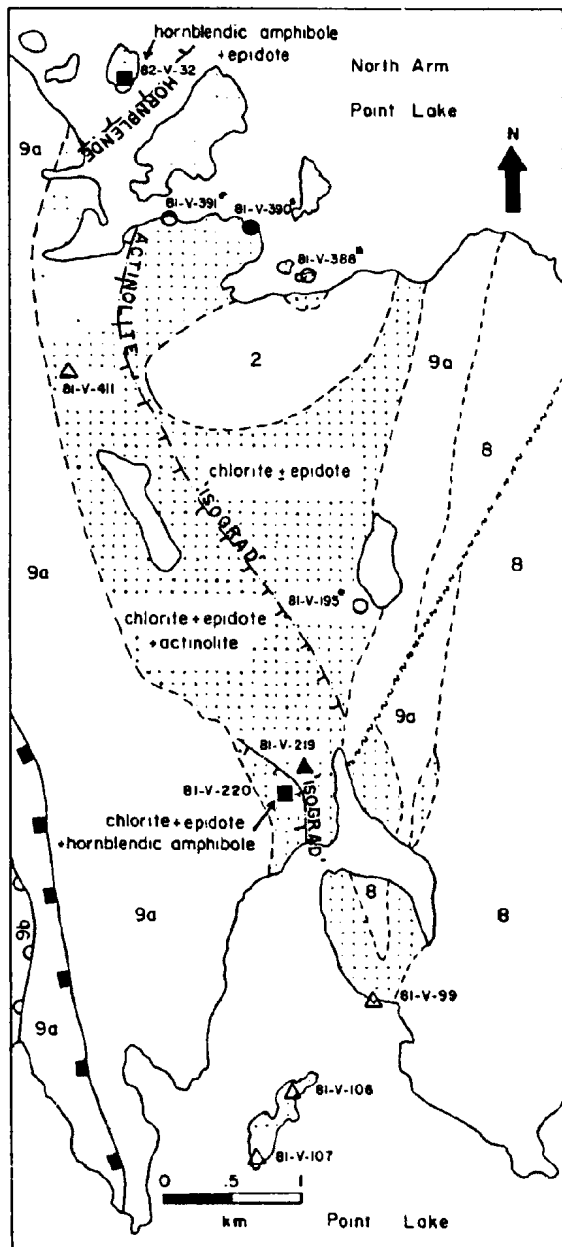
Figure 46: Distribution of metamorphic zones in central exposures of metabasites (unit 4; stippled pattern). Sample numbers correspond to those examined in thin section and analysed by electron microprobe (see Table 13).
Ticks on high-grade side of isograds. Biotite and cordierite isograds in unit 9 also indicated (symbols as in Figure 6).

○   chlorite - biotite - calcite

●   chlorite - epidote - biotite - calcite

△   chlorite - epidote - actinolite - calcite

▲   chlorite - epidote - actinolite - biotite - calcite

■   epidote - hornblendic amphibole ± chlorite

♭   abundant carbonate

Figure 47: ACF diagram showing phase relations in unit 4 metabasites and the progression from actinolite to more hornblendic amphibole with increasing metamorphic grade (see also inset diagram to right).

■ whole rock analyses of metabasites (units 3 and 4) in the Keskarrah Bay area plotted from unpublished data of R.M. Easton.

$A = [Al_2O_3] + [Fe_2O_3] + ([Na_2O] - [K_2O])$

$C = [CaO] - 3.3[P_2O_5]$

$F = [MgO] + [MnO] + [FeO]$
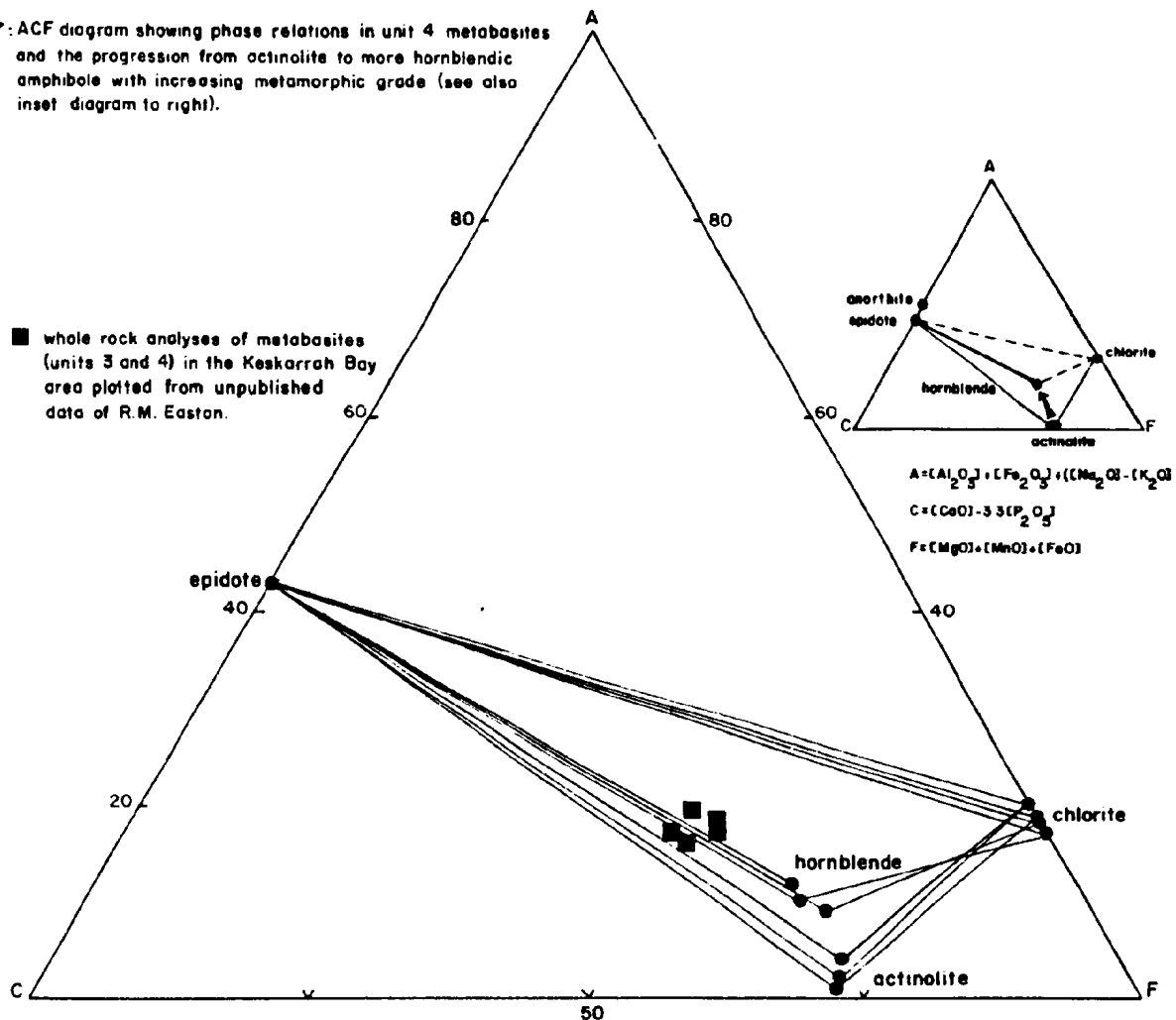
10-20% FeO (probably as Fe_2O_3). Plagioclase compositions (as identified optically) are variable, ranging from albite to andesine, but no systematic variation was determined.

Chlorite is a ubiquitous member of the equilibrium assemblage and on this basis the metabasites document low-grade metamorphic conditions (Winkler, 1976, p.170). The appearance of actinolite in the equilibrium assemblage, possibly through the reaction chlorite + calcite + quartz = epidote + actinolite + CO_2 + H_2O (Deer et al, 1966, p. 67), may indicate the change from lower to upper low-grade, but a reaction of this type is strongly dependent on the composition of the vapor phase present. The blue-green color of hornblende in these rocks is indicative of the upper portion of low-grade metamorphism (Miyashiro, 1973, p.254).

Moody et al. (1983) noted the following changes across the low-grade/medium-grade boundary that characterize the transition zone and are pertinent to this study: 1) the first appearance of actinolite or actinolitic hornblende and a decrease in the amount of chlorite below the boundary; 2) above the boundary amphiboles contain increasingly more Al, Ti and Na until in medium-grade hornblende is present without chlorite; 3) chlorite becomes Mg-richer as its abundance diminishes; and 4) the disappearance of chlorite marks the end of the transition.

The mineralogical changes noted within these mafic metavolcanics are comparable to those cited by Moody et al. (1983) and indicate that metamorphic conditions reached the

low/medium-grade transition zone but did not breach the boundary (hornblende and chlorite stable). This conclusion is in contrast with the metamorphic grade determined for the adjacent metagreywackes, which record uniquely low-grade (muscovite-chlorite) conditions. However, given the abundance of calcite in the metabasites, it seems likely that the fluid phase was enriched in CO_2 relative to that of the metagreywackes and that this resulted in the reactions occurring at lower temperatures than those predicted for an H_2O-rich fluid phase. It is, however, also possible that the pattern of metamorphic zonation between these two units reflects a structural overprint - a combination of folding and faulting of the isograds. The present data are insufficient to distinguish between these two hypothesis.

Mineral assemblages observed in the banded mafic volcanics (unit 3) lack chlorite; the dominant equilibrium assemblage is hornblende-plagioclase. The stability field of low-grade metamorphism has therefore been surpassed for these rocks (Winkler, 1976; Moody et al, 1983). This is in accord with the medium-grade assemblages recorded by the neighbouring metagreywackes.

2.9.2 Metafelsites, Point Lake Formation

Metamorphism of the felsic volcanic rocks (units 5 and 6) predominantly resulted in the development of muscovite, biotite and chlorite, with less aluminous compositions being muscovite-free and containing garnet-biotite+/-amphibole.

Microprobe analyses of garnet, biotite and amphibole from two widely separated samples (81-V-170, 82-V-73; Appendix A) are given in Table A.14; the data from sample 81-V-170 are of poor quality, but they are included in the text for illustrative purposes. The amphiboles are within the compositional range of ferro-tschermakite to ferro-tschermakitic hornblende (Leake, 1978); and biotite is relatively Fe-rich, having M/FM values comparable to those of biotite in iron formation. Garnets from both samples are almandine-rich, although compared to garnets from iron formation they contain more Ca and Mn. The analysed garnet from sample 82-V-73 is compositionally zoned, with rims containing more Fe and Mg and less Ca and Mn than the core (normal zoning).

The presence of hornblende and absence of chlorite in the felsic volcanics indicates that medium-grade metamorphic conditions were approached or reached, with precise definition being hampered by the quartzofeldspathic compositions. No variation in metamorphic grade could be determined within the felsic volcanic unit and it appears that the presence or absence of garnet is controlled by bulk composition rather than the physical conditions of metamorphism.

Amphibole from the siliceous carbonate formation (unit 7; sample 81-V-430a), which is associated with the felsic volcanics, approximates hornblende in composition (Table A.14).

2.9.3 Keskarrah Formation Conglomerate

Chlorite and muscovite are the only Fe-Mg-Al silicates identified within the conglomerate (unit 8) and lithic clasts show a variety of intricate primary textures. The absence of biotite and preservation of primary textures indicates the low metamorphic grade of the unit.

2.10 Geothermometry and Geobarometry

2.10.1 General Statement

The garnet-biotite geothermometer and garnet-aluminosilicate-plagioclase-quartz geobarometer have been applied to two samples of the medium-grade metasediments of the Contwoyto Formation (unit 9c) and one sample of the Itchen Formation (unit 10). Two domains were analysed in each of the Contwoyto Formation samples to yield two pressure and temperature estimates, which are used to determine consistency and accuracy of the analyses. Results from several garnet-biotite assemblages, including one sample from the felsic volcanics, provide additional geothermometric constraints. The conditions of metamorphism and predominance of Fe-poor whole-rock compositions precluded the widespread development of garnet-bearing assemblages and so there is a limited distribution of pressure and temperature estimates.

The compositions of coexisting garnet-biotite pairs have been previously listed (Table A.12). Atomic proportion of

Fe^{3+} in garnet is estimated by assuming electrical neutrality, with any site vacancies being occupied by Fe^{3+}; Fe^{3+} content of the garnets thus calculated is small. The garnets are zoned and calculations have been performed on core, inner rim and outer rim compositions (see 2.10.4). Biotites display no evidence of zoning; Fe in biotite is assumed to be all Fe^{2+}.

2.10.2 Geothermometry

Ferry and Spear (1978) calibrated the partitioning of Fe^{2+} and Mg^{2+} between coexisting garnet and biotite to estimate temperatures of metamorphism. Their polybaric-polythermal equation has been applied to the medium-grade rocks of this study. Garnets fall within the compositional brackets of ((Ca + Mn) / (Ca + Mn + Fe + Mg)) < 0.20 and 0.80 < (Fe / (Fe + Mg)) < 1.0, respectively, that were recommended by Ferry and Spear. Temperatures thus derived are estimated to be accurate to within 50°C. Table 5 presents the data relevant to Ferry and Spear's calibration, with sample locations given in Appendix A.

2.10.3 Geobarometry

Metamorphic pressures are estimated using the equilibrium constant equations for the assemblage plagioclase-garnet-aluminosilicate-quartz derived by Ghent (1976) and modified by Ghent et al. (1979). The latter authors empirically estimated a value of -0.4 for the activity coefficient product to relate the grossular-

TABLE 5: Results from Geothermometry and Geobarometry

sample no.	Mg/Fe GARN O.R	I.R	CORE	BIO	ln Kd O.R	I.R	CORE	Temp(°C)* O.R	I.R	CORE	XCa** GARN O.R	I.R	CORE	PLAG	log Kd O.R	I.R	CORE	Pressure(kbar)*** O.R	I.R	CORE
81-V-143 (1)	.120	.133	.133	.687	-1.745	-1.642	-1.642	565	605	605	.037	.037	.038	.286	-2.664	-2.664	-2.630	3.1	3.6	3.8
(2)	.110	.122	.133	.687	-1.832	-1.728	-1.642	535	578	605	.031	.037	.038	.286	-2.895	-2.664	-2.630	2.0	3.4	4.0
81-V-15a (1)	.100	.110	.110	.672	-1.905	-1.801	-1.801	510	545	545	.047	.050	.048	.456	-2.961	-2.880	-2.933	1.5	2.2	2.0
(2)	.101	.111	.099	.657	-1.873	-1.778	-1.893	520	551	515	.046	.050	.047	.450	-2.972	-2.863	-2.944	1.6	2.3	1.6
81-V-252		.197		1.114		-1.733			565			.028		.243		-2.816			2.7	
81-V-38# (1)	.113	.108	.095	.655	-1.757	-1.803	-1.931	558	543	504										
(2)	.119	.113	.114	.667	-1.724	-1.775	-1.767	569	552	554										
81-V-23#	.127	.132	.108	.816	-1.860	-1.822	-2.022	525	537	479										
81-V-214b#		.075	.072	.445		-1.781	-1.821		550	537										
81-V-383d#		.107		.705		-1.885			518											
82-V-73#		.086	.083	.681		-2.069	-2.105		467	458										

Ferry and Spear (1978) calibration at 2.07kb: (ln K= -2109/T(°K) + 0.782, where ln K= [(Mg/Fe;garnet)/(Mg/Fe;bioite)].

*   Except for those samples marked with # temperature is derived from Ferry and Spear's (1978) polybaric/polythermal equation (see text).

**   XCa= (Ca)/[(Ca)+(Mn)+(Fe)+(Mg)] for garnet and XCa= (Ca)/[(Ca)+(Na)+(K)] for plagioclase, where ()= atomic proportion.

***   Ghent (1976) calibration modified by Ghent et al. (1979): 0= -2551.4/T(°K) + 7.1711 - 0.2842(P-1)/T(°K) + log Kd = (-0.4), where log Kd= 3log Xgarnet/grossular - 3log Xplagioclase/anorthite.

anorthite curve to the kyanite-sillimanite isograd. This value has been adopted in the calibration of this study although the samples used here approximately straddle the andalusite-sillimanite isograd. Data relevant to this geobarometer are listed in Table 5 and the calculated pressures are considered to be accurate to within 1.6 kbar (Ghent et al., 1979).

2.10.4 P-T Estimates

The Ferry and Spear (1978) and Ghent et al. (1979) calibrations can be simultaneously solved to yield a unique P-T estimate for each mineral association providing it is assumed that the geothermometer (exchange reaction) and geobarometer (net transfer reaction) both blocked at the same point on their P-T trajectory. This assumption has been made in the P-T estimates that follow even though the zoning in garnets indicate continued reaction subsequent to peak conditions. Results of this study are shown graphically in Figure 48 and are also tabulated (Table 5).

Tracy et al. (1976) noted that at medium grades of metamorphism (such as in this study) growth zoning (both prograde and retrograde) in garnets may be preserved. Previous studies (for example Ghent, 1976; St.Onge, 1984) have concluded that it is the inner rim portion of a zoned garnet that is in equilibrium with compositionally homogeneous minerals such as biotite and plagioclase. However, Tracy et al. (1976) reasoned that Kd determined for

Figure 48: P-T estimates from garnet-biotite-plagioclase-
aluminosilicate-bearing assemblages. Sample 81-V-
143 (A and B), andalusite-bearing; sample 81-V-
15a (C and D), andalusite-sillimanite-bearing;
sample 81-V- 252 (E), Itchen Formation,
sillimanite not observed in thin section but is
present in outcrop. See text for explanation.
Relevant data presented in Table 5.

C 81-V-15a

D 81-V-15a
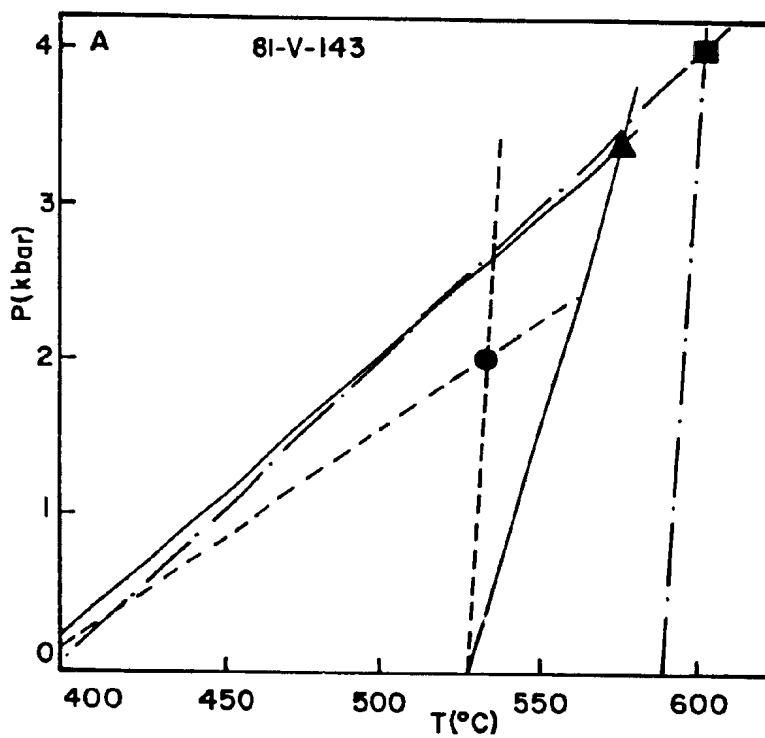
Core
Inner rim
Outer rim

- 167 -

81-V-252
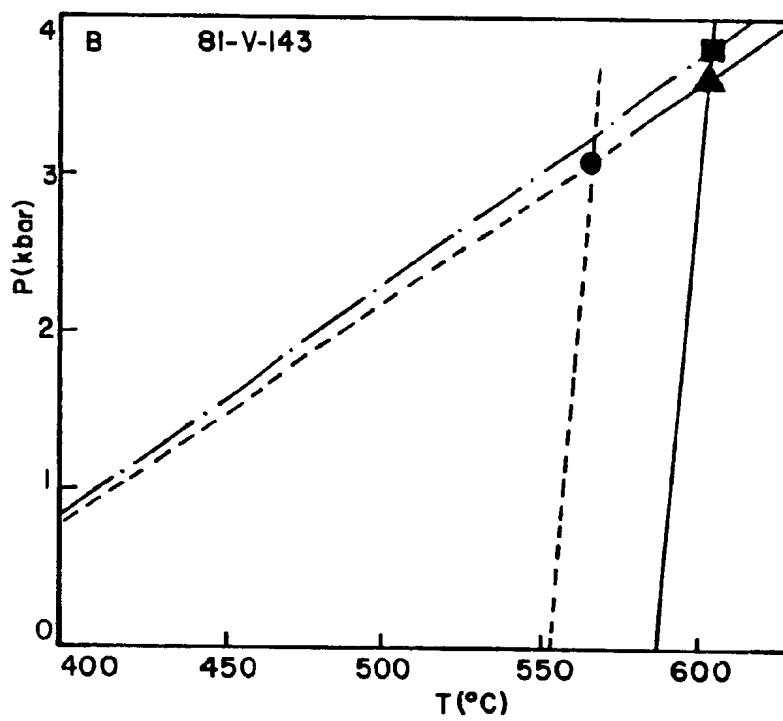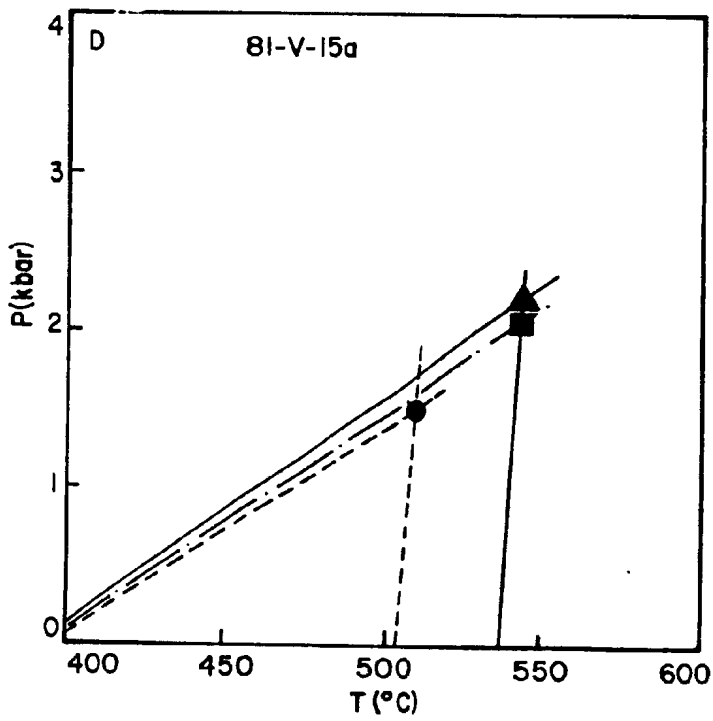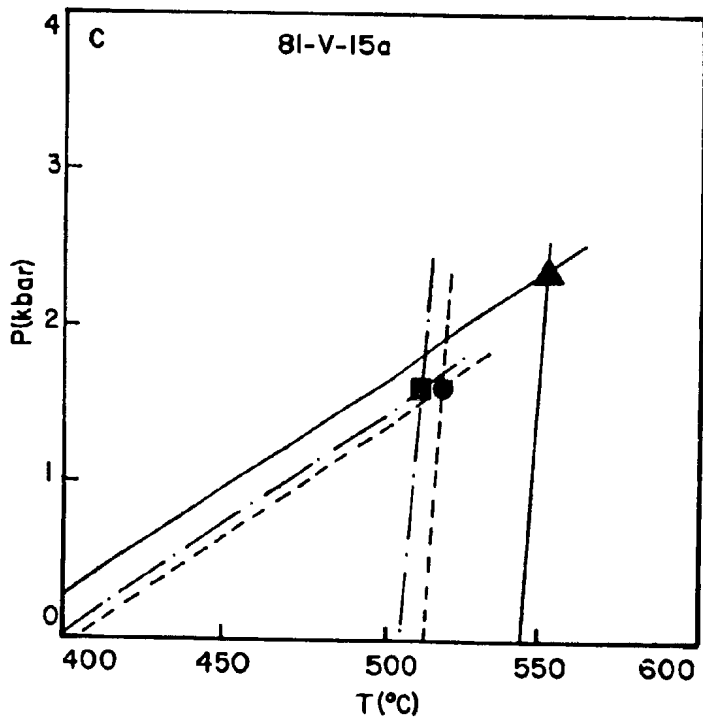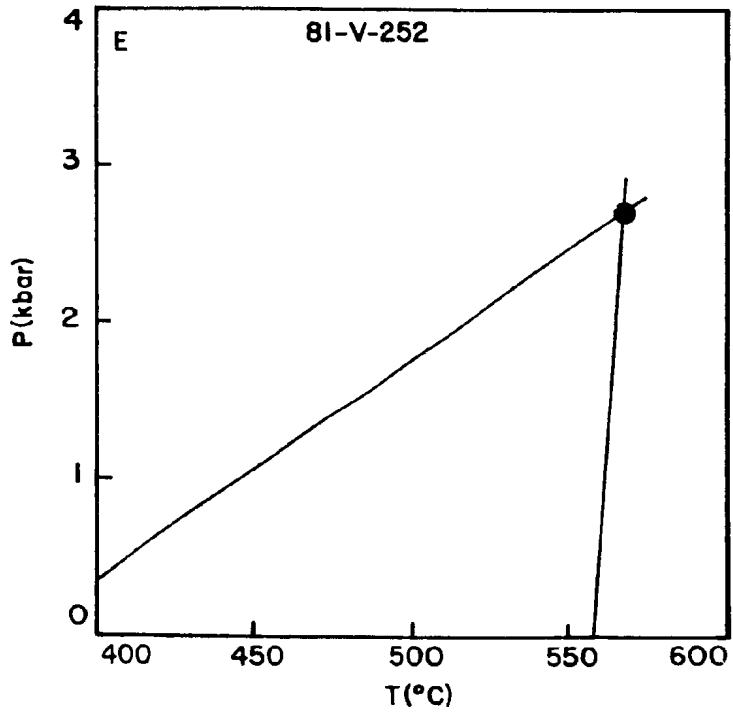
garnet cores and matrix biotite should yield a substantially correct estimate of prograde temperature provided that the rock contains very little garnet, and/or retrograde outer rims of the garnets are extremely narrow and there are no other abundant Fe-Mg-Mn phases. The studies of Spear and Selverstone (1983) and Spear et al. (1984) have utilized garnet zoning profiles to determine quantitative P-T paths (see below). Because most of the analysed garnets of this study are zoned, results are shown for core, inner rim and outer rim portions (Figure 48; Table 5).

Three samples were analysed to provide P-T estimates, two of which contain zoned garnets. Garnet analyses was not carried out in the detail required to determine zoning profiles (or composition maps), therefore the width of the garnet retrograde rims is unknown. However, the relative modal mineralogy of these samples is compatible with the criteria recommended by Tracy et al. (1976), enabling the use of the composition of garnet cores and matrix biotite to determine prograde temperatures. Sample 81-V-15a (containing about 5-10% garnet and 1% staurolite) comes from just above the sillimanite isograd, while sample 81-V-143 (containing about 3% garnet and 1% staurolite) was collected 4 km further up-grade within the SZ (Figure A.1; Appendix A). Using inner rim compositions, P-T estimates for the samples range from 2.2 kbar and 545°C to 3.6 kbar and 605°C (Table 5). While both samples yielded internally consistent P-T estimates, there is considerable variation between the

samples (Figure 48), so the variation in the P-T data may reflect actual differences in metamorphic conditions. However, estimates from sample 81-V-15a place this sample within the AZ according to the aluminosilicate phase diagram of Holdaway (1971), which is inconsistent with the observed SZ mineral assemblage.

As indicated in Figure 48 (a,b,d) garnet cores appear to have equilibrated at higher temperatures and pressures than the outer rims, suggesting that garnet growth continued during decompression associated with retrograde metamorphism (Spear and Selverstone, 1983). Figure 48c could indicate garnet growth during initial prograde compression, followed by decompression and retrograde metamorphism (Spear and Selverstone, 1983).

Geothermometric data from samples lacking sillimanite (Table 5) also suggest prograde garnet growth, with cores recording lower temperatures than rims. This is also supported by the normal compositional zoning of these garnets (Table A.12). The range of temperatures (from about 480° - 550°C) for these samples (derived from Ferry and Spear's (1978) calibration at 2.07 kbar) is within the realm of medium-grade metamorphism. The sample from the felsic volcanic unit gives temperatures of approximately 460°C (Table 5), slightly lower than the range of temperatures from the medium-grade iron formation.

Sample 81-V-252 is from the SZ of the Itchen Formation and contains the assemblage garnet-biotite-cordierite-

staurolite. Garnet is compositionally homogeneous and is present as embayed relics within cordierite. Because of the scarcity of garnet in the mineral assemblages of the Itchen Formation, P-T estimates were carried-out on this sample even though it is not part of an equilibrium assemblage with plagioclase and biotite. P-T determinations of 2.7 kbar and 565°C (Table 5, Figure 48e) place this sample within the field of andalusite (Holdaway, 1971), however within the limits of analytical error results are consistent with the observed SZ mineral assemblage.

2.11 Petrogenetic Grid

A petrogenetic grid has been constructed for both the metagreywackes and iron-rich metasediments of the area (Figure 49a,b) to illustrate the P-T relationships of many of the reactions. In estimating the P-T path the following have been considered: 1) observed textural relationships between coexisting phases; 2) observed sequential development of mineral phases; and 3) results of geothermometry and geobarometry.

Continuous reactions occur in P-T space as bands or zones across which reactions affect different rock compositions. Most of the continuous reactions affecting the rocks of this area have not been bracketed by experimental calibration and so most are not illustrated in Figure 49. The curves on the P-T grid thus correspond mainly to the

Figure 49: P-T grids constructed for the Keskarrah Bay area;
(A) for greywacke compositions; (B) for iron-rich
compositions; (C) estimated P-T path from garnet
zoning profiles. Curves representing reactions
R.11, R.12, R.14, R.16 and the breakdown of
muscovite to form K-feldspar and Al_2SiO_5 are from
the unpublished works of Carmichael, presented in
Bailes and McRitchie (1978) and Ermanovics and
Froese (1978). Solid circles in A and B show
present erosion level. Aluminosilicate triple
point after Holdaway (1971). Numbered curves
correspond to reactions discussed in the text:

1) generalized "biotite-in" reaction from Winkler
(1976)

3) chl+celadonite+Mg-bio+qtz+/-plag = cord+musc+
Fe-bio+H_2O (modified after Thompson, 1978)

4) cord+musc+/-ilm = and+bio+qtz+/-plag+/-rut
(Thompson, 1978)

5) chl+musc+qtz = cord+and+bio+H_2O (modified from
Hess, 1969)

7) cord+musc = sill+bio+qtz+H_2O (Thompson, 1978)

11) garn+chl+musc = staur+bio+H_2O

12) chl+musc+qtz = staur+cord+bio+H_2O

14) staur+cord+musc+qtz = and+bio+H_2O

16) staur+musc+qtz = garn+and+bio+H_2O

A: P-T grid for metagreywackes

B: P-T grid for Fe-rich metasediments

C: Estimated P-T-t path

- 173 -
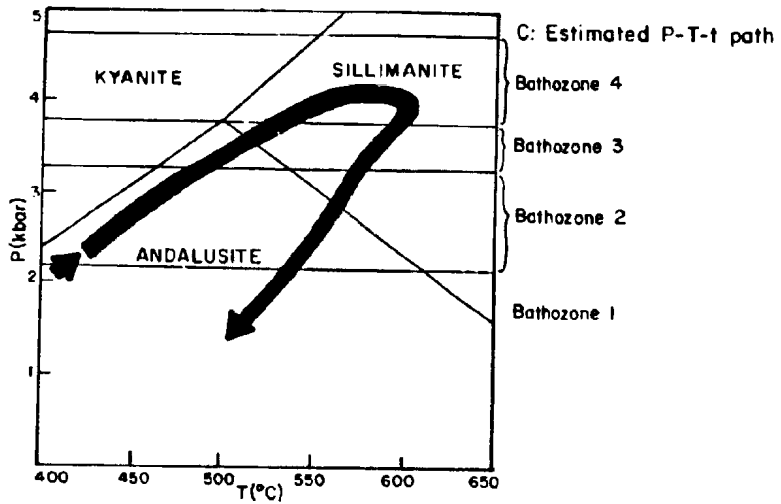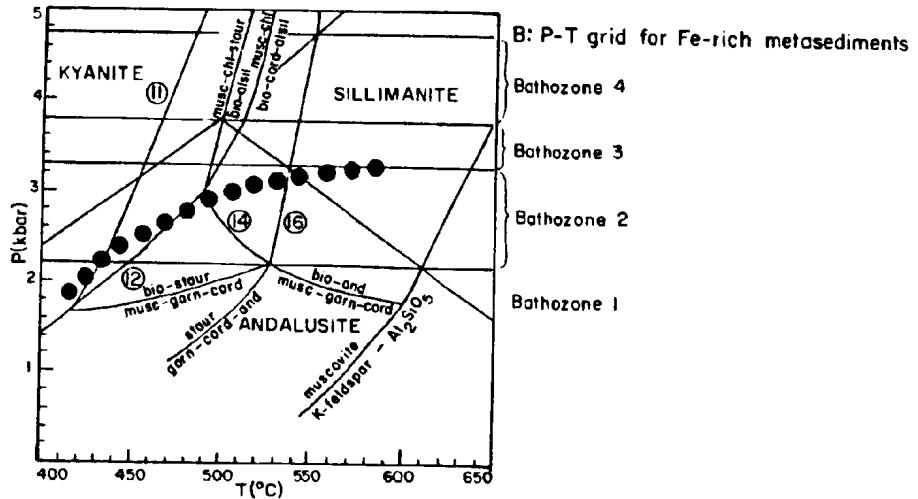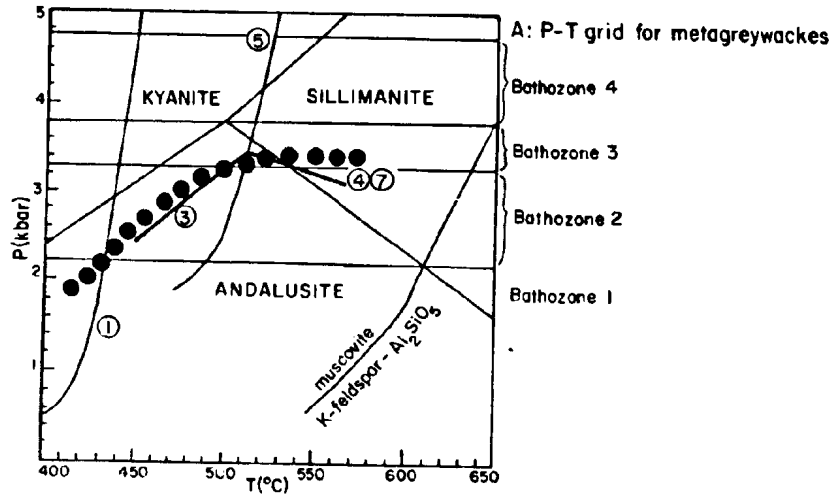
discontinuous reactions proposed in the text. The
aluminosilicate triple point of Holdaway (1971) is employed
as it is the most congruous with observed mineral
assemblages and estimated pressures and temperatures
obtained from geobarometry and geothermometry. Curve (1)
represents the generalized biotite-in continuous reaction of
Winkler (1976) and is used to depict the biotite-forming
reaction (R.1) of this study. Curves representing the
continuous reactions leading to the formation of cordierite
(R.2) and andalusite and sillimanite (R.4 and R.7) are
compiled from the works of Thompson (1978) and King (1981),
with the combined consideration of the isograd spacing found
in this study aiding in the positioning of the curves.
Although the positions of these curves are poorly controlled
in P-T space, their relative locations can be determined.
For instance, reaction R.2 is constrained by its occurrence
subsequent to the formation of biotite, its intersection
with the discontinuous reaction R.5 within the stability
field of andalusite and the position of the andalusite-
kyanite boundary.

Reactions illustrated on the P-T grid that correspond to
the more Fe-rich garnet and/or staurolite-bearing
assemblages (Figure 49b) have been compiled from the
unpublished works of D.M. Carmichael presented in Bailes and
McRitchie (1978) and Ermanovics and Froese (1978).

Figure 49 also shows that there is a slight discrepancy
(of about 0.25 kbar) between the placement of the

metamorphic field gradient (erosion surface P-T curve) indicated for metagreywacke compositions (Figure 49a) and that for Fe-rich compositions (Figure 49b). This discrepancy may reflect inaccurate positioning of the continuous reactions R.3, R.4 and R.5 (Figure 49a), which have not been experimentally calibrated.

Although the pressure is poorly constrained at low-grade, it is better defined at medium-grade as a result of the andalusite/sillimanite transition and the geothermometric and geobarometric investigations. The erosion surface P-T path thus delineated falls within bathozones 1 to 3 of Carmichael (1978): the andalusite-sillimanite assemblages are diagnostic of bathozones 1 to 3 and reaction R.16 occurs within bathozone 2.

Geothermobarometric results using zoned garnets have been used to construct both a P-T-t path for the highest grade rocks (Figure 49c). The retrograde part of this path is determined largely from the P-T data illustrated in Figures 48a and b. The prograde path represents the combined data from the erosion surface P-T path and maximum P-T estimates from geothermobarometry (using garnet core-matrix biotite data; Figure 48a). The P-T-t path indicates decompression (uplift) from about 4 to about 2 kbar accompanied by a decline in temperature from 600°C to 500°C. This pattern emphasizes the importance of cooling and uplift as suggested by England and Thompson (1984) and Thompson and England (1984). These authors investigated P-T-t (time)

- 175 -

paths of regional metamorphism and noted that metamorphism to andalusite-sillimanite facies series is not likely without additional heat supply from intrusives. In the Keskarrah Bay area such intrusives are not immediately apparent, other than the volumetrically small amount of pegmatite and adamellite within the SZ metaturbidites, which may have been derived by partial melting of the sediments at conditions of about 660°C and 5 kbar (McKinnon, 1982). However, the Keskarrah Bay area is situated between two batholith terranes (the Yamba batholith to the east and 'Pointless' batholith to the west) which could conceivably have provided additional heat sources.

3.0 STRUCTURE

3.1 Introduction

Structural elements observed in supracrustal and basement rocks of the Keskarrah Bay area are indicative of polyphase deformation and depict a complex tectonic history for the area. Dominant structural trends in the supracrustal rocks parallel the gneiss-greenstone boundary (Henderson and Easton, 1977b) and elsewhere throughout the Itchen Lake region these trends parallel the arcuate shape of the greenstone belt (Bostock, 1980; King, 1981). Large scale folds formed in the supracrustal rocks are mainly overturned toward the western margin of the belt (Bostock, 1980; King, 1981), a relationship that is also observed over a large part of the southern Slave Province (Fyson, 1981; Fyson and Helmstaedt, 1988). Deformation of the basement rocks in part pre-dates that of the supracrustals and also involved several phases of deformation (Easton, et al., 1981; Kusky, pers. comm.).

The map area is divisible into two lithotectonic elements; the basement gneiss terrane and the supracrustal terrane. The important structural features of each of these terranes are described in the following sections and are summarized in Table 6. Figure 50 shows the salient structural characteristics of the area and is included in the text for ease of reference.

TABLE 6: Summary of Deformational Events in the Keskarrah Bay Area

DEFORMATIONAL EVENT	SUPRACRUSTAL TERRANE	BASEMENT GNEISS TERRANE
Post-D_2	Crenulation and kinking of S_2. Biotite porphyroblasts aligned into L-S fabric (E-SE plunge, down-dip of S_2 plane). Formation of biotite foliation at a high angle to S_2. Formation of SE and NE trending biotite foliation (S_3 and S_4?).	NOT RECOGNIZED
D_2	F_2: Macroscopic N-trending folds of S_0/S_1. Steep to moderate plunges, variable plunge direction. F_1 isoclines refolded. S_2: Dominant foliation. N-trending, steep east-dipping. Axial planar to F_2.	F_2: Macroscopic NE-plunging folds of gneissic banding and F_1 isoclines (?). S_2: Weak axial plane foliation. Mineral lineations subparallel F_2 fold axis.
D_1	F_1: Isoclinal folds of bedding, developed in western areas; E-trending. S_1: Penetrative axial plane cleavage in western areas. Weak cleavage developed in east-central areas; E-trending.	Formation of isoclinal folds of gneissic banding or flattening of pre-existing folds (?) with development of axial plane foliation.
D_x	NOT RECOGNIZED	Formation of gneisses, accompanied by high grade metamorphism and anatexis. Development of gneissosity, possibly E-trending.

ITCHEN
LAKE

S₁ ,easterly

S₂ , northerly

S₄ ?, northeasterly

L–S fabric (biotite porphyroblasts)

POINT LAKE

NORTH

TREE
BAY

ARM

POINT

KESKARRAH
BAY

LAKE

bedding tops known: inclined, overturned, tops unknown

S₁,S₁ dip<60°

S₂ & undifferentiated

S₃,S₄

gneissosity:steep dip, dip <60°

lineation: post-D₂ biotite shallow (gneiss terrane)

F₁:anticline, syncline   ~ ~ fault   Fubar fault

F₂:antiform, synform (plunge may be indicated)

F overturned:antiform, synform

R: recumbent fold (gneiss terrane)

pillow top, inclined

geologic contact

mylonite (gneiss-supracrustal boundary)

kilometers
0 1 2 3 4 5

gneiss   banded mafic volcanics   mafic flows   carbonate   turbidites
granodiorite   gabbro   felsic volcanics   conglomerate   granite,pegmatite

Figure 50: Structural features of the Keskarrah Bay area. Isograd patterns as Figures 5 and 6. Inset diagram shows zonation of foliation trends

It is appropriate to note here that inland exposures
have a ubiquitous lichen cover which obscures some
structural relaticnships. Much structural information was
gleaned from the wave-washed and ice-scoured exposures on
the shoreline of Point Lake, but in many instances attempts
to trace structures inland from the shoreline were
fruitless.

3.2 Deformation of the Supracrustal Terrane

3.2.1 Folding Events

i) D_1 Structures in the Volcanic Units

Compositional layering (S_0?) within banded mafic
volcanics (unit 3) was interpreted by Bostock (1980) as
bedding within a tuffaceous unit. However, Kusky (pers.
comm., 1986) suggested that the layering in these volcanics
is, at least in part, tectonic in origin. A conclusion was
not drawn in the course of this study regarding the origin
of this layering. Therefore, should Kusky's interpretation
be correct, the sequence of deformational events presented
below may be incomplete.

In the southwestern part of the map area, compositional
layering (S_0?) within the banded mafic volcanics is folded
into isoclinal, horizontal to shallow east-plunging F_1 folds
(Figure 50). The associated east-trending axial planar
foliation (S_1) is defined by the alignment of micas and
amphiboles. Interbedded mafic flows (unit 4) also contain

the easterly trending S_1 foliation (see also the map of Henderson and Easton, 1977b) and S_1 maintains a relatively consistent trend implying that the steeply plunging F_2 folds are little developed in this area (east of this area F_2 folds have reoriented D_1 structures; Henderson and Easton, 1977b). Toward the south, S_1 dip directions change from south to north and the amount of dip varies from steep to shallow (Figures 5 and 50). Thus the east-trending F_1 isoclines change from upright folds in the north to folds that are overturned toward the south in the southern part of the area.

In the northwestern map area several synformal folds within the banded mafic volcanics have been designated F_1 structures (Figures 5 and 50) on the basis of: the presence of a foliation that is considered to be S_1 is parallel to the compositional layering and both this fabric and the compositional layering are folded about later phase F_2 folds.

Mafic flows (unit 4) exposed on the islands in the north arm of Point Lake have east-trending flow contacts (S_0) and foliations (S_1?; Figures 5 and 50). These D_1 structural trends are preserved between domains that are overprinted by D_2 structural trends. Felsic volcanics (units 5 and 6) locally contain east-trending compositional laminations (S_0?) which are parallel to a mica foliation that may represent S_1.

ii) D_1 in Metaturbidites

F_1 folds are defined largely on the basis of changes in younging directions as obtained from graded bedding. Several fold hinges have been seen, however, in the shoreline exposures of the low-grade Contwoyto Formation (Figure 51). The F_1 folds are long limbed isoclines (Figure 52) that are in all cases refolded by later phase folds such that their initial orientation cannot be precisely defined over a large area. However, many observations of F_1 fold closures were made where bedding has an easterly strike (Figures 51,52) and is steeply dipping suggesting F_1 folding was about easterly or westerly trending horizontal axes with steep axial planes.

Elsewhere in the turbidite succession opposing bedding facing directions are also observed and some are interpreted to be indicative of F_1 folding. However, the axial traces defined by many of these bedding reversals have a northerly orientation (Figure 51) creating uncertainty as to whether they are the result of F_1 or F_2 folding. For instance, in the medium-grade Itchen Formation schists these axial traces parallel second phase fold traces in the eastern Point Lake area (King, 1981). King has, however, indicated that F_1 folds with probable easterly orientations are present in the eastern Point Lake area, suggesting that easterly trending D_1 structures were once more widespread.

Deformation of the metaturbidites during D_1 was associated with the development of an S_1 cleavage, which has

Figure 51: Locations of observed F_1 folds in low - grade metaturbidites (unpatterned). Folds not drawn to scale. Bedding form lines, faults and F_2 axial trace and plunge direction (if known) are also indicated. Ticks on bedding form lines indicate tops. F_1 folds in 1 and 2 are associated with a penetrative S_1 axial plane cleavage; those in 3 and 4 are not. An S_2 axial plane cleavage is associated with all F_2 folds shown.

v = volcanic rocks; + = granodiorite; dotted pattern = Keskarrah Formation conglomerate.
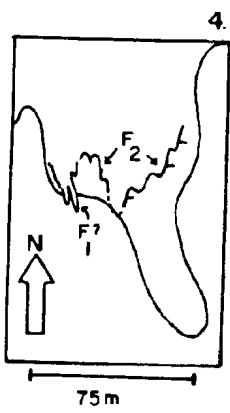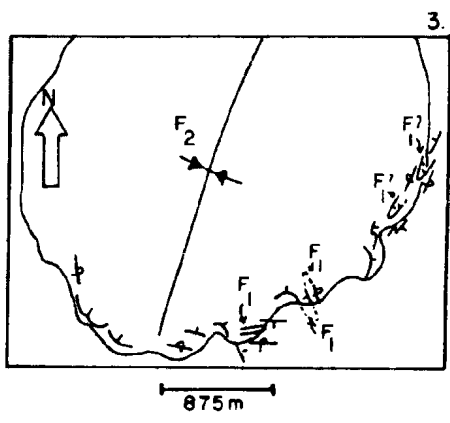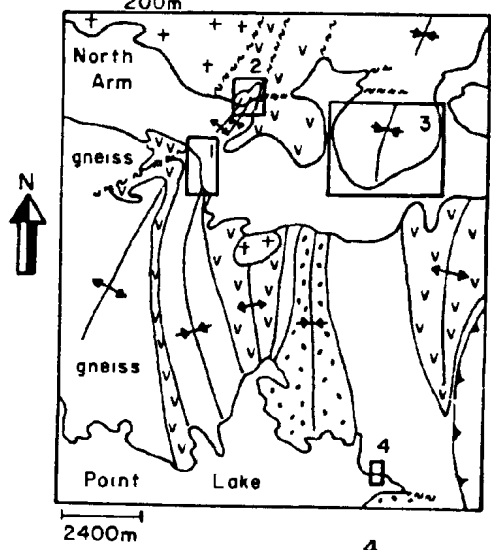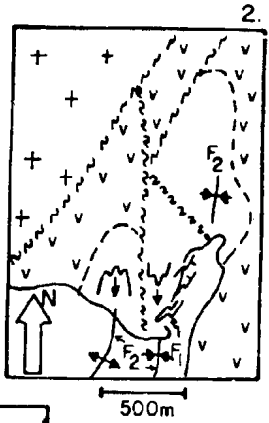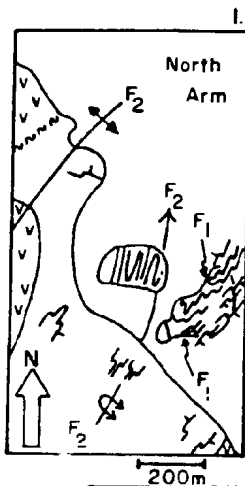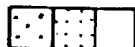
Figure 52: Mesoscopic F_1 fold styles showing the relationship between F_1, S_1, F_2 and S_2. A is from location 1 and B from location 2 on Figure 52. Note the tight style of F_1 folds versus the more open F_2 folds. S, z and m symmetry of F_1 minor folds are defined by small scale folds of compositional layering in the turbidites (A and B) and quartz veinlets (B). Fault in (B) shows sinistral offset. Sketches are drawn from photographs, with viewing direction oriented approximately north. Rapidograph pen for scale in A. Hammerhead for scale in B.
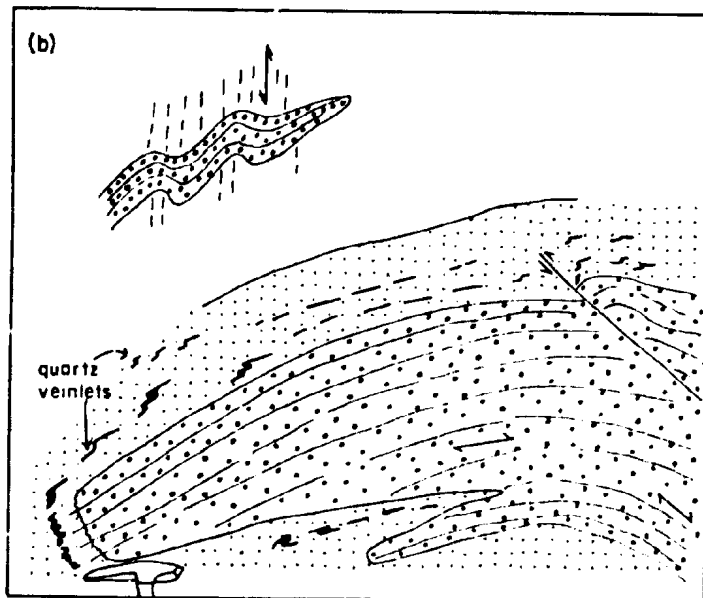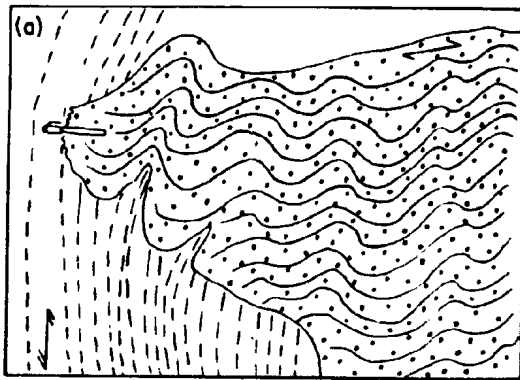
coarse-grained, medium-grained greywacke, shale

S_1: best developed in greywacke portions

S_2: best developed in shale portions

a variable character. In the western area a penetrative, S_1 cleavage is developed that is axial planar to F_1 isoclines (Figure 52). In eastern areas a weak, non-penetrative axial planar S_1 cleavage is locally developed in the hinge zones of isoclinal F_1 folds. S_1 here is defined by thin seams of opaque Fe-oxides and a weak alignment of micas (pressure solution seams). Locally a weak bedding-parallel cleavage is noted and since both of these surfaces are folded by later F_2 folds, this cleavage is likely an S_1 fabric. An S_1 fabric has not been recorded in the medium-grade rocks. The characteristics of the S_1 fabric developed in the metaturbidites are discussed in a later section (3.2.4).

iii) Inferred Macroscopic F_1 Folds

Large scale F_1 folds have not been directly mapped out in this study; documentation of bedding facing directions and bedding-cleavage relationships to substantiate these folds is lacking. However, small scale F_1 folds and a penetrative S_1 cleavage are present in two areas along the western margin of the supracrustal belt (see above) and in Figure 53 it can be seen that these are interpreted to represent the locations of major F_1 synclinal fold axes. Evidence presented above (section 3.2.1 ii) suggests that F_1 structures may have been developed throughout the entire Point Lake area (see also King, 1981), but are best preserved in the western Keskarrah Bay area. Figure 53 shows that these rather tight or keel-like synclines are separated
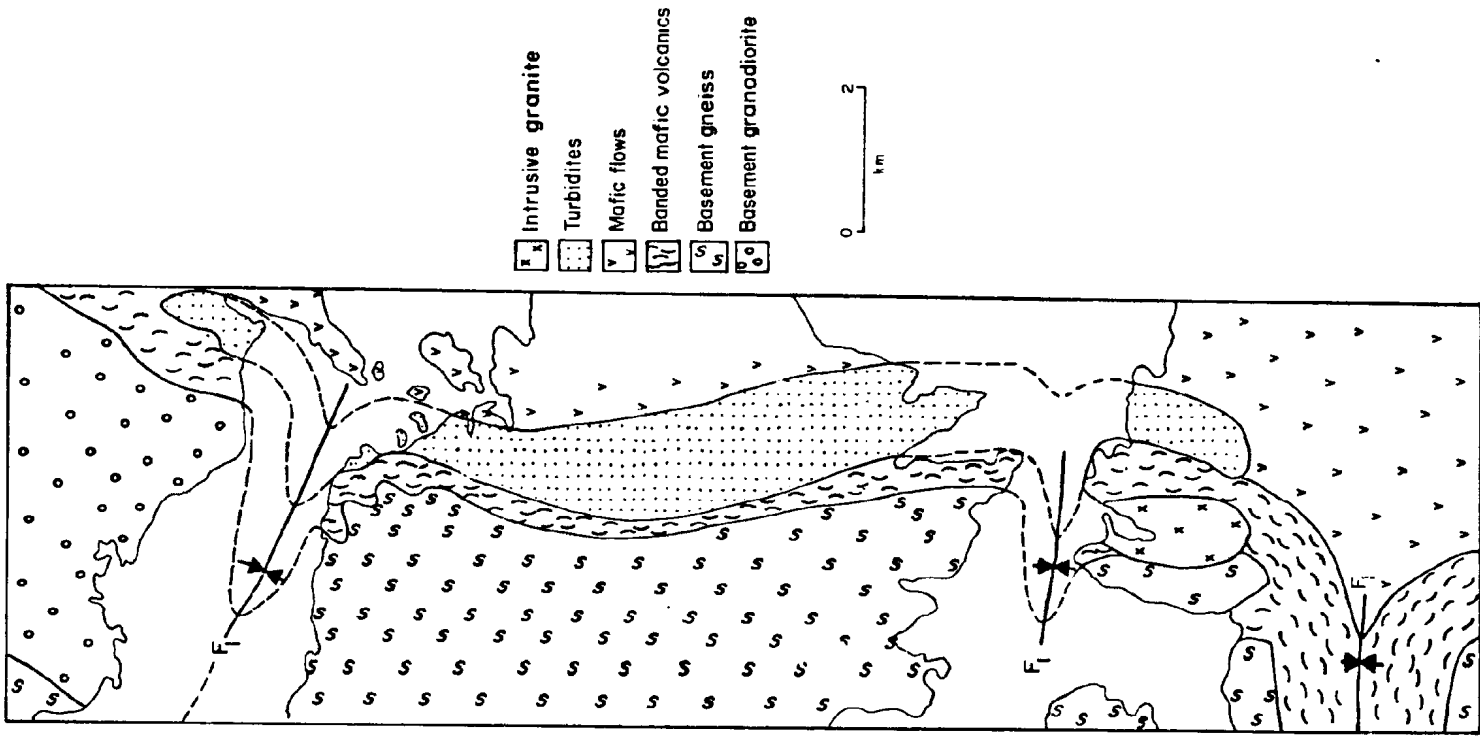
Figure 5.3: Inferred macroscopic F_1 folds along the west edge of the supracrustal belt (shoreline of Point Lake is indicated).

Legend:
- Intrusive granite
- Turbidites
- Mafic flows
- Banded mafic volcanics
- Basement gneiss
- Basement granodiorite

km scale: 0 — 2

by a broader, dome-like anticlinal structure. Ramsay (1967, p. 383) describes this type of fold pattern as being common at basement-cover interfaces in other orogenic belts and suggests that it is due to the competency contrast between the relatively dry rigid basement rocks and their more ductile cover.

iv) D_2 in Metaturbidites

Large scale north-trending F_2 folds are characteristic of the main phase of folding throughout the supracrustal terrane (Figure 50). Westward overturning of these folds is suggested by the predominance of steep east-dipping beds and easterly dips of the S_2 axial plane foliation.

Throughout much of the map area a northerly to northwesterly foliation is the dominant planar feature. This foliation is locally axial planar to both F_2 minor and major folds and thus it is ascribed to the D_2 event. The S_2 foliation is predominantly defined by the alignment of planar minerals such as micas (muscovite, biotite +/- chlorite). Cordierite and andalusite porphyroblasts have overgrown the S_2 foliation. The nature of the S_2 foliation developed in turbiditic rocks is discussed in greater detail below (3.2.3).

Within the low-grade Contwoyto Formation two major F_2 synformal fold traces are delineated (Figure 50). While the western synform was defined by Henderson and Easton (1977a, b) and substantiated during this study, the eastern synform

is poorly documented; Bostock (1980) noted an antiformal fold trace to the north of this eastern structure. F_2 fold axes are steeply plunging (Figures 5 and 50); this reflects the initial orientation of the steeply dipping beds on the limbs of the F_1 folds. In exposures of the western Contwoyto Formation on the north arm of Point Lake, F_2 fold axes plunge to the south on the north shore, but to the north on the south shore. A similar orientation is noted in shoreline exposures on the main part of Point Lake. This suggests that the Point Lake topographic low is a plunge depression. These opposing plunge directions may partly account for the elliptical map pattern of the western Contwoyto Formation, inferring a basin-type of fold interference pattern.

The geometry of the F_2 minor folds seen in the metaturbidites is interpreted to reflect that of the major folds (compare areas 1 and 2 with 3 in Figure 51). Open folds with round closures characterize minor folds in the eastern part of the map area. In the western part of the map area, minor folds on the limbs of the F_2 synforms are typically tight with angular closures (Figure 51, areas 1 and 2). Hinge zones are often not observed and Bostock (1980) suggested that this may indicate removal of isoclinal fold closures along shear planes. Evidence of shearing related to F_2 folding was not found in the turbidite units, however D_2-related shear zones are noted within volcanic units (see 3.2.1 v, below).

Throughout much of the turbidites macroscopic F_2 folds have not been inferred. The F_2 minor folds are tight to open, steeply plunging reclined folds with axial planes dipping steeply to the east and subangular to round fold closures. F_2 minor folds in some shoreline exposures can be seen to fold an earlier cleavage (S_1?) that parallels bedding: these folds are moderately northeast-plunging and have a dominant s-sense of asymmetry. Most of the minor folds within the low-grade Contwoyto Formation have this same pervasive s-sense of asymmetry, while those in the medium-grade rocks have no dominant sense of asymmetry.

F_2 fold axes in the turbidites have rather variable plunges and trends, which may indicate either: 1) variations in strain during D_2; 2) the variable orientation of bedding surfaces prior to D_2 or 3) the effects of later deformation. A combination of these factors seems likely.

v) D_2 in Conglomerate and Volcanic Units

Sandstone and carbonate-rich lenses and beds within the conglomerate serve as marker horizons, albeit discontinuous, that define a large, steeply north-plunging synform (Figure 54a). An axial planar foliation (S_2), defined by the parallel alignment of micas within the matrix and mafic volcanic clasts (Figure 54b), indicates a north-trending, steep to vertical axial surface. This foliation is the dominant fabric in the conglomerate and is an L-S fabric as indicated by the elongation direction of mafic volcanic

Figure 54: A; Photograph showing calcareous sandstone beds
that outline the F_2 synform in the Keskarrah

Formation conglomerate. View is to the north.

Rock face is approximately 10 meters high.

B; mafic volcanic clasts of Keskarrah Formation

conglomerate aligned in S_2 foliation (parallel to

hammer handle). Note that granitic clasts are

relatively undeformed. Hammer points

approximately north.

clasts. The long axes of the stretched clasts, which are contained within the foliation plane, plunge steeply and appear to parallel the major F_2 fold axis. Granitic clasts are generally little deformed (Figure 54b) and only locally contribute to a linear or planar fabric.

Banded mafic volcanics and turbiditic sediments in the western part of the map area are folded into a large scale, moderate northeast-plunging F_2 antiform (Figure 50; see also section 3.2.1 iv). In the hinge zone area the volcanics contain a weak S_2 axial plane foliation. On the north side of the lake, the turbidites are folded into a steeply south-plunging F_2 synform and antiform associated with a strong axial plane S_2 cleavage.

The hinge zones of the large scale antiforms within the felsic volcanic and mafic flow unit (Figure 50) are not readily observed in the field and were defined by Henderson and Easton (1977a, b) largely on the basis of stratigraphic relationships. The felsic volcanics contain a penetrative north-trending S_2 mica foliation. Near the F_2 hinge zone on the north arm of Point Lake, easterly trending compositional laminations (S_0/S_1?) are offset on a millimeter to centimeter scale along the S_2 foliation. A consistent sense of displacement was not determined.

Throughout the area the highly deformed state of many pillows within the mafic flow unit precludes top determinations. Flattened pillows are parallel to the S_2 foliation (defined by the alignment of chlorite, biotite and

amphiboles). Locally the pillows are also elongate and have steep to vertical plunges down the dip of the S_2 foliation plane, parallel to mineral lineations (amphiboles) and small scale crenulations. Steep amphibole lineations, which form an L-S fabric, indicate that D_2 involved extension as well as flattening. The S_2 foliation is often defined by discrete north-trending high strain zones in which randomly oriented amphiboles are progressively aligned into the north-trending foliation. These zones vary from several centimeters to tens of meters in width, but neither the sense nor amount of displacement was determined.

3.2.2 Post-D_2 Foliation-forming Events

Throughout the turbidite sequence, although dominantly within the eastern exposures, there is evidence of deformation that post-dates the main phase D_2 fold and fabric-forming event. Documentation of post-D_2 deformation comes largely from microstructural evidence, with field observations being limited. Deformation subsequent to D_2 resulted in fabric formation and modification of the pre-existing and dominant S_2 foliation. Associated folds have not been found.

The evidence for post-D_2 deformation includes:

1) At low metamorphic grades small scale crenulations or kinks of the S_2 mica schistosity, which may be accompanied by the formation of a discrete or zonal

crenulation cleavage (Powell, 1979), are oriented at a high angle (approximately easterly) to S_2;

2) In some BZ and a few medium-grade (CZ and AZ) rocks, biotite porphyroblasts are preferentially aligned parallel to the axial surfaces of the small scale crenulations. The same high angle orientation to S_2 is noted (Figure 51 and 55);

3) Many samples from the SZ contain two equally developed biotite schistosity trends, one being the northerly S_2 trend, the other being at a high angle to S_2;

4) In some samples from the AZ and SZ, muscovite laths have consistent conjugate orientations suggesting that they were once kinked or crenulated but subsequently annealed. In addition an annealed crenulation texture of muscovite may be retained within cordierite porphyroblasts but is not observed within the matrix;

5) Although most cordierite and andalusite porphyroblasts have overgrown both S_2 and post-S_2 fabrics (specifically those fabrics noted in points 3 and 4 above), some that grew post-S_2 schistosity show evidence of rotation;

6) Within the northeastern exposures of the sillimanite-grade Itchen Formation there is an isolated occurrence of a southeast-trending biotite schistosity that post-dates the north-northwest-trending S_2 foliation (Figure 50). King (1981) has established a D_3 fabric-forming event that resulted in a southeast-trending regional foliation

- 196 -

with which this later schistosity is tentatively correlated;

7) A biotite schistosity with a northeast trend is recorded within some low to medium-grade rocks, but becomes much more apparent in the eastern exposures of the Itchen Formation, where it is locally seen to post-date the northerly to northwesterly S_2 biotite schistosity (Figure 50). This northeasterly trend is consistent with the S_4 foliation trend of King (1981) which is well developed in the adjacent eastern Point Lake map area.

i) Biotite Porphyroblasts

Biotite porphyroblasts developed in the prograde metamorphic sequence adjacent to the Fubar fault, in the eastern BZ, have a distinctly angular, poikiloblastic habit (Figure 12). They define an L-S fabric (Figure 55), the planar component of which is marked by the preferred alignment of the porphyroblasts at a high angle (easterly) to the northerly trending S_2 foliation. The linear fabric is contained within the S_2 plane, with the long axes of the porphyroblasts plunging to the east or southeast, maintaining a roughly perpendicular relationship with the Fubar fault. In one outcrop cordierite porphyroblasts show a weak alignment parallel to this linear fabric (Figure 55b). The biotite porphyroblasts show evidence of having been deformed (kink bands, undulatory extinction, development of pressure shadows and deflection of the S_2 foliation around them). Although the biotite porphyroblasts often contain

Figure 55: Orientation of linear fabric defined by biotite
porphyroblasts and cordierite porphyroblasts.
Stereonet (A) represents data from the EBZ, near
the Fubar fault and the eastern medium - grade
zones (lower hemisphere projection using Schmidt
net). Schematic block section (B) taken from a
hand specimen (about 1/2 actual size) showing the
orientation of the L-S fabric defined by biotite
porphyroblasts and less commonly cordierite
porphyroblasts. S_0 and S_2 are oriented
approximately north-northwesterly and dip about
60°.

N

S
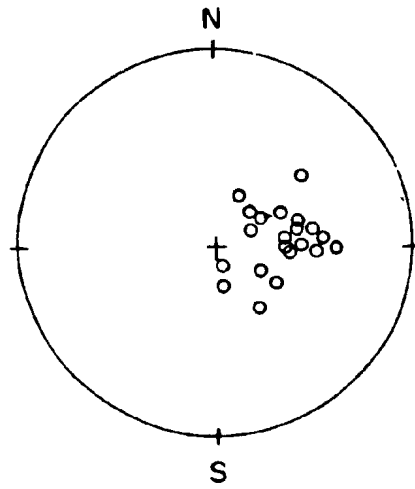
A

Crenulated S$_2$ muscovite-biotite schistosity

biotite porphyroblast

cordierite porphyroblast

S$_2$

S$_0$

B

L$_{bio/cord}$ + crenulation axis
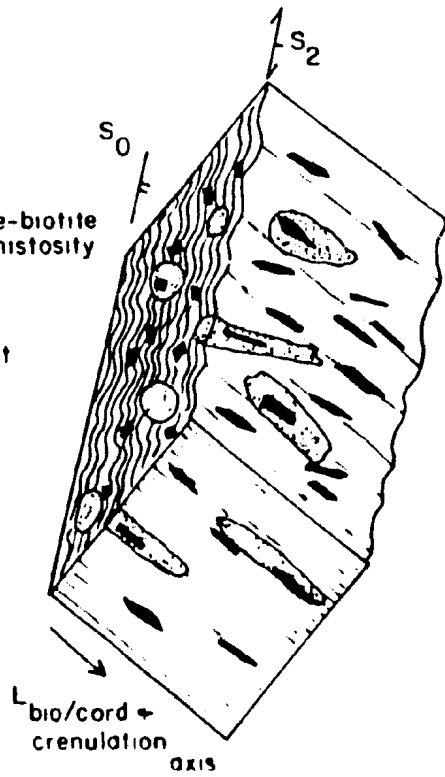
quartz inclusions, these inclusions were not seen to define trails, such as those described by Fyson (1975, 1980).

Characteristic habits and relationships of the biotite porphyroblasts to the northerly striking S_2 foliation are illustrated in Figure 56. The textural evidence indicates that while some of these porphyroblasts clearly truncate (and therefore post-date) S_2, others deflect (and may either pre-date or have formed during) S_2. This suggests either two periods of biotite porphyroblast growth, or alternatively porphyroblast growth was initiated during S_2 and continued during post-S_2 fabric formation.

Lister et al. (1986) examined the mechanism of porphyroblast growth in a detailed optical and electron microscope study of biotite porphyroblasts in pelitic schists from the Pyrenees. Their proposed mechanism involved the growth of biotite porphyroblasts into their own dilating pressure shadows. While no attempt was made to examine mechanisms of porphyroblast growth in this study, it is interesting to note that the biotite porphyroblasts studied by Lister et al. (1986) exhibit features similar to those of this study, notably: evidence of growth of the porphyroblasts during and after small scale folding, and crenulation of a pre-existing fabric resulting in porphyroblasts with crenulated or kinked basal cleavage planes and the formation of quartz-rich pressure shadows (Figure 56).

Figure 56: Characteristic habits of biotite porphyroblasts

from the BZ (A - D), AZ (E) and SZ (F). In A and

B biotite porphyroblasts overgrow the S_2

foliation and are approximately aligned axial

planar to open warps and small scale kinks in

S_0/S_2. B is an enlarged view of the small circled

area in A. The biotite porphyroblast in C

overgrows the kinked and crenulated S_2 fabric but

also contains evidence of deformation (kinked

basal cleavage planes). S_2 foliation in D (upper)

is deflected around the biotite porphyroblast and

quartz and chlorite have grown in pressure

shadows. The biotite porphyroblast in D (lower)

may have grown syn-S_2 as it has been kinked

during deformation of S_2. Biotite porphyroblasts

in E contain muscovite, the external muscovite

fabric is deflected around the porphyroblasts,

the biotite cleavage planes are kinked and there

is quartz growth in the pressure shadows. Biotite

porphyroblasts in F overgrow the external

muscovite fabric but display kinked cleavage

planes and coarse grained quartz has grown in the

pressure shadows.

epidote and opaque-filled fracture

quartz-rich, mica-poor layer (S_0)

mica-rich layer (S_0)

a.

1mm

b.

.250 mm

c.

.300 mm

d.

.300 mm

muscovite

e.

.750mm

inclusions

f.

.750mm
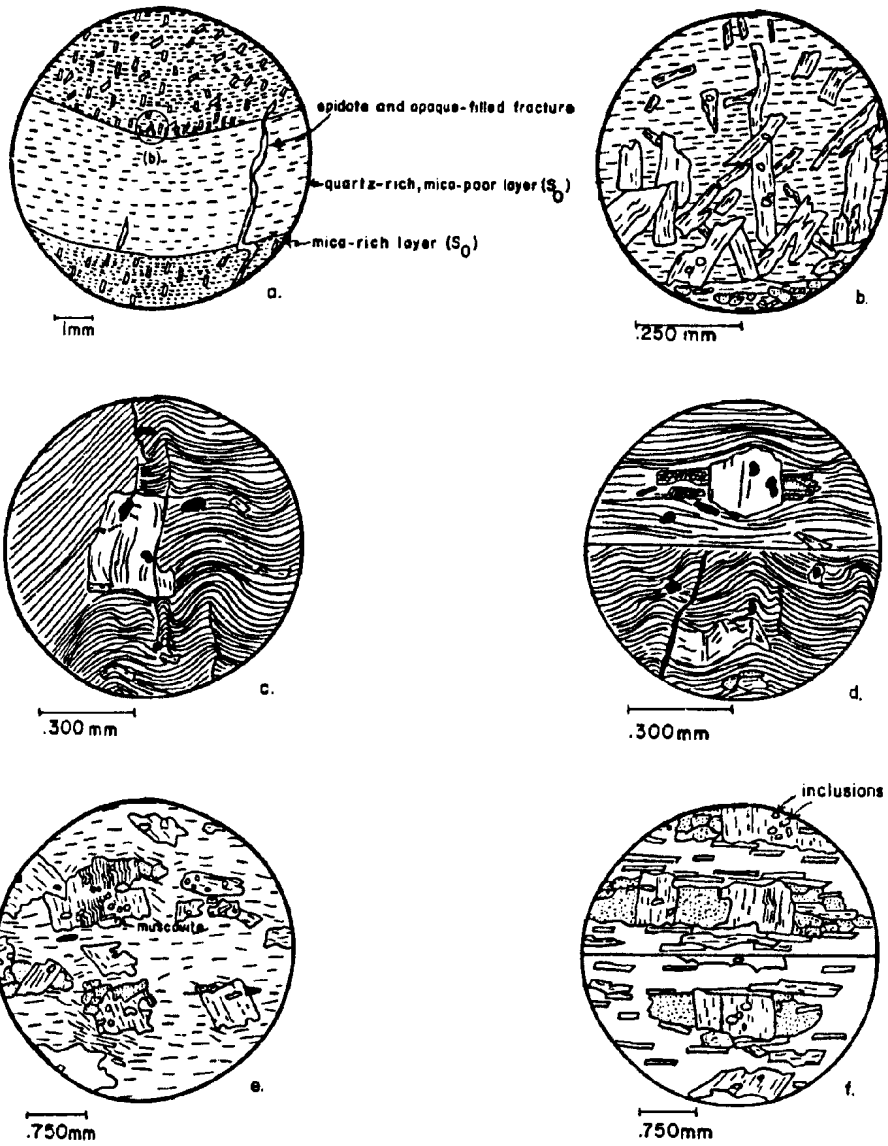
fine-grained muscovite-chlorite-biotite schistosity (S_2) of BZ rocks (a-d).

coarse-grained muscovite schistosity (S_2) of AZ, SZ rocks (e-f).

coarse-grained quartz (b, d-f).   chlorite (d)   tourmaline (d)

opaque

Note: in b-f detail in biotite porphyroblasts represents basal cleavage traces; those with no cleavage detail represent basal sections.

3.2.3 Fabric Development

i) General Statement

This section contains a more rigorous examination of the foliations formed during the D_1 and D_2 deformational events. In addition possible mechanism(s) of fabric formation are discussed. The terminology of Powell (1979) has been adopted in the classification of cleavage, foliation and crenulation types and is summarized in Appendix D.

ii) S_1

In the WCHZ, S_1 forms a well defined rough cleavage or a schistosity defined by the planar alignment of chlorite and muscovite and the preferred dimensional orientation of quartz clasts and opaques. Quartz-mica beard overgrowths have formed on some of the quartz clasts (Figure 57). The majority of quartz clasts are strained, exhibiting undulatory extinction and many show evidence of recrystallization. Within the WBZ detrital quartz clasts were extensively recrystallized during D_1 (Figure 13). In southern exposures of the WCHZ the S_1 foliation is a well developed rough cleavage partly defined by opaque seams, and the cleavage may be refracted across layers of different competency.

Samples from the vicinity of F_1 folds in the eastern low-grade rocks contain a discrete S_2 crenulation cleavage, with S_1 preserved in closely-spaced microlithons in which

Figure 57: Photomicrograph of quartz-mica beards developed in pressure shadows between quartz clasts. Note recrystallization of smaller quartz clast (center bottom of photograph). Top, plane light. Bottom, crossed nicols. Length of sections shown approximately 0.6 mm.
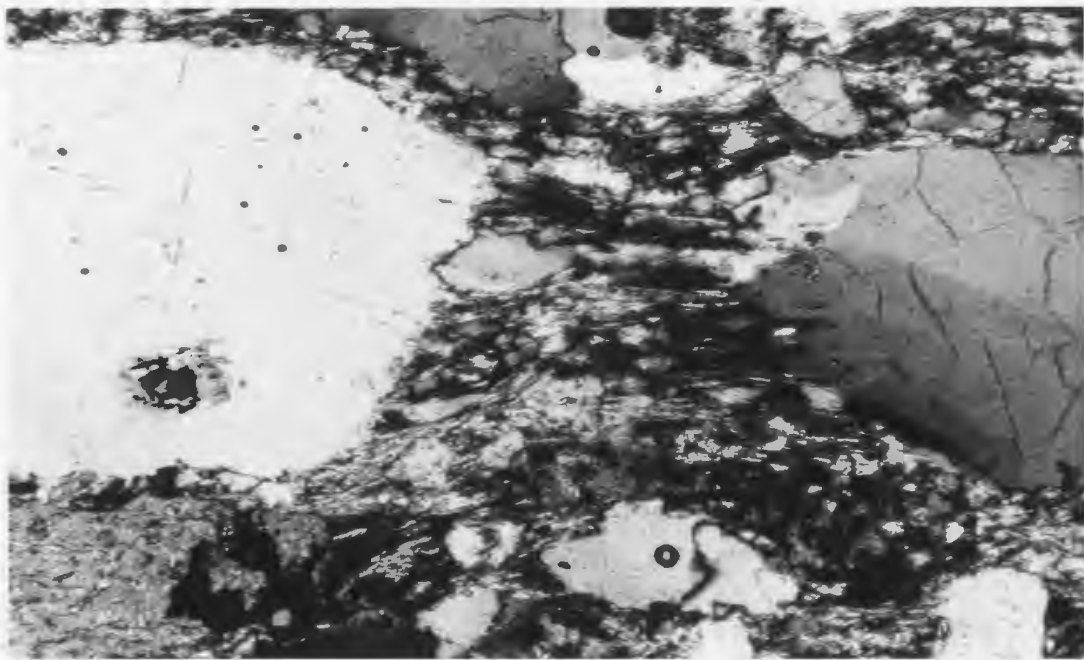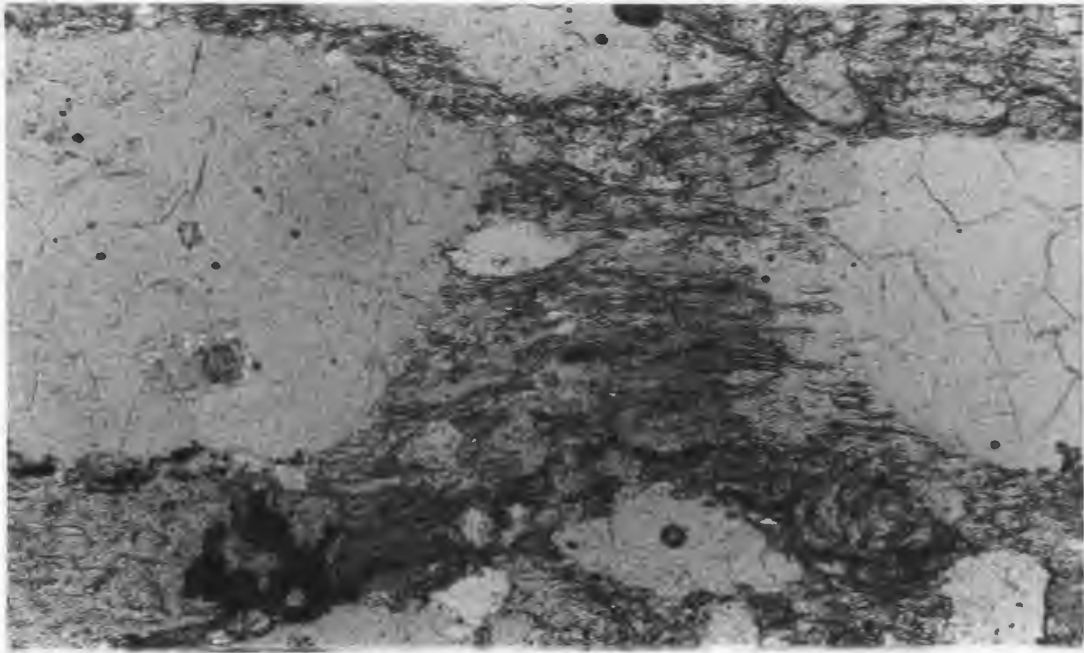
fine-grained micas are aligned parallel to the bedding surfaces (S_0).

iii) S_2

The northerly striking S_2 foliation is heterogeneously developed throughout the turbidite sequence. This variation results from metamorphic grade contrasts, varying lithologies and the presence or absence and intensity of the earlier formed S_1 cleavage.

Within the CHZ, where there is no visible evidence of an earlier fabric, the S_2 cleavage in the greywackes varies from a weak anastomosing rough cleavage to a well defined rough cleavage (Figures 9, 58) defined by the alignment of opaque seams and very fine-grained micas. The degree of microlithon fabric alignment appears to vary with the grain size of the phyllosilicates, which is in turn a function of metamorphic grade. The finest grained micas are randomly oriented while the coarser-grained micas display a stronger preferred orientation. Detrital quartz and plagioclase grains in greywackes have weak to well developed quartz-mica beard overgrowths and while both grain types may show a near random orientation, the long axis of quartz clasts are often aligned parallel to the cleavage. Quartz grains and quartz aggregates both tend to be strained, although there is some indication that in those rocks that have the weakest cleavage development there is a higher proportion of unstrained grains. Plagioclase grains on the other hand

Figure 58: Photomicrograph of an eastern BZ metagreywacke showing weak development of quartz-mica beards and a strong disjunctive cleavage that is defined by opaque-mica seams. Length of section shown approximately 3.4 mm.

Figure 59: Photomicrograph of F_2 folds, spaced S_2 axial plane cleavage and penetrative S_1 cleavage (folded) in a western CHZ metagreywacke. Length of section shown approximately 3.4 mm.
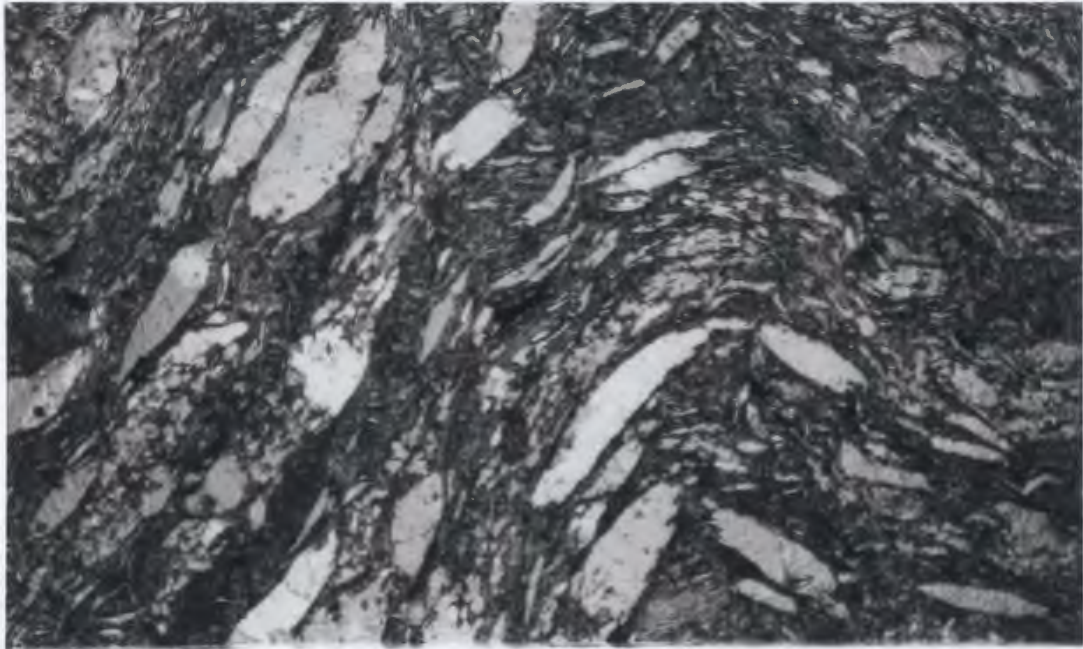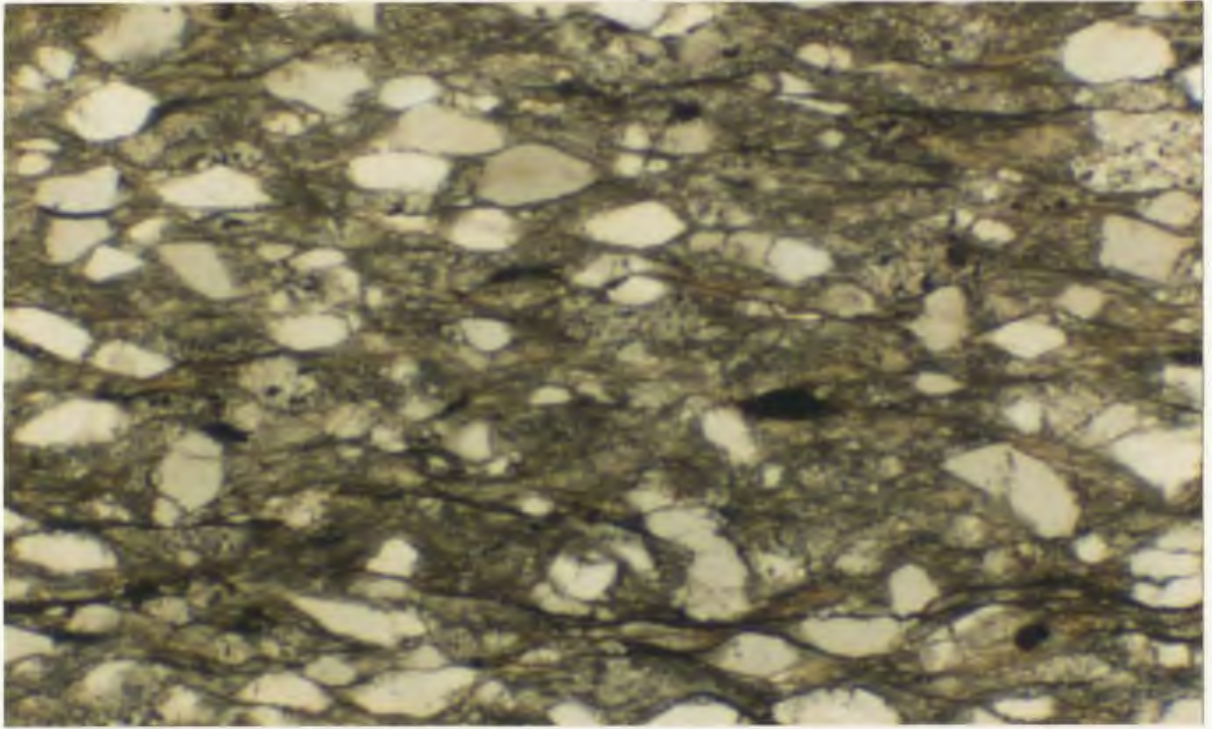
rarely show any evidence of strain. In some of the coarser-grained greywackes from the WCHZ, S_2 forms a continuous schistosity.

Pelitic or more shaly compositions always show a stronger cleavage development than the greywackes and possess a close-spaced smooth cleavage or continuous cleavage. Refraction of the cleavage is common in passing from a shale to a greywacke layer. The rare detrital quartz grains have a preferred alignment parallel to the slaty cleavage or schistosity that forms at higher grades.

Within the BZ the phyllosilicates are coarser grained and their dimensional orientation defines a continuous cleavage or schistosity. Quartz and plagioclase are generally recrystallized, although detrital grain shapes are retained and quartz-mica beard overgrowths can be observed in some samples. Within the upper portion of the EBZ (where biotite porphyroblasts are observed) and in the medium-grade rocks, the S_2 fabric is defined by a biotite-muscovite+/- chlorite schistosity. In these rocks quartz and plagioclase form equant polygonal crystals; only rarely are detrital grain shapes retained and quartz-mica beards are not developed.

Where the eastern low-grade rocks contain a pre-existing planar anisotropy (thought to result from development of the S_1 cleavage), S_2 may form a closely spaced crenulation cleavage of either the discrete or zonal type. The S_2 discrete crenulation cleavage is formed by discontinuous

opaque seams on the limbs of crenulations that are axial planar to F_2 minor folds. Where observed, the S_2 zonal crenulation cleavage is defined by the parallel alignment of micas rather than opaque seams.

In the western part of the map area S_1 forms a penetrative schistosity which is folded and kinked by F_2 folds (Figure 59), with the S_2 cleavage localized in micaceous layers, forming a zonal crenulation cleavage. Two samples from the hinge zone area of the western F_2 synform are shown in Figure 60. The samples contain a compositional layering (S_0?) of quartz clast-rich (psammitic) layers and micaceous (pelitic) layers. Quartz clasts have weakly developed quartz-mica beards. Both S_1 and S_2 cross-cut the layering and both cleavages are refracted across the layering. In the psammite, S_1 is defined by the preferred alignment of micas, quartz clasts (most prominent in Figure 60a) and widely spaced, poorly defined opaque seams. Whereas S_2 in psammitic layers forms a spaced crenulation cleavage, partly defined by opaque seams and a weak alignment of quartz clasts (Figure 60b). In pelite the S_1 mica cleavage is tightly crenulated by S_2 and S_2 is defined by prominent close spaced opaque seams. The apparent offset of the quartz vein in Figure 60b does not require a component of shearing as it may be explained by folding during S_2, with removal of the fold limbs accomplished by a combination of attenuation and pressure solution processes.
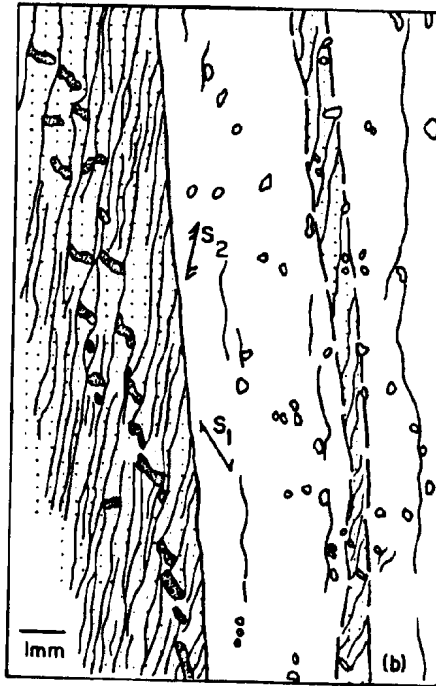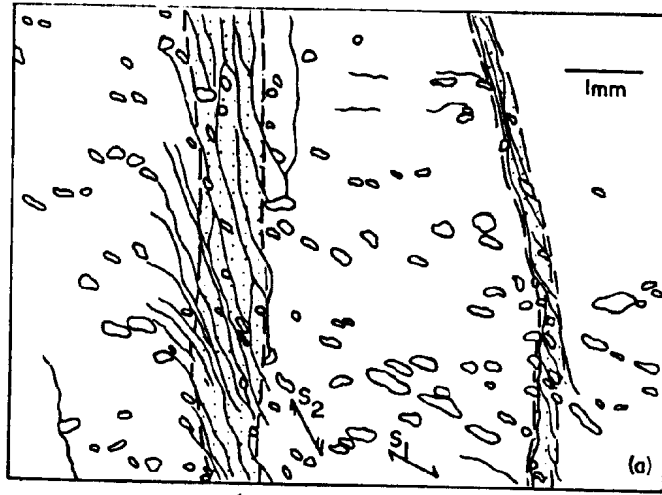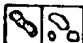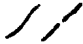
shale, greywacke   cleavage trace

quartz vein segments, quartz clasts

compositional boundary (bedding):distinct, approximate

Figure 60:(a) and (b) sketches from thin sections of WCHZ metagreywackes
showing penetrative S_1 and S_2 crenulation cleavage. See text
for explanation.

iv) Summary of Cleavage Development

At the lowest metamorphic grades recorded in the study area (ECHZ and part of the WCHZ), both S_1 and S_2 foliations in the greywackes are defined as rough cleavages that vary from weak and anastomosing to well-defined. Quartz clasts often have corroded and indistinct boundaries with the fine-grained mica-rich siliceous matrices. Quartz-mica beard overgrowths are common on quartz and plagioclase clasts, but are variable in degree of development.

Gray (1978) concluded that, while the alignment of phyllosilicates is partly due to crystallization/recrystallization, this type of cleavage formed dominantly by a solution transfer mechanism, with the opaque-mica seams representing pressure solution surfaces. Inherent in this process is the lack of internal deformation structures and evidence of recrystallization within the clast-forming phases. However, in the samples from Keskarrah Bay it is evident that although feldspar clasts are typically undeformed, the quartz clasts invariably show evidence of deformation. It is uncertain whether the deformation reflects an original feature of the source rock or was acquired during cleavage formation. Should the latter be the case then the solution transfer mechanism envisaged by Gray (1978) cannot be solely responsible for the formation of the cleavages, and some ductile deformation of quartz must have accompanied it.

Within the BZ and parts of the WCHZ, the micas are coarser-grained, have a strong preferred alignment and the S_1 and S_2 cleavages are of the continuous rather than disjunctive type (Powell, 1979). Quartz-mica beard overgrowths can still be observed and quartz clasts are recrystallized. At grades higher than, and within parts of, the BZ polygonal grain aggregates and triple junctions (between quartz grains) indicate that recrystallization and plastic deformation are likely responsible for schistosity development. It is to be expected that these processes would obliterate evidence of solution transfer mechanisms that may have taken place at lowest grades.

3.3 Deformation of the Basement Terrane

3.3.1 Gneiss-forming Event (D_x)

The earliest deformational event (D_x) in the study area is recognized only in the basement gneiss terrane and led to the formation of gneissic banding. Complex relationships observed between different phases of the gneiss suggest that the gneisses were formed during more than one event. For example: 1) on the north arm of Point Lake (about 1.5 km west of the supracrustal contact), unit 1a contains an enclave (unit 1b) in which Easton et al. (1981) recognized three phases of folding and 2) about 2.5 km west of the supracrustal contact, on the north shore of Point Lake, a basin and dome interference pattern is noted in hornblende

tonalite gneiss which is cross-cut by later migmatitic and intrusive phases. The evidence therefore indicates that D_x included multiphase deformation accompanied by extensive migmatization, intrusive activity and medium to high-grade metamorphism.

The lack of migmatization in the schistose rocks of the Yellowknife Supergroup suggests D_x pre-dated deformation in the supracrustals. Other evidence that D_x pre-dated deposition of the Yellowknife Supergroup includes the documentation of an angular unconformity between the gneisses and supracrustals and the recognition of gneissic cobbles in the Keskarrah Formation conglomerate, that are lithologically comparable to units within the gneiss terrane (Easton et al., 1981, 1982).

Other structural elements superimposed on D_x are also observed in the basement terrane. These may be correlative with the structures in the supracrustal terrane, and are discussed below.

3.3.2 Isoclinal Folds (D_1?)

Locally the gneissic banding is folded into small scale, tight, upright folds (Figure 50) that vary from long limbed isoclines to intrafolial folds. The initial orientation of these folds is uncertain as they are refolded by F_2 (see below). In the thickened hinge zones of the folds, micaceous minerals are aligned in an axial plane foliation. Major folds related to these small scale structures have not been

identified. These isoclines may be correlative with D_1 in the supracrustal terrane as a similar style of folding is documented within the banded mafic volcanics (unit 3). However, it is also possible that these folds were formed pre-D_1 and that during D_1 they were tightened into isoclines.

3.3.3 D_2 Northerly Oriented Structures

The northeast to east-trending gneissic banding prevalent in western exposures of the gneiss terrane becomes progressively reoriented towards northerly trends near the contact with the supracrustals (Figure 50). This change in structural trend is partly accomplished through the development of macroscopic folds formed during the D_2 event, which also affected the supracrustals.

Macroscopic F_2 folds initially outlined from aerial photographs (Figure 50) are defined by the trace of the gneissic banding, the contact between the gneisses and banded mafic volcanics and the asymmetry of minor folds. The synformal and antiformal folds thus outlined (Figure 50) plunge moderately to steeply to the northeast. Minor folds, representative of D_1 or D_x folds, are folded about these major structures. Locally, a weak biotite +/- chlorite schistosity is axial planar to these folds and small scale crenulations are parallel to the fold axes in the hinge zones of some folds. Mineral lineations (defined by

plagioclase and epidote) are rare, but where present are also parallel to F_2 fold axes.

Adjacent to the supracrustal terrane the steeply dipping, northerly trends of gneissic banding indicate a complete reorientation of earlier structural trends into the D_2 orientation (Figure 50). In this area the gneisses and granitoids commonly have mylonitic textures which are partly defined by muscovite and chlorite, indicating that they were formed during low-grade metamorphism.

3.3.4 Recumbent Structures

Southern exposures of the basement gneiss terrane (Figure 50) are characterized by recumbent folds and gently to moderately dipping and plunging planar and linear features. To the west of the gneiss-supracrustal boundary Easton et al. (1981) noted a west-verging recumbent fold in banded mafic volcanics. Kusky (1987) has re-interpreted the outlier of Yellowknife Supergroup rocks (Figure 3; identified by Easton et al., 1981) as a klippe. On the north shore of Point Lake west-verging recumbent folds, a few meters (Figure 61a) to tens of meters in amplitude on vertical outcrops, have shallow north to northeast-plunging fold axes and shallow east-dipping axial planes. Typical of these folds is a progressive steepening of the limbs from the antiforms into the synforms, so that the antiforms are recumbent but the synforms are upright. This relationship is sketched in Figure 61b which also illustrates a possible
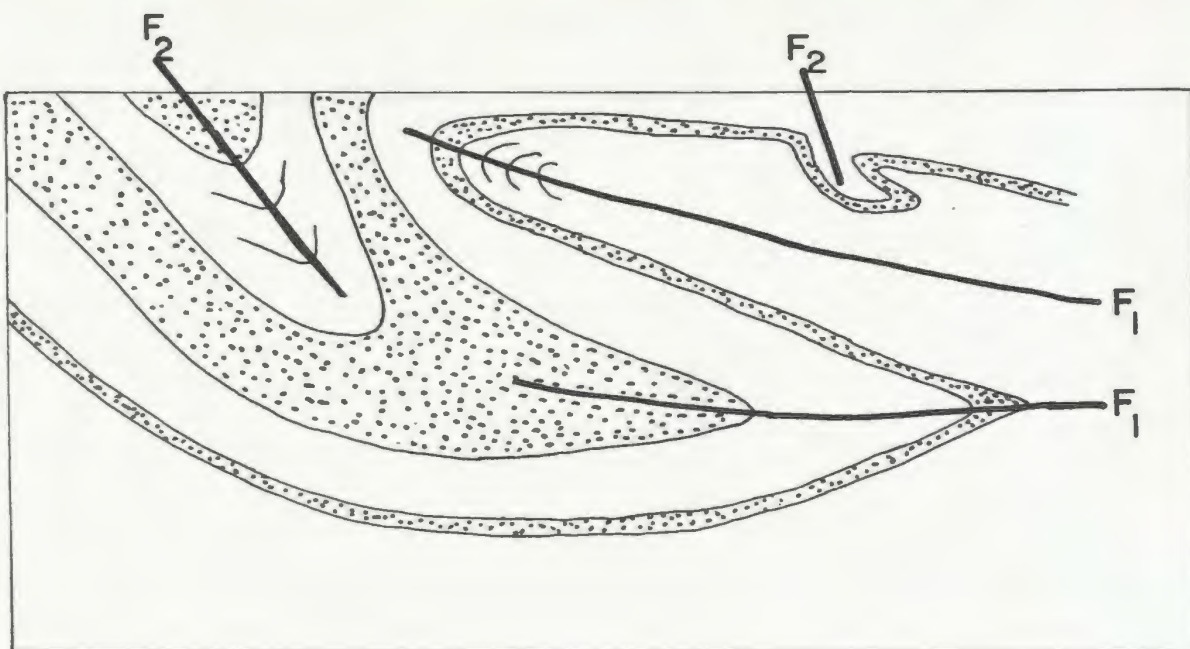
Figure 61 : Top; photograph of granitic gneiss showing possible
interference between recumbent and upright folds.
Bottom; interpretative sketch of above photograph.

interpretation of the upright folds refolding earlier formed recumbent folds. Alternatively the folds may be of the same generation. Kusky (1987 and pers. comm.) is investigating the possible existence of nappe structures in this area of the basement gneiss terrane. The relationship of the recumbent structures to the previously described macroscopic F_2 folds is uncertain due to limited outcrop and an abundance of intrusive rocks. However the shallow east-dips of granitic sheets and gneissosities progressively steepen toward the contact with the supracrustals suggesting reorientation into D_2 structural trends. Thus the formation of the recumbent structures may predate D_2.

3.3.5 Basement Granodiorite-granite

Exposures of the basement granodiorite on the north arm of Point Lake (Figure 4; Henderson and Easton, 1977b) contain thin (about 10 cm wide) southwest to east-west-trending retrograde shear zones with mylonitic textures. Mafic dikes which intrude the granodiorite also contain an east-west oriented foliation. Elsewhere the granodiorite contains localized north-trending shear zones. The shear zones are composed of quartz-eye chlorite schist or phyllonite which is interpreted to have formed contemporaneously with the metamorphism of the supracrustals. Thus it is likely that this basement terrane acted as a relatively rigid block during deformation of the supracrustals and responded to deformation through the

development of localized shear zones rather than a
penetrative fabric.

3.4 Faulting

3.4.1 Gneiss-supracrustal Boundary

Henderson and Easton (1977a, b) recognized a series of
four faults, which Henderson (1981) speculated were active
during basin development. The most westerly of these faults
is represented by the gneiss-supracrustal boundary (Figure
50; Henderson and Easton, 1977a, b). Along this boundary
volcanics of the Yellowknife Supergroup contain thin
chlorite-rich shear zones while the gneisses and younger
granitic phases (units 1f, 12) contain narrow mylonite zones
also of low metamorphic grade (see 3.3.3). Within the
gneisses these textures become less apparent with increasing
distance from the contact and 2 to 3 kilometers to the west
only discrete 1 meter wide shear zones are recognized. It
was previously suggested (section 3.3.3) that some of the
mylonitic textures formed during D_2. Easton (1985; his
Figures 2 and 3) indicates that the mylonite zone along the
gneiss-supracrustal boundary is folded by F_2, suggesting
some mylonitization pre-dated D_2. While these observations
do not relate mylonitic processes to basin formation they
suggest that deformation processes related to faulting along
the boundary were long-lived. Kusky (1987) suggested the
gneiss-supracrustal boundary may represent a deep level
thrust and the presence of recumbent folds within the gneiss

terrane may indicate that the basement terrane was also involved in westward directed thrusting.

3.4.2 Faults in the Supracrustals

Two major north-trending faults are found within the central exposures of the turbidite units (Figure 50). The Fubar fault occurs within the Contwoyto Formation whereas the easternmost fault marks the contact between the Contwoyto and Itchen Formations for most of its length. South of Point Lake the two faults may merge (Figure 5), but neither can be traced into the northern area because of extensive drift cover.

The eastern fault is steeply dipping and marked by chloritization of biotite and pinnitization of cordierite. Widespread chloritization of the Itchen Formation schists is noted to the east of this fault, suggesting that it may have been the locus of extensive fluid mobility post-dating peak metamorphism.

Fubar fault is a moderately east-dipping fault zone that forms a gentle arc concave to the east, approximately parallel to bedding and S_2 schistosity trends. It is clearly a post-metamorphic feature as it juxtaposes AZ rocks against the lower grade BZ equivalents along part of its length and southeast of the map area SZ rocks are displaced against those of the BZ (Henderson and Easton, 1977b; Bostock, 1980). Medium-grade rocks within the Fubar fault zone are extensively hematized and chloritized and quartz veins are

abundant indicating the previous passage of hydrous fluids. Axial traces of folded quartz veins within the fault zone are parallel to the strike of the fault, with axes plunging down the dip of the fault plane (reclined folds). Folding of the quartz veins into long limbed isoclines and conjugate kink banding within muscovite-rich layers indicate that deformation associated with faulting took place, at least in part, in the ductile regime and may indicate a prolonged movement history on this fault. Although movement along the Fubar fault is indicated to have been combined dip-slip and strike-slip, telescoping of the metamorphic zones suggests a significant dip-slip component. The Fubar fault is suggested to be an east-side-up contraction fault.

Numerous northeast-southwest-trending faults transect the map area (Figure 50; Henderson and Easton, 1977b). Some of these faults offset lithologic boundaries and foliations and possibly also some of the north-trending faults, suggesting they formed late in the deformational history.

3.5 Structural Overprinting and Refolding

Throughout the supracrustal terrane there is a map scale zonation of structural elements associated with each deformational episode that can be viewed as the result of structural overprinting. This zonation is illustrated in Figure 50 and is based on the relative intensity or dominance of one fabric element over another. Given two

fabric-forming events, the preservation of the earlier
fabric depends, amongst other factors, on the relative
intensity of the event that follows, as does the type of
interference pattern observed between two folding events
(Pearson and Lewry, 1974).

In the supracrustal rocks in the western part of the map
area, it has been shown that S_1 is locally an intense,
penetrative axial plane cleavage associated with F_1
isoclines. Although F_2 resulted in folding of this S_1
foliation, there was little fabric development associated
with D_2 folding. Thus the preservation of S_1 in this area
indicates D_1 was more intense than D_2. The resultant
refolding of the inferred F_1 isoclines by large scale F_2
folds (Figure 62) has given rise to interference patterns
similar to the type 3 patterns described by Ramsay (1967).
Interference patterns such as this are observed along the
shores of Point Lake (Figure 51, 52).

Throughout most of the map area, however, D_2 fabric
elements dominate (F_2, S_2: Figure 50) and evidence of D_1 is
either lacking or only preserved as a weak cleavage. S_2 is
generally northerly trending and F_2 folds plunge moderately
to the north and south.

The development of a post-D_2 fabric is noted only in
central and eastern exposures of the turbidite sequence. In
the central area S_2 is the dominant mesoscopic fabric and
post-S_2 fabrics are noted at the microscopic scale, but in
extreme eastern exposures this relationship is reversed with
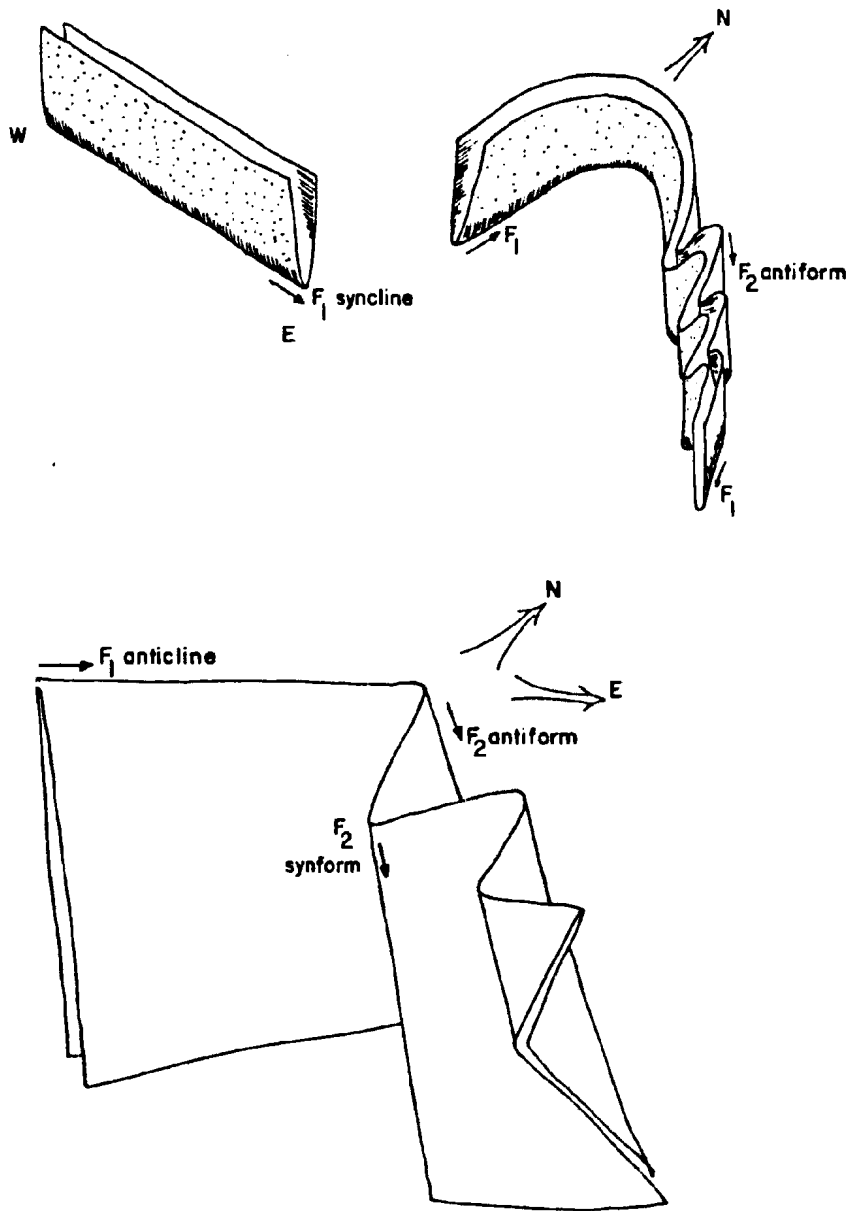
Figure 62 : Schematic representation of F_1 and F_2 fold interference pattern.

post-S_2 fabrics dominating at the mesoscopic scale and S_2 being recognized only in thin section.

3.6 Basement Control During Deformation of the Supracrustals

It has already been noted that the presence of basement rocks may have exerted some control on the style of deformation and the orientation of structures within the supracrustal terrane. This is discussed further below.

The metavolcanics and metasediments that form the inferred macroscopic F_1 synclines (Figure 53) were intensely deformed during D_1, the main fabric-forming event locally. This is considered to be due to the local infolding of the cover sequence into the basement, with narrow pinched in synforms of cover rocks separated by wide antiformal arches of basement in a pattern similar to that described by Ramsay (1967, p. 383) from the Alps.

Basement control on D_2 structures in the supracrustals may be illustrated by contrasting the tight, angular folds of the western area adjacent to the basement with the more open, rounded folds observed further east. F_2 folds in both areas are overturned towards the west, i.e. towards the basement gneisses. Considering the evidence presented above that the basement was a relatively rigid block during the deformation of the supracrustals, it is likely that it acted as a buttress against which the supracrustals were deformed. This situation would explain why F_2 folds formed adjacent to

the buttress at the margin of the deforming belt exhibit a tighter style of folding than those nearer the center.

Evidence that the degree of overturning of these folds increases toward the basement-cover interface was not found during the course of this study. However, west-verging recumbent folds are abundant to the west of the gneiss-supracrustal boundary (Easton et al., 1981; Kusky, 1987) and the presence of large. scale recumbent structures are suggested in this area (Kusky, 1987). In addition these relationships can be used to postulate that the gneiss-supracrustal boundary represents a crustal detachment zone, perhaps the deep level thrust that Kusky (1987) suggested, along which the cover rocks were transported.

4.0 RELATIVE TIMING OF METAMORPHISM AND DEFORMATION

4.1 General Statement

The time relationship between metamorphism and deformation within the area has been determined largely from observations made within the turbidite units. Fabric development is best documented in these rocks and the growth of porphyroblasts enables the establishment of the relative timing of peak metamorphic conditions relative to fabric formation.

Metamorphism associated with the deformation (D_x) of the basement gneisses was at medium to high-grades and was accompanied by anatexis. These rocks were subsequently partly retrogressed during the low-medium grade metamorphism of the supracrustal sequence. Evidence of this retrogression of the basement rocks is the replacement of hornblende and biotite by chlorite and the presence of low grade foliations correlated with those in the supracrustals, which are defined by the alignment of chlorite, biotite and muscovite. The basement granodiorite was also affected by retrogression, as indicated by chlorite-filled fractures and extensive alteration of feldspars.

4.2 Metamorphic Mineral Growth Relative to Fabric Formation

Throughout the study area, the predominant fabrics (S_1, S_2, post-S_2) are mainly defined by the preferred alignment of micaceous minerals, and in the case of volcanic rocks, by amphiboles. Porphyroblastic phases, with the local exception of biotite, amphiboles and rarely cordierite, do not define planar or linear fabrics. Prograde metamorphic mineral growth in relation to the fabrics and folds formed during deformational episodes is summarized in Figure 63.

In the low-grade Contwoyto Formation, metamorphic mineral growth accompanied the formation of S_1 and S_2. Although metaturbidites in the western belt have undergone a retrograde metamorphic event, muscovite, chlorite and biotite are seen to define both S_1 and S_2. In the western area retrograde chlorite growth occurred during and after S_2 fabric formation. While in the eastern sequence biotite growth during D_1 has not been established, it defines S_2 as well as post-S_2 fabrics.

Western exposures of medium-grade metaturbidites of the Contwoyto Formation have been disrupted by faulting and have undergone retrograde metamorphism so that a precise determination of the relative timing of metamorphism to deformation cannot be made. However, completely pinnitized cordierite porphyroblasts have overgrown a mica schistosity (S_1?) and have been rotated prior to or during the development of a second mica schistosity (S_2?). In view of

Figure 63

		Western Sequence		Eastern Sequence				
		D₁	D₂	D₁	D₂	Post-D₂(SE/NE schistosity)		
low-grade metasediments	Chl						Chl	low-grade metasediments
	Musc						Musc	
	Bio						Bio	
medium-grade metasediments	Chl						Chl	medium-grade metasediments
	Bio						Bio	
	Musc						Musc	
	Cord		?				Gar	
mafic flow volcanics	Chl						Staur	
	Bio						Cord	
	Actin						Andal	
	Hornbl						Sill	
banded mafic volcanics	Chl	?			?		Chl	felsic volcanics
	Bio				?		Musc	
	Actin	?			?		Bio	
	Hornbl						Gar	
							Amph	
							Chl	conglomerate
							Musc	

———— fabric-forming mineral phase

▬▬▬▬ porphyroblastic phase

Figure 63: Relative timing of prograde metamorphism and deformation in the Keskarrah Bay area. Note that in the western sequence, the timing of retrograde metamorphism, during which much chlorite was produced, has not been established but clearly post-dates D₂.

these relationships, in Figure 63 cordierite is indicated to have grown between D_1 and D_2 in the western sequence.

In the medium-grade Contwoyto and Itchen Formations of the eastern prograde sequence, evidence of the formation of either S_1 or F_1 has not been established, and peak metamorphic conditions in this area post-date D_2. Chlorite was not observed in the equilibrium assemblage of the medium-grade rocks, of either greywacke or Fe-rich composition. However, several of the previously proposed reactions require the presence of chlorite, for example in the initial formation of cordierite . Therefore chlorite is indicated in Figure 63 as a fabric-forming phase, it's stability slightly overlapping with that of cordierite and andalusite. Growth of porphyroblasts of garnet and staurolite may have occurred prior to D_2, however porphyroblasts of cordierite and andalusite, have overgrown and contain the S_2 biotite schistosity.

Many samples from the CZ, AZ and western parts of the SZ contain cordierite and andalusite porphyroblasts that have also overgrown the L-S biotite fabric and the post-S_2 biotite schistosity. This indicates that porphyroblast growth post-dated the development of all these fabrics (see 3.2.2). However, although rarely observed, cordierite is also seen to form a linear fabric parallel to the lineation of biotite porphyroblasts. These relationships indicate that the growth of some cordierite was initiated during post-D_2 deformation but outlasted it.

The metamorphic minerals defining the foliations within the mafic volcanic rocks indicate prograde metamorphism during D_1 and D_2. The locally developed S_1 foliation in the mafic flows is defined by chlorite (+/- biotite, actinolite), as is the more widespread S_2 foliation. Hornblende porphyroblasts are reoriented into north-trending S_2 shear zones, indicating the metamorphic peak was attained during or slightly before D_2. The banded mafic volcanics may have been within medium-grade metamorphic conditions throughout both D_1 and D_2 as both foliations are defined by the alignment of hornblende +/- biotite.

In summary (Figure 63), peak metamorphic conditions were attained prior to or during D_2 in the western prograde sequence. In the eastern sequence evidence from porphyroblasts of cordierite and andalusite indicates peak conditions post-dated D_2 and occurred before, during and after the post-D_2 event(s). Limited observations place growth of these porphyroblastic phases prior to the formation of the northeast-trending biotite schistosity (S_4 of King, 1981).

4.3 Disposition of Metamorphic Isograds

Fabric analysis in the eastern prograde sequence indicates the metamorphic peak was established subsequent to the formation of the S_2 foliation, suggesting the metamorphic pattern post-dates large scale F_2 folding and

was not significantly affected by this main phase of deformation.

The attitude of the isograds in central and western parts of the area is problematical. In this area the lowest grade rocks, which also partly represent the youngest lithostratigraphic units, (Keskarrah Formation conglomerate and sandstone and Contwoyto Formation turbidites) are exposed in the core of a syncline. This fact, combined with the pre- to syn-D_2 metamorphic mineral growth recorded in both volcanic and sedimentary units, suggests that the central and western isograds have been folded.

At least one major discontinuity in the isograd pattern, coinciding with the Fubar fault, indicates westward telescoping of the metamorphic zones. A second discontinuity may be indicated in the central map area by the discrepancy in metamorphic grade recorded by mafic volcanics (unit 4) and the adjacent turbiditic sediments.

5.0 REGIONAL COMPARISONS AND DISCUSSION AND SUMMARY

5.1 Regional Comparisons

5.1.1 General Statement

The dispositions of metamorphic isograds and structural trends in the supracrustal rocks of the Itchen Lake region are roughly parallel to the arcuate shape of the greenstone belt (Figure 3). The metamorphic grade increases toward the major batholiths east and north of the study area (Tremblay, 1976; Bostock, 1980; King, 1981) and westward, toward the basement gneiss and 'Pointless' batholith terrane in the Keskarrah Bay area (Henderson and Easton, 1977a; this study). Since the eastern edge of the Keskarrah Bay map area adjoins the eastern Point Lake area examined by King (1981), the metamorphic and structural evolution of the present study area can be compared and correlated with the results therein (Figures 64-67; King, 1981).

5.1.2 Metamorphism

The eastward increase in metamorphic grade in the study area continues progressively through the eastern Point Lake area (Figure 64) to the Yamba batholith (Figure 3). West of this batholith schists of the Itchen Formation are transformed into gneisses (cordierite + granitic melt isograd), the highest metamorphic grade mapped by King

Figure 64: Metamorphic zonation of both the Keskarrah Bay and eastern Point Lake areas. Isograd ornaments are on the high grade side.

METAMORPHIC ISOGRADS

Biotite
Cordierite
Andalusite
Sillimanite
K-feldspar
Cordierite + granitic melt

Thrust fault
Fault
Basement
Granitoids

CHZ   chlorite zone
BZ   biotite zone
CZ   cordierite zone
AZ   andalusite zone
SZ   sillimanite zone
KZ   K-feldspar zone
C2Z   cordierite + granitic melt zone

ITCHEN LAKE

NORMA FAULT

FUBAR FAULT

POINT

LAKE

0   5
km

KESKARRAH BAY AREA | EASTERN POINT LAKE AREA (King, 1981)

(1981; Figure 64). In the Keskarrah Bay area metamorphic grade also increases westward towards the basement gneisses (Figure 64) and the granitoids of the 'Pointless' batholith (Figure 3). In this terrane outliers of the Yellowknife Supergroup are thought to have been metamorphosed to medium and possibly high grade (Easton et al., 1981, 1982).

The dominantly continuous metamorphic reactions leading to the formation of cordierite, andalusite and sillimanite documented in this study are similar to those suggested for the eastern Point Lake area by King (1981). One notable difference between the two areas is the absence of muscovite from the equilibrium assemblage of some of the AZ and SZ rocks noted in this study. King does not record this assemblage in the eastern Point Lake area, as muscovite is apparently present below the second sillimanite isograd in the K-feldspar zone (KZ). In the case of muscovite-absent assemblages, the higher grade KZ equivalent would be the assemblage sillimanite + quartz.

P-T estimates indicate that temperatures ranged from 450°C in the low-grade rocks to about 700°C in the high-grade gneissic rocks of the eastern Point Lake area (King, 1981). Pressures operative during regional metamorphism were relatively constant at about 3.0 kbar for low- to medium-grade rocks, but increased to about 4.5 kbar for the high-grade region of the eastern Point Lake area (King, 1981). These pressure estimates imply burial of the

supracrustal pile to depths of about 10-15 km and some
degree of differential uplift or tilting of the crust.

5.1.3 Deformation

Prior to deformation of the supracrustal rocks the
basement gneiss terrane underwent anatexis, migmatization
and several phases of folding. This early deformation of the
basement terrane is poorly understood at present. Subsequent
deformation of the gneisses can be correlated with that
which affected the cover sequence and resulted primarily in
a marginal overprint of F_2 folds and localized mylonitic
fabrics (S_2?). West-verging recumbent folds within the
gneisses may have developed during or before D_2 deformation
of the cover sequence, although their relative age is not
precisely defined.

In Table 7 the characteristic structural elements of the
supracrustal rocks of the Keskarrah Bay and eastern Point
Lake areas are compared and in Figure 65 foliation trends
for both areas are compiled.

F_1 folds are only locally observed in the eastern Point
Lake area, but may have been widespread and are everywhere
refolded by second phase folds (King, 1981). In both the
Keskarrah Bay and eastern Point Lake areas F_1 isoclines are
easterly trending, but the associated S_1 fabric is variably
developed. It is absent in the eastern Point Lake area
(King, 1981), but as already noted it forms a penetrative

TABLE 7: Comparison of deformational events and characteristic structural elements recognized in the supracrustal terrane of the Keskarrah Bay and eastern Point Lake areas.

		KESKARRAH BAY AREA	EASTERN POINT LAKE AREA
D_1	F_1:	E-W isoclinal folds of S_0, large scale folds in western area. Refolded during D_2.	F_1: E-W folds of S_0.
	S_1:	E-trending axial plane cleavage, penetrative (continuous chl-musc+/-bio schistosity) in western exposures, weakly developed (preserved in spaced microlithons) in eastern areas. Folded during D_2. chl-musc+/-bio growth.	S_1: Not developed, no metamorphic mineral growth.
D_2	F_2:	Major phase folds. N-S trends of axial planes and some fold axes. Moderate to steep or vertical plunges. Steeply overturned to west. Reclined folds.	F_2: Major phase folds. NE-SW trends common. Upright to overturned with subhorizontal plunges or upright to steeply reclined isoclines with moderate south plunges. Disposed in convergent and divergent fan axes.
	S_2:	Dominant N-trending foliation throughout most of the area, axial planar to F_2. Varies from first phase rough cleavage to discrete and zonal crenulation cleavages to continuous bio-musc+/-chl schistosity. Chl-musc-bio growth.	S_2: Local axial plane foliation to some folds. Biotite growth?
Post-D_2	Folds:	Small scale crenulations and kinks of S_2 foliation.	
	Fabric:	High angle orientation to S_2 (easterly). Varies from discrete and zonal crenulation cleavage to biotite schistosity. Biotite and rare cordierite porphyroblasts define L-S fabric (E-SE plunges). Correlative to S_4? Musc-bio-cord+/-chl+/ and growth.	
D_3	F_3:	No major folds recognized.	D_3: No major folds; small scale folding of quartz veins.
	S_3:	SE-trending biotite schistosity in eastern exposures of Itchen Formation.	S_3: Regional foliation (140-160° trends), dominant in medium-high grade (gneissic) Itchen Formation.
D_4	F_4:	No major folds recognized.	F_4: No major folds; strong axial plane crenulation cleavage, warps F_2 in high grade terrane. Steeply plunging folds of S_0 and F_2 axial traces.
	S_4:	NE-trending biotite schistosity noted throughout medium grade Contwoyto and Itchen Formation. Predominant in far eastern exposures.	S_4: Regional foliation (010-060° trend) dominant in low to medium grade Itchen Formation.

Figure 65:
FOLIATION
TRENDS
of the
POINT LAKE
AREA

Itchen Lake

POINT LAKE

S₁

S₂ and undifferentiated foliation

S₃

S₄

gneissosity in basement rocks

gneissosity in high grade
supracrustal rocks

granitic rocks
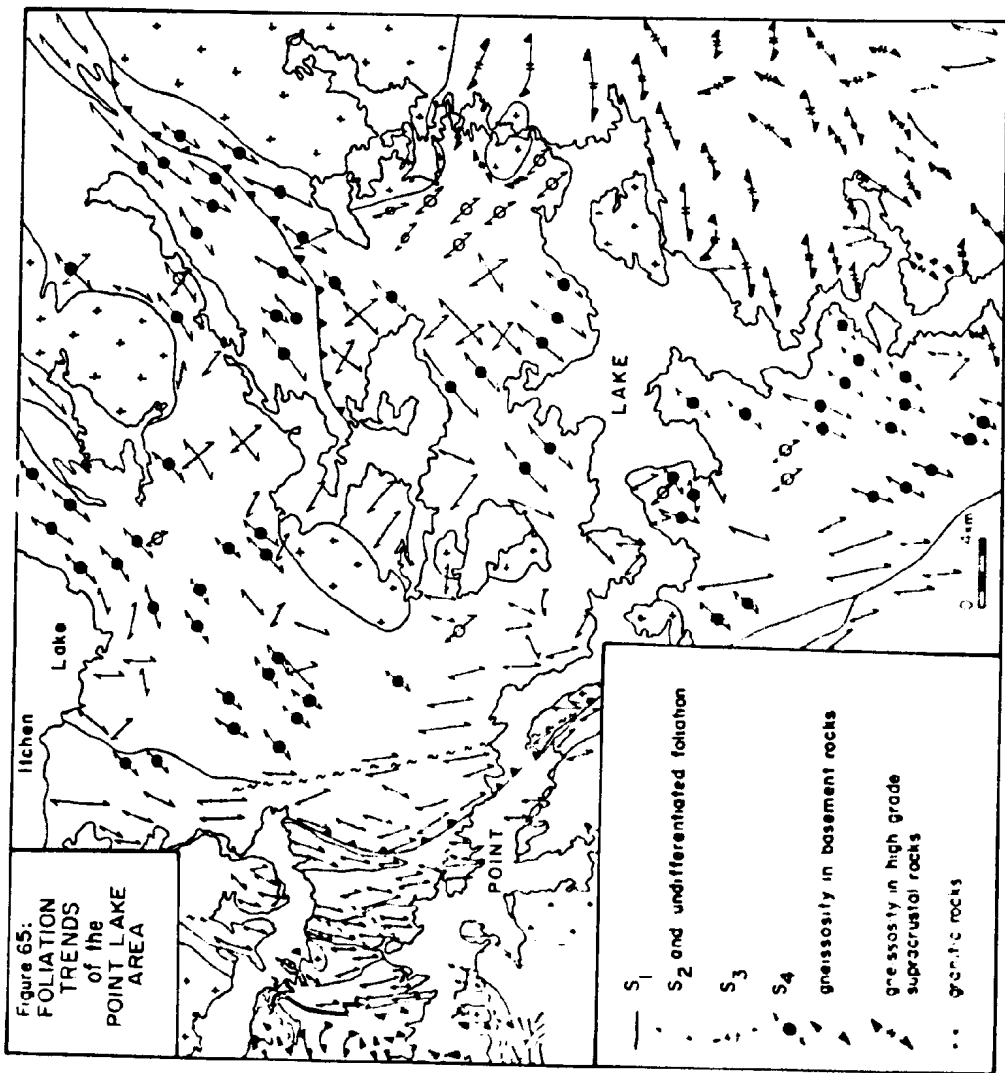
axial plane cleavage in the western part of the Keskarrah
Bay area.

The main phase of folding in both areas occurred during
D_2, although differences occur in the degree of S_2 fabric
development, the orientation of the F_2 folds and the
direction of overturning of these folds. In the Keskarrah
Bay area these folds are consistently overturned to the west
and are associated with a regional foliation (S_2). In the
eastern Point Lake area F_2 folds are overturned about
divergent and convergent fan axes and these folds are
associated with only a locally developed axial plane
foliation (King, 1981). In the southern parts of this area,
where the supracrustal belt narrows between the basement
granodiorite and Yamba batholith (Figure 3), F_2 fan axes are
absent and bedding steepens (King, 1981). In addition, in
the western parts of the eastern Point Lake area westward
overturning of F_2 folds is noted (Bostock, 1980; King,
1981). Axial traces of F_2 folds conform to the arcuate shape
of the supracrustal belt and the geometry of both F_2 folds
and that of the greenstone belt may have been established
during D_2 (King, 1981).

In the eastern Point Lake area two events (D_3 and D_4)
led to the formation of the southeast-trending (S_3) and
northeast-trending (S_4) regional foliations (King, 1981). S_3
and S_4 transect F_2 axial traces (King, 1981) and therefore
post-date D_2 regional folding. Both fabrics can be related
in time and intensity of development to emplacement of the

Yamba batholith (King, 1981; King and Helmstaedt, 1989).
However, these fabrics maintain a consistent high-angle
orientation to the margin of the Yamba batholith, suggesting
that the stresses that dictated their orientation were not
solely related to batholith emplacement (King and
Helmstaedt, 1989). These foliations have apparent
correlatives in the eastern part of the Keskarrah Bay area
(Figure 65), although definite documentation of this is
lacking. On the basis of its northeast orientation, the
predominant post-D_2 fabric recognized in the Keskarrah Bay
area is correlated with S_4 mapped in the eastern Point Lake
area by King (1981).

The Fubar fault (this study) and the Norma fault
(Tremblay, 1976; initially named Point Lake fault by King,
1981) display several characteristics in common, including:
1) a dip-slip component, suggested by the juxtaposition of
higher metamorphic grade rocks against those of lower grade;
2) they transect metamorphic isograds; 3) both are concave
to the east and southeast, with an inferred west to
northwest sense of tectonic transport and 4) both occur
within the sedimentary terrane, displacing the metasediments
against volcanic rocks and toward the basin margin. King et
al. (1988) re-interpreted the Point Lake fault of King
(1981) to be an extension of the Norma fault which is a
dextrally oblique dip-slip (north-side-down) Proterozoic
fault. However, King et al. (1988) also noted that in the
eastern Point Lake area displacement along the Norma fault

is predominantly dip-slip. Therefore, within the Point Lake area, both the Fubar fault and the Norma fault are considered steep contraction or thrust faults that may connect southeast of the Keskarrah Bay area (King, 1981).

Thus throughout both the Keskarrah Bay and eastern Point Lake areas there is a broad similarity in the sequential deformational events recorded in the supracrustals (Table 7). The noticeable differences are: 1) the prominence of F_1 folds and formation of a penetrative S_1 axial plane fabric in the supracrustals near the contact with the basement; 2) the orientation of main phase folds and degree of development of the associated S_2 fabric and; 3) the prominence of post-S_2 fabrics. These differences may be related to two factors: the involvement of the basement terrane during deformation and proximity to the Yamba batholith.

It has been argued previously in this text that the presence of basement in the Keskarrah Bay area influenced the orientation of structures formed in the supracrustal pile during the first two phases of deformation. A penetrative S_1 fabric is recognized only in the Keskarrah Bay area, along the west edge of the supracrustal belt. Proceeding eastward away from the basin margin, S_1 becomes progressively less intensely developed until in the eastern Point Lake area D_1 was not accompanied by metamorphic mineral growth or fabric formation. F_2 fold fan structures, which were noted in the eastern Point Lake area (King,

1981), are absent around the Keskarrah Bay area where F_2 axial traces are vertical or dip steeply to the east, indicative of westward overturning toward the basin margin and basement gneiss terrane. F_2 folds also appear to tighten toward the gneisses. The north-trending S_2 foliation is dominant in the Keskarrah Bay area, but only locally associated with F_2 folds in the eastern Point Lake area. These contrasts are considered to reflect the increased intensity of deformation adjacent to the basement buttress.

The development of regional foliations (S_3, S_4) post-dating the main phase of folding (F_2) and toward the end of the metamorphic culmination may be a result of thermal zonation formed in response to granitic plutonism and batholith emplacement (King, 1981), similar to relationships observed in the southern part of the Slave Province (Fyson and Frith, 1979; Fyson, 1980). The Keskarrah Bay area is relatively distant to the main area of granitic emplacement, possibly accounting for the less widespread development of these foliations.

5.1.4 Relationships Between Metamorphism and Deformation

Figure 66 (modified from King, 1981) summarizes the relationships between metamorphism and deformation in both the Keskarrah Bay and eastern Point Lake areas. Throughout much of the Itchen Lake region, the metamorphic peak was attained late in the deformational history (Tremblay, 1976; Bostock, 1980; King, 1981; this study). In both the eastern
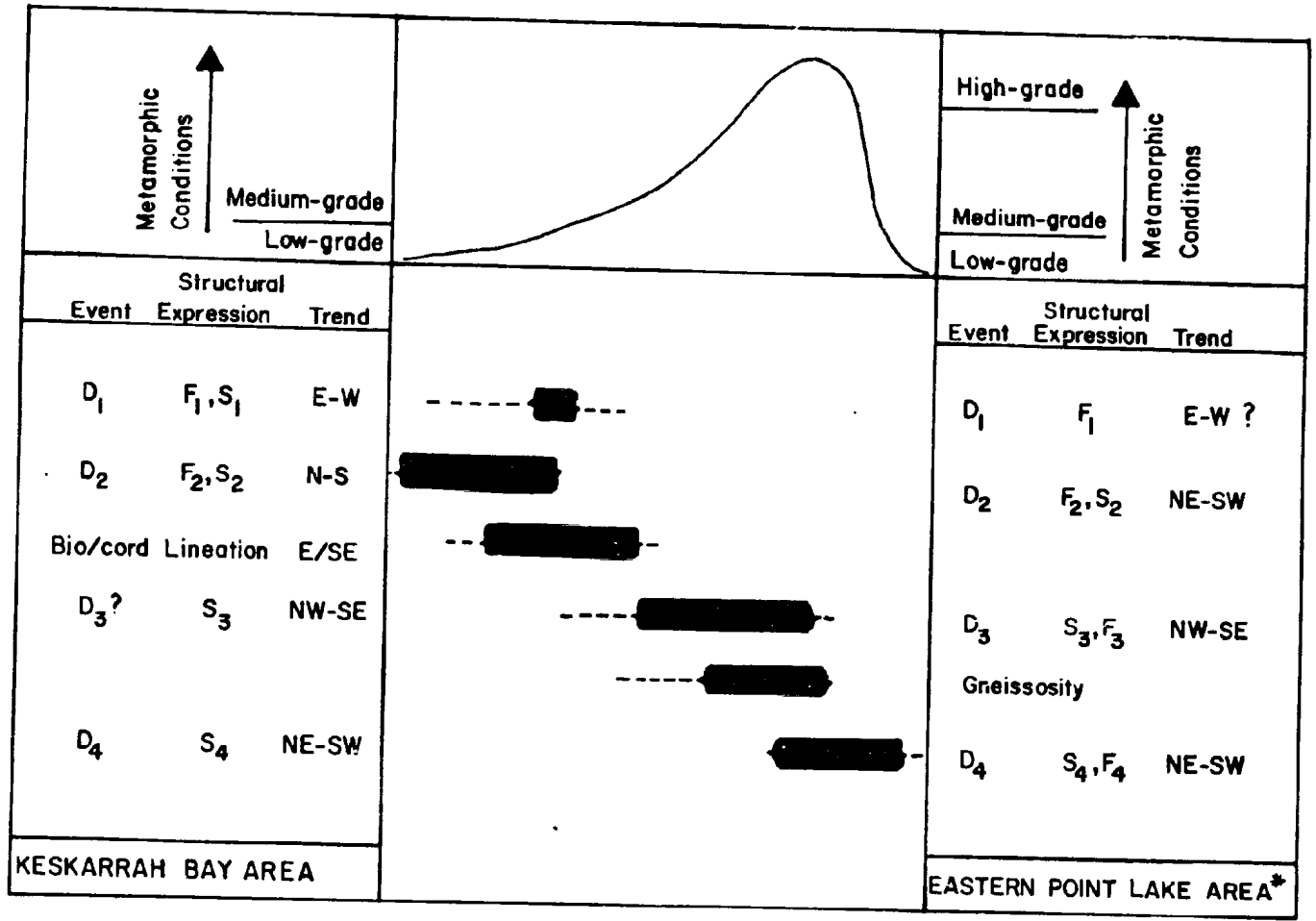
Figure 66: Relationship of metamorphism to deformation in the Keskarrah Bay and eastern Point Lake areas. Diagram is adapted from King (1981).

part of the Keskarrah Bay area and the eastern Point Lake area cordierite and andalusite porphyroblasts post-date D_2 and in the eastern Point Lake area they are also post D_3 (King 1981). In both areas these porphyroblasts locally pre-date the last phase of deformation (D_4). The gneissic fabric developed in the Itchen Formation metasediments adjacent to the Yamba batholith was formed prior to or during D_3 but before D_4 (King, 1981). However, in the western part of the Keskarrah Bay area the metamorphic peak probably pre-dated that in the eastern area, with metamorphism initiated during D_1 and continuing up to or through D_2. In metabasites hornblende is aligned in the S_2 foliation plane and in metaturbidites cordierite porphyroblasts have overgrown a mica schistosity (S_1?) and were subsequently rotated (during the formation of S_2?).

The data presented above illustrate the P-T distribution during peak metamorphism across this part of the Itchen Lake region. In addition, Thompson (1978) constructed a P-T profile for part of the Slave Province that included the Point Lake area and concluded that: 1) the metamorphic pattern of the Slave Province can be accounted for by "differential erosion of an irregularly spaced group of thermal highs and lows" and 2) "...granitoid rocks produced in the core of a thermal dome may intrude overlying metamorphic rocks related to the same thermal dome...". Thompson (1978) indicates that the P-T distribution in the Keskarrah Bay area may be comparable to the metamorphic

pattern that formed on the distal part of a thermal dome which accompanied granitoid emplacement (Yamba batholith).

In both the eastern part of the Keskarrah Bay area and the eastern Point Lake area the metamorphic peak is suggested to have been established subsequent to main phase F_2 folding. Later deformational events did not result in large scale folding and it is presumed that the isograd pattern in these areas is not folded. The broad expanse in the central part of Figure 64 is underlain by the SZ. The presence of pockets of AZ rocks within the SZ is interpreted to reflect the shallow, undulatory nature of the isograds (see King (1981) for discussion of the attitude of isobars and isotherms). The close spacing of the isograds in the high-grade Itchen Formation towards the east of Figure 64 is attributed to an increase in the thermal gradient at the margin of a thermal dome into which the Yamba batholith was emplaced (King, 1981). King (1981) also notes an increase in the slope of the isobars in the gneissic metasediments adjacent to the Yamba batholith, which may indicate structural doming of both isotherms and isobars. The batholith may have dragged up its metamorphic envelope in a manner similar to that described by Flood and Vernon (1978) for the Cooma granodiorite. However, in Flood and Vernon's model the metamorphic envelope is compressed around the intrusion, whereas such a situation is rather unlikely around the Yamba batholith, given the aerial extent of the gneissic envelope.

Assuming that the metamorphic zonation in the eastern Keskarrah Bay and Point Lake areas is related solely to emplacement of the Yamba batholith, then the thermal overprint extends at least to the low-grade zones of the Keskarrah Bay area, a minimum distance of 50-60 km from the present position of the batholith (Figure 3). Such distances are well within reason, given the extent of the regional metamorphic aureoles suggested by Thompson (1978). However, McKinnon (1982) indicated that some pegmatite and granite intrusions in the SZ rocks may have formed through partial melting of the sedimentary rocks at depth. Thus it is possible that a granitic intrusion, perhaps part of the Yamba batholith, underlies the SZ and provided an additional heat source for metamorphism in this area.

In the Keskarrah Bay area, the westward increase in metamorphic grade may be explained by a thermal dome lying to the west of the study area, into which the 'Pointless' batholith (Easton et al., 1981) was emplaced (Figure 3). The presently exposed low-grade metamorphic zones in the Keskarrah Bay area may thus form a very narrow (5 km or less) thermal depression or trough between two regional thermal domes. Although radiometric age data are unavailable for the Pointless batholith, Easton (pers. comm., 1982) has suggested it is a late syntectonic intrusion, which is compatible with the above interpretation. However, in the central and western area the metamorphic peak was attained prior to or during D_2, suggesting that the isograds in this

area were deformed during main phase F_2 folding. Therefore an alternative explanation is that the low-grade zones represent a structural depression in the regional metamorphic zonation that forms the distal part of the thermal dome surrounding the Yamba batholith.

5.2 Discussion and Summary

Much of the early (D_1 and earlier) deformational history of the Itchen Lake region is poorly understood. However, the documentation of structural elements related to subsequent deformation is of sufficient detail to attempt tectonic modelling (King, 1981; Kusky, 1987; King and Helmstaedt, 1989; this study).

Across the Itchen Lake region supracrustal belt F_2 folds exhibit a progression westward from the fan structures defined in the central part of the belt (King, 1981), to westward overturned folds near the basement terrane and the margin of the belt (Bostock, 1980; this study) and to west-verging recumbent folds west of the gneiss-supracrustal boundary (Easton et al., 1981; Kusky, 1987; this study). The gneiss-supracrustal boundary is marked by mylonite zones for much of it's length and Kusky (1987) suggested it represents a ductile detachment zone along which the cover rocks were thrust over the basement gneisses. The combination of these structures has led to the recent interpretation of the deformational history of the Itchen Lake region supracrustal

belt as that of a west-verging fold-and-thrust belt (Kusky, 1987, 1989; King and Helmstaedt, 1989). The driving forces for development of the fold-and-thrust belt are considered to be independent of batholith emplacement (King and Helmstaedt, 1989).

Several factors point to subsequent modification of the west-verging structures: 1) the shallow-dipping gneissosity and recumbent folds within the gneiss terrane progressively steepen toward the gneiss-supracrustal boundary; 2) along the gneiss-supracrustal contact mylonitic foliations within the basement rocks and the compositional layering within the banded mafic volcanics (suggested by Kusky (1987) to be tectonic in origin) are vertical to steeply east-dipping; 3) east of the gneiss-supracrustal contact F_2 main phase folds are steeply plunging, have vertical to steep east-dipping axial planes and appear to tighten toward the gneisses and 5) a prominent north-trending, steeply east-dipping S_2 foliation is developed in the Keskarrah Bay area, but is only locally developed in central parts of the belt. Many of these points suggest that the proposed buttressing effect of the basement terrane was superimposed on the cover sequence subsequent to westward directed thrusting over basement.

The development of the regional foliations during D_3 and D_4 can be related to the thermal but not the strain aureole that accompanied intrusion of the Yamba batholith (King, 1981). King and Helmstaedt (1989) suggest that horizontally

directed forces, external to the dynamics of batholith intrusion, were responsible for their orientation.

Regional metamorphism of supracrustal rocks across the Itchen Lake region has been shown to be that of a single progressive event which documents low-pressure andalusite-sillimanite facies metamorphism. The metamorphic zonation is interpreted to reflect the thermal pattern produced during granite batholith emplacement. Subsequent modification of this pattern is indicated by: 1) suggested folding of the isograds in the western Keskarrah Bay area during main phase F_2 folding; 2) structural doming of the high-grade isograds in the eastern Point Lake area, which may have occurred during emplacement of the Yamba batholith and 3) telescoping of the isograds across two fault zones, the Fubar and Norma faults.

Some of the structural elements of the Itchen Lake greenstone belt described in this text and the studies of King (1981), Kusky (1986, 1987) and King and Helmstaedt (1989) appear to lend support to the previously described contractional tectonic models. The development of recumbent folds in the western area, geometry of main phase F_2 folds and arcuate outline of the belt may have resulted from westward directed folding and thrusting of the cover rocks during an accretionary stage. King and Helmstaedt (1989) suggest that the two regional foliations formed in response to ongoing metamorphism and convergence of the belt. Modification of the metamorphic zonation along the Fubar and

Norma faults resulted in telescoping of the metamorphic isograds.

Although the accretionary theory proposed by Kusky (1986, 1987, 1989) presents a convincing argument for D_2 and younger deformational events, some important features are not explained in this model. For instance: 1) the relationship of easterly trending F_1 folds to the suggested westerly directed tectonism; 2) the apparent lack of recumbent folds within the supracrustal terrane and 3) the orthogonal relationships observed between successive phases of deformation eg. easterly-trending F_1 folds are overprinted by north-trending F_2 folds and the regional southeast-trending S_3 foliation is overprinted by a northeast-trending S_4 regional fabric. In addition, the early tectonometamorphic history of the basement gneiss terrane remains poorly understood.

This thesis has examined the metamorphic and structural history of a small part of the Slave Province. Correlation and comparison with studies in adjacent areas has allowed the integration of data for a large part of one supracrustal belt within this Archean terrane. However, much detailed information remains to be acquired throughout the Slave Province to allow precise testing of the various proposed tectonic models.

REFERENCES

Atkinson, D.J. (1987): Report on preliminary mapping and geochemistry of the Western Plutonic Complex; in Exploration Overview, Mining, Exploration and Geological Investigations, INAC, NAP, Geology Division, Yellowknife, N.W.T., ed. Ellis, C.E., p. 17-18.

Bailes, A.H. and McRitchie, W.D. (1978): The transition from low to high grade metamorphism in the Kisseynew sedimentary gneiss belt, Manitoba; in Metamorphism in the Canadian Shield, eds. Fraser, J.A. and Heywood, W.W., Geol. Surv. Can., Paper 78-10, p. 155-178.

Baragar, W.R.A. and McGlynn, J.C. (1976): Early Archean basement in the Canadian Shield: a review of the evidence; Geol. Surv. Can., Paper 76-14, 20p.

Bartholomé, P. (1962): Iron-magnesium ratio in associated pyroxenes and olivines; Geol. Soc. Am. Buddington Volume, p. 1-20.

Bostock, H.H. (1977): The composition of hornblende, grunerite and garnet in Archean iron-formation of the Itchen Lake area, District of Mackenzie; Can. J. Earth Sci., v. 14, p. 1740-1752.

Bostock, H.H. (1980): Geology of the Itchen Lake area, District of Mackenzie; Geol. Surv. Can., Memoir 391, 101p.

Brown, E.H. (1967): The greenschist facies in part of eastern Otago, New Zealand; Contr. Mineral. Petrol., v. 14, p. 259-292.

Butler, B.C.M. (1967): Chemical study of minerals from the Moine schists of the Ardnamurchan area, Argyllshire, Scotland; J. Petrology, v.8, p. 233-267.

Carmichael, D.M. (1969): On the mechanism of prograde metamorphic reactions in quartz-bearing pelitic rocks; Contr. Min. Petrology, v. 20, p. 244-267.

Carmichael, D.M. (1978): Metamorphic bathozones and bathograds: a measure of the depth of post-metamorphic uplift and erosion on the regional scale; Am. J. Sci., v.278, p. 769-797.

Carmignani, L., Franceschelli, M., Pertusati, P.C., Memmi, I., and Ricci, C.A. (1982): An example of compositional control of the celadonitic content of muscovite and the incoming of biotite in metapelites (Nurra, NW Sardinia); N. Jb. Miner. Mh., v. 19, p. 289-311.

Chakraborty, K.R. and Sen, S.K. (1967): Regional metamorphism of pelitic rocks around Kandra, Singhbkum, Bihar; Contr. Mineral. Petrol., v. 16, p. 210-232.

Cipriani, C., Sassi, F.P., and Viterbo-Bassani, C. (1968): Metamorphic white micas: definition of paragenetic field; Schweiz. Petrol. Mitt., v. 51, p. 259-302.

Cooper, A.F. (1972): Progressive metamorphism of basic rocks from the Haast Schist Group of southern New Zealand; J. Petrology, v. 13, p. 457-492.

Craw, D. (1981): Oxidation and microprobe induced potassium mobility in Fe-bearing phyllosilicates from Otago schists, New Zealand; Lithos, v. 14, p.49 -57.

Davidson, A. (1972): Granite studies in the Slave Province (parts of 85I); Geol. Surv. Can., Paper 72-1A, p. 109-115.

Deer,W.A., Howie, R.A. and Zussman, J. (1966): An introduction to the rock forming minerals. Longman Group Limited, London, 528 p.

Drury, S.A. (1977): Structures induced by granite diapirs in the Archaean greenstone belt at Yellowknife, Canada: implications for Archaean geotectonics; J. Geology, v. 85, p. 345-358.

Easton, R.M. (1985): The nature and significance of pre-Yellowknife Supergroup rocks in the Point Lake area, Slave Structural Province, Canada; in Evolution of Archean Supracrustal Sequences, eds. Ayers, L.D., Thurston, P.C., Card, K.D. and Weber, W.; Geol. Assoc. Can., Special Paper 28, p. 153-167.

Easton, R.M., Boodle, R.L., Zalusky, L., Eiche, G. and McKinnon, D. (1981): Geology of 86H/3, H/4, H/5 and H/6, District of Mackenzie; Department of Indian Affairs and Northern Development, NAP, Geology Division, Preliminary Geological Map, EGS-1981-5.

Easton, R.M., Boodle, R.L. and Zalusky, L. (1982): Evidence for gneissic basement to the Archean Yellowknife Supergroup in the Point Lake area, Slave Structural Province, District of Mackenzie, N.W.T.; Geol. Surv. Can., Paper 82-1B, p. 33-41.

England, P.C. and Thompson, A.B. (1984): Pressure - temperature - time paths of regional metamorphism I. Heat transfer during the evolution of regions of thickened continental crust; J. Petrol., v. 25, p. 894-928.

Ermanovics, I.F. and Froese, E. (1978): Metamorphism of the Superior Province in Manitoba; in Metamorphism in the Canadian Shield, eds. Fraser, J.A. and Heywood, W.W., Geol. Surv. Can., Paper 78-10, p. 17-24.

Ernst, W.G. (1963): Significance of phengitic micas from low-grade schists; Am. Mineral., v. 48, p. 1357-1373.

Evans, B.W. and Guidotti, C.V. (1966): The sillimanite-potash feldspar isograd in western Maine, U.S.A.; Beitr. Mineral. Petrol., v. 12, p. 25-62.

Ferguson, C.C., Harvey, P.K. and Lloyd, G.E. (1980): On the mechanical interaction between a growing porphyroblast and its surrounding matrix; Con. Mineral. Petrol., v. 75, p. 339-352.

Ferry, J.M. and Spear, F.S. (1978): Experimental calibration of the partitioning of Fe and Mg between biotite and garnet; Con. Mineral. Petrol., v. 66, p. 113-117.

Flood, R.H. and Vernon, R.H. (1978): The Cooma Granodiorite, Australia: an example of in situ crustal anatexis?; Geology, v. 6, p. 81-84.

Ford, C.R. (1988): Comparative geology of gold-bearing Archean iron formation, Slave Structural Province, Northwest Territories; Unpubl. M.Sc. thesis, University of Western Ontario, 233p.

Fraser, J.A. (1964): Geological notes on northeastern District of Mackenzie, Northwest Territories; Geol. Surv. Can., Paper 63-40.

Frith, R.A. (1982): Advances in our knowledge of the Slave Structural Province; Geol. Assoc. Can., Program with Abstracts, v. 7, p.50.

Frith, R.A. and Hill, J.D. (1975): The geology of the Hackett - Back River greenstone belt - preliminary account; in Report of Activities, Part C, Geol. Surv. Can., Paper 75 - 1c, p. 366-370.

Frith, R., Frith, R.A. and Doig (1977): The geochronology of the granitic rocks along the Bear-Slave Structural Province boundary, northwest Canadian Shield; Can. J. Earth Sci., v. 14, p. 1356-1373.

Frith, R.A. and Roscoe, S.M. (1980): Tectonic setting and sulfide deposits, Hackett River Belt, Slave Province; Can. Mining Metallur. Bull., v. 73, p. 143-153.

Frith, R.A. and Loveridge, W.D. (1982): Ages of Yellowknife
    Supergroup volcanic rocks, granitoid intrusive rocks and
    regional metamorphism in the northeastern Slave
    Structural Province; Geol. Surv. Can., Paper 82-1A, p.
    225-237.

Fyson, W.K. (1975): Fabrics and deformation of Archean
    metasedimentary rocks, Ross Lake-Gordon Lake area, Slave
    Province, Northwest Territories; Can. J. Earth Sci.,
    v.12, p. 765-776.

Fyson, W.K. (1980): Fold fabrics and emplacement of an
    Archean granitoid pluton, Cleft Lake, Northwest
    territories; Can. J. Earth Sci., v. 17, p. 325-332.

Fyson, W.K. (1981): Divergent fold overturning and regional
    tectonics, southern Slave Province, Northwest
    Territories; Precambrian Res., v. 14, p. 107-118.

Fyson, W.K. (1982): Complex evolution of folds and cleavages
    in Archean rocks, Yellowknife, N.W.T.; Can. J. Earth
    Sci., v.19, p. 878-893.

Fyson, W.K. (1984a): Fold and cleavage patterns in Archean
    metasediments of the Yellowknife supracrustal domain,
    Slave Province, Canada; in Precambrian Tectonics, eds. A
    Kroner and R. Greiling v.19, p. 281-293.

Fyson, W.K. (1984b): Basement-controlled structural fronts
    forming an apparent major refold pattern in the
    Yellowknife domain, Slave Province; Can. J. Earth Sci.,
    v.21, p. 822-828.

Fyson, W,K, (1987): Map patterns and tectonics of the Slave
    Province; in Geol. Assoc. Can., Summer Field Meeting,
    Abstracts with Programs, p. 21.

Fyson, W.K. and Frith, R.A. (1979): Regional deformations
    and emplacement of granitoid plutons in the Hackett
    River greenstone belt, Slave Province, Northwest
    Territories; Can. J. Earth Sci., v. 16, p. 1187-1195.

Fyson, W.K. and Helmstaedt, H. (1988): Structural patterns
    and tectonic evolution of supracrustal domains in the
    Archean Slave Province, Canada; Can. J. Earth Sci., v.
    25, p. 301-315.

Ghent, E.D. (1976): Plagioclase-garnet-Al_2SiO_5-quartz: a
    potential geobarometer-geothermometer; Am. Mineral., v.
    61, p. 710-714.

Ghent, E.D., Robbins, D.B. and Stout, M.Z. (1979):
    Geothermometry, geobarometry and fluid compositions of

metamorphosed calc-silicates and pelites, Mica Creek, British Columbia; Am. Mineral., v. 64, p. 874-885.

Gibbins, W.A. (1986): High magnesium or komatiitic peridotite from the Archean Hope Bay volcanic belt, Slave Province, Northwest Territories; Geol. Assoc. Can., Program with Abstracts, v. 11, p. 72.

Goodwin, A.M. (1981): Archaean plates and greenstone belts; in Precambrian Plate Tectonics, ed. Kröner, A., Elsevier, Amsterdam, p.105-135.

Gray, D.R. (1978): Cleavages in deformed psammitic rocks from southeastern Australia: Their nature and origin; G.S.A. Bull., v. 89, p. 577-590.

Green, D.C. and Baadsgaard, H. (1971): Temporal evolution and petrogenesis of an Archaean crustal segment at Yellowknife, N.W.T.; J. Petrology, v. 12, p. 177-217.

Guidotti, C.V. (1966): Variations of the basal spacings of muscovite in sillimanite-bearing pelitic schists of northwestern Maine; Am. Mineral., v. 51, p. 1778-1786.

Guidotti, C. V. (1969): A comment on chemical study of minerals from the Moine Schists of Ardnamurchan area, Argyllshire, Scotland by B.C.M. Butler, and its implications for the phengite problem; J. Petrol., v. 10, p. 164-170.

Guidotti, C.V. (1970): The mineralogy and petrology of the transition from the lower to upper sillimanite zone in the Oquossoc area, Maine; J. Petrology, v. 11, p. 277-336.

Guidotti, C.V. (1973): Compositional variation of muscovite as a function of metamorphic grade and assemblage in metapelites from N.W. Maine; Con. Mineral. Petrol., v. 42, p. 33-42.

Guidotti, C.V. (1974): Transition from staurolite to sillimanite zone, Rangeley Quadrangle, Maine; Geol. Soc. Am. Bull., v. 85, p. 475-490.

Guidotti, C.V. and Sassi, F.P. (1976): Muscovite as a petrogenetic indicator mineral in pelitic schists; N. Jb. Miner. Abh., v. 127, p. 97-142.

Helmstaedt, H. (1985): Report on status of Yellowknife Volcanic Belt project; in Exploration Overview, Mining Exploration and Geological Investigations, Northwest Territories 1985, Geology Division, Indian and Northern Affairs Canada, Northern Affairs Program, Yellowknife, N.W.T., p. 18-19.

Helmstaedt, H. and Padgham, W.A. (1986): A new look at the stratigraphy of the Yellowknife Supergroup at Yellowknife, N.W.T. - implications for the age of gold-bearing shear zones and Archean basin evolution; Can. J. Earth Sci., v. 23, p. 454 - 475.

Henderson, J.B. (1970): Stratigraphy of the Archean Yellowknife Supergroup, Yellowknife Bay-Prosperous Lake area, District of Mackenzie; Geol. Surv. Can., Paper 70-26, 12p.

Henderson, J.B. (1975): Sedimentology of the Archean Yellowknife Supergroup at Yellowknife, District of Mackenzie; Geol. Surv. Can. Bull. 246, 62p.

Henderson, J.B. (1981): Archean basin evolution in the Slave Province, Canada; in Precambrian Plate Tectonics, ed. A. Kroner, Elsevier, Amsterdam, p. 213-235.

Henderson, J.B. and Easton, R.M. (1977a): Archean supracrustal-basement rock relationships in the Keskarrah Bay map area, Slave Structural Province, District of Mackenzie; Geol. Surv. Can., Paper 77-1A, p. 217-221.

Henderson, J.B. and Easton, R.M. (1977b): Geology of Keskarrah Bay, Point Lake, Northwest Territories; Geol. Surv. Can., Open File 447.

Henderson, J.B. and Thompson, P.H. (1980): The Healey Lake map area (northern part) and the enigmatic Thelon Front, District of Mackenzie; Geol. Surv. Can., Paper 80-1A, p. 165-169.

Henderson, J.B. and Thompson, P.H. (1981): The Healey Lake map area and the enigmatic Thelon Front, District of Mackenzie; Geol. Surv. Can., Paper 81-1A, p. 175-180.

Henderson, J.B., van Breemen, O. and Loveridge, W.D. (1987): Some U-Pb zircon ages from Archean basement, supracrustal and intrusive rocks, Yellowknife-Hearne Lake area, District of Mackenzie; in Radiogenic ages and isotopic studies: Report 1, Geol. Surv. Can., Paper 87-2, p. 111-121.

Hess, P.C. (1969): The metamorphic paragenesis of cordierite in pelitic rocks; Contr. Mineral. and Petrol., v. 24, p. 191-207.

Hey, M.H. (1954): A new review of the chlorites; Min. Mag., v. 30, p. 277-292.

Heywood, W.W. and Davidson, A. (1969): Geology of Benjamin Lake map-area, District of Mackenzie, 75M/2; Geol. Surv. Can., Memoir 361, 35p.

Hoffman, P.F. (1986): Crustal accretion in a 2.7-2.5 Ga "granite-greenstone" terrane, Slave Province, N.W.T: a prograding trench-arc system?; Geol. Assoc. Can., Program with Abstracts, v. 11, p. 82.

Holdaway, M.J. (1971): Stability of andalusite and the aluminum silicate phase diagram; Am. J. Sci., v. 271, p. 97-131.

Hollister, L.S. (1966): Garnet zoning: an interpretation based on the Rayleigh fractionation model; Science, v. 154, p. 1647-1651.

Hosheck, G. (1969): The stability of staurolite and chloritoid and their significance in metamorphism of pelitic rocks; Contr. Mineral. and Petrol., v. 22, p. 208-232.

Jackson, V.A. (1983): A preliminary report on the Keskarrah Bay map area, Slave Structural Province, NWT. (N.T.S. 86H/2, 86H/6 and 86H/7); in Mineral Industry Report-1978; INAC, NAP, Geology Division, Yellowknife, EGS-1983-2, p.213-222.

Jackson, V.A. (1984): Structure and metamorphism of the Keskarrah Bay area, Point Lake, NWT. Second preliminary report; in Contributions to the Geology of the Northwest Territories, v. 1, INAC, NAP, Geology Division, Yellowknife, EGS-1984-6, p.47-54.

Jackson, V.A., Chawrun, P.C., Edbrooke, S., Falck, H., Gault, C.D., Hamilton, A-M., Kerr, D., Mayor, T., McCorquodale, J. and Potts, G. (1987): Preliminary geology of the Kathawachaga Lake area (north half); Indian and Northern Affairs Canada, Northern Affairs Program, Geology Division, Yellowknife, EGS 1987-10, map with accompanying notes and legend.

Jenner, G.A., Fryer, B.J. and McLennan, S.M. (1981): Geochemistry of the Archean Yellowknife Supergroup; Geochim. et Cosmochim. Acta, v. 45, p. 1111-1129.

Kamineni, D.C. and Carrara, A. (1973): Comparison of the composition of porphyroblastic and fabric-forming biotite in two metamorphic rocks; Can. J. Earth Sci., v. 10, p. 948-953.

King, J.E. (1981): Low pressure regional metamorphism and progressive deformation in the eastern Point Lake area,

Slave Province, N.W.T.; unpublished M.Sc. thesis, Queen's University, Kingston, Ontario, 187p.

King, J.E., Davis, W.J., Relf, C. and Avery, R.W. (1988): Deformation and plutonism in the western Contwoyto Lake map area, central Slave Province, District of Mackenzie, N.W.T; in Current research, Part C, Geol. Surv. Can., Paper 88-1C, p. 161-176.

King, J.E. and Helmstaedt, H. (1989): Deformational history of an Archean fold belt, eastern Point Lake area, Slave Structural Province, N.W.T; Can. J. Earth Sci., v. 26, p. 106-118.

Kretz, R. (1961): Some applications of thermodynamics to coexisting minerals of variable composition: examples, orthopyroxene - clinopyroxene and orthopyroxene-garnet; J. Geol., v. 69, p. 361-387.

Kretz, R. (1969): Study of pegmatite bodies and enclosing rocks, Yellowknife-Beaulieu region, District of Mackenzie, Geol. Surv. Can., Bull. 159, p.

Krogh, T.E. and Gibbins, W.A (1978): U-Pb isotopic ages of basement and supracrustal rocks in the Point Lake area of the Slave Structural Province; Geol. Assoc. Can., Abstracts with Programs, v. 3, p. 438.

Kusky, T.M. (1986): Are greenstone belts in the Slave Province, N.W.T. allochthonous?; in Workshop on Tectonic Evolution of Greenstone Belts, eds. de Wit, M.J. and Ashwal, L.D., Lunar and Planetary Institute, Technical Report 86-10, p. 135-139.

Kusky, T.M. (1987): An Archean fold-and-thrust belt at Point Lake, N.W.T.; Geol. Assoc. Can., Summer Field Meeting, Program with Abstracts, p. 22.

Kusky, T.M. (1989): Accretion of the Archean Slave Province; Geology, v. 17, p. 63-67.

Kwak, T.A.P. (1968): Ti in biotite and muscovite as an indication of metamorphic grade in almandine amphibolite facies rocks from Sudbury, Ontario; Geochim. et Cosmochim. Acta, v. 32, p. 1222-1229.

Lambert, M.B. (1976): The Back River volcanic complex, District of Mackenzie; Geol. Surv. Can., Paper 76-1A, p. 363-367.

Lambert, M.B. (1978): The Back River volcanic complex - a cauldron subsidence structure of Archean age; Geol. Surv. Can., Paper 78-1A, p. 153-157.

Lambert, M.B. (1982a): Felsic domes and flank deposits of the Back River volcanic complex, District of Mackenzie; Geol. Surv. Can., Paper 82-1A, p. 159-164.

Lambert, M.B. (1982b): Synvolcanic intrusions in the Cameron River volcanic belt, District of Mackenzie; Geol. Surv. Can., Paper 82-1A, p. 165-167.

Lambert, M.B. and Henderson, J.B. (1980): A uranium-lead age of zircons from volcanics and sediments of the Back River Volcanic Complex, Eastern Slave Province, District of Mackenzie; in Loveridge, W.D. Rubidium-strontium and uranium-lead isotopic age studies, Report 3; in Current Research, Part C, Geol. Surv. Can., Paper 80-1C, p. 239-242.

Leake, B.E. (1978): Nomenclature of amphiboles; Can. Mineral., v. 16, p. 501-520.

Lhotka, P.G. and Nesbitt, B.E. (1989): Geology of unmineralized and gold-bearing iron formation, Contwoyto Lake - Point Lake region, Northwest Territories, Canada; Can. J. Earth Sci., v. 26, p. 46-64.

Lister, G.S., Boland, J.N. and Zwart, H.J. (1986): Step-wise growth of biotite porphyroblasts in pelitic schists of the western Lys-Caillaouas massif (Pyrenees); J. Struct. Geol., v. 8, p. 543-562.

Mather, J.D. (1970): The biotite isograd and the lower greenschist facies in the Dalradian rocks of Scotland; J. Petrology, v. 11, p. 253-275.

McGlynn, J.C. (1977): Geology of the Bear-Slave Structural Provinces; Geol. Surv. Can., Open File 445.

McGlynn, J.C. and Henderson, J.B. (1970): Archean volcanism and sedimentation in the Slave Structural Province; in Basins and geosynclines in the Canadian Shield, ed. Baer, A.J., Geol. Surv. Can., Paper 70-40, p. 31-44.

McGlynn, J.C and Henderson, J.B. (1972): The Slave Province; in Variations in Tectonic Styles in Canada, eds. Price, R.A and Douglas, R.J.W.; Geol. Assoc. Can., Special Paper 11, p. 516-526.

McKinnon, D.F. (1982): Origin of the pegmatite-adamellite bodies within the Itchen Formation at Point Lake, N.W.T.: evidence for partial melting of metasedimentary rocks?; Unpublished B.Sc. thesis, University of Western Ontario, London, Ontario, 90p.

McNamara, M. (1965): The lower greenschist facies in the Scottish Highlands; Geologiska Foreningens i Stockholm Forhandlinger, v. 87, p. 347-389.

Meintzer, R.E. and Cerny, P. (1983): Geological studies of rare-element pegmatites in the Yellowknife basin of the N.W.T; in Mineral Industry Report, 1978, N.W.T., Canada; Dept. Indian Affairs and Northern Dev., EGS 1983-2, p. 189-202.

Miyashiro, A. (1973): Metamorphism and Metamorphic Belts. George Allen and Unwin, Great Britain, 492p.

Moody, J.B., Meyer, D. and Jenkins, J.E. (1983): Experimental characterization of the greenschist/amphibolite boundary in mafic systems; Am. J. Sci., v. 283, p. 48-92.

Nikic, Z., Baadsgaard, H., Folinsbee, R.E. and Leech, A.P. (1975): Diatreme containing boulders of 3030M.Y. old tonalite gneiss, Con Mine, Yellowknife, Slave Craton: Geol. Soc. Am., Abstracts with Programs, v. 7, p. 1213-1214.

Osberg, P.H. (1971): An equilibrium model for Buchan-type metamorphic rocks, south-central Maine: Am. Mineral., v. 56, p. 570-586.

Padgham, W.A. (1981): Archean crustal evolution - a glimpse from the Slave Province; in Archaean Geology, eds. Glover, J.E. and Groves, D.I, Second International Archaean Symposium; Geol. Soc. Aust., Special Publication 7, p. 99-110.

Padgham, W.A. (1985): Observations and speculations on supracrustal successions in the Slave Structural Province; in Evolution of Archean Supracrustal Sequences, eds. Ayers, L.D., Thurston, P.C., Card, K.D. and Weber, W.; Geol. Assoc. Can., Special Paper 28, p. 130-151.

Pearson, D.E. and Lewry, J.F. (1974): Large-scale fold interference structures in the Mudjatik River area of northern Saskatchewan; Can. J. Earth Sci., v. 11, p. 619-634.

Percival, J.A. (1979): Kyanite-bearing rocks from the Hackett River area, N.W.T.: implications for Archean geothermal gradients; Contr. Miner. and Petrol., v. 69, p. 177-184.

Powell, C.M.A. (1979): A morphological classification of rock cleavage; Tectonophys., v. 58, p. 21-34.

Ramamohana Rao, T. (1977): Distribution of elements between coexisting phengite and chlorite from greenschist facies of the Tennant Creek area, Central Austria; Lithos, v. 10, p. 103-112.

Ramsay, C.R. (1973a): The origin of biotite in Archaean meta-sediments near Yellowknife, N.W.T., Canada; Contr. Mineral. and Petrol., v. 42, p. 43-54.

Ramsay, C.R. (1973b): Controls of biotite zone mineral chemistry in Archaean meta-sediments near Yellowknife, Northwest Territories, Canada; J. Petrology, v. 14, p. 467-488.

Ramsay, C.R. (1974): The cordierite isograd in Archaean meta-sediments near Yellowknife, N.W.T., Canada - variations on an experimentally established reaction; Contr. Mineral. Petrol., v. 47, p. 27-40.

Ramsay, C.R. and Kamineni, D.C. (1977): Petrology and evolution of an Archaean metamorphic aureole in the Slave Craton, Canada; J. Petrol., v. 18, p. 460-486.

Ramsay, J.G. (1967): Folding and fracturing of rocks. McGraw - Hill Book Company. U.S.A. 568p.

Richardson, S.W. (1970): The relation between a petrogenetic grid, facies series' and geothermal gradient in metamorphism; Fortschr. Miner., v. 47, p. 65-76.

Schärer, U. and Allègre, C.J. (1982): Investigation of the Archean crust by single-grain dating of detrital zircon: a graywacke of the Slave Province, Canada; Can. J. Earth Sci., v. 19, p. 1910-1918.

Schreyer, W. and Yoder, H.S. (1961): Petrographic guides to the experimental petrology of cordierite; Yb. Carnegie Instn. Wash., v. 60, p. 147-152.

Seifert, F. (1970): Low-temperature compatibility relations of cordierite in haplopelites of the system $K_2O-MgO-Al_2O_3-SiO_2-H_2O$; J. Petrology, v. 11, p. 73-99.

Spear, F.S. and Selverstone, J. (1983): Quantitative P-T paths from zoned minerals: theory and tectonic applications; Contr. Mineral. Petrol., v. 83, p. 348-357.

Spear, F.S., Selverstone, J., Hickmott, D., Crowley, P. and Hodges, K.V. (1984): P-T paths from garnet zoning: a new technique for deciphering tectonic processes in crystalline terranes; Geology, v. 12, p. 87-90.

St. Onge, M.R. (1984): Geothermometry and geobarometry in pelitic rocks of north-central Wopmay Orogen (early Proterozoic), Northwest Territories, Canada; Geol. Soc. Am. Bull., v. 95, p. 196-208.

Stockwell, C.H. (1933): Great Slave Lake-Coppermine River area, N.W.T.; Geol. Surv. Can., Summary Report 1932, Part C, p. 37-63.

Stockwell, C.H. (1961): Structural provinces, orogenies and time classification of rocks of the Canadian Precambrian Shield; in Age Determinations by the Geological Survey of Canada, compiled by J.A. Lowdon, Geol. Surv. Can., Paper 61-17, p. 108-118.

Thompson, A.B. (1976): Mineral reactions in pelitic rocks: I. Prediction of P-T-X(Fe-Mg) phase relations; Am. J. Sci., v. 276, p. 401-424.

Thompson, A.B. and England, P.C. (1984): Pressure - temperature - time paths of regional metamorphism II. Their influence and interpretation using mineral assemblages in metamorphic rocks; J. Petrol., v. 25, p.929-955.

Thompson, J.B., Jr. (1957): The graphical analysis of mineral assemblages in pelitic schists; Am. Miner., v. 42, p. 65-103.

Thompson, P.H. (1978): Archean regional metamorphism in the Slave Province - A new perspective on some old rocks; in Metamorphism in the Canadian Shield, eds. Fraser, J.A. and Heywood, W.W.; Geol. Surv. Can., Paper 78-10, p. 85-102.

Thompson, P.H. and Bard, J.P. (1982): Isograds and mineral assemblages in the eastern axial zone, Montagne Noire (France): implications for temperature gradients and P-T history; Can. J. Earth Sci., v. 19, p. 129- 143.

Thompson, P.H. and Frey, M. (1984): Illite "crystallinity" in the Western River Formation and it's significance regarding the regional metamorphism of the Early Proterozoic Goulburn Group, District of Mackenzie; in Current Research, Part A, Geol. Surv. Can., Paper 84-1A, p. 409-414.

Tilley, C.E. (1926): Some mineralogical transformations in crystalline schists; Mineral. Mag., v. 21, p. 34-46.

Tracy, R.J., Robinson, P. and Thompson, A.B. (1976): Garnet composition and zoning in the determination of temperature and pressure of metamorphism, Central Massachusetts; Am. Mineral., v. 61, p. 762-775.

Tremblay, L.P. (1976): Geology of northern Contwoyto Lake
    area, District of Mackenzie; Geol. Surv. Can., Memoir
    381, p.

Turner, F.J. (1981): Metamorphic Petrology, Mineralogical,
    Field and Tectonic Aspects. Second Edition. McGraw-Hill
    Book Company, Hemisphere Publishing Corporation, U.S.A.,
    524p.

van Breemen, O., Henderson, J.B., Sullivan, R.W. and
    Thompson, P.H. (1987): U-Pb, zircon and monazite ages
    from the eastern Slave Province, Healey Lake area,
    N.W.T.;in Radiogenic ages and isotopic studies: Report
    1, Geol. Surv. Can., Paper 87-2, p. 101-110.

Velde, B. (1965): Phengitic micas: synthesis, stability and
    natural occurrence; Am. J. Sci., v. 263, p. 886-913.

Winkler, H.J.F. (1976): Petrogenesis of Metamorphic Rocks.
    Fourth Edition. Springer-Verlag, New York, 334p.

Appendix A: Electron Microprobe Analysis

Appendix A contains the following tables of electron microprobe analyses, which are discussed in the text:

Table   A.5; Chemical compositions of CHZ minerals.

Table   A.6; Chemical compositions of BZ minerals.

Table   A.7; Chemical compositions of CZ minerals.

Table   A.8; Chemical compositions of AZ minerals.

Table   A.9; Chemical compositions of SZ minerals.

Table A.10; Microprobe analyses of minerals from amphibole-bearing iron formation.

Table A.11; Chemical compositions of low-grade Fe-rich minerals.

Table A.12; Chemical compositions of minerals in garnet/staurolite-bearing assemblages.

Table A.13; Microprobe analyses of minerals from mafic flows.

Table A.14; Chemical compositions of minerals in felsic volcanics.

The tables are arranged in an order that corresponds with the text and are presented following the discussions on Methods and Problems in Analysing Phyllosilicates by Electron Microprobe. Locations of all samples examined in thin section and analysed by electron microprobe, x-ray diffraction or for whole-rock composition are shown in Figure A.1.

Contwoyto and Itchen Formations (units 9a,b,10)
* muscovite-free, A*Z, S*Z

Contwoyto Formation (iron-rich; unit 9c) and garnetiferous Itchen Formation.

△ Metabasites (unit 4 mafic flows)

☐ Felsic volcanics (unit 5).

▧ Carbonate (unit 7).

⬡ Gneisses (unit 1).

N O R T H   A R M

Itchen Lake

82-V-180*
82-V-176
82-V-173
82-V-54
82-V-22
82-V-21
82-V-23
82-V-183*
82-V-34
82-V-38*
82-V-39
82-V-33
82-V-42*
82-V-40*
82-V-58
82-V-76
81-V-383d
81-V-450
81-V-366
81-V-373
82-V-32
81-V-392
81-V-451
81-V-396
81-V-395
81-V-391
81-V-356
82-V-73
81-V-427
81-V-442a*
81-V-398
81-V-411
81-V-357
81-V-430
81-V-444*
81-V-191
81-V-170
81-V-439
81-V-171
81-V-220
81-V-437
81-V-221
-223
81-V-163
81-V-128
81-V-132
81-V-226
+225
81-V-99
81-V-108a
82-V-133
81-V-105
81-V-155
82-V-163
81-V-112
81-V-106
81-V-122
81-V-135
81-V-109
81-V-107
81-V-137
81-V-29
81-V-139
81-V-39
81-V-307
81-V-304*
81-V-302
81-V-38
P O I N T
81-V-05
81-V-277
81-V-01
81-V-36
81-V-343
81-V-153
82-V-214
81-V-200, 201
81-V-342
81-V-198, 199
81-V-340
81-V-15
81-V-143
81-V-45
81-V-55
81-V-346
81-V-347
81-V-350*
Keskarrah Bay
L A K E
81-V-252
81-V-67
*81-V-268
*81-V-250
81-V-264
81-V-413

FIGURE A.I: Locations of all samples analysed by electron microprobe, x-ray diffraction and for whole-rock geochemistry.

N

0   2.5   5
km

Methods

Samples were chosen that: a) contained little or no evidence of alteration or retrograde metamorphism and b) contained representative mineral assemblages.

Thin sections were hand polished using 1.0, 0.3 and a final .05 micron synthetic powders. The amount of time required to achieve the necessary degree of polish varied with grain size and mineralogy of the sample: micaceous minerals in fine-grained greywackes were the most difficult to polish. Areas were selected in the thin section for analysis and circled and the section was then carbon-coated.

Samples were analysed with a JEOL JXA-50A wavelength dispersive electron probe microanalyser with Krisel control probe system and built-in Bence Albee correction factors housed at the Department of Earth Sciences Memorial University, St. John's, Nfld. In most cases each mineral was analysed for 11 elements (Na, Mg, Al, Si, K, Ca, Ti, Cr, Mn, Fe, Ni) with an analysis time of 30 seconds and/or 60,000 counts (for analysis of some plagioclases and opaque phases analysis time was cut to 5 seconds and 30,000 counts).

The internal standard used for analysis was clinopyroxene (ACPX) and occasional checks were made using other standards (garnet, plagioclase). Oxide abundances for the ACPX clinopyroxene standard are given in Table A.1 along with other standards used for element calibration.

TABLE A.1: Chemical Composition of ACPX Clinopyroxene Standard and Other Standards Used During Electron Microprobe Analyses

Standard	ACPX	FCPX	2442GARN	K-GNT	LC PLAG	BENS	HEDEN	MCKAY	KREEP	LOWK	K-HB*	JOPX
Na_2O	1.27	1.27	n.d	n.d	3.45	.36	.44	n.d	1.06	n.d	2.60	.13
MgO	16.65	15.47	11.53	18.504	.134	.00	1.47	7.38	10.84	7.16	12.80	26.79
Al_2O_3	7.86	7.86	22.10	23.732	30.91	19.24	1.58	13.42	17.31	9.94	14.90	1.23
SiO_2	50.73	49.85	39.00	41.46	51.25	63.42	47.12	44.65	48.80	39.18	40.37	54.09
K_2O	n.d	n.d	n.d	n.d	.175	15.34	.05	.02	.52	.05	2.05	n.d
CaO	15.82	17.75	4.20	5.163	13.64	.08	21.97	12.25	10.00	12.07	10.30	1.52
TiO_2	.74	.83	.08	.47	.045	.00	.01	6.59	1.68	10.12	4.72	.16
Cr_2O_3	n.d	n.d	n.d	..d	.01	.00	n.d	.14	n.d	n.d	n.d	.75
MnO	.13	.14	.49	.28	.446	.10	2.62	13.95	.19	18.63	.09	.49
FeO	6.768	6.17	22.04	10.678	n.d	.02	24.41	n.d	8.90	n.d	10.919	15.22
NiO	n.d	n.d	n.d	n.d	n.d	.62	n.d	.25	.18	.35	n.d	n.d
TOTAL	99.97	99.34	99.44	100.287	100.06	99.18	99.67	98.65	99.48	97.50	96.69	100.25

*H2O content 0.94 weight percent

A large muscovite grain from pegmatite was used as an external monitor during analysis of the phyllosilicates. The composition of the muscovite monitor as determined by wet chemical analysis (Table A.2) differs from that determined by electron microprobe analysis (Table A.3): K is lower in almost every microprobe analysis relative to wet chemical analysis (higher K-contents were determined during one set of analyses) and Si-contents are inconsistent: L.O.I. indicates a water content of 5.4% but microprobe oxide totals are in the range of 90 to 95 indicating water contents of 5 to 10%.

Problems in Analysing Phyllosilicates by Electron Microprobe

The discrepancies in K-contents determined for the muscovite monitor by the 2 different methods is a problem that was recognized buc could not be rectified. Craw (1981) observed that in K-bearing phyllosilicates K ions will migrate within the sample due to volatization of OH ions by the microprobe beam and that the beam causes internal oxidation of Fe^{2+}. Initially K ions migrate to the beam spot, but subsequently the ions migrate away from the spot, apparently as the result of the oxidation of Fe^{2+}. Craw (1981) also noted that the direction of change in Fe:Mg:Al ratios during oxidation is unpredictable. Table A.4 presents microprobe analyses carried out repeatedly on one spot of

TABLE A.2: Chemical Composition of Muscovite Monitor from Atomic
Adsorption Analyses

Analyses no.	1	2	3	4	Trace Elements	
SiO_2	45.8	45.8	45.8	45.6	Pb	3
TiO_2	.10	.10	.10	.10	Th	1
Al_2O_3	32.0	32.0	32.0	32.0	U	4
Li	.13	.13	.13	.13	Rb	2095, 0.2%
Fe_2O_3*	4.25	4.25	4.22	4.21	Sr	4
MnO	.10	.10	.10	.10	Y	38
MgO	.39	.39	.40	.40	Zr	2
CaO	.07	.06	.11	.08	Nb	246
Na_2O	.67	.66	.66	.66	Zn	432
K_2O	10.36	10.46	10.42	10.46	Cu	7
P_2O_5	.05	.03	.05	.05	Ni	17
LOI	5.43	5.43	5.43	5.43	La	26
TOTAL	99.35	99.41	99.42	99.22	Ba	88
					Ti	14
					V	11
					Ce	13
					Cr	0
					Ga	165

* Fe_2O_3 = Fe total.
Trace element data in ppb.

TABLE A.3:Chemical Composition of Muscovite Monitor from
Electron Microprobe Analyses (using ACPX standard)

batch no.	1	2	3	4	5	Average
no. of analyses	4	6	6	4	3	23
Na_2O	.57	.58	.55	.66	.73	.60
MgO	.43	.44	.44	.47	.43	.44
Al_2O_3	31.61	32.50	33.04	31.46	31.35	32.16
SiO_2	47.12	45.70	46.78	44.58	45.10	45.96
K_2O	9.57	9.50	10.77	9.39	9.73	9.86
CaO	.00	.00	.00	.00	.00	.00
TiO_2	.14	.13	.14	.12	.13	.14
Cr_2O_3	.00	.00	.00	.00	.00	.00
MnO	.08	.09	.06	.11	.04	.08
FeO	3.02	3.19	3.02	2.87	3.00	3.04
NiO	.04	n.d	.01	.00	.00	.00
TOTAL	92.56	92.12	94.81	89.66	90.52	92.28
Na	:149	.154	.143	.179	.198	.160
Mg	.084	.089	.087	.096	.091	.089
Al	5.109	5.294	5.260	5.262	5.206	5.236
Si	6.466	6.316	6.318	6.329	6.356	6.350
K	1.675	1.675	1.855	1.700	1.749	1.736
Ca	.000	.000	.000	.000	.000	.000
Ti	.012	.012	.012	.012	.012	.012
Cr	.000	.000	.000	.000	.000	.000
Mn	.008	.008	.004	.012	.004	007
Fe	.347	.365	.341	.337	.357	.350
Ni	.004	n.d	.000	.000	.000	.000
TOTAL	13.849	13.913	14.019	13.927	13.967	13.940

formula basis: 22 oxygens per formula unit

TABLE A.4: Repeated One Spot Electron Microprobe Analyses of Muscovite Monitor
(using ACPX standard)

analysis no.	1	2	3	4	5	6	7	8
Na_2O	1.01	.64	.21	.18	.28	.07	.11	.18
MgO	.54	.49	.46	.29	.52	.50	.45	.34
Al_2O_3	30.99	32.22	30.75	32.97	29.95	31.86	29.00	29.54
SiO_2	42.61	43.57	43.54	45.60	42.44	41.27	38.45	41.38
K_2O	10.79	9.48	7.38	6.37	5.33	3.31	5.58	3.52
CaO	.00	.00	.00	.00	.00	.00	.05	.00
TiO_2	.13	.17	.17	.12	.14	.19	.11	.17
Cr_2O_3	.02	.00	.03	.06	.00	.00	.00	.00
MnO	.04	.15	.11	.06	.00	.20	.00	.11
FeO	2.58	2.71	2.80	2.92	3.32	2.57	2.80	2.70
NiO	.00	.18	.13	.01	.00	.00	.00	.00
TOTAL	88.70	89.60	85.57	88.59	81.98	79.97	76.55	77.94
Na	.282	.175	.056	.049	.080	.018	.033	.055
Mg	.115	.100	.099	.057	.115	.111	.110	.078
Al	5.315	5.414	5.318	5.445	5.345	5.719	5.565	5.448
Si	6.199	6.213	6.390	6.391	6.425	6.287	6.264	6.477
K	2.002	1.724	1.378	1.135	1.026	.644	1.157	.698
Ca	.000	.000	.000	.000	.000	.000	.004	.000
Ti	.013	.017	.017	.012	.013	.018	.009	.018
Cr	.000	.000	.000	.004	.000	.000	.000	.000
Mn	.004	.017	.013	.004	.000	.022	.000	.014
Fe	.312	.322	.340	.341	.417	.326	.377	.354
Ni	.000	.017	.013	.000	.000	.000	.000	.000
TOTAL	14.241	13.998	13.623	13.439	13.422	13.144	13.520	13.141
M/FM	.267	.228	.219	.142	.216	.242	.226	.175
Na/Na+K	.123	.092	.039	.041	.072	.027	.028	.073
Al^{vi}	3.514	3.627	3.708	3.836	3.770	4.006	3.829	3.925
Al^{iv}	1.801	1.787	1.610	1.609	1.575	1.713	1.736	1.523

formula basis: 22 oxygens per formula unit

the muscovite monitor, from which it can be seen that K-contents decreased and Fe-contents increased during the course of the analyses.

Craw (1981) suggested that defocusing the beam (increasing the width and decreasing the intensity) is a solution to alleviate K ion migration. In the rocks of this study the width of the phyllosilicates (especially muscovite) often approximates the smallest beam width obtainable, so beam defocusing could not be attempted.

Other problems encountered include: a) difficulties in precisely locating the beam; b) the beam position must be constantly checked for wandering during analysis of fine-grained micas; c) in some instances it is possible to focus on a mica that is just beneath another grain (quartz, feldspar); d) basal sections of the micas are almost impossible to polish and e) none of the internal standards used during analysis for this study compare closely enough to muscovite or biotite mineral chemistry.

TABLE A.5: Chemical Composition of CHZ Minerals
EASTERN BELT

	MUSCOVITE					CHLORITE	
Sample no.	05a	277a	171	356	122	05a	277a
no. of analyses	7	3	3	6	3	3	2
Na_2O	.44	.46	.46	.43	.47	.26	.13
MgO	1.13	.69	.57	.80	.50	12.99	13.03
Al_2O_3	32.23	32.58	34.01	33.00	33.92	21.99	21.44
SiO_2	48.43	46.87	44.81	47.18	45.96	26.32	26.23
K_2O	9.35	10.06	9.2	10.31	10.08	.07	.35
CaO	.00	.00	.00	.00	.00	.02	.01
TiO_2	.34	.40	.24	.23	.20	.05	.06
Cr_2O_3	.00	.03	.04	.00	.02	.01	.19
MnO	.02	.02	.00	.03	.03	.14	.14
FeO	2.04	1.30	1.22	1.27	.82	26.47	26.70
NiO	.02	.01	.03	.03	.04	.00	.03
TOTAL	94.00	92.42	90.59	93.29	92.04	88.32	88.41
Na	.111	.120	.122	.111	.123	.067	.029
Mg	.223	.136	.115	.159	.100	2.597	2.624
Al	5.090	5.245	5.569	5.270	5.474	3.475	3.417
Si	6.490	6.405	6.220	6.396	6.293	3.572	3.558
K	1.455	1.751	1.629	1.782	1.760	.009	.055
Ca	.000	.000	.000	.000	.000	.001	.000
Ti	.030	.040	.023	.023	.020	.003	.004
Cr	.000	.001	.002	.000	.001	.000	.018
Mn	.001	.001	.000	.000	.003	.015	.014
Fe	.226	.145	.138	.143	.092	2.969	3.019
Ni	.001	.001	.001	.000	.003	.000	.002
TOTAL	13.627	13.845	13.819	13.884	13.869	12.708	12.740
M/FM	.497	.484	.455	.527	.521	.467	.465
Na/Na-K	.071	.064	.070	.059	.065		
AlVI	3.580	3.650	3.789	3.666	3.767	2.444	2.465
AlIV	1.510	1.595	1.780	1.604	1.707	2.961	2.850
formula basis#:	22	22	22	22	22	18	18

number of oxygens per formula unit

	MUSCOVITE							CHLORITE						
Sample no.	105	392a	108	225	221	395	223	105	392a	108	225	221	395	223
no. of analyses	3	3	8	3	4	6	10	2	3	6	7	5	10	4
Na$_2$O	.60	.45	.44	.50	.50	.30	.77	.04	.01	.03	.01	.03	.03	.04
MgO	.48	.69	.75	.70	.62	.65	.69	19.06	18.05	16.94	19.11	16.34	11.73	12.99
Al$_2$O$_3$	35.21	33.53	34.96	34.28	36.39	33.31	33.99	23.41	22.74	22.60	23.55	23.30	22.69	23.65
SiO$_2$	47.79	44.46	48.35	46.80	47.18	46.08	46.30	26.91	24.56	27.28	26.02	25.59	24.65	25.53
K$_2$O	8.70	10.09	9.34	9.03	9.03	9.79	9.29	.02	.03	.01	.07	.02	.01	.05
CaO	.00	.00	.00	.00	.00	.00	.00	.01	.01	.03	.01	.01	.01	.01
TiO$_2$	.10	.55	.39	.11	.20	.29	.19	.03	.06	.05	.03	.03	.06	.04
Cr$_2$O$_3$	.03	.07	.08	.02	.01	.08	.01	.09	.06	.07	.03	.02	.01	.02
MnO	.02	.03	.01	.02	.02	.08	.02	.13	.19	.20	.20	.52	.19	.24
FeO	.39	.72	.89	.59	.81	1.51	1.21	17.80	21.96	22.69	18.77	24.32	29.98	27.57
NiO	.01	.00	.02	.00	.03	.02	.03	.09	.06	.05	.01	.03	.03	.03
TOTAL	93.37	90.59	95.23	92.05	96.89	92.11	92.50	87.59	87.73	89.94	87.81	89.31	89.40	90.17
Na	.163	.120	.109	.128	.123	.078	.202	.007	.003	.005	.001	.007	.004	.007
Mg	.092	.168	.114	.140	.118	.130	.137	3.682	3.583	3.266	3.708	3.191	2.369	2.567
Al	5.523	5.517	5.411	5.479	5.518	5.383	5.450	3.575	3.571	3.447	3.898	3.596	3.635	3.695
Si	6.360	6.201	6.350	6.346	6.328	6.318	6.294	3.487	3.269	3.525	3.389	3.352	3.351	3.363
K	1.476	1.797	1.563	1.561	1.482	1.712	1.612	.002	.002	.000	.008	.002	.000	.006
Ca	.000	.000	.000	.000	.000	.000	.000	.000	.000	.002	.000	.000	.000	.000
Ti	.008	.056	.037	.009	.018	.031	.017	.000	.005	.002	.000	.001	.003	.001
Cr	.002	.007	.006	.001	.000	.001	.000	.007	.005	.001	.000	.000	.004	.001
Mn	.000	.003	.000	.001	.002	.003	.001	.013	.021	.018	.016	.023	.014	.025
Fe	.043	.081	.096	.065	.086	.170	.136	1.929	2.447	2.454	2.040	2.662	3.410	3.057
Ni	.000	.000	.001	.000	.002	.001	.002	.005	.004	.003	.001	.001	.002	.002
TOTAL	13.667	13.950	13.687	13.730	13.677	13.827	13.851	12.707	12.910	12.726	13.062	12.835	12.788	12.724
M/FM	.682	.675	.543	.683	.578	.433	.502	.656	.594	.571	.645	.545	.411	.456
Na/Na+K	.100	.063	.065	.076	.077	.044	.111							
Al^{vi}	3.883	3.718	3.761	3.825	3.846	3.701	3.744	2.576	2.915	2.517	2.728	2.786	2.787	2.769
Al^{iv}	1.640	1.799	1.650	1.654	1.672	1.682	1.706	2.985	2.640	2.845	3.335	2.808	2.867	2.979
Al/Mg+Fe+Mn								.531	.436	.496	.579	.478	.495	.527
formula basis#:	22	22	22	22	22	22	22	18	18	18	18	18	18	18

number of oxygens per formula unit

TABLE A.5 (continued): PLAGIOCLASE

	Western CHZ						Eastern CHZ		356		matrix		357a	
Sample no.	105	392a	223	392	05a	277a	clast		clast		matrix		clast	matrix
no. of analyses	2	2	1	1	1	1	1	1	1	1	2	1	1	1
Na_2O	11.58	11.42	6.07	11.30	10.29	12.10	12.25	12.34	11.43	10.89	11.69	12.54	10.82	12.70
MgO	.00	.00	.00	.00	.00	.10	.03	.00	.00	.00	.02	.00	.00	.00
Al_2O_3	19.15	20.00	27.35	19.48	18.49	19.01	20.82	19.33	21.75	19.96	19.09	19.37	20.43	18.67
SiO_2	64.46	70.31	56.16	67.71	69.60	7_.53	68.18	70.05	67.95	68.75	69.16	71.60	66.62	70.48
K_2O	.00	.02	.13	.04	.03	.10	.01	.01	.03	.07	.04	.05	.06	.04
CaO	.19	.62	9.13	.66	.06	.08	1.93	.15	2.71	1.58	.29	.11	2.16	.16
TiO_2	.00	.00	.06	.00	.00	.00	.05	.00	.03	.03	.00	.02	.00	.02
Cr_2O_3	.00	.00	.00	.00	.00	.00	.00	.00	.00	.00	.01	.00	.00	.00
MnO	.00	.00	.01	.00	.01	.02	.06	.14	.00	.00	.05	.04	.00	.00
FeO	.02	.03	.07	.12	.08	.34	.16	.06	.18	.13	.05	.00	.10	.01
NiO	.08	.04	.00	.05	.00	.01	.06	.00	.00	.01	.05	.08	.06	.01
TOTAL	95.48	102.44	98.98	99.36	98.56	103.28	103.54	102.08	104.09	101.04	100.45	103.80	100.26	102.08
Na	1.031	.944	.528	.964	.875	.992	1.012	1.025	.939	.915	.985	1.023	.920	1.055
Mg	.000	.000	.000	.000	.000	.005	.001	.000	.000	.000	.000	.000	.000	.000
Al	1.037	1.004	1.456	1.010	.957	.948	1.046	.976	1.086	1.021	.979	.962	1.056	.943
Si	2.956	2.996	2.544	2.979	3.060	3.028	2.908	3.002	2.882	2.963	3.009	3.017	2.923	3.023
K	.000	.001	.000	.001	.001	.005	.000	.000	.001	.003	.001	.002	.002	.001
Ca	.008	.028	.440	.031	.002	.002	.087	.006	.123	.072	.013	.005	.102	.006
Ti	.000	.000	.000	.000	.000	.000	.001	.000	.000	.000	.000	.000	.000	.000
Cr	.000	.000	.000	.000	.000	.000	.000	.000	.000	.000	.000	.000	.000	.000
Mn	.000	.000	.000	.000	.000	.000	.001	.005	.000	.000	.001	.001	.000	.000
Fe	.000	.000	.005	.003	.002	.011	.005	.001	.006	.003	.001	.000	.002	.000
Ni	.006	.003	.000	.001	.000	.000	.001	.000	.000	.000	.001	.002	.001	.000
TOTAL	5.038	4.976	4.973	4.990	4.898	4.991	5.063	5.015	5.039	4.976	4.990	5.013	5.006	5.028
An-content (molecular %)	0.8	2.9	45.5	3.1	0.2	0.2	7.9	0.6	11.6	0.7	1.3	0.5	10.0	0.6

formula basis#: 8 oxygens per formula unit

TABLE A.6: Chemical Compositions of BZ Minerals

EASTERN BELT

	MUSCOVITE						CHLORITE						
Sample no.	01a	199a	200	201a	201b	2-33	01a	199a	200	201a	201b	2-33	2-54a
no. of analyses	3	4	2	7	6	11	1	4	2	6	5	5	3
Na_2O	.12	.25	.41	.33	.30	.55	.01	.04	.09	.02	.03	.02	.01
MgO	1.75	1.04	.99	.79	.90	.67	14.98	15.05	12.59	14.51	14.92	15.83	18.06
Al_2O_3	30.94	34.25	32.47	35.02	34.50	35.51	20.61	22.33	21.55	22.09	22.61	23.40	21.74
SiO_2	44.92	48.58	46.44	47.83	48.76	48.75	24.32	25.97	27.07	26.37	25.91	25.34	25.94
K_2O	10.82	10.39	10.09	10.90	10.70	10.33	.01	.10	.34	.21	.05	.03	.04
CaO	.01	.01	.00	.01	.01	.01	.02	.02	.03	.03	.01	.03	.03
TiO_2	.51	.40	.39	.29	.34	.33	.07	.06	.06	.11	.07	.07	.06
Cr_2O_3	.01	.06	.04	.04	.04	.05	.03	.04	.03	.06	.04	.07	.14
MnO	.06	.02	.01	.02	.02	.01	.21	.22	.22	.16	.27	.31	.32
FeO	2.26	1.33	2.18	1.15	1.38	.84	25.13	25.60	25.53	25.70	25.27	23.81	21.56
NiO	.04	.02	.02	.02	.04	.02	.05	.03	.06	.02	.01	.04	.05
TOTAL	91.58	96.35	93.04	96.40	96.99	97.07	85.45	89.46	87.57	89.28	89.19	88.95	87.95
Na	.030	.060	.106	.083	.075	.136	.000	.010	.020	.002	.007	.005	.000
Mg	.365	.201	.198	.152	.172	.126	3.122	2.971	2.545	2.874	2.950	3.117	3.562
Al	5.108	5.284	5.233	5.421	5.301	5.153	3.392	3.488	3.422	3.453	3.534	3.644	3.562
Si	6.291	6.361	6.347	6.280	6.355	6.319	3.396	3.411	3.660	3.502	3.438	3.349	3.432
K	1.930	1.734	1.758	1.825	1.778	1.707	.000	.016	.054	.033	.006	.003	.005
Ca	.000	.000	.000	.000	.000	.000	.000	.001	.002	.003	.000	.002	.001
Ti	.052	.037	.036	.026	.030	.030	.004	.003	.008	.009	.005	.004	.002
Cr	.010	.003	.000	.001	.002	.003	.000	.002	.000	.004	.001	.005	.012
Mn	.005	.001	.000	.000	.001	.000	.024	.021	.022	.016	.028	.032	.034
Fe	.263	.143	.244	.124	.149	.089	2.937	2.837	2.905	2.855	2.801	2.632	2.386
Ni	.001	.001	.002	.000	.003	.009	.004	.002	.006	.001	.000	.002	.005
TOTAL	14.055	13.825	13.924	13.912	13.866	13.572	12.879	12.762	12.642	12.752	12.770	12.795	12.829
M/FM	.581	.584	.448	.551	.536	.586	.513	.510	.465	.500	.511	.539	.595
Na/Na+K	.015	.033	.057	.044	.040	.074							
Al^{vi}	3.399	3.645	3.580	3.701	3.656	3.472	2.718	2.694	2.307	2.553	2.652	2.791	2.662
Al^{iv}	1.709	1.639	1.653	1.720	1.645	1.681	2.558	2.732	3.016	2.818	2.845	2.877	2.611
Al/Fe+Mg+Mn							.421	.469	.551	.491	.492	.498	.436
formula basis#:22	22	22	22	22	22	18	18	18	18	18	18	18	

number of oxygens per formula unit

EASTERN BELT
BIOTITE

Sample no.	01a	198a	199a	201a	201b	2-33	2-54a
no. of analyses	4	7	3	3	6	7	7
Na_2O	.11	.10	.03	.03	.07	.10	.19
MgO	9.71	7.96	10.38	10.09	10.51	11.05	12.67
Al_2O_3	18.38	18.97	18.60	18.88	18.81	19.04	17.76
SiO_2	35.52	35.78	35.96	36.83	36.20	36.97	36.28
K_2O	9.89	9.87	9.98	10.36	9.93	10.03	9.11
CaO	.00	.00	.01	.00	.01	.01	.00
TiO_2	1.74	1.74	1.73	1.62	1.77	1.42	1.36
Cr_2O_3	.05	.05	.06	.08	.05	.07	.16
MnO	.07	.08	.08	.08	.11	.14	.16
FeO	19.46	21.75	19.15	19.87	19.30	17.70	17.34
NiO	.00	.03	.06	.01	.01	.03	.01
TOTAL	94.67	96.33	96.04	97.85	96.77	96.56	95.05
Na	.033	.027	.009	.014	.020	.025	.050
Mg	2.225	1.906	2.339	2.237	2.347	2.450	2.866
Al	3.333	3.407	3.314	3.307	3.325	3.338	3.132
Si	5.423	5.452	5.437	5.476	4.472	5.501	5.522
K	1.939	1.917	1.924	1.962	1.897	1.902	1.704
Ca	.001	.000	.000	.000	.000	.001	.000
Ti	.200	.197	.195	.177	.197	.156	.149
Cr	.004	.003	.004	.008	.004	.007	.018
Mn	.006	.009	.007	.008	.012	.015	.019
Fe	2.503	2.771	2.420	2.470	2.420	2.201	2.136
Ni	.000	.002	.004	.001	.001	.001	.001
TOTAL	15.667	15.590	15.653	15.660	15.560	15.597	15.597
M FM	.471	.412	.492	.475	.492	.527	.573
Na Na+K	.017	.014	.005	.007	.010	.013	.029
AlVI	.756	.859	.751	.783	.752	.839	.654
AlIV	2.577	2.548	2.563	2.524	2.573	2.499	2.478

formula basis: 22 oxygens per formula unit

TABLE A.6: (continued)

WESTERN BELT

	MUSCOVITE				CHLORITE				BIOTITE			
Sample no.	398	396	112	373	398	396	112	373	398	396	112	373
no. of analyses	5	3	3	5	3	2	6	3	4	3	7	4
Na_2O	.63	.22	.38	.32	.01	.04	.02	.02	.08	.04	.07	.02
MgO	.41	.84	.74	.75	12.58	14.51	12.94	14.35	9.04	10.04	8.84	8.95
Al_2O_3	34.31	32.96	35.60	33.25	22.65	23.77	22.78	19.14	18.68	19.74	19.27	17.73
SiO_2	44.41	47.65	48.31	47.00	24.52	24.71	25.33	27.35	35.97	34.50	36.69	37.08
K_2O	9.40	10.05	9.30	9.42	.03	.07	.02	.02	9.14	9.59	9.15	8.81
CaO	.00	.00	.00	.01	.01	.01	.03	.01	.00	.01	.03	.00
TiO_2	.29	.43	.29	.45	.06	.06	.08	.04	1.53	1.96	1.53	1.41
Cr_2O_3	.04	.02	.04	.01	.05	n.d	.02	.02	.07	n.d	.05	.02
MnO	.01	.02	.02	.02	.42	.44	.37	.47	.19	.22	.16	.23
FeO	.85	1.07	1.00	1.10	28.38	25.25	28.67	27.49	21.78	18.82	21.86	22.01
NiO	.02	.04	.01	.03	.00	n.d	.03	.04	.06	n.d	.04	.03
TOTAL	90.37	93.30	95.69	92.36	88.71	88.86	90.27	88.95	96.54	94.92	97.68	96.29
Na	.167	.055	.094	.082	.003	.000	.003	.005	.021	.007	.019	.004
Mg	.084	.167	.143	.149	2.551	2.889	2.574	2.886	2.041	2.296	1.964	2.010
Al	5.634	5.239	5.482	5.327	3.637	3.735	3.584	3.044	3.337	3.555	3.388	3.165
Si	6.185	6.429	6.314	6.386	3.332	3.294	3.383	3.689	5.451	5.275	5.474	5.614
K	1.670	1.728	1.549	1.631	.002	.009	.001	.001	1.766	1.868	1.741	1.702
Ca	.000	.000	.000	.000	.002	.009	.001	.001	.000	.000	.002	.000
Ti	.028	.041	.027	.044	.005	.000	.006	.001	.171	.226	.169	.160
Cr	.002	.000	.002	.000	.004	n.d	.000	.000	.009	n.d	.003	.000
Mn	.001	.001	.001	.001	.047	.036	.040	.050	.022	.026	.019	.026
Fe	.097	.118	.107	.123	3.231	2.808	3.200	3.100	2.760	2.405	2.726	2.787
Ni	.000	.003	.000	.002	.000	n.d	.001	.003	.003	n.d	.003	.000
TOTAL	13.841	13.781	13.719	13.745	12.812	12.771	12.794	12.779	15.581	15.648	15.508	15.477
M/FM	.464	.586	.572	.548	.438	.504	.443	.478	.425	.487	.419	.420
Na/Na+K	.091	.031	.057	.048					.012	.004	.011	.002
Al^{vi}	3.819	3.668	3.796	3.713	2.817	2.876	2.738	2.262	.788	.830	.862	.779
Al^{iv}	1.815	1.571	1.686	1.614	2.840	2.934	2.837	2.473	2.549	2.725	2.526	2.386
Al/Fe+Mg+Mn					.487	.512	.488	.410				
formula basis#:	22	22	22	22	18	18	18	18	22	22	22	22

PLAGIOCLASE

	WESTERN BELT				EASTERN BELT						
Sample no.	112 M	398 M	373 C	373 M	01a C	01a M	199a C	201a M	201b C	2-33 M	2-54a M
no. of analyses	1	1	1	2	1	1	1	1	2	2	1
Na_2O	6.68	8.26	11.59	9.20	11.78	12.08	11.10	8.20	11.81	8.71	7.08
MgO	.00	.00	.02	.01	.01	.00	.00	.30	.01	.10	.00
Al_2O_3	25.06	24.36	20.66	23.33	19.00	19.82	19.62	25.01	20.17	23.43	24.52
SiO_2	59.98	60.05	71.03	62.23	66.45	69.07	73.21	62.03	73.60	63.08	59.95
K_2O	.04	.07	.03	.05	.04	.04	.03	.08	.03	.13	.03
CaO	9.45	6.73	1.56	5.52	.25	.68	.17	7.54	.39	5.59	6.95
TiO_2	.00	.04	.00	.02	.00	.04	.01	.00	.00	.01	.02
Cr_2O_3	.00	.00	.00	.00	.00	.00	.01	.00	.02	.01	.01
MnO	.05	.00	.01	.02	.00	.04	.01	.00	.02	.01	.01
FeO	.11	.12	.03	.09	.08	.05	.09	.09	.05	.32	.01
NiO	.00	.14	.00	.00	.02	.05	.00	.00	.05	.02	.02
TOTAL	101.39	99.78	104.93	100.47	97.64	101.87	104.24	102.95	106.13	101.40	98.59
Na	.572	.715	.938	.789	1.023	1.007	.895	.689	.941	.740	.616
Mg	.000	.000	.001	.000	.000	.000	.000	.000	.000	.006	.000
Al	1.358	1.162	1.015	1.219	1.004	1.005	.962	1.278	.975	1.209	1.296
Si	2.610	2.812	2.965	2.755	2.980	2.972	3.047	2.690	3.021	2.764	2.696
K	.001	.002	.001	.002	.001	.001	.001	.003	.001	.007	.000
Ca	.446	.249	.068	.262	.012	.030	.007	.350	.017	.262	.336
Ti	.000	.001	.000	.000	.000	.010	.000	.000	.000	.000	.000
Cr	.000	.000	.000	.000	.000	.000	.000	.000	.000	.000	.000
Mn	.001	.000	.000	.000	.000	.001	.000	.000	.000	.000	.000
Fe	.003	.004	.000	.003	.002	.001	.002	.002	.001	.011	.000
Ni	.000	.004	.000	.000	.000	.001	.000	.000	.001	.000	.000
TOTAL	4.992	5.018	4.989	5.029	5.022	5.020	4.915	5.013	4.957	4.999	4.944
An-content (molecular %)	44.0	30.5	7.0	24.8	1.0	2.9	0.1	33.6	0.8	26.0	35.3

formula basis: 8 oxygens per formula unit
M = recrystallized matrix plagioclase
C = recrystallized "?" plagioclase grains

TABLE A.7: Chemical Compositions of C2 Minerals

	MUSCOVITE					BIOTITE			
Sample no	2-54b	2-34	132	2-163		.-54b	2-34	132	2-163
no. of analyses	6	7	7	4		7	5	8	6
Na$_2$O	.97	1.18	1.29	1.39		.14	.17	.15	.12
MgO	.48	.43	.43	.43		10.83	9.53	10.73	10.26
Al$_2$O$_3$	36.01	36.00	36.25	34.55		19.64	20.00	19.62	18.85
SiO$_2$	49.04	48.67	49.10	45.47		36.45	36.71	37.17	35.43
K$_2$O	8.61	8.70	8.23	8.56		8.53	8.69	8.57	8.77
CaO	.00	.02	.00	.00		.00	.01	.00	.00
TiO$_2$	.31	.31	.36	.37		1.35	1.36	1.43	1.36
Cr$_2$O$_3$	.05	.06	.05	.05		.06	.06	.06	.06
MnO	.01	.01	.01	.02		.08	.10	.08	.08
FeO	.72	.70	.73	.54		19.81	19.77	20.15	18.26
NiO	.03	.01	.02	.03		.05	.02	.03	.03
TOTAL	96.23	96.09	96.47	91.41		96.75	96.42	97.99	93.22
Na	.242	.295	.321	.367		.037	.047	.042	.035
Mg	.091	.081	.080	.085		2.396	2.117	2.347	2.354
Al	5.491	5.504	5.507	5.578		3.440	3.515	3.394	3.423
Si	6.344	6.318	6.329	6.229		5.414	5.475	5.455	5.461
K	1.420	1.438	1.351	1.495		1.581	1.653	1.602	1.724
Ca	.000	.002	.000	.000		.000	.000	.000	.000
Ti	.027	.027	.032	.036		.148	.150	.156	.155
Cr	.002	.004	.002	.002		.006	.005	.005	.007
Mn	.000	.000	.000	.001		.008	.011	.008	.009
Fe	.076	.074	.076	.061		2.460	2.465	2.473	2.351
Ni	.002	.000	.000	.002		.003	.002	.002	.003
TOTAL	13.695	13.743	13.698	13.856		15.493	15.440	15.484	15.522
M/FM	.545	.523	.513	.582		.493	.462	.487	.500
Na/Na+K	.146	.170	.192	.197		.023	.028	.026	.020
Al^{vi}	3.835	3.822	3.836	3.807		.854	.990	.849	.884
Al^{iv}	1.656	1.682	1.671	1.771		2.586	2.525	2.545	2.539

formula basis: 22 oxygens per formula unit

TABLE A.7: (continued)

Sample no.	CORDIERITE				PLAGIOCLASE		
	2-54b	2-34	132	2-163	2-54b	132	2-163
no. of analyses	11	5	3	5	1	1	1
Na_2O	.38	.52	.27	.19	8.65	8.34	10.10
MgO	8.42	8.00	8.41	8.16	.00	.00	.00
Al_2O_3	32.18	31.69	32.15	31.55	22.72	23.30	22.19
$SiO2$	49.66	51.80	49.09	48.49	64.79	64.36	62.30
K_2O	.01	.01	.00	.01	.06	.05	.04
CaO	.01	.02	.00	.00	4.48	5.00	3.54
TiO_2	.01	.01	.00	.00	.01	.00	.01
Cr_2O_3	.00	.00	.00	.01	.00	.00	.00
MnO	.27	.44	.19	.29	.03	.00	.00
FeO	8.04	8.77	8.15	7.77	.01	.03	.16
NiO	.00	.00	.00	.00	.04	.00	.05
TOTAL	98.98	101.26	98.28	96.49	100.79	101.08	98.38
Na	.075	.098	.054	.038	.732	.705	.881
Mg	1.282	1.192	1.289	1.271	.000	.000	.000
Al	3.874	3.793	3.900	3.894	1.169	1.198	1.177
Si	5.074	5.186	5.051	5.090	2.832	2.809	2.804
K	.000	.000	.000	.000	.002	.002	.001
Ca	.000	.000	.000	.000	.209	.233	.170
Ti	.000	.000	.000	.000	.000	.000	.000
Cr	.000	.000	.000	.000	.000	.000	.000
Mn	.022	.035	.015	.024	.000	.000	.000
Fe	.686	.733	.699	.679	.000	.000	.005
Ni	.000	.000	.000	.000	.001	.000	.001
TOTAL	11.013	10.993	11.008	10.996	4.946	4.944	5.038
X FM	.644	.608	.644	.644			
An-content (molecular %					22.2	24.8	16.2
formula basis#:	18.0	18.0	18.0	18.0	8.0	8.0	8.0

number of oxygens per formula unit

TABLE A.8: Chemical Compositions of A2 Minerals

	MUSCOVITE							BIOTITE						
Sample no.	439	2-176	427	2-173	39	2-22b	135	439	2-176	427	2-173	39	2-22B	135
no. of analyses	2	5	7	3	3	7	6	7	11	9	5	7	15	3
Na_2O	1.52	1.11	1.42	.98	1.16	1.09	.85	.22	.13	.18	.13	.22	.07	.14
MgO	.46	.49	.44	.48	.50	.56	.52	10.41	10.83	10.16	10.69	9.93	9.87	10.21
Al_2O_3	36.22	36.00	36.06	34.86	35.16	34.75	37.88	19.63	19.46	19.78	19.32	18.94	19.69	20.45
SiO_2	48.13	47.87	48.09	46.17	48.65	45.17	46.90	36.993	36.90	37.51	37.30	35.52	36.37	37.69
K_2O	9.37	9.46	7.99	8.66	8.89	8.55	8.79	9.63	9.40	8.85	8.71	8.91	8.56	8.84
CaO	.00	.01	.00	.00	.00	.00	.01	.00	.00	.00	.01	.01	.00	.00
TiO_2	.30	.45	.27	.45	.39	.41	.33	1.52	1.50	1.53	1.43	1.81	1.47	1.27
Cr_2O_3	.05	.05	.04	.04	.06	.06	.05	.10	.06	.05	.06	.09	.06	.05
MnO	.04	.02	.02	.01	.01	.01	.02	.07	.14	.09	.09	.07	.08	.06
FeO	.58	.62	.67	.74	.76	.74	.82	19.28	18.32	20.20	19.38	19.25	19.85	20.36
NiO	.04	.00	.02	.01	.01	.01	.02	.00	.03	.04	.01	.05	.04	.08
TOTAL	96.71	96.08	95.02	92.40	95.59	91.35	96.19	97.85	96.82	98.39	97.13	94.80	96.06	99.15
Na	.379	.278	.358	.257	.293	.286	.211	.061	.048	.050	.034	.061	.017	.038
Mg	.087	.092	.084	.095	.095	.110	.099	2.287	2.363	2.214	2.350	2.254	2.198	2.206
Al	5.540	5.538	5.558	5.560	5.416	5.529	5.804	3.410	3.359	3.410	3.360	3.402	3.474	3.494
Si	6.245	6.247	6.289	6.249	6.356	6.194	6.092	5.455	5.406	5.486	5.512	5.415	5.454	5.462
K	1.549	1.572	1.332	1.493	1.483	1.494	1.455	1.809	1.756	1.650	1.638	1.733	1.632	1.634
Ca	.000	.000	.000	.000	.000	.000	.000	.000	.000	.000	.001	.000	.000	.000
Ti	.027	.043	.024	.044	.036	.040	.031	.165	.164	.166	.157	.206	.163	.134
Cr	.003	.003	.002	.001	.005	.003	.033	.009	.006	.004	.006	.010	.005	.004
Mn	.002	.001	.001	.000	.000	.000	.001	.007	.014	.007	.009	.006	.008	.005
Fe	.061	.066	.072	.082	.082	.084	.087	2.376	2.213	2.469	2.391	2.453	2.483	2.469
Ni	.000	.000	.001	.000	.000	.000	.001	.000	.000	.003	.001	.007	.002	.007
TOTAL	13.893	13.840	13.721	13.781	13.766	13.740	13.784	15.579	15.539	15.459	15.459	15.547	15.436	15.453
M/FM	.588	.582	.538	.537	.537	.567	.532	.490	.512	.472	.495	.478	.469	.471
Na/Na+K	.197	.150	.212	.147	.165	.161	.127	.033	.027	.029	.020	.034	.010	.023
Al^{vi}	3.785	3.785	3.847	3.809	3.772	3.723	3.896	.865	.765	.896	.872	.817	.928	.956
Al^{iv}	1.755	1.753	1.711	1.751	1.644	1.806	1.908	2.545	2.594	2.514	2.488	2.585	2.546	2.538

formula basis: 22 number of oxygens per formula unit

TABLE A.8: (continued)

	CORDIERITE						PLAGIOCLASE					
Sample no.	439	2-176	427	2-173	39	135	2-176	427	2-173	39	2-22b	135
no. of analyses	4	8	3	7	3	3	1	1	?	3	2	1
Na_2O	.21	.17	.35	.20	.74	.26	9.01	11.30	8.38	9.43	9.19	7.68
MgO	8.38	8.53	8.20	8.63	7.72	7.69	.00	.02	.01	.02	.00	.00
Al_2O_3	32.18	32.00	31.74	31.92	32.04	36.68	23.13	21.65	23.78	22.16	22.44	26.50
SiO_2	51.82	49.91	49.53	50.96	50.88	46.59	64.59	68.91	65.00	62.53	64.10	61.31
K_2O	.01	.00	.01	.01	.01	.01	.04	.04	.07	.14	.06	.03
CaO	.01	.01	.01	.01	.03	.01	4.52	2.57	6.30	3.33	5.21	6.50
TiO_2	.01	.00	.00	.00	.00	.01	.00	.00	.00	.01	.01	.01
Cr_2O_3	.01	.01	.01	.01	.00	.0.	.00	.01	.00	.00	.01	.00
MnO	.28	.42	.23	.33	.27	.38	.01	.02	.00	.00	.02	.01
FeO	8.95	7.71	7.67	8.12	7.98	7.86	.04	.03	.16	.10	.07	.18
NiO	.02	.05	.03	.03	.00	.04	.00	.00	.05	.00	.00	.01
TOTAL	101.89	98.73	97.78	100.22	99.67	99.54	101.35	104.55	103.75	97.72	101.11	102.23
Na	.039	.031	.069	.038	.143	.049	.759	.922	.693	.825	.773	.646
Mg	1.242	1.307	1.260	1.295	1.165	1.167	.000	.000	.000	.001	.000	.000
Al	3.771	3.854	3.353	3.733	3.827	4.403	1.186	.074	1.197	1.178	1.200	1.356
Si	5.152	5.093	5.110	5.137	5.156	4.744	2.810	2.993	2.777	2.823	2.783	2.663
K	.000	.000	.000	.001	.000	.000	.001	.001	.003	.007	.002	.001
Ca	.002	.000	.001	.000	.002	.000	.213	.116	.287	.160	.241	.302
Ti	.000	.000	.000	.000	.000	.000	.000	.000	.000	.000	.000	.000
Cr	.000	.000	.000	.000	.000	.000	.000	.000	.000	.000	.000	.000
Mn	.022	.035	.013	.026	.021	.031	.000	.000	.000	.000	.001	.000
Fe	.743	.650	.660	.663	.675	.665	.001	.000	.005	.003	.002	.006
Ni	.001	.003	.001	.001	.000	.000	.000	.000	.001	.000	.000	.000
TOTAL	11.970	10.952	10.977	10.973	11.989	11.724	4.968	5.017	4.963	4.997	5.001	4.975
% FM	.613	.663	.651	.646	.626	.625						
An content (molecular %)							21.7	11.2	29.2	16.1	23.7	31.8
formula basis*	18	18	18	18	18	14	8	8	8	8	8	8

* number of oxygens per formula unit

TABLE A.8: (continued)

	A*Z BIOTITE				A*Z CORDIERITE				A*Z PLAGIOCLASE			
Sample no.	2-40a	2-42	2-180	2-183	2-40a	2-42	2-180	2-183	2-40a	2-42	2-180	2-183
no. of analyses	5	5	5	7	8	14	7	5	1	1	1	1
Na_2O	.23	.10	.11	.20	.22	.23	.24	.17	6.88	8.43	9.39	9.43
MgO	10.60	9.53	9.88	10.80	8.90	7.84	8.61	8.78	.00	.00	.00	.01
Al_2O_3	19.90	19.84	19.45	19.50	32.59	31.70	32.58	32.53	22.57	23.20	22.79	22.49
SiO_2	37.69	35.93	36.63	37.22	50.68	49.47	50.08	50.96	64.61	63.61	64.71	64.00
K_2O	8.77	9.61	8.79	9.40	.01	.01	.00	.01	.07	.02	.04	.05
CaO	.01	.03	.02	.01	.01	.02	.01	.01	5.13	5.39	4.38	4.27
TiO_2	2.01	1.40	1.95	1.83	.00	.00	.01	.01	.00	.00	.00	.00
Cr_2O_3	.08	.10	.08	.08	.01	.01	.01	.01	.00	.01	.00	.00
MnO	.12	.10	.12	.12	.30	.36	.31	.35	.00	.02	.02	.00
FeO	19.02	19.88	18.99	19.39	7.78	8.87	7.77	8.16	.08	.04	.00	.07
NiO	.01	.02	.02	.02	.03	.02	.02	.02	.02	.03	.00	.01
TOTAL	98.44	96.54	96.04	98.57	100.53	98.53	99.64	101.01	99.37	100.77	101.32	100.34
Na	.063	.028	.029	.055	.041	.044	.045	.031	.587	.717	.792	.805
Mg	2.296	2.133	2.200	2.353	1.331	1.203	1.299	1.308	.000	.000	.000	.000
Al	3.407	3.515	3.425	3.359	3.856	3.849	3.890	3.836	1.172	1.200	1.169	1.167
Si	5.478	5.402	5.474	5.441	5.087	5.097	5.074	5.100	2.849	2.792	2.819	2.818
K	1.624	1.842	1.674	1.751	.000	.000	.000	.000	2.849	2.792	2.819	2.818
Ca	.000	.002	.003	.000	.000	.000	.000	.000	.003	.001	.001	.002
Ti	.216	.154	.217	.199	.000	.000	.000	.000	.242	.252	.203	.200
Cr	.007	.009	.007	.008	.000	.000	.000	.000	.000	.000	.000	.000
Mn	.014	.010	.013	.013	.024	.030	.025	.028	.000	.000	.000	.000
Fe	2.311	2.496	2.371	2.370	.652	.763	.657	.682	.000	.000	.000	.002
Ni	.001	.001	.001	.002	.001	.001	.001	.001	.002	.001	.000	.002
TOTAL	15.417	15.592	15.414	15.551	10.992	10.987	10.991	10.986	4.856	4.963	4.985	4.994
M/FM	.497	.460	.480	.497	.663	.603	.656	.648				
Na/Na+K	.037	.015	.017	.031								
Al^{vi}	.885	.917	.899	.800								
Al^{iv}	2.522	2.598	2.526	2.559								
An-content (molecular %)									29.1	26.0	20.4	19.9
formula basis#:	22	22	22	22	18	18	18	18	8	8	8	8

number of oxygens per formula unit

TABLE A.8 (continued): Cordierite-free Assemblage - ABM

sample no.		437			128c	
no. of analyses	MUSC 3	BIO 6	PLAG 1		MUSC 3	BIO 4
Na_2O	1.39	.12	9.94		1.34	.18
MgO	.36	10.06	.00		.48	10.16
Al_2O_3	35.20	19.42	21.86		34.03	19.16
SiO_2	46.72	36.83	65.36		45.84	35.97
K_2O	8.19	8.88	.04		8.49	9.05
CaO	.00	.00	3.42		.00	.00
TiO_2	.35	1.62	.00		.31	1.40
Cr_2O_3	.04	.04	.02		.04	.03
MnO	.02	.09	.00		.01	.08
FeO	.53	20.26	.00		.69	19.85
NiO	.03	.03	.00		.02	.05
TOTAL	92.82	97.35	100.64		91.25	95.93
Na	.358	.033	.843		.353	.048
Mg	.071	2.222	.000		.096	2.280
Al	5.572	3.393	1.128		5.501	3.405
Si	6.277	5.460	2.861		6.287	5.429
K	1.404	1.678	.001		1.484	1.740
Ca	.000	.000	.159		.000	.000
Ti	.031	.180	.000		.029	.155
Cr	.000	.003	.000		.001	.000
Mn	.000	.010	.000		.000	.009
Fe	.059	2.510	.000		.076	2.502
Ni	.000	.002	.000		.000	.004
TOTAL	13.772	15.491	4.992		13.827	15.573
M/FM	.546	.469			.558	.476
Na Na+K	.203	.019			.192	.027
AlVi	3.849	.850			3.788	.834
Aliv	1.723	2.540			1.713	2.571
An-content (molecular %)			15.9			
formula basis#:	22	22	8		22	22

\# number of oxygens per formula unit

TABLE A.9: Chemical Compositions of S2 Minerals

	MUSCOVITE					BIOTITE				
Sample no.	2-21	342	346	340	307	2-21	342	346	340	307
no. of analyses	4	5	4	4	5	5	7	3	6	5
Na$_2$O	1.23	1.07	1.08	1.42	1.29	.13	.18	.22	.13	.20
MgO	.53	.52	.55	.48	.44	10.83	10.28	10.57	10.60	9.81
Al$_2$O$_3$	36.02	35.72	33.81	35.88	35.86	19.51	19.43	19.25	19.60	19.36
SiO$_2$	48.20	47.77	43.90	47.91	47.93	37.30	36.57	36.84	36.90	36.93
K$_2$O	9.15	9.80	8.58	8.96	9.21	9.04	9.90	8.87	8.90	9.71
CaO	.01	.00	.00	.00	.00	.00	.00	.00	.00	.00
TiO$_2$	.51	.44	.91	.40	.61	1.93	1.95	1.97	1.94	1.49
Cr$_2$O$_3$	.07	.03	.08	.04	.05	.08	.06	.09	.07	.07
MnO	.01	.02	.03	.03	.02	.11	.13	.15	.15	.09
FeO	.64	.58	.72	.68	.62	20.26	18.94	18.62	21.32	19.88
NiO	.02	.01	.01	.02	.02	.03	.03	.01	.04	.02
TOTAL	96.21	95.96	89.67	95.82	96.05	99.22	97.47	96.59	99.65	97.56
Na	.309	.269	.385	.360	.323	.034	.051	.061	.042	.057
Mg	.101	.101	.113	.092	.083	2.348	2.271	2.336	2.300	2.197
Al	5.514	5.513	5.583	5.513	5.513	3.345	3.396	3.368	3.363	3.431
Si	6.262	6.256	6.149	6.270	6.253	5.426	5.421	5.469	5.373	5.415
K	1.514	1.634	1.533	1.494	1.532	1.675	1.873	1.679	1.652	1.859
Ca	.000	.000	.000	.000	.000	.000	.000	.000	.000	.000
Ti	.048	.041	.094	.038	.057	.208	.216	.218	.209	.166
Cr	.004	.001	.007	.002	.003	.006	.003	.008	.006	.007
Mn	.000	.000	.002	.002	.001	.012	.015	.017	.013	.009
Fe	.067	.062	.083	.072	.065	2.464	2.347	2.313	2.595	2.497
Ni	.002	.000	.000	.001	.001	.002	.002	.001	.003	.001
TOTAL	13.821	13.877	13.949	13.844	13.831	15.520	15.595	15.470	15.556	15.639
M/FM	.601	.620	.577	.561	.561	.487	.490	.501	.469	.467
Na/Na+K	.170	.141	.201	.194	.174	.020	.027	.035	.025	.030
Al^{vi}	3.776	3.769	3.732	3.783	3.766	.771	.817	.837	.736	.846
Al^{iv}	1.738	1.744	1.851	1.730	1.747	2.574	2.579	2.531	2.627	2.585
formula basis#:	22	22	22	22	22	22	22	22	22	22

number of oxygens per formula unit

TABLE A.9: (continued)

(Cordierite - free; SABM)

	CORDIERITE				PLAGIOCLASE					MUSC	BIO	PLAG
Sample no.	2-21	346	340	307	2-21	342	346	340	307	343	343	343
no. of analyses	13	3	5	14	1	1	2	1	1	4	6	1
Na_2O	.22	.37	.31	.28	9.19	9.55	9.47	10.68	9.78	1.41	.29	11.25
MgO	8.60	8.73	8.59	8.18	.00	.00	.00	.00	.00	.55	10.57	.00
Al_2O_3	32.40	31.64	32.47	32.27	23.22	22.09	22.29	20.93	21.96	35.07	19.04	21.24
SiO_2	51.40	48.57	51.04	48.66	66.23	65.78	61.80	68.34	67.50	47.49	36.85	65.84
K_2O	.00	.00	.01	.01	.04	.05	.05	.04	.06	8.11	8.62	.04
CaO	.01	.02	.01	.01	4.38	4.41	4.01	1.74	3.70	.00	.00	2.29
TiO_2	.00	.01	.00	.00	.00	.00	.00	.03	.00	.43	1.75	.00
Cr_2O_3	.00	.00	.01	.01	.00	.00	.00	.02	.02	.04	.05	.01
MnO	.33	.34	.32	.32	.00	.01	.04	.03	.03	.01	.17	.03
FeO	8.06	7.46	8.32	8.20	.01	.03	.08	.05	.06	.69	18.43	.13
NiO	.02	.01	.01	.03	.01	.00	.02	.05	.05	.03	.05	.00
TOTAL	101.24	97.15	101.09	97.98	103.08	101.93	97.76	101.90	103.15	93.84	95.82	100.82
Na	.041	.074	.058	.055	.761	.802	.831	.890	.809	.362	.082	.954
Mg	1.306	1.352	1.279	1.258	.000	.000	.000	.000	.000	.105	2.352	.000
Al	3.507	3.683	3.829	3.931	1.168	1.127	1.183	1.060	1.104	5.486	3.352	1.095
Si	5.126	5.050	5.108	5.034	2.830	2.849	2.798	2.938	2.860	6.304	5.504	2.881
F	.000	.000	.000	.000	.001	.002	.002	.001	.002	1.372	1.641	.001
Ca	.000	.000	.000	.000	.199	.205	.194	.079	.169	.000	.000	.106
Ti	.000	.000	.000	.000	.000	.000	.000	.000	.000	.042	.195	.000
Cr	.000	.000	.000	.000	.000	.000	.000	.000	.000	.003	.004	.000
Mn	.027	.028	.025	.027	.000	.000	.000	.000	.000	.000	.019	.000
Fe	.670	.648	.695	.706	.000	.000	.000	.001	.001	.074	2.301	.003
Ni	.000	.000	.000	.000	.000	.000	.000	.001	.001	.000	.003	.000
TOTAL	10.977	11.035	10.994	11.012	4.960	4.985	5.017	4.969	4.967	13.749	15.453	5.041
M/FM	.650	.667	.647	.632						.587	.503	
Na/Na+K										.209	.048	
AlVI										3.790	.856	
AlIV										1.696	2.496	
An-content (molecular %)					20.7	20.8	18.9	8.1	17.2			10.0
formula basis*=	18	18	18	18	8	8	8	8	8	22	22	8

* number of oxygens per formula unit

	BIOTITE					CORDIERITE				
Sample no.	268	264	350b	2-38	444	268	264	350b	2-38	444
no. of analyses	11	8	5	6	3	12	4	8	4	6
Na_2O	.22	.18	.12	.19	.19	.21	.19	.50	.26	.27
MgO	10.60	9.74	10.32	10.32	10.18	8.65	8.45	8.56	8.76	8.72
Al_2O_3	19.83	19.62	19.62	19.30	19.54	32.32	32.48	32.31	32.45	32.44
SiO_2	36.38	36.86	37.15	37.40	35.84	48.86	50.28	49.31	50.20	50.66
K_2O	8.66	8.76	8.60	9.85	8.70	.01	.01	.01	.01	.01
CaO	.00	.00	.01	.01	.00	.01	.02	.02	.01	.01
TiO_2	2.02	2.59	2.15	1.92	2.05	.00	.01	.01	.01	.01
Cr_2O_3	.08	.09	.09	.12	.10	.01	.01	.00	.01	.00
MnO	.13	.11	.12	.10	.12	.44	.30	.46	.27	.30
FeO	18.09	18.79	17.83	19.18	19.40	7.62	7.71	7.19	7.45	7.52
NiO	.04	.03	.02	.06	.04	.02	.04	.02	.01	.02
TOTAL	96.05	96.77	96.03	98.45	96.16	98.15	99.50	98.39	99.44	99.96
Na	.061	.050	.035	.050	.054	.040	.034	.097	.048	.051
Mg	2.351	2.149	2.280	2.254	2.273	1.326	1.276	1.307	1.322	1.309
Al	3.478	2.424	3.427	3.334	3.453	3.923	3.879	3.907	3.876	3.853
Si	5.415	5.458	5.506	5.484	5.371	5.032	5.096	5.058	5.087	5.107
K	1.642	1.653	1.626	1.840	1.663	.000	.000	.000	.001	.000
Ca	.000	.000	.001	.000	.000	.000	.001	.000	.000	.000
Ti	.223	.285	.237	.210	.228	.000	.000	.000	.000	.000
Cr	.007	.008	.008	.011	.008	.000	.000	.000	.000	.000
Mn	.016	.012	.013	.011	.011	.037	.025	.039	.022	.024
Fe	2.251	2.326	2.208	2.351	2.432	.655	.652	.616	.630	.633
Ni	.002	.003	.002	.005	.003	.001	.002	.001	.000	.001
TOTAL	15.446	15.404	15.343	15.550	15.496	11.014	10.965	11.025	10.986	10.978
M/FM	.509	.479	.507	.488	.482	.657	.653	.666	.670	.666
Na/Na+K	.036	.029	.021	.027	.032					
Al^{vi}	.893	.882	.933	.818	.824					
Al^{iv}	2.585	2.542	2.494	2.516	2.629					
formula basis#:	22	22	22	22	22	18	18	18	18	18

number of oxygens per formula unit

287

TABLE A.9 (continued): S*Z

Sample no.	(SCAB)					(SCB)			(SAB)			
	268	264	350b	2-38	444	250b			442a		304	
	PLAGIOCLASE					BIO	CORD	PLAG	BIO	PLAG	BIO	PLAG
no. of analyses	4	4	2	1	1	4	6	2	6	1	6	7
Na₂O	8.87	8.95	9.54	9.39	9.73	.24	.28	9.48	.28	9.46	.23	9.83
MgO	.01	.01	.11	.00	.01	10.63	8.82	.00	10.60	.00	10.55	.00
Al₂O₃	23.74	23.32	24.26	22.95	21.75	19.83	32.02	22.77	19.21	22.59	18.90	21.69
SiO₂	62.22	64.38	64.63	61.43	65.79	37.06	50.00	64.53	36.66	64.21	35.99	63.00
K₂O	.04	.06	.08	.06	.04	8.90	.01	.10	8.67	.05	9.07	.04
CaO	5.58	4.88	4.02	4.20	2.68	.00	.02	4.27	.00	4.14	.00	3.73
TiO₂	.00	.01	.01	.01	.00	1.84	.01	.00	2.05	.00	2.00	.00
Cr₂O₃	.00	.00	.00	.01	.02	.06	.01	.00	.06	.00	.07	.00
MnO	.02	.01	.03	.02	.04	.18	.52	.03	.17	.00	.21	.00
FeO	.02	.04	.17	.07	.12	18.28	7.77	.05	17.80	.10	17.87	.02
NiO	.01	.00	.04	.00	.05	.03	.03	.02	.00	.00	.05	.02
TOTAL	100.53	101.66	102.87	98.15	100.22	97.05	99.49	101.26	95.51	100.57	94.96	98.35
Na	.759	.754	.795	.821	.825	.067	.054	.802	.078	.806	.065	.856
Mg	.000	.006	.006	.000	.000	2.332	1.335	.000	2.383	.000	2.377	.000
Al	1.235	1.194	1.228	1.221	1.122	3.444	3.837	1.172	3.416	1.169	3.370	1.149
Si	2.749	2.780	2.778	2.773	2.882	5.461	5.084	2.816	5.430	2.820	5.444	2.831
K	.002	.003	.004	.002	.001	1.671	.006	.004	1.666	.002	1.748	.002
Ca	.264	.227	.185	.203	.125	.000	.003	.200	.000	.134	.000	.179
Ti	.000	.000	.000	.000	.000	.204	.000	.000	.231	.000	.225	.000
Cr	.000	.000	.000	.000	.000	.004	.000	.000	.006	.000	.007	.000
Mn	.000	.000	.000	.000	.001	.020	.043	.001	.021	.000	.024	.000
Fe	.001	.001	.005	.000	.003	2.253	.659	.001	2.244	.002	2.259	.000
Ni	.000	.000	.001	.000	.001	.002	.000	.001	.000	.000	.002	.000
TOTAL	5.036	4.977	5.000	5.023	4.960	15.456	11.013	4.997	15.474	4.994	15.522	5.017
Mg FM						.506	.655		.513		.510	
Na Na+K						.039			.045		.036	
An-content molecular %	25.8	23.1	20.5	19.8	13.1			20.0		13.4		17.3
AlVI						.905			.846		.814	
AlIV						2.539			2.570		2.556	
formula basis#:8	8	8	8	8	22	28	8	22	8	22	8	

number of oxygens per formula unit

TABLE A.10: Microprobe Analyses of Minerals from Amphibole-bearing Iron Formation

Sample no.	2-58a		2-76a		36b					
Mineral	AMPH	BIO	AMPH	BIO	GARN			BIO	AMPH	CHL
					O.R	I.R	Core			
no.of analyses	3	3	3	1	3	3	5	1	4	2
Na_2O	.08	.09	1.45	.04	.03	.00	.00	.05	.00	.01
MgO	11.80	7.61	5.12	7.09	3.48	1.66	1.46	11.84	10.08	16.51
Al_2O_3	.43	16.19	14.05	15.82	21.02	20.34	20.27	17.54	13.88	21.88
SiO_2	53.07	35.90	42.25	35.21	35.66	37.28	37.46	36.53	28.34	24.20
K_2O	.01	10.33	.50	9.70	.01	.01	.00	8.56	.13	.04
CaO	.31	.00	10.98	.02	2.02	3.28	3.36	.02	.04	.00
TiO_2	.00	1.48	.29	.99	.00	.05	.02	1.47	.01	.09
Cr_2O_3	.03	.07	.03	.03	.00	.00	.00	.12	.02	.02
MnO	.42	.14	.14	.11	.26	.74	.60	.13	.06	.04
FeO	34.94	26.26	25.59	29.24	36.75	35.70	36.39	17.39	34.34	22.90
NiO	.03	.03	.04	.05	.00	.05	.00	.00	.03	.04
TOTAL	101.11	98.11	100.44	98.27	99.23	99.11	99.57	93.65	86.93	85.72
Na	.000	.027	.414	.009	.005	.000	.000	.013	.000	.000
Mg	2.599	1.744	1.150	1.639	.424	.201	.176	2.687	2.640	3.378
Al	.069	2.938	2.484	2.899	2.025	1.954	1.942	3.148	2.872	3.543
Si	7.889	5.527	6.371	5.479	2.914	3.038	3.047	5.567	4.976	3.322
K	.000	2.029	.092	1.922	.001	.000	.000	1.663	.025	.004
Ca	.046	.000	1.771	.000	.177	.284	.291	.000	.005	.000
Ti	.000	.171	.023	.114	.000	.002	.000	.165	.000	.008
Cr	.000	.004	.000	.000	.000	.000	.000	.013	.000	.000
Mn	.046	.013	.000	.014	.018	.050	.041	.013	.005	.004
Fe	4.324	3.380	3.220	3.803	2.512	2.432	2.474	2.213	5.043	2.628
Ni	.000	.000	.000	.004	.000	.002	.000	.000	.000	.000
TOTAL	14.996	15.833	15.548	15.884	8.076	7.962	7.971	15.483	15.567	12.887
M/FM	.387	.340	.275	.300	.144	.075	.065	.547	.470	.562
Fe^{2+}	4.117		3.036		2.511	2.388	2.452		2.974	
Fe^{3+}	.207		.184		.001	.044	.022		2.069	
Alman					80.2	81.7	83.6			
Pyrope					13.6	6.9	6.0			
Gross					5.7	9.7	9.8			
Spess					0.6	1.7	1.4			
formula basis#:	23	22	23	22	12	12	12	22	23	18

\# number of oxygens per formula unit

TABLE A.11: Chemical Composition of Low-grade Fe-rich Minerals

	MUSC	CHLORITE					BIOTITE	
Sample no.	226	226	122	137	163	109a	226	122
no. of analyses	1	4	1	3	3	5	3	3
Na$_2$O	.11	.00	.00	.00	.00	.01	.06	.07
MgO	.52	6.68	7.79	5.50	10.33	13.20	4.12	6.97
Al$_2$O$_3$	34.91	.41	20.78	19.31	21.05	22.81	20.17	15.49
SiO$_2$	52.05	22.30	24.35	24.53	25.04	24.92	32.78	37.19
K$_2$O	8.50	.04	.04	.02	.00	.00	9.03	9.02
CaO	.09	.01	.05	.02	.02	.02	.00	.03
TiO$_2$	.18	.07	.14	.05	.11	.04	2.25	2.33
Cr$_2$O$_3$	n.d	n.d	.00	.00	.03	.00	n.d	.01
MnO	.00	.13	.16	.00	.20	.17	.06	.02
FeO	5.49	37.24	35.27	41.63	33.33	28.07	27.31	35.27
NiO	n.d	n.d	.05	.00	.00	.00	n.d	.04
TOTAL	99.86	90.48	88.63	91.06	90.10	89.23	95.78	98.34
Na	.022	.000	.000	.000	.000	.000	.015	.016
Mg	.095	1.391	1.642	1.166	2.114	2.651	.967	1.581
Al	5.160	3.857	3.467	3.239	3.409	3.625	3.747	2.781
Si	5.160	3.200	3.450	3.495	3.441	3.360	5.168	5.669
K	1.359	.005	.004	.000	.000	.000	1.815	1.752
Ca	.011	.000	.004	.000	.000	.000	.000	.003
Ti	.015	.000	.012	.004	.008	.000	.265	.265
Cr	n.d	n.d	.000	.000	.000	.000	n.d	.000
Mn	.000	.000	.017	.000	.020	.016	.007	.001
Fe	.364	4.356	4.178	4.958	3.829	3.166	3.600	3.463
Ni	n.d	n.d	.004	.000	.000	.000	n.d	.004
TOTAL	13.554	12.810	12.777	13.861	12.822	12.818	15.584	15.535
M FM	.207	.242	.282	.190	.356	.456	.212	.313
formula basis#:	22	18	18	18	18	18	22	22

\# number of oxygens per formula unit
'n.d' = not determined

Table A.12: Chemical compositions of minerals in
garnet/staurolite-bearing assemblages. This
Table consists of 7 pages of analyses, presented
according to mineral assemblage.

$Ca*$ = (Ca+Mn)/(Ca+Mn+Fe+Mg)

$Al**$ = $(Al^{vi}+Ti)/(Al^{vi}+Ti+Fe+Mg)$

O.R, I.R = garnet outer rim and inner rim

Formula basis# = number of oxygens per formula unit.

Garnet end members calculated using molecular %.

Garnet analyses for 81-V-143: (1) near

plagioclase contact, (2) near biotite contact.

Fe^{2+} and Fe^{3+} in garnet calculated by charge

balance.

TABLE A.12: Chemical Compositions of Minerals in Garnet/Staurolite-Bearing Assemblages

Assemblage: GARNET-BIOTITE

Sample no.				81-V-38									81-V-383d	
Mineral				GARNET						BIO	BIO	GAR	BIO	PLAG
		(1)			(2)			(3)		(1)	(2)			
	O.R	I.R	CORE	O.R	I.R	CORE	O.R	I.R	CORE					
no. of analyses	1	2	2	1	1	1	2	1	2	3	3	8	3	2
Na_2O	.04	.01	.03	.00	.15	.08	.07	.05	.05	.11	.17	n.d	.35	10.13
MgO	2.50	2.34	2.04	2.52	2.41	2.43	2.55	2.57	2.31	8.02	7.95	2.27	8.80	.01
Al_2O_3	21.11	20.98	21.06	20.55	20.63	20.68	20.78	21.21	20.97	19.27	19.34	20.53	19.82	22.45
SiO_2	34.73	36.96	35.56	36.70	37.21	38.42	34.47	34.83	35.83	35.03	35.30	36.63	35.53	64.52
K_2O	.00	.01	.00	00	.02	.00	.01	.02	.00	8.67	8.82	n.d	8.70	.07
CaO	1.77	2.04	2.18	1.73	1.73	1.79	1.58	1.80	1.83	.00	.00	.79	.00	3.82
TiO_2	.01	.05	.04	.00	.00	.00	.01	.03	.05	1.23	1.18	.01	1.30	.00
Cr_2O_3	.00	.00	.03	.00	.00	.00	.02	.00	.02	.04	.02	.00	.05	.00
MnO	.06	.03	.12	.12	.11	.12	.13	.04	.14	.02	.01	.52	.04	.01
FeO	39.70	38.89	38.93	38.03	38.38	38.51	37.55	38.43	38.87	21.85	21.21	37.75	22.28	.15
NiO	.00	.03	.07	.00	.00	.00	.01	.00	.02	.05	.01	.03	.03	.01
TOTAL	99.90	101.34	100.06	99.15	100.65	102.02	97.18	98.98	100.09	94.29	94.01	98.52	96.89	101.16
Na	.004	.000	.004	.000	.023	.011	.010	.007	.007	.032	.050	n.d	.097	.858
Mg	.304	.279	.247	.305	.289	.286	.318	.315	.279	1.851	1.833	.277	1.979	.000
Al	2.047	1.986	2.029	1.985	1.960	1.930	2.061	2.065	2.017	3.520	3.528	1.990	3.524	1.156
Si	2.859	2.970	2.913	2.967	3.003	3.044	2.897	2.877	2.926	5.429	5.470	3.014	5.357	2.822
K	.000	.000	.000	.000	.000	.000	.000	.000	.000	1.714	1.741	n.d	1.673	.002
Ca	.154	.175	.187	.151	.149	.151	.141	.157	.160	.000	.000	.067	.000	.178
Ti	.000	.001	.002	.000	.000	.000	.000	.000	.001	.141	.136	.000	.146	.000
Cr	.000	.000	.000	.000	.000	.000	.000	.000	.000	.000	.000	.000	.004	.000
Mn	.002	.000	.007	.007	.007	.007	.008	.002	.008	.000	.000	.036	.004	.000
Fe	2.733	2.613	2.659	2.606	2.588	2.551	2.639	2.654	2.654	2.828	2.747	2.599	2.807	.005
Ni	.000	.001	.004	.000	.003	.000	.000	.000	.001	.004	.000	.000	.000	.000
TOTAL	8.104	8.026	8.051	8.021	8.020	7.970	8.074	8.076	8.053	15.518	15.505	7.984	15.592	5.022
Fe^{2+}	2.696	2.590	2.605	2.567	2.569	2.518	2.635	2.620	2.620			2.583		
Fe^{3+}	.037	.024	.054	.039	.019	.033	.004	.034	.034			.016		
M FM	.046	.002	.081	.111	.096	.095	.103	.100	.091	.396	.038	.094	.413	
Ca*	.044	.038	.064	.052	.052	.053	.048	.051	.055			.033		
Al**									.189	.198		.155		
Alman	85.4	85.1	85.5	84.7	85.2	85.3	85.0	84.7	85.4			87.2		
Pyrope	9.6	9.2	8.2	11.2	9.6	9.5	10.3	11.2	9.1			9.4		
Gross	4.5	5.5	6.2	5.0	4.9	5.0	4.6	5.1	5.2			2.3		
Spess	.5	.2	.1	.1	.3	.2	.30	.20	.30			1.2		
formula basis=#	12	12	12	12	12	12	12	12	12	22	22	12	22	8

An-content "molecular" of plagioclase is 17

TABLE A.12: (continued)

Assemblage: GARNET-BIOTITE-CORDIERITE-STAUROLITE-ALUMINOSILICATE

Sample no.   81-V-143

Mineral	GARN					BIO	STAUR	PLAG
	(1)			(2)				
	O.R	I.R	CORE	I.R	O.R			
no. of analyses	3	3	3	3	3	3	5	3
Na$_2$O	n.d	n.d	n.d	n.d	n.d	.15	.02	8.42
MgO	2.46	2.69	2.67	2.47	2.29	8.48	1.56	.00
Al$_2$O$_3$	20.76	21.07	21.00	20.41	21.01	19.11	52.43	23.63
SiO$_2$	36.48	37.60	37.08	37.60	36.30	35.39	26.95	62.02
K$_2$O	n.d	n.d	n.d	n.d	n.d	8.91	.01	.05
CaO	1.29	1.27	1.30	1.25	1.09	.00	.00	6.13
TiO$_2$	.01	.00	.00	.00	.01	1.51	.35	.01
Cr$_2$O$_3$	.00	.01	.00	.04	.02	.07	.01	.00
MnO	1.16	1.28	1.48	1.19	1.41	.04	.08	.01
FeO	37.16	36.31	36.04	36.24	37.20	22.00	14.61	.10
NiO	.00	.04	.00	.00	.00	.02	.03	.00
TOTAL	99.32	100.26	99.57	99.17	99.33	95.68	96.05	100.38
Na	n.d	n.d	n.d	n.d	n.d	.040	.003	.722
Mg	.299	.321	.321	.298	.278	1.933	.170	.000
Al	1.996	1.996	2.004	1.955	2.024	3.440	4.559	1.232
Si	2.979	3.021	3.002	3.053	2.970	5.410	2.017	2.745
K	n.d	n.d	n.d	n.d	n.d	1.736	.000	.002
Ca	.112	.108	.111	.107	.093	.000	.000	.290
Ti	.000	.000	.000	.000	.000	.170	.018	.000
Cr	.000	.000	.000	.000	.000	.004	.000	.000
Mn	.079	.084	.100	.081	.096	.004	.004	.000
Fe	2.538	2.441	2.441	2.462	2.545	2.813	.901	.002
Ni	.000	.000	.000	.000	.000	.000	.002	.000
TOTAL	8.003	7.972	7.979	7.956	8.006	15.551	7.674	4.994
FE^{2+}	2.498	2.421	2.407	2.453	2.521			
Fe^{3+}	.040	.020	.034	.027	.024			
M/FM	.100	.110	.109	.102	.093	.407	.159	
Ca*	.063	.065	.071	.064	.063			
Al**						.177		
Almand	83.6	82.5	81.9	83.4	84.8			
Pyrope	10.1	11.0	10.9	10.2	9.3			
Gross	3.8	3.7	3.8	3.7	3.1			
Spess	2.6	2.9	3.4	2.8	3.2			
formula basis#:12	12	12	12	12	22	12	8	

An-content (molecular %) of plagioclase 29

Assemblage: GARNET-BIOTITE-STAUROLITE-ALUMINOSILICATE

Sample no. 81-V-15a

Mineral	GARNET						BIO (1)	BIO (2)	BIO(G)	STAUR	PLAG (1)	PLAG (2)
	(1)			(2)								
	O.R	I.R	CORE	O.R	I.R	CORE						
no. of analyses	3	3	3	3	3	3	3	3	3	3	2	2
Na$_2$O	n.d	n.d	n.d	n.d	n.d	n.d	.11	.13	.08	.00	6.23	6.51
MgO	2.13	2.26	2.30	2.14	2.32	1.97	7.95	7.82	8.08	1.02	.00	.00
Al$_2$O$_3$	20.18	20.24	20.17	20.51	19.90	20.06	19.68	19.39	19.33	55.83	26.34	26.75
SiO$_2$	37.93	37.89	37.48	37.13	37.27	38.15	36.45	35.42	35.91	28.13	58.31	57.28
K$_2$O	n.d	n.d	n.d	n.d	n.d	n.d	9.15	9.14	8.90	.00	.04	.04
CaO	1.64	1.70	1.67	1.57	1.78	1.67	.00	.00	.00	.02	9.50	9.68
TiO$_2$	.00	.00	.00	00	.02	.02	1.78	1.95	1.84	.54	.00	.00
Cr$_2$O$_3$	.00	.00	.00	.00	.00	.00	.05	.07	.05	.05	.00	.00
MnO	.80	1.26	1.88	.76	1.23	3.30	.02	.03	.04	.03	.04	.00
FeO	38.06	36.53	36.99	37.91	37.80	35.79	21.09	21.55	21.99	13.50	.11	.08
NiO	.01	.00	.05	.03	.01	.01	.03	.01	.06	.03	.00	.00
TOTAL	100.75	99.88	100.55	100.05	100.32	100.96	96.30	95.49	96.28	99.15	100.58	100.35
Na	n.d	n.d	n.d	n.d	n.d	n.d	.026	.036	.022	.000	.538	.565
Mg	.255	.270	.275	.257	.281	.236	1.788	1.781	1.823	.107	.000	.000
Al	1.915	1.928	1.921	1.951	1.904	1.899	3.495	3.495	3.451	4.678	1.382	1.411
Si	3.055	3.062	3.029	3.014	3.026	3.067	5.495	5.415	5.443	2.001	2.596	2.565
K	n.d	n.d	n.d	n.d	n.d	n.d	1.756	1.781	1.716	.000	.001	.001
Ca	.142	.147	.145	.136	.152	.141	.000	.000	.000	.001	.452	.464
Ti	.000	.000	.000	.000	.000	.000	.199	.220	.209	.028	.000	.000
Cr	.000	.000	.000	.000	.000	.000	.004	.004	.004	.002	.000	.000
Mn	.054	.085	.128	.050	.083	.224	.000	.000	.004	.001	.001	.000
Fe	2.563	2.469	2.500	2.573	2.566	2.407	2.659	2.754	2.784	.802	.004	.002
Ni	.000	.000	.012	.000	.000	.000	.000	.000	.004	.001	.000	.000
TOTAL	7.963	7.961	7.999	7.991	8.012	7.975	15.423	15.435	15.461	7.621	4.974	5.009
Fe^{2+}	2.556	2.443	2.475	2.544	2.544	2.388						
Fe^{3+}	.007	.026	.025	.029	.022	.019						
X FM	.065	.094	.092	.056	.092	.079	.400	.392	.396	.118		
Ca*	.065	.075	.09	.062	.075	.120						
Al**							.211	.199				
Almand	85.0	83.0	81.9	85.0	83.1	79.9						
Pyrope	8.6	9.0	9.1	8.6	9.0	7.9						
Gross	4.7	5.0	4.9	4.5	5.0	4.7						
Spess	1.8	2.9	4.2	1.7	2.7	7.5						
formula basis#	12	12	12	12	12	12	22	22	22	2	8	8

An-content (molecular %) of Plag 1 is 45.
G = biotite in contact with garnet.

TABLE A.12: (continued)

Assemblage:	GARNET-BIOTITE-CORDIERITE					STAUR-CORD-BIO-ALSILICATE			
Sample no.	82-V-23					81-V-153			
Mineral	GARN			BIO	PLAG	STAUR	CORD	BIO	PLAG
	C.R	I.R	CORE						
no. of analyses	3	3	3	4	1	1	7	6	4
Na₂O	n.d	n.d	n.d	.23	8.75	.04	.37	.19	9.37
MgO	2.73	2.78	2.22	9.81	.00	1.36	8.38	10.08	.00
Al₂O₃	20.47	20.42	20.52	18.53	23.43	52.22	32.01	19.65	23.60
SiO₂	37.96	37.65	36.79	35.51	61.16	28.41	49.29	35.79	63.29
K₂O	n.d	n.d	n.d	8.69	.06	.00	.01	8.78	.04
CaO	1.00	1.20	1.14	.01	5.76	.01	.02	.00	4.95
TiO₂	.00	.02	.02	1.53	.00	.57	.01	1.69	.00
Cr₂O₃	.00	.01	.00	.06	.00	.03	.00	.07	.00
MnO	.16	.13	.98	.01	.03	.39	.31	.10	.00
FeO	38.38	37.82	36.80	21.41	.16	13.25	7.86	18.79	.05
NiO	.02	.02	.05	.05	.01	.05	.01	.03	.00
TOTAL	100.72	100.05	98.51	95.86	99.40	96.37	98.27	95.18	101.29
Na	n.d	n.d	n.d	.067	.759	.004	.072	.054	.794
Mg	.325	.334	.270	2.224	.000	.148	1.284	2.269	.000
Al	1.937	1.942	1.987	3.323	1.236	4.512	3.883	3.500	1.217
Si	3.046	3.039	3.024	5.404	2.739	2.083	5.073	5.407	2.769
K	n.d	n.d	n.d	1.684	.002	.000	.000	1.690	.001
Ca	.084	.102	.099	.000	.276	.000	.000	.000	.231
Ti	.000	.000	.000	.174	.000	.030	.000	.190	.000
Cr	.000	.000	.000	.004	.000	.004	.000	.007	.000
Mn	.009	.007	.067	.000	.000	.023	.025	.010	.000
Fe	2.575	2.553	2.527	2.724	.005	.811	.675	2.374	.001
Ni	.000	.000	.002	.004	.000	.002	.000	.002	.000
TOTAL	7.977	7.977	7.976	15.607	5.018	7.617	11.012	15.503	5.013
Fe²⁺	2.556	2.527	2.510						
Fe³⁺	.019	.026	.017						
M/FM	.109	.113	.092	.450		.154	.655	.489	
Ca*	.031	.036	.056						
Al**					.154				
Almand	86.0	85.1	85.2						
Pyrope	10.9	11.3	9.2						
Gross	2.8	3.4	3.4						
Spess	.3	.2	2.3						
formula basis#:	12	12	12	22	8	12	18	22	8

An-content of plagioclase (82-V-23) is 27.

Assemblage: GARNET-BIOTITE-STAUROLITE STAUROLITE-CORDIERITE-BIOTITE

Sample no.	81-V-252				81-V-347a				82-V-39			
	GARN	BIO	CORD	PLAG	STAUR	CORD	BIO	PLAG	STAUR	CORD	BIO	PLAG
no. of analyses	3	6	4	5	2	7	9	2	7	6	6	3
Na_2O	.00	.21	.21	9.26	.00	.29	.19	8.54	.00	.23	.17	9.41
MgO	3.72	11.40	9.03	.01	1.41	8.53	10.32	.00	1.66	8.46	10.08	.00
Al_2O_3	20.69	18.29	31.93	23.21	52.46	32.61	19.86	24.20	51.62	32.19	19.24	22.77
SiO_2	37.75	37.24	49.72	63.02	27.77	50.65	36.62	63.20	27.42	49.83	36.37	62.64
K_2O	n.d	8.75	.00	.05	.01	.01	8.74	.05	.00	.00	8.96	.04
CaO	1.00	.00	.02	5.38	.01	.02	8.74	5.75	.00	.00	8.96	4.54
TiO_2	.00	1.98	.00	.01	.54	.01	1.69	.01	.56	.00	1.90	.00
Cr_2O_3	.00	.12	.02	.01	.36	.00	.09	.00	.14	.00	.14	.00
MnO	2.98	.06	.21	.01	.40	.30	.10	.00	.35	.27	.11	.03
FeO	33.70	18.24	7.52	.03	12.93	7.90	19.05	.05	12.89	7.96	18.97	.04
NiO	.03	.02	.01	.03	.00	.01	.03	.00	.02	.03	.03	.01
TOTAL	99.87	96.31	98.67	101.02	95.89	100.33	96.69	101.62	94.66	98.98	95.97	99.48
Na	.000	.058	.039	.784	.000	.055	.051	.722	.000	.045	.049	.811
Mg	.443	2.522	1.374	.000	.153	1.279	2.283	.000	.184	1.287	2.250	.000
Al	1.959	3.201	3.845	1.208	4.556	3.868	3.472	1.243	4.452	3.870	3.399	1.194
Si	3.032	5.532	5.082	2.768	2.045	5.096	5.436	2.750	2.046	5.085	5.454	2.789
K	n.d	1.656	.000	.002	.000	.000	1.654	.002	.000	.000	1.712	.001
Ca	.084	.000	.002	.252	.000	.000	.000	.267	.000	.000	.000	.215
Ti	.000	.218	.000	.000	.028	.000	.187	.000	.031	.000	.211	.000
Cr	.000	.012	.000	.000	.019	.000	.008	.000	.006	.000	.015	.000
Mn	.200	.005	.016	.000	.023	.024	.010	.000	.021	.022	.012	.000
Fe	2.263	2.264	.642	.000	.795	.663	2.363	.001	.803	.677	2.377	.001
Ni	.000	.001	.000	.001	.000	.000	.000	.000	.001	.002	.001	.000
TOTAL	7.981	15.469	11.000	5.013	7.622	10.985	15.464	4.984	7.643	10.988	15.480	5.011
Fe^{2+}	2.248											
Fe^{3+}	.015											
M/FM	.149	.526	.676		.161	.659	.492		.186	.655	.486	
Almand	75.6											
Pyrope	14.9											
Gross	2.8											
Spess	6.7											
Ca*	.095											
Al**			.266									
An-content (molecular %)				24.3				26.9				20.9
formula basis#:	12	22	18	8	12	18	22	8	12	18	22	8

296

TABLE A.12: (continued)

Assemblage:			GARNET-BIOTITE-STAUROLITE						FE-RICH AND-CORD-BIO-MUSC (A2?)				
Sample no.			81-V-214b						81-V-55b				
	I.P	GARNET O.P	BIO	BIO(St)	BIO(G)	STAUR	PLAG		CORD	BIO(M)	BIO(S)	BIO(C)	MUSC
no. of analyses	3	2	4	2	3	6	3		4	3	2	2	2
Na₂O	n.d	n.d	.12	.06	.12	.01	8.81		1.10	.22	.19	.21	1.41
MgO	1.61	1.48	6.74	6.40	6.70	.64	.04		7.52	9.39	9.27	10.83	.38
Al₂O₃	20.18	19.29	19.74	19.37	19.67	53.19	21.78		30.27	19.48	19.33	20.02	35.13
SiO₂	37.54	37.90	35.18	33.21	34.34	28.31	66.10		50.68	36.48	37.97	35.98	50.34
K₂O	n.d	n.d	8.23	7.70	7.97	.00	.93		.00	8.54	8.81	7.62	8.53
CaO	.41	.57	.00	.00	.00	.00	2.57		.00	.00	.00	.00	.01
TiO₂	.00	.04	1.15	1.38	1.38	.29	.00		.00	1.46	1.50	1.25	.38
Cr₂O₃	.00	.00	.03	.07	.06	.04	.02		.00	.06	.07	.14	.05
MnO	2.09	3.81	.05	.00	.03	.05	.00		.27	.06	.07	.08	.00
FeO	38.30	36.73	26.95	27.61	26.04	13.64	.19		10.07	23.53	22.73	21.83	.87
NiO	.00	.00	.03	.03	.05	.04	.00		.01	.05	.04	.04	.00
TOTAL	100.13	99.82	98.22	95.81	96.36	96.21	100.44		99.93	99.27	99.97	98.01	97.10
Na	n.d	n.d	.031	.014	.033	.000	.747		.216	.061	.051	.061	.349
Mg	.193	.180	1.522	1.493	1.537	.069	.001		1.147	2.060	2.007	2.384	.060
Al	1.935	1.858	3.530	3.575	3.574	4.596	1.122		3.648	3.384	3.314	3.485	5.310
Si	3.055	3.096	5.333	5.198	5.294	2.076	2.892		5.186	5.380	5.526	5.314	6.453
K	n.d	n.d	1.593	1.535	1.570	.000	.051		.000	1.605	1.636	1.435	1.396
Ca	.033	.048	.000	.000	.000	.000	.119		.000	.000	.000	.000	.000
Ti	.000	.002	.129	.161	.157	.015	.000		.000	.160	.162	.139	.035
Cr	.000	.000	.000	.004	.006	.002	.000		.000	.004	.004	.013	.002
Mn	.143	.261	.004	.000	.001	.002	.000		.021	.004	.008	.008	.000
Fe	2.606	2.508	3.418	3.612	3.357	.834	.006		.862	2.899	2.763	2.696	.084
Ni	.000	.000	.000	.000	.003	.000	.000		.000	.004	.004	.000	.000
TOTAL	7.966	7.953	15.561	15.591	15.532	7.594	4.938		11.080	15.561	15.476	15.534	13.689
Fe²⁺	2.581	2.498											
Fe³⁺	.025	.010											
M/FM	.065	.060	.308	.293	.314	.076	.565		.415	.421	.469		
Ca*	.059	.103											
Al**			.167	.155	.173								
Almand	87.5	83.6											
Pyrope	6.5	6.0											
Gross	1.1	1.6											
Spess	4.9	8.7											
formula basis#:	12	12	22	22	22	12	8		18	22	22	22	22

St= bio in contact with staur. G = bio in contact with garn. M = matrix bio. S = bio oriented at a high angle to BIO (M). C = bio included in cord porphyroblast.
An-content of plagioclase (molecular %) is 13.0

TABLE A.13: Microprobe Analyses of Minerals from Mafic Flows

	AMPHIBOLE					CHLORITE							PLAG
Sample no.	99a	106	107	220	2-32a	99a	106	107	220	32a	391	411a	2-32a
no.of analyses	3	3	3	1	2	3	3	3	1	1	2	2	1
Na_2O	.12	.20	.20	.21	1.58	.00	.00	.00	.01	.00	.03	.03	8.96
MgO	18.96	14.38	14.44	12.04	9.05	22.31	14.40	17.73	15.43	20.18	13.86	17.20	.00
Al_2O_3	1.33	2.36	4.02	8.20	13.32	19.82	19.75	20.71	17.44	17.59	21.38	20.71	24.49
SiO_2	56.32	52.96	51.58	42.60	43.74	28.13	26.44	27.13	26.64	28.08	25.18	25.93	61.49
K_2O	.04	.04	.09	.16	.37	.00	.00	.00	.09	.20	.02	.00	.08
CaO	12.84	11.98	11.74	11.31	11.55	.13	.01	.02	.03	.02	.00	.03	6.22
TiO_2	.00	.16	.03	.02	.21	.00	.03	.02	.06	.01	.05	.06	.00
Cr_2O_3	.06	.00	.10	.77	.02	.49	.00	.00	.73	.02	.02	.04	.00
MnO	.23	.36	.29	.30	.24	.25	.41	.43	.34	.22	.14	.51	.00
FeO	9.07	16.73	15.98	18.87	19.20	18.56	28.32	24.78	27.02	26.67	28.64	25.93	.14
NiO	.01	.04	.04	.03	.00	.14	.05	.14	.01	.10	.05	.03	.02
TOTAL	98.90	99.21	98.50	94.50	99.28	89.83	89.41	90.96	87.80	89.09	89.37	90.46	101.40
Na	.023	.046	.046	.046	.046	.000	.000	.000	.000	.000	.008	.003	.763
Mg	3.933	3.082	3.128	2.806	2.001	4.239	2.892	3.434	3.154	3.960	2.794	3.377	.000
Al	.207	.391	.690	1.495	2.323	2.978	3.138	3.170	2.820	2.728	3.405	3.219	1.269
Si	7.843	7.659	7.475	6.670	6.463	3.584	3.565	3.525	3.658	3.697	3.405	3.417	2.704
K	.000	.000	.000	.023	.069	.000	.000	.000	.016	.031	.004	.000	.003
Ca	1.909	1.863	1.817	1.886	1.817	.015	.000	.000	.004	.000	.000	.003	.293
Ti	.000	.000	.000	.000	.000	.000	.000	.000	.004	.000	.004	.003	.000
Cr	.000	.000	.000	.092	.000	.048	.000	.000	.076	.000	.000	.003	.000
Mn	.023	.023	.023	.023	.023	.026	.043	.045	.036	.023	.012	.054	.000
Fe	1.058	2.001	1.932	2.461	2.369	1.979	3.193	2.693	3.102	2.496	3.239	2.855	.003
Ni	.000	.000	.000	.000	.000	.011	.004	.011	.000	.007	.004	.000	.000
TOTAL	14.996	15.098	15.134	15.502	15.525	12.879	12.835	12.878	12.870	12.941	12.875	12.936	5.035
M FM	.310	.632	.642	.547	.537	.682	.475	.560	.504	.612	.463	.542	
Fe^{2+}	.??	1.794	1.748	2.323	1.725								
Fe^{3+}	.139	.207	.184	.138	.644								
formula basis#:	23	23	23	23	23	19	18	18	18	18	18	18	8

number of oxygens per formula unit

TABLE A.14: Chemical Compositions of Minerals in Felsic Volcanics

Sample no. Mineral	GARN		2-73 BIO	AMPH	PLAG	170 GARN	BIO	AMPH	430a BIO	AMPH
	Rim	Core								
no. of analyses	2	3	2	2		3	3	3	:	3
Na_2O	.01	.00	.00	1.71	3.88	.00	.13	1.04	.05	.86
MgO	1.55	1.29	8.69	17.94	.00	.82	5.94	3.91	10.12	7.23
Al_2O_3	20.37	19.82	16.87	17.94	28.60	20.43	17.19	14.49	17.18	11.95
SiO_2	37.45	34.98	35.21	39.23	52.21	38.54	35.31	39.89	37.06	43.37
K_2O	.01	.02	9.04	.30	.03	.00	10.63	.07	9.13	.90
CaO	3.22	4.20	.02	9.78	12.07	5.29	.00	10.89	.05	11.25
TiO_2	.07	.07	.96	.14	.03	.05	1.04	.08	1.50	.48
Cr_2O_3	.00	.00	.00	.00	.00	.02	.02	.00	.08	.06
MnO	3.93	8.56	.04	.62	.12	9.46	.27	.43	.23	.38
FeO	32.24	27.88	22.77	21.80	.15	29.46	27.97	25.93	20.60	19.58
NiO	.00	.02	.09	.01	.00	.00	.04	.00	.04	.00
TOTAL	98.85	96.82	93.67	95.81	97.08	104.12	98.55	97.46	96.04	96.06
Na	.000	.000	.000	.515	.349	.004	.036	.299	.000	.253
Mg	.187	.161	2.040	.984	.000	.094	1.368	.920	2.288	1.656
Al	1.958	1.972	3.132	1.567	3.283	1.887	3.136	2.668	3.058	2.162
Si	3.054	2.953	5.552	6.097	2.429	3.022	5.468	6.256	5.610	6.670
K	.000	.000	1.813	.054	.001	.000	2.100	.138	1.760	.161
Ca	.280	.379	.000	1.628	.601	.444	.000	1.817	.000	1.840
Ti	.002	.002	.111	.014	.000	.002	.118	.000	.154	.046
Cr	.000	.000	.000	.000	.000	.000	.000	.000	.000	.000
Mn	.270	.612	.004	.077	.004	.628	.032	.046	.000	.046
Fe	2.200	1.967	2.998	2.832	.005	1.931	3.623	3.381	2.596	2.507
Ni	.000	.000	.009	.000	.000	.000	.004	.000	.000	.000
TOTAL	7.950	8.045	15.659	15.484	4.956	8.013	15.885	15.525	15.488	15.341
M/FM	.079	.077	.405	.290		.047	.274	.225	.469	.411
Fe^{2+}	2.172	1.941		2.412		1.886		3.174		2.369
Fe^{3+}	.028	.026		.420						
$Ca*$	.189	.320				.045		.207		.138
$Al**$				.136						
Alman	74.7	62.8								
Pyrope	6.4	5.2								
Gross	9.6	12.3								
Spess	9.3	19.8								
formula basis#:	12	12	22	23	8	12	22	23	22	23

\# number of oxygens per formula unit
Plagioclase has an An-content of 63.

APPENDIX B: Additional Analyses

The compositions of various minerals referred to in the
text are tabulated and compared in: 1) Table B.1 - biotite
and muscovite included in cordierite porphyroblasts compared
to those in the matrix; 2) Table B.2 - matrix biotite or
biotite in the S_2 foliation plane versus biotite
porphyroblasts or biotite oriented at a high angle to S_2
(post-S2 fabric orientation); 3) Table B.3 - late
(post-tectonic) muscovite and; 4) Table B.4 and Figure B.1 -
altered cordierite porphyroblasts.

TABLE 8.1: Chemical Composition of Muscovite and Biotite Included in Cordierite Porphyroblasts Compared to those Defining the Matrix

Sample no. Metamorphic Zone	2-163				2-34		439		2-173	
	CZ				CZ		AZ		AZ	
Mineral	MUSCOVITE		BIOTITE		BIOTITE		BIOTITE		BIOTITE	
	MATRIX	PORPH	MATRIX	PORPH	MATRIX	PORPH	MATRIX	PORPH	MATRIX	PORPH
no. of analyses	4	3	6	5	4	3	5	2	3	3
Na_2O	1.39	1.57	.12	.23	.14	.25	.21	.29	.09	.20
MgO	.43	.38	10.26	10.56	9.70	11.47	10.45	10.47	10.68	10.79
Al_2O_3	34.55	34.71	18.85	19.26	19.93	19.38	19.46	19.70	19.29	19.68
SiO_2	45.47	44.47	35.43	35.81	36.61	37.03	36.73	37.59	37.77	36.02
K_2O	8.56	8.60	8.77	8.7?	8.58	8.41	9.66	8.93	8.63	8.35
CaO	.00	.00	.00	.00	.00	.00	.00	.00	.00	.00
TiO_2	.37	.26	1.36	1.30	1.36	1.39	1.54	1.57	1.41	1.37
Cr_2O_3	.05	.09	.06	.10	.05	.37	.10	.22	.05	.18
MnO	.02	.03	.08	.08	.0?	.15	.07	.05	.11	.08
FeO	.54	.58	18.26	18.59	19.94	18.89	19.34	20.87	19.48	19.31
NiO	.03	.00	.03	.05	.02	.00	.00	.01	.00	.02
TOTAL	91.41	90.73	93.22	94.72	96.43	97.34	97.56	99.69	97.53	95.??
Na	.367	.422	.035	.065	.039	.069	.056	.076	.025	.057
Mg	.085	.077	2.354	2.388	2.156	2.490	2.307	2.258	2.335	2.403
Al	5.578	5.661	3.423	3.445	3.506	3.362	3.394	3.364	3.335	3.471
Si	6.229	6.153	5.461	5.434	5.465	5.435	5.436	5.449	5.546	5.391
K	1.495	1.515	1.724	1.689	1.630	1.578	1.825	1.650	1.616	1.590
Ca	.000	.000	.000	.000	.000	.000	.000	.000	.000	.000
Ti	.036	.028	.155	.145	.149	.151	.169	.170	.155	.153
Cr	.002	.008	.007	.010	.004	.040	.008	.021	.004	.017
Mn	.001	.000	.009	.008	.008	.017	.008	.004	.013	.008
Fe	.061	.065	2.351	2.357	2.489	2.325	2.394	2.526	2.392	2.417
Ni	.002	.000	.003	.003	.003	.000	.000	.000	.000	.000
TOTAL	13.856	13.929	15.522	15.546	15.445	15.485	15.597	15.519	15.421	15.507
M/FM	.582	.540	.500	.503	.493	.514	.491	.472	.494	.499
Na/Na+K	.197	.220	.020	.037	.023	.034	.030	.044	.015	.035
Al^{vi}	3.807	3.814	.884	.873	.854	.800	.830	.813	.881	.862
Al^{iv}	1.771	1.847	2.539	2.572	2.586	2.57?	2.564	2.551	2.454	2.609

formula basis: 22 oxygens per formula unit

- 301 -

TABLE B.1 (continued)

Sample no.	2-21		340				346			
Metamorphic Zone	SZ		SZ				SZ			
Mineral	MUSCOVITE		MUSCOVITE		BIOTITE		MUSCOVITE		BIOTITE	
	MATRIX	PORPH	MATRIX	PORPH	MATRIX	PORPH	MATRIX	PORPH	MATRIX	PORPH
No. of analyses	4	2	3	3	3	3	2	2	3	3
Na_2O	1.23	1.27	1.39	1.41	.16	.26	1.05	1.07	.21	.18
MgO	.53	.52	.50	.46	10.57	10.79	.49	.61	10.56	11.13
Al_2O_3	36.01	35.77	35.75	35.54	19.60	20.23	33.75	33.87	19.24	19.42
SiO_2	48.22	48.74	48.72	48.53	36.74	37.04	43.93	43.87	36.83	36.49
K_2O	9.15	8.66	9.04	8.67	9.03	8.31	8.62	8.55	8.87	8.83
CaO	.00	.00	.00	.00	.00	.02	.00	.00	.00	.00
TiO_2	.51	.63	.43	.43	2.00	1.45	.87	.93	1.97	1.58
Cr_2O_3	.07	.09	.04	.15	.07	.10	.09	.07	.09	.08
MnO	.00	.01	.03	.00	.13	.11	.03	.03	.15	.12
FeO	.64	.79	.73	.72	21.09	19.72	.71	.73	18.62	16.84
NiO	.00	.04	.02	.00	.04	.05	.00	.02	.00	.03
TOTAL	96.35	96.50	96.64	95.92	99.43	98.06	89.53	89.73	96.55	94.69
Na	.309	.315	.346	.355	.042	.073	.284	.288	.061	.048
Mg	.099	.099	.095	.087	2.296	2.347	.103	.123	2.338	2.491
Al	5.511	5.453	5.463	5.451	3.371	3.484	5.577	5.588	3.368	3.439
Si	6.262	6.308	6.315	6.318	5.363	5.415	6.162	6.143	5.475	5.481
K	1.513	1.428	1.495	1.436	1.679	1.549	1.539	1.524	1.679	1.693
Ca	.000	.000	.000	.000	.000	.000	.000	.000	.000	.000
Ti	.049	.061	.038	.042	.218	.159	.090	.094	.218	.176
Cr	.003	.007	.000	.015	.008	.008	.008	.004	.008	.009
Mn	.000	.000	.000	.000	.013	.013	.000	.000	.017	.013
Fe	.068	.083	.076	.076	2.574	2.411	.082	.082	2.312	2.116
Ni	.000	.003	.000	.000	.000	.004	.000	.000	.000	.000
TOTAL	13.814	13.757	13.826	13.781	15.564	15.462	13.844	13.846	15.476	15.467
M FM	.593	.544	.556	.534	.472	.493	.557	.600	.503	.541
Na Na+K	.170	.181	.169	.193	.024	.045	.156	.159	.035	.028
AlVI	3.773	3.761	3.778	3.769	.734	.899	3.739	3.731	.843	.920
AlIV	1.738	1.692	1.685	1.682	2.637	2.585	1.838	1.857	2.525	2.519

formula basis: 22 oxygens per formula unit

TABLE B.2: Chemical Composition of Biotite in S_2 Foliation (BIO_1) Versus Biotite Oriented at a High Angle to S_2 (BIO_2)

Sample no.	132		427		439		2-176		22b	
Metamorphic Zone	CZ		AZ		AZ		AZ		AZ	
	BIO_1	BIO_2	BIO_1	BIO_2	BIO_1	BIO_2	BIO_1	BIO_2	BIO_1	BIO_2
no. of analyses	5	3	4	5	2	5	6	5	6	9
Na_2O	.19	.10	.18	.19	.24	.21	.16	.20	.07	.06
MgO	10.79	10.62	10.19	10.15	10.31	10.46	10.82	10.84	9.67	10.01
Al_2O_3	19.65	19.57	19.93	19.67	20.05	19.46	19.41	19.53	19.68	19.71
SiO_2	37.72	36.24	37.55	37.47	37.63	36.73	36.80	37.02	36.53	36.27
K_2O	8.70	8.36	8.57	9.08	9.52	9.67	9.43	9.36	8.80	8.40
CaO	.00	.00	.00	.00	.00	.00	.00	.01	.00	.00
TiO_2	1.41	1.43	1.48	1.57	1.46	1.54	1.47	1.55	1.48	1.46
Cr_2O_3	.05	.05	.05	.05	.11	.10	.07	.06	.07	.05
MnO	.07	.11	.06	.10	.07	.07	.14	.13	.09	.08
FeO	19.82	20.68	20.11	20.27	19.14	19.33	18.45	18.17	20.16	19.64
NiO_2	.00	.04	.04	.05	.00	.01	.04	.02	.02	.04
TOTAL	98.40	97.19	98.61	98.60	98.53	97.58	96.79	96.89	96.57	95.72
Na	.051	.026	.049	.050	.066	.059	.044	.053	.017	.017
Mg	2.344	2.350	2.219	2.210	2.240	2.306	2.368	2.357	2.147	2.232
Al	3.375	3.427	3.434	3.390	3.448	3.395	3.358	3.360	3.455	3.486
Si	5.497	5.385	5.492	5.481	5.493	5.439	5.404	5.409	5.470	5.443
K	1.617	1.583	1.597	1.693	1.771	1.824	1.767	1.742	1.671	1.606
Ca	.000	.000	.000	.000	.000	.000	.000	.000	.000	.000
Ti	.154	.157	.161	.170	.156	.168	.161	.169	.165	.163
Cr	.004	.004	.003	.004	.008	.010	.006	.005	.005	.004
Mn	.004	.013	.005	.009	.006	.007	.015	.014	.009	.008
Fe	2.417	2.568	2.459	2.478	2.332	2.394	2.265	2.217	2.512	2.465
Ni	.000	.000	.002	.004	.000	.000	.000	.000	.001	.003
TOTAL	15.461	15.513	15.421	15.489	15.520	15.602	15.388	15.326	15.452	15.427
M/FM	.490	.480	.474	.471	.489	.490	.509	.514	.460	.474
Na/Na+K	.030	.020	.030	.029	.036	.031	.024	.030	.010	.010
Al^{vi}	.872	.812	.926	.871	.941	.834	.762	.769	.925	.929
Al^{iv}	2.503	2.615	2.508	2.519	2.507	2.561	2.596	2.591	2.530	2.557

formula basis: 22 oxygens per formula unit

TABLE B.2 (continued)

Sample no.	342		340		307	
Metamorphic Zone	SZ		SZ		SZ	
	BIO$_1$	BIO$_2$	BIO$_1$	BIO$_2$	BIO$_1$	BIO$_2$
no. of analyses	2	5	3	3	3	2
Na$_2$O	.15	.20	.10	.15	.22	.18
MgO	10.27	10.29	10.57	10.62	9.54	10.22
Al$_2$O$_3$	19.40	19.44	19.61	19.59	19.20	19.61
SiO$_2$	36.76	36.49	36.73	37.07	37.14	36.60
K$_2$O	9.88	9.92	9.03	8.77	9.75	9.65
CaO	.00	.00	.00	.00	.00	.00
TiO$_2$	1.96	1.95	2.00	1.87	1.56	1.39
Cr$_2$O$_3$	.06	.05	.07	.08	.07	.07
MnO	.14	.13	.13	.16	.10	.08
FeO	18.89	18.96	21.09	21.54	19.70	20.16
NiO	.04	.02	.05	.03	.02	.02
TOTAL	97.55	97.45	99.38	99.87	97.30	97.98
Na	.041	.055	.042	.041	.062	.050
Mg	2.261	2.275	2.302	2.298	2.158	2.255
Al	3.386	3.400	3.373	3.354	3.436	3.424
Si	5.441	5.413	5.360	5.386	5.412	5.419
K	1.862	1.877	1.679	1.624	1.885	1.821
Ca	.000	.000	.000	.000	.000	.000
Ti	.216	.216	.217	.202	.175	.152
Cr	.004	.003	.007	.005	.007	.006
Mn	.015	.015	.013	.014	.010	.006
Fe	2.339	2.351	2.576	2.613	2.498	2.496
Ni	.002	.002	.003	.003	.001	.000
TOTAL	15.567	15.607	15.572	15.540	15.644	15.629
M FM	.500	.490	.471	.466	.462	.474
Na Na+K	.022	.029	.024	.025	.032	.027
AlVi	.827	.813	.733	.740	.848	.843
AlIV	2.559	2.587	2.640	2.614	2.588	2.581

formula basis: 22 oxygens per formula unit

TABLE B.3: Microprobe Analyses of Post-tectonic Muscovites

Metamorphic Zone	A*Z CAB	A*Z CAB	A*Z CAB	S*Z SCAB	S*Z SCAB	S*Z SAB	S*Z SAB
Sample no.	2-180	2-183	2-40a	268	2-36	304	442a
no.of analyses	3	2	2	4	1	1	2
Na_2O	1.08	1.23	1.09	.84	1.10	1.16	1.18
MgO	.44	.35	.43	.48	.39	.54	.48
Al_2O_3	35.69	36.06	36.70	36.01	36.04	34.50	34.54
SiO_2	47.20	48.23	47.32	46.82	48.05	43.00	44.16
K_2O	9.45	8.69	8.51	8.93	9.31	8.79	8.74
CaO	.00	.00	.01	.00	.02	.05	.05
TiO_2	.31	.60	.52	.39	.36	.64	.55
Cr_2O_3	.04	.06	.05	.02	.09	.00	.02
MnO	.01	.01	.01	.00	.02	.05	.05
FeO	.68	.63	.51	.62	.79	.77	.72
NiO	.01	.02	.02	.03	.04	.00	.04
TOTAL	94.91	95.88	95.17	94.14	96.19	89.46	90.49
Na	.274	.306	.272	.215	.275	.314	.319
Mg	.084	.065	.083	.093	.072	.111	.098
Al	5.560	5.529	5.666	5.636	5.533	5.723	5.654
Si	6.242	6.276	6.199	6.218	6.260	6.054	6.132
K	1.592	1.440	1.419	1.511	1.545	1.578	1.548
Ca	.000	.000	.000	.000	.000	.000	.000
Ti	.030	.058	.050	.037	.034	.066	.057
Cr	.003	.003	.003	.001	.007	.000	.000
Mn	.000	.000	.000	.000	.000	.004	.004
Fe	.073	.067	.052	.065	.084	.091	.081
Ni	.000	.000	.000	.000	.003	.000	.003
TOTAL	13.858	13.744	13.744	13.839	13.814	13.940	13.896
M/FM	.535	.492	.615	.589	.462	.550	.548
Na/Na+K	.147	.175	.161	.125	.151	.166	.171
Al^{vi}	3.802	3.805	3.865	3.854	3.793	3.777	3.786
Al^{iv}	1.758	1.724	1.801	1.782	1.740	1.946	1.868

formula basis#: 22 oxygens per formula unit

Figure B.4: Schematic diagram of cordierite porphyroblast from the AZ (sample 81-V-135) showing the areas analysed by electron microprobe (analyses given in Table B.4). Area 1 is the only area analysed that shows visible signs of alteration (orange coloration due to pinnitization ;in plane light and isotropic in crossed nicols). Dashed line marks area of pinnitization. Porphyroblast has indistinct boundaries with the matrix and has overgrown recrystallized quartz grains and possibly a crenulated fabric (see dashed lines marking zones of different mica orientations and different crystallographic orientation of porphyroblast). Muscovite is more abundant than biotite within the porphyroblast, but biotite is more abundant in the matrix.
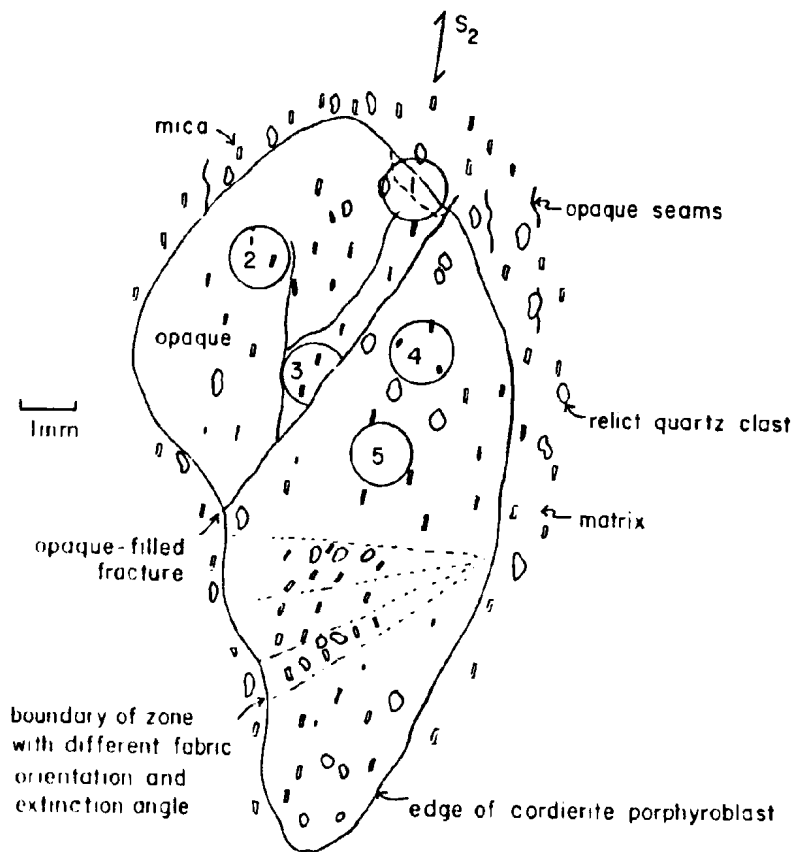
TABLE B.4: Chemical Compositions of Isotropic Rims of Cordierite Porphyroblasts (A) and of an Altered Cordierite Porphyroblast (B)

	(A)					(B)			
sample no.	340	2-21	2-21	307	2-135				
area analysed					1	2	3	4	5
no. of analyses	2	3	2	1	2	3	3	3	3
Na_2O	.01	.03	.07	.00	.04	.20	.20	.34	.26
MgO	4.55	5.58	4.76	4.13	3.06	6.00	7.07	8.00	7.69
Al_2O_3	33.41	30.40	31.37	30.86	34.94	47.07	40.75	35.79	36.68
SiO_2	40.19	43.95	45.46	42.48	41.80	36.90	42.57	47.91	46.59
K_2O	.17	1.73	3.42	.13	.19	.02	.02	.01	.01
CaO	.25	.31	.12	.43	.16	.04	.02	.02	.01
TiO_2	.00	.00	.02	.00	.00	.01	.00	.00	.00
Cr_2O_3	.00	.00	.00	.02	.00	.00	.00	.00	.00
MnO	.08	.10	.08	.11	.04	.29	.34	.35	.38
FeO	9.23	8.73	7.16	7.13	6.36	6.54	7.52	8.23	7.86
NiO	.04	.00	.01	.03	.03	.00	.01	.00	.04
TOTAL	87.93	90.83	92.46	85.30	86.63	97.07	98.55	100.64	99.52
Na	.000	.000	.000	.000	.000	.040	.048	.065	.051
Mg	.774	.936	.774	.720	.522	.934	1.085	1.201	1.166
Al	4.590	4.050	4.104	4.284	4.752	5.806	4.950	4.250	4.404
Si	4.680	4.968	5.040	5.004	4.824	3.861	4.387	4.830	4.748
K	.018	.252	.468	.000	.018	.003	.000	.000	.000
Ca	.018	.036	.000	.036	.000	.003	.000	.000	.000
Ti	.000	.000	.000	.000	.000	.000	.000	.000	.000
Cr	.000	.000	.000	.000	.000	.000	.000	.000	.000
Mn	.000	.000	.000	.000	.000	.024	.027	.029	.030
Fe	.882	.810	.666	.702	.612	.571	.647	.692	.669
Ni	.000	.000	.000	.003	.000	.000	.000	.000	.000
TOTAL	10.962	11.052	11.052	10.746	10.728	11.242	11.145	11.166	11.068
M FM	.467	.536	.538	.506	.460	.611	.617	.625	.625

formula basis: 18 oxygens per formula unit

APPENDIX C: X-ray Diffraction Studies of Low-Grade

Metaturbidites

X-ray diffraction patterns of five whole rock samples
from the central exposures of the CHZ Contwoyto Formation
and one sample from near the Fubar Fault on the south shore
of Point Lake (sample 81-V-413a) are shown in Figure C.1.
These samples were chosen for XRD analyses to determine the
relative degree of low-grade metamorphism by establishing:
a) whether paragonite or pyrophyllite are present and; b)
the crystallinity of the micas.

Analyses were run at 1,000 cps with a goniometer speed
of both 1° 2θ/min and 1/2° 2θ/min and the graph rate set at
10 mm/min; 1/2° 2θ/min runs on samples 81-V-139 and 413a had
a graph setting of 2.5 mm/min (Figure C.1).

The characteristic peaks of some of the minerals
identified during analyses are labelled on Figure C.1. The
characteristic peaks for paragonite and muscovite are very
similar, but the diffraction patterns obtained from these
low-grade samples are more comparable to muscovite than
paragonite (the peak for paragonite at 27.7 and those at
approximately 37, 41, 43 and 47 2° theta (θ) are absent).
Pyrophyllite is not present, at least not in sufficient
quantities to be determined. The sharpness or width of a
peak measured at half height gives an index of the

crystallinity of the mica (Thompson and Frey, 1984, and references therein). Although actual measurements were not made in this study, the sharpness of the muscovite peaks is taken to indicate a high degree of crystallinity.

Figure C.1

- 311 -
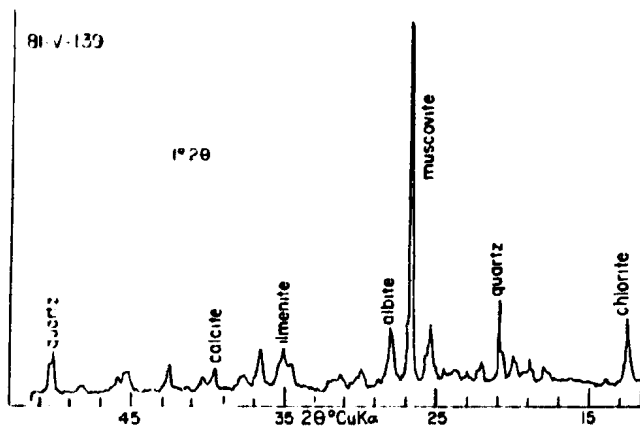
Figure C.1 (continued)
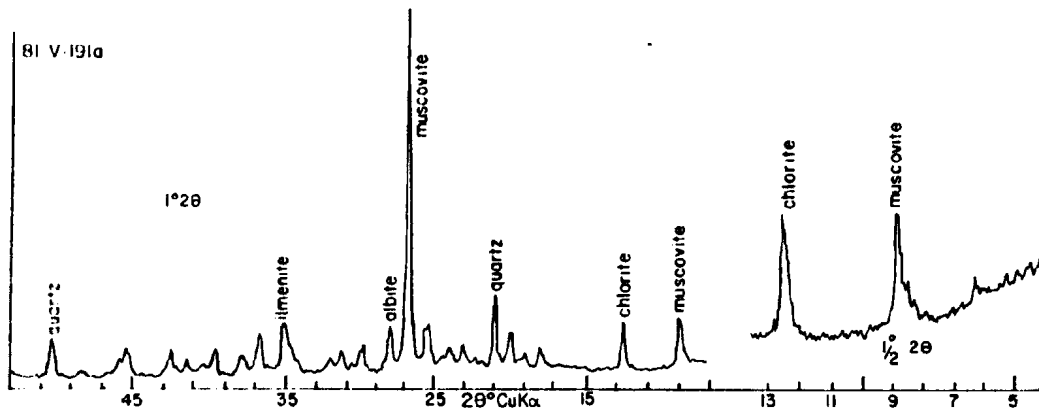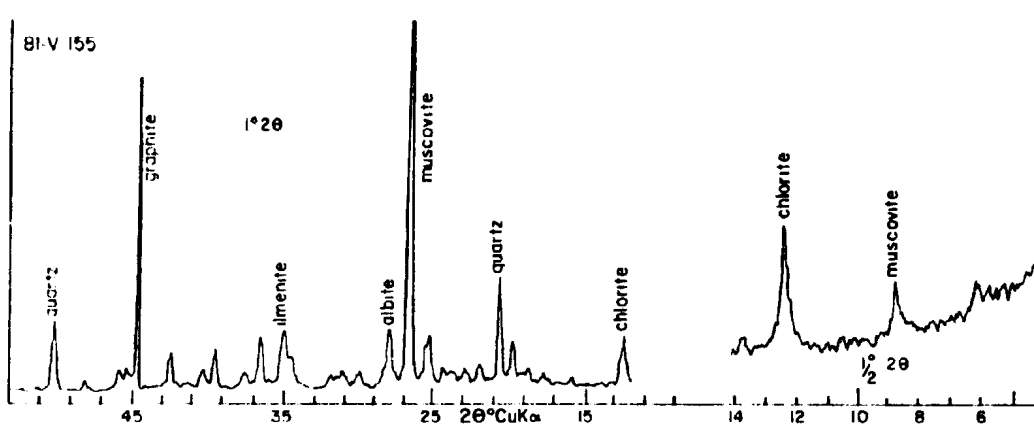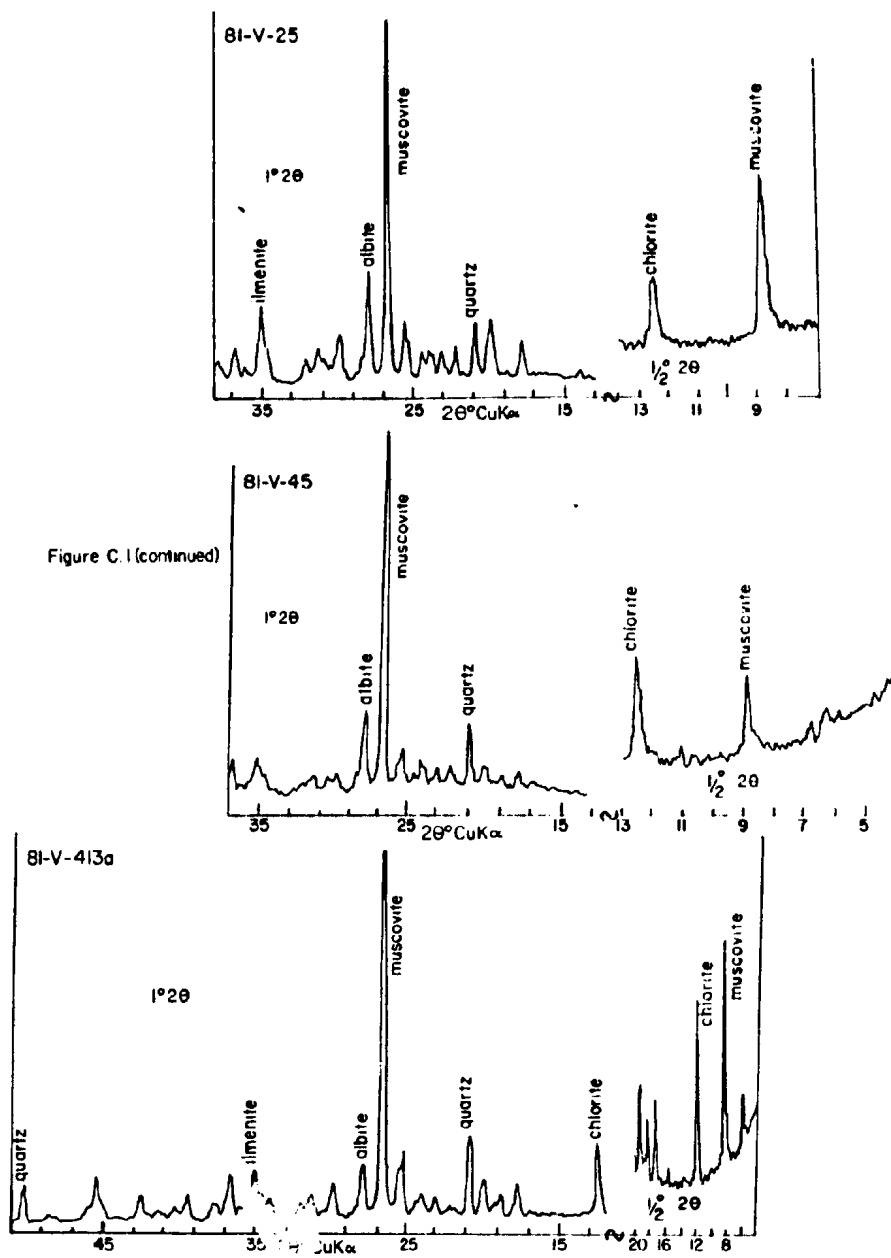
APPENDIX D : Summary of Cleavage Terminology (after Powell, 1979)

CLASSIFICATION OF CLEAVAGE

I) Continuous

II) Spaced:

Disjunctive Cleavage (no pre-existing planar anisotropy):

stylolitic and anastomosing; typical of weakly deformed
rocks with little or no fabric development in the
microlithons.

rough; typical of psammites.

smooth; typical of slates.

Crenulation Cleavage (pre-existing planar anisotropy):

discrete; thin, sharply defined discontinuities in the
crenulated fabric. Pre-existing foliation in the
microlithons is truncated by the cleavage domains.

zonal; cleavage domains represent wide lamellar zones
coincident with fold limbs. Zones have diffuse,
gradational boundaries. Crenulated fabric can be traced
through cleavage domains.

- discrete and zonal may grade into one another.
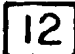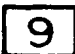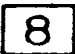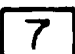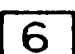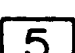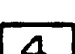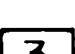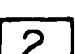
Degree of microlithon fabric alignment:

Random: no alignment of detrital grains, no preferred orientation of
            phyllosilicates, no beard overgrowths.
Weak: slight detrital grain alignment, visible preferred orientation
            of phyllosilicates, some beard overgrowths.
Strong: prominent elongation of detrital grains, strong preferred
            orientation of phyllosilicates, detrital grain boundaries are
            indistinct, with prominent beard overgrowths.
Complete: schistose microfabric, all detrital grain shapes lost, strongly
            oriented intergrowth of quartz, feldspars and micas, where
            cleavage domains are indistinct passes into continuous
   cleavage.

random   weak   strong   complete

cm scale   mm scale
spacing   spacing

stylolitic anastomosing rough ←-----→smooth

Type A   Type B   Type C
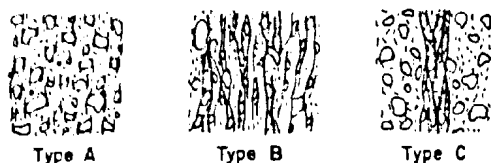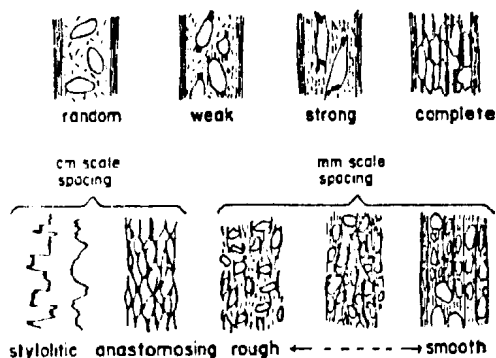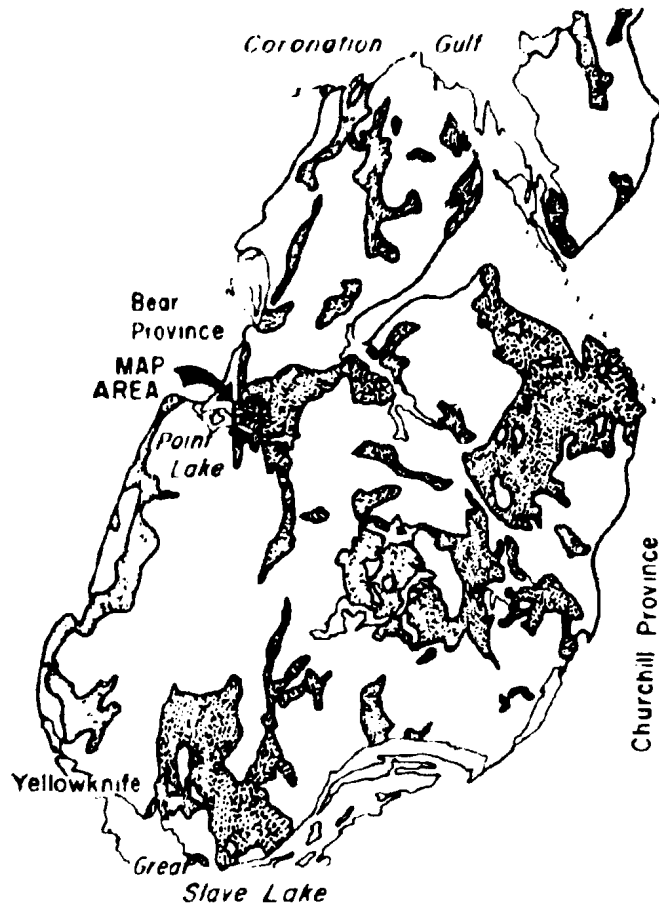
Map of the Slave Province showing the location
of the Keskarrah Bay map area (outlined) and
distribution of supracrustal rocks (stippled) within
granitoids and gneisses (unpatterned) of various
ages relative to the Yellowknife Supergroup

Diabase

12 Granite

11 Pegmatite

10 Itchen For

9 Contwoyto

8 Keskarrah

7 Carbonate

6 Rhyolite

5 Dacite

4 Mafic flow

3 Banded mc

2 Granite gra

1 Gneisses to
p
a

e dikes   includes Proterozoic and older dikes

e   intrusive into banded mafic volcanics and gneisses

itite (IIa) and granite (IIb) intrusive into metaturbidites

Intrusive Contact

YELLOWKNIFE SUPERGROUP

Formation medium-grade

yto Formation low-grade (9a), medium-grade (9b), iron formation (9c) } turbiditic metasediments

rah Formation conglomerate and sandstone

ate

e

Point Lake Formation

flows

mafic volcanic , gabbro (3a)

BASEMENT (Unconformity)

granodiorite

tonalite granodiorite orth gneiss with variable amounts of amphibolite and diorite (Ia),
paragneiss (Ia), granitic gneiss, massive to foliated granitoids and porphyroclastic granite
and amphibolite (Ie-t), deformed pegmatite and granite   possible equivalent
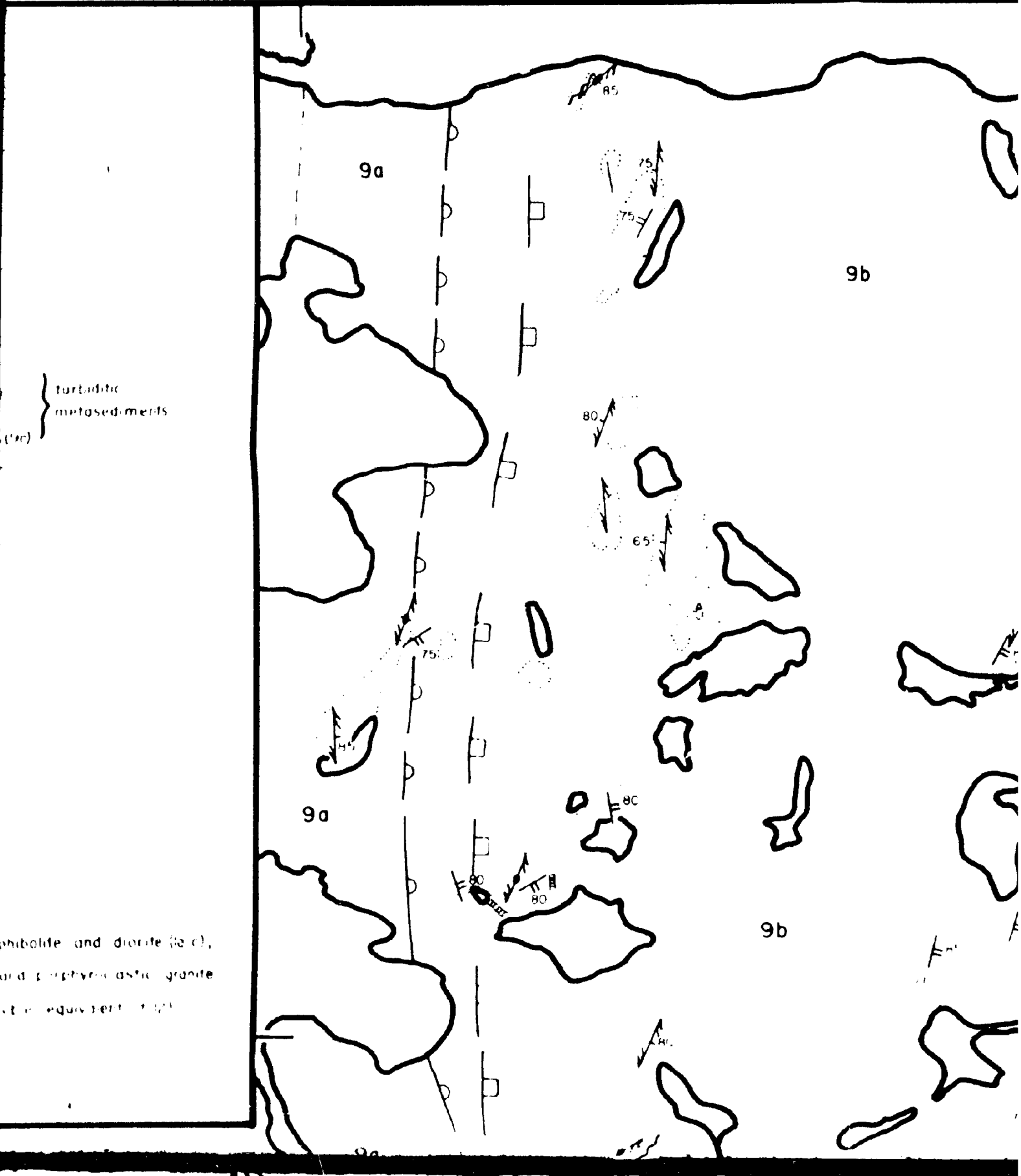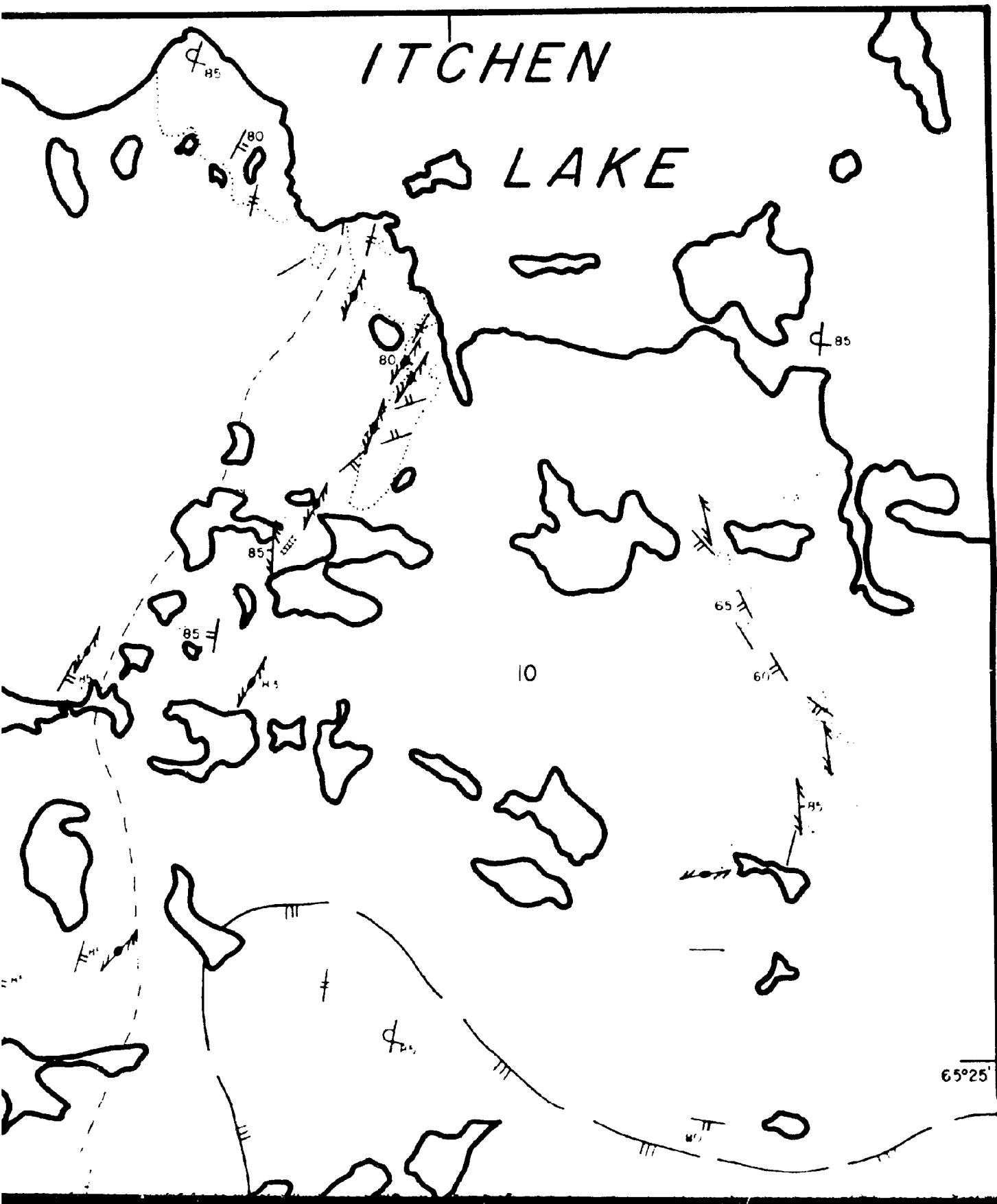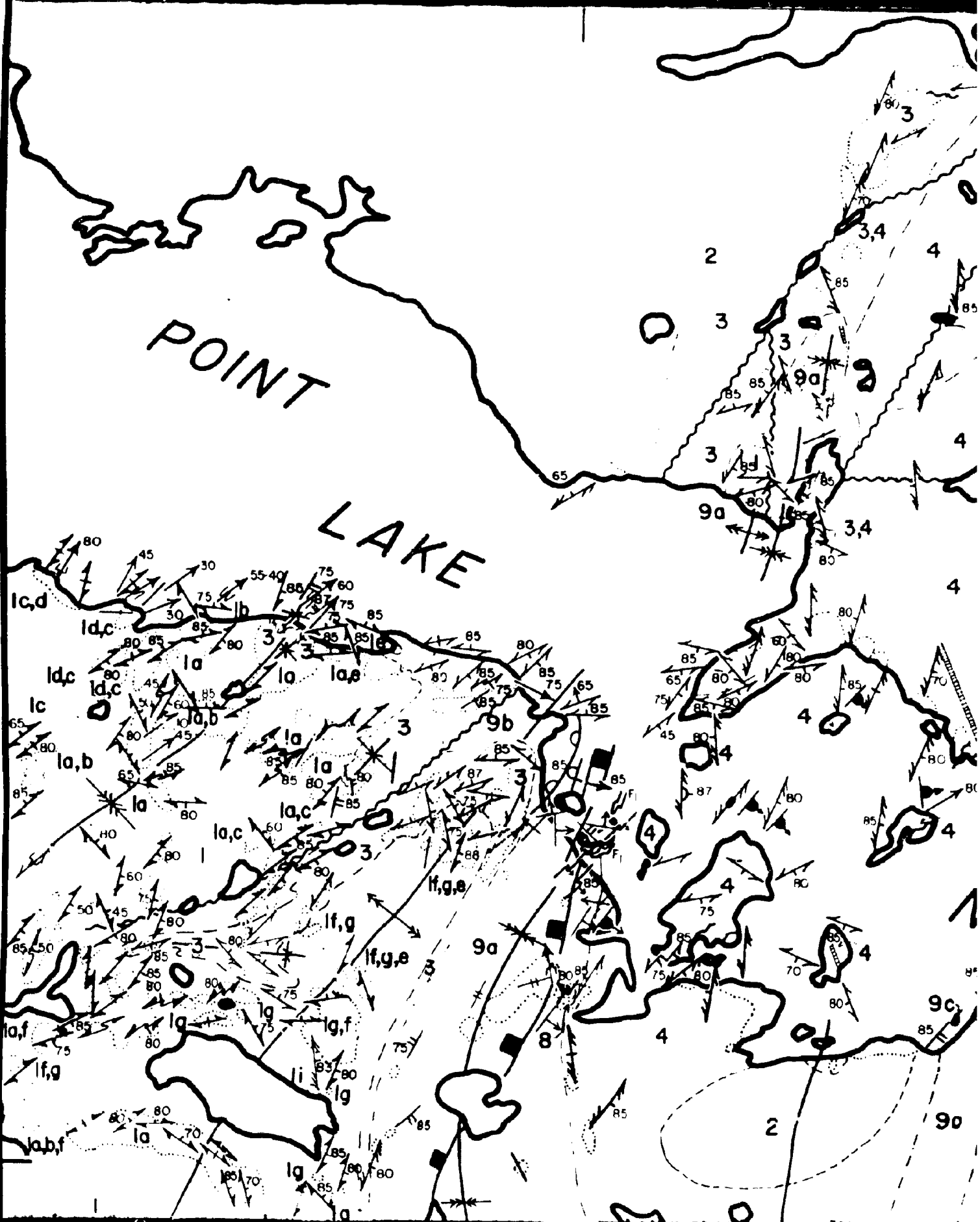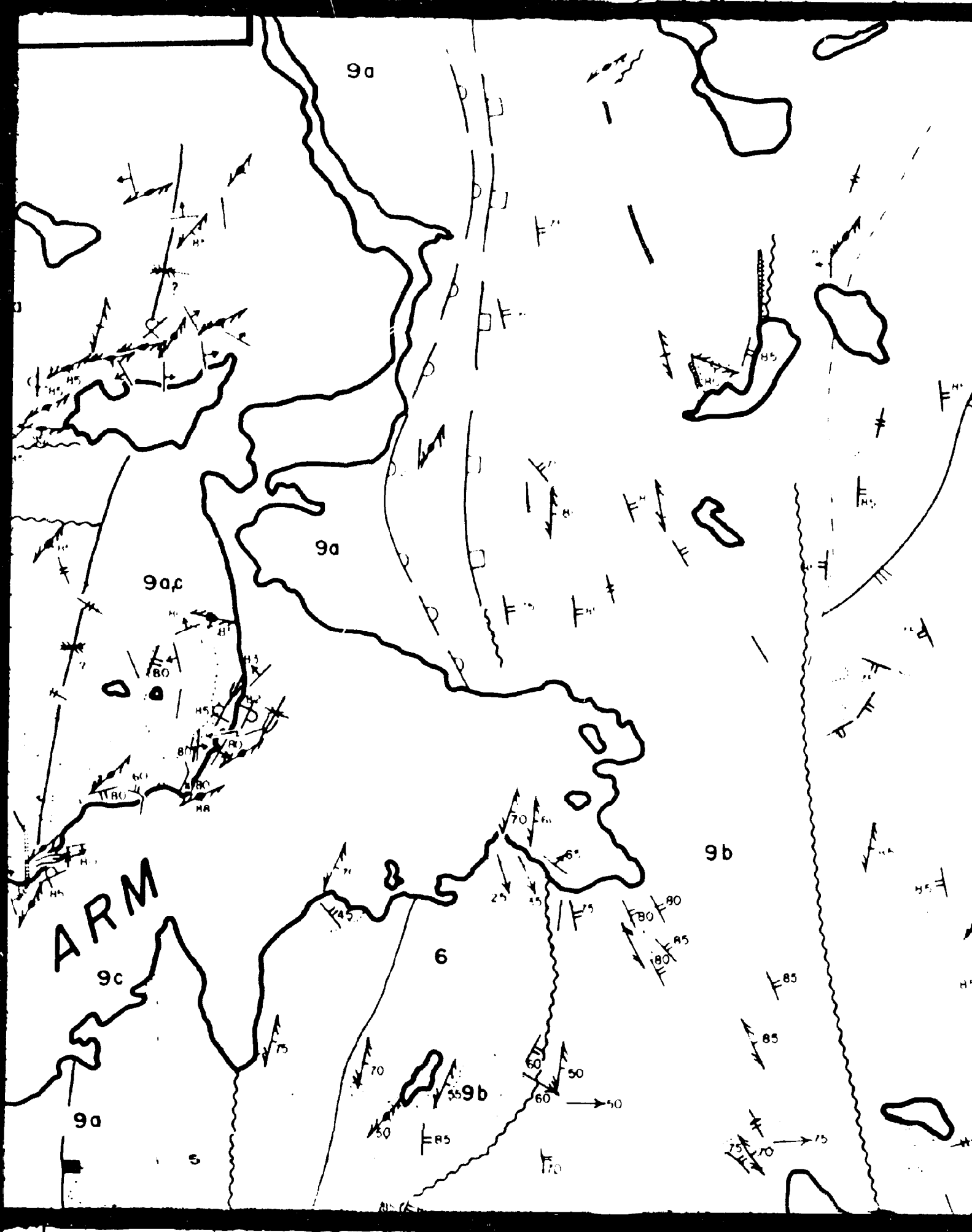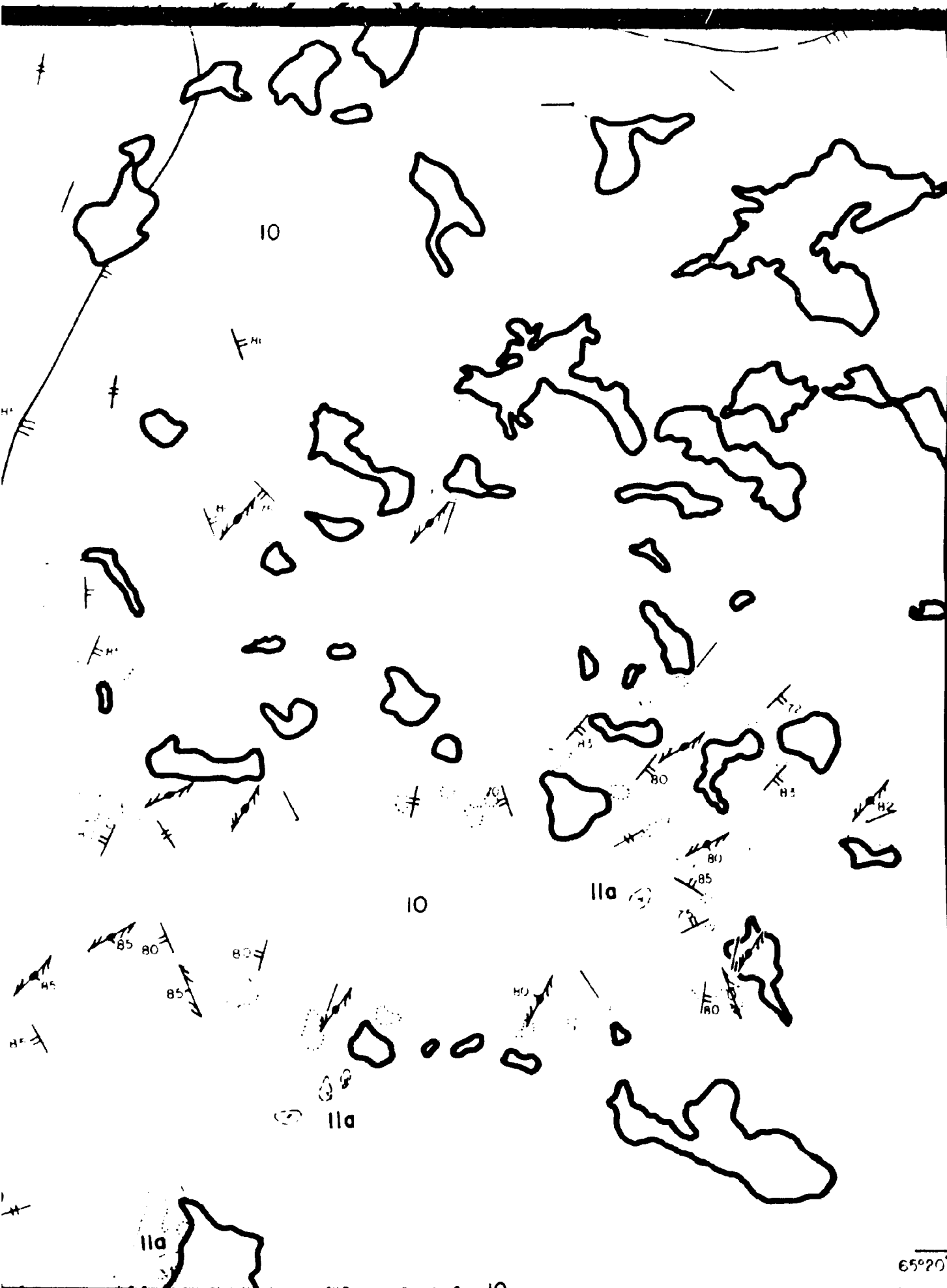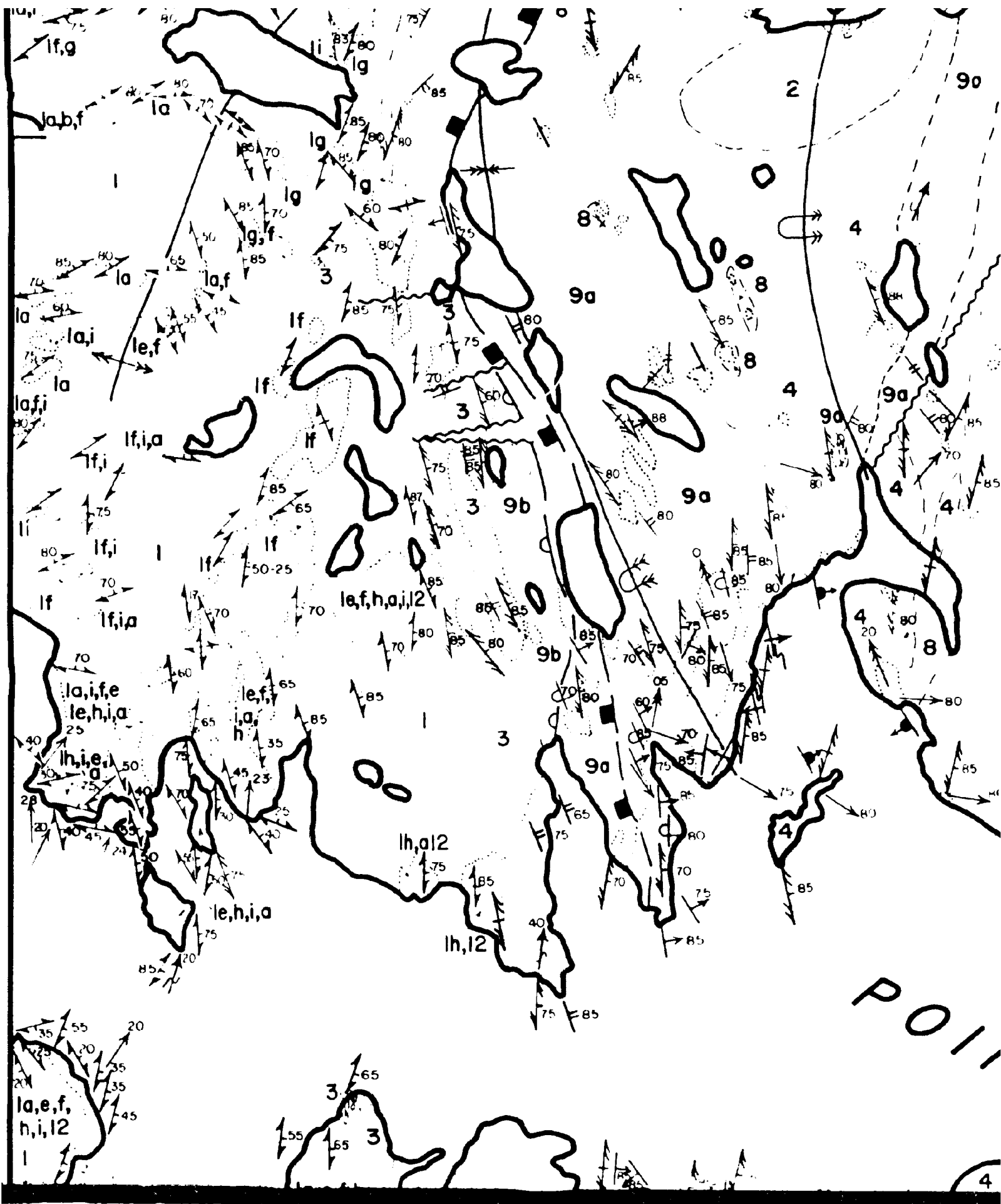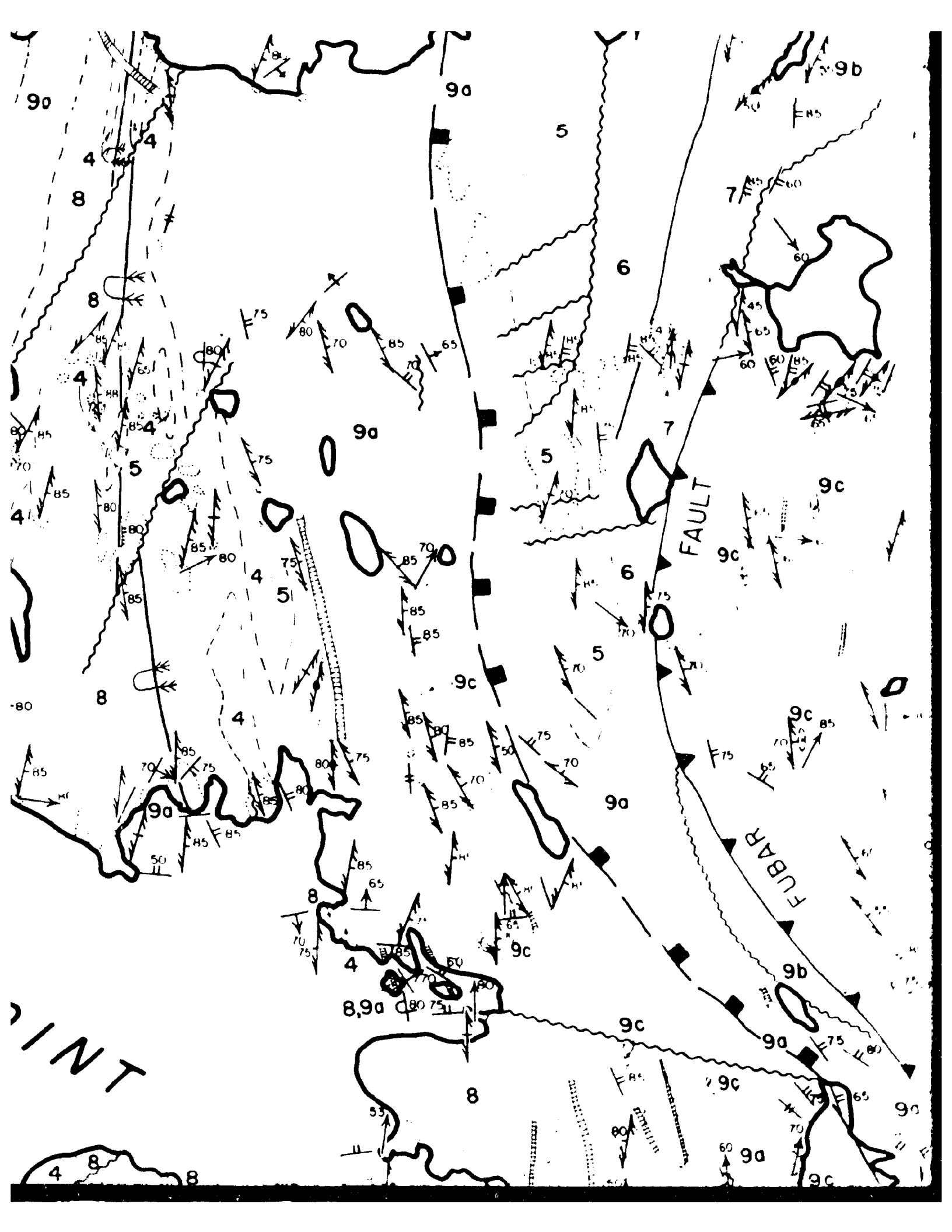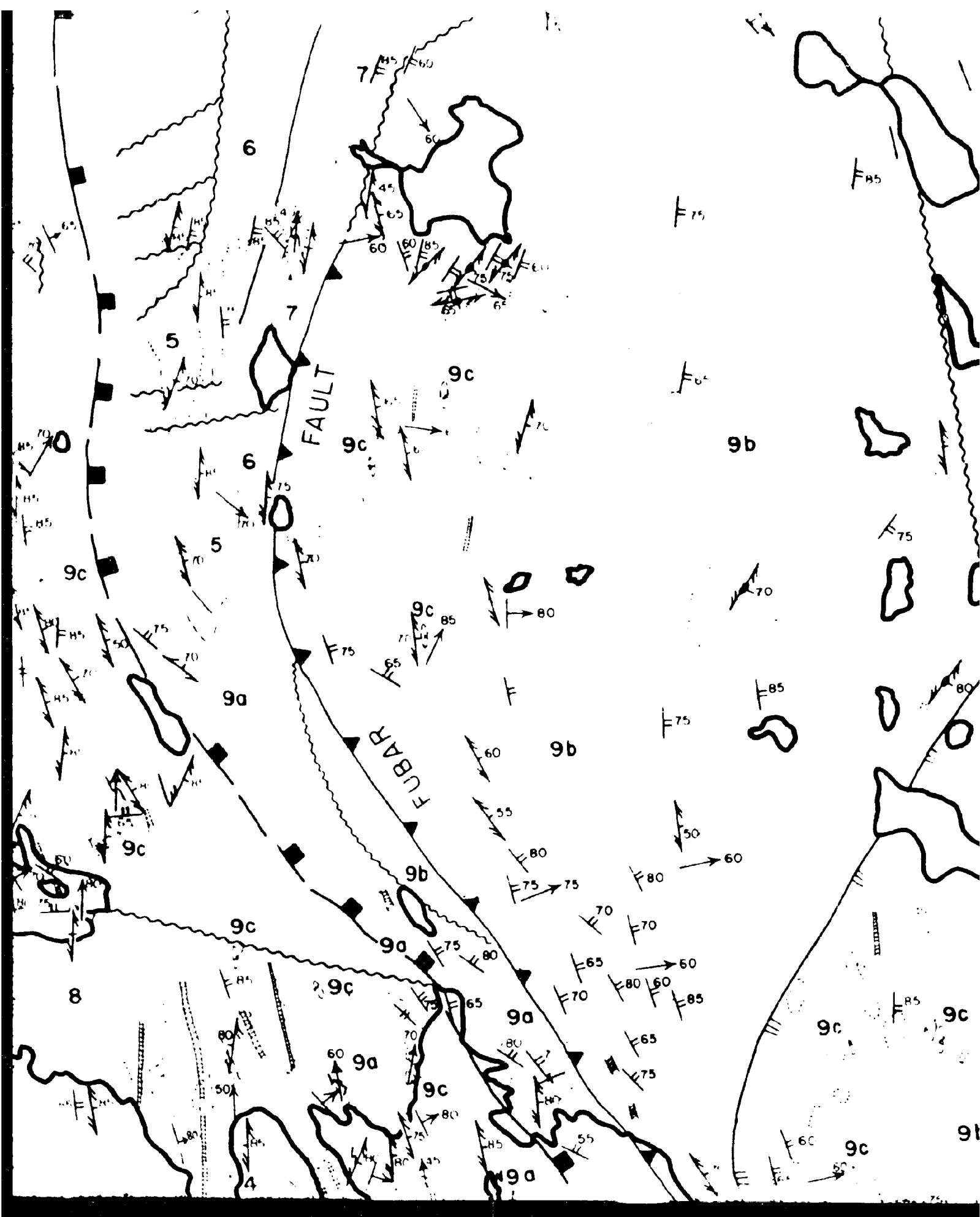
9a

9a

9a

9b

85

75

75

80

65

{ turbiditic
metasediments

('9c)

75

45

9a

80

80

80

9b

amphibolite and diorite (9 d),
and porphyroclastic granite
st e equivalent (9e)

ITCHEN

LAKE

65°25'

POINT LAKE

10

10

11a

11a

11a

65°20'

IIa

IIa

65°20'

10

IIa

IIa

IIa

IIa

IIa

IIa

85

80

85

80

IIa

IIa

IIa

IIa

IIa

IIa

80

IIa

IIa

IIa

IIa

IIa

10

IIa

60

85

85

75

85

85

IIa

80 85

80

IIa

c

85

55

IIa

75

75

IIa

IIa

9b

IIa

10

75 75

IIa

la,e,f,h,
i,12

113°10'

Legend:
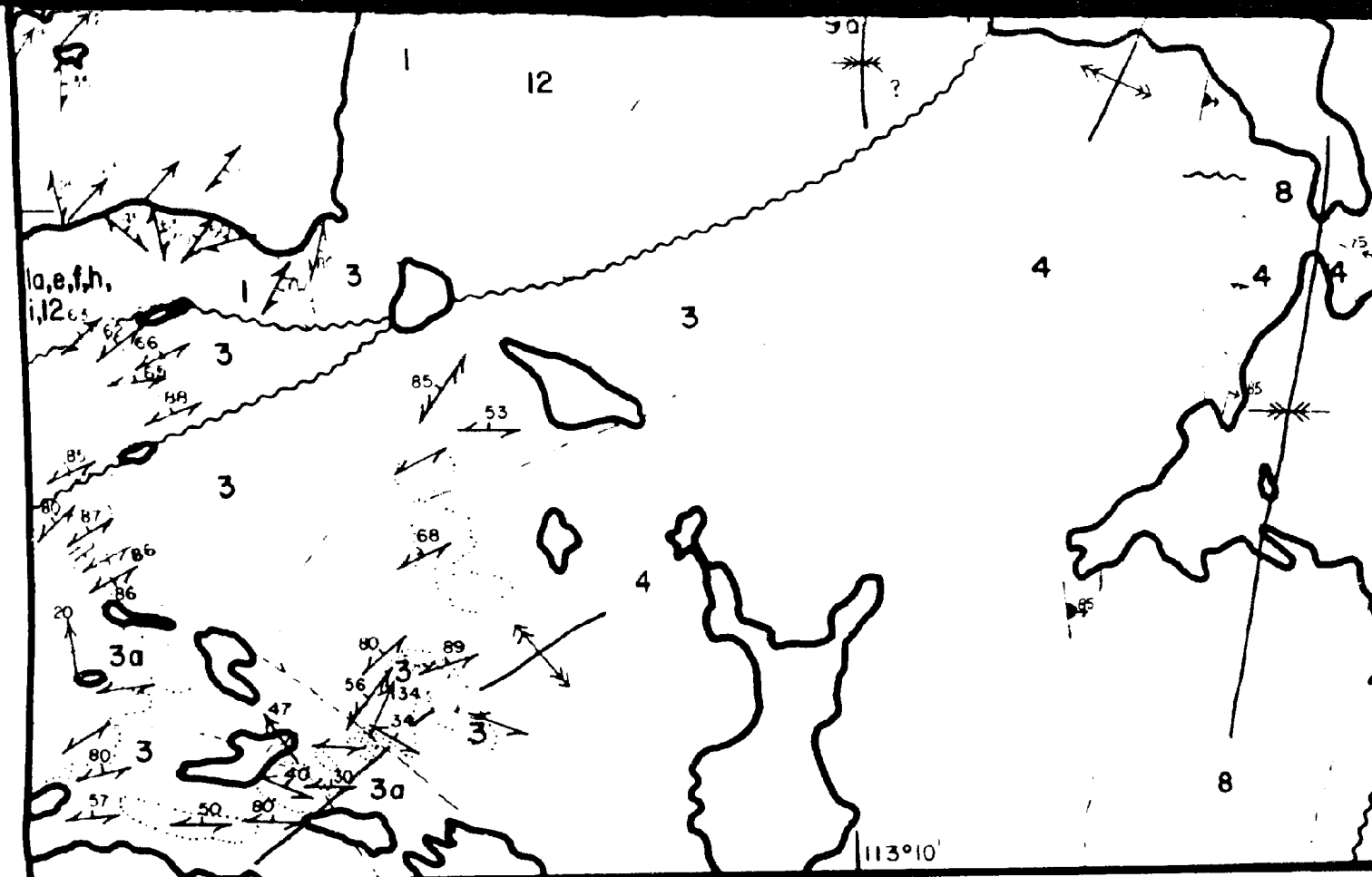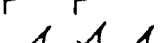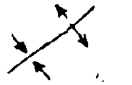
- Bedding tops known : inclined , vertical, overturned
- Bedding tops unknown : inclined , vertical, trend
- Pillows : tops known , unknown (trend)
- S_1 inclined , vertical, trend
- S_2 inclined , vertical, trend
- Pillow elongation parallel to S_2 (with arrow tops known)
- S_3 (largely inferred) : inclined , vertical , trend
- S_4 (largely inferred) and undifferentiated : inclined , vertical , trend
- Gneissosity : inclined , vertical, trend
- Minor fold axis (may include fold shape /sense of asymmetry)
- Mineral /clast/ intersection lineation , crenulation axis
- Late sub-horizontal slickensides

LAKE

KESKARRAH

BAY

55

113°00'

L A K E

9c

9a

11a

8

KESKARRAH

8

BAY

8

4

4

5

4

8

4

9a

4

9a

8

4

53

45

75

75

65

75

4

75

80

80

9a

4

2

8

8

4

8

2

4

113°00'

9a

9a

0   1   2

65°15'

10

11a

9c

9b

10

11a

11a

5

9a

9a

9a

8

8

8

8

50

2

2

5

9a

11a

11a

10

10

9b

112°50'

11b

9a

9b

1:30,000

2   3   4   5

KILOMETERS